

Examining the Role of ZIP7 in Zinc Signalling Mechanisms and its Relevance to Cancer

A thesis submitted in accordance with the conditions
governing candidates for the degree
of:

Philosophiae Doctor in Cardiff University

by

Sara Almadani

January 2022

**Cardiff School of Pharmacy and Pharmaceutical Sciences
Cardiff University**

Summary

Zinc is an essential trace element in the human body. The cellular zinc level is tightly regulated by zinc transporters, including the ZIP family, which has a role in increasing cytosolic zinc levels. The aberrant function of many ZIP channels has been associated with human diseases, including cancer. Our main focus is zinc transporter ZIP7 which is uniquely placed on the endoplasmic reticulum membrane. Despite this cellular localisation, ZIP7 appears to stain the nuclear membrane raising the issue that it can transport zinc into the nucleus as well as the cytosol. The present study evaluated the significance of ZIP7 gene expression in breast cancer using comprehensive bioinformatic analysis. Findings within this project support the hypothesis that ZIP7 might be considered a predictive biomarker for breast cancer prognosis and a novel therapeutic target for breast cancer.

Imaging ZIP7 in MCF7 cells has suggested that ZIP7 and the active form of ZIP7 (pS275/S276 ZIP7) are located in the nuclear membrane. These data highlighted that ZIP7 could transport zinc from the endoplasmic reticulum store into the nucleus. This nuclear localisation of ZIP7 may play an essential role in cell growth but also position it to increase cancer development through access to transcription factors which have a zinc finger domain. It is crucial to understand the function of ZIP7 in the nuclear envelope so having discovered three potential nuclear localisation motifs in ZIP7, these were mutated by site-directed mutagenesis for experimental confirmation. The different functions of nuclear-located ZIP7 mutants were assessed by phospho-kinase arrays to examine the effect on the activation of downstream pathways. This study revealed that NLS3 (²⁸⁸AAAGGSTVPKDGPVRPQNAEEEEAA³¹¹) is required for ZIP7 maximal activation. ZIP7 has already been implicated in cancer growth and proving the role of ZIP7 in nuclear zinc transport could have significant implications for future cancer therapy.

Acknowledgment

First of all, I would like to thank ALLAH (God) almighty, the most merciful and compassionate, for his support, help, and generosity.

Second, I would like to thank and express my sincere appreciation and gratitude to my supervisor Dr Kathryn Taylor for her continuous support, dedicated help, valuable advice, and immense knowledge. Her guidance and comments helped me in all the time of research and writing of this thesis.

Also, I would like to thank all breast cancer molecular pharmacology group members for their help and support. A deep thanks to my friend, Olivia, for her continuous help, kindness, encouragement, and support, especially during the most challenging times of my PhD. Thank you, Silvia, for your help in the lab and your kindness. An extended thanks to all my friends for their constant support during my PhD. Their help and friendship will always be remembered. I would like to thank my sponsor, Taibah University, College of Pharmacy, for the full scholarship and for giving me the opportunity to finish my higher degree at Cardiff University. I am deeply grateful to my husband, Ahmad, for his love, support, encouragement, and patient. To my lovely daughter, Tala, thank you for giving me the happiness and cheering me up during my studies. I love you to the moon and back.

Finally, it is impossible to mention everybody who impacted this work; however, those whose spiritual support is even more important. I feel a deep sense of gratitude for my father and mother, who formed part of my vision and taught me good things that matter in life. Their love, prayers and support have always been my strength. Their patience and sacrifice will remain my inspiration throughout my life. Also, A special thanks to all my family members for their constant love, inspiration and encouragement are immeasurable.

Table of Contents

Summary	<i>i</i>
Acknowledgment	<i>ii</i>
Table of Contents	<i>iii</i>
List of Figures	<i>vi</i>
List of Tables:	<i>ix</i>
List of Abbreviations:	<i>x</i>
1 Chapter 1: Introduction:	1
1.1 The Important of Zinc in the Body:	1
1.2 Biological and Physiological Function of Zinc:	2
1.3 Zinc Signaling:	3
1.4 Zinc Transporters:	5
1.5 Structure of ZIP Family of Zinc Transporters:	7
1.6 Handling of Zinc in Cells:	10
1.7 ZIP Cellular Location and Phosphorylation Site:	12
1.8 Nuclear Membrane:	13
1.7 Integral membrane protein targeting to the inner nuclear membrane:	16
1.9 Role of Zinc in Oncogenesis:	17
1.10 Zinc Transporters and Cancer	20
1.11 ZIP7 and breast cancer:	21
1.12 Hypotheses, aims and objectives of this project	22
1.12.1 Hypothesis.....	22
1.12.2 Aims and objectives:	23
2. Chapter 2: Materials and Methods:	24
2.1 Cell Preparation and Treatment	24
2.1.1 Cell Culture.....	24
2.1.2 Transfection	24
2.1.3 Zinc Treatment.....	25
2.2 Site-directed mutagenesis	25
2.3 Plasmid Preparation:	27
2.4 Immunofluorescence:	28
2.5 Western Blot	31
2.5.1 Cell lysis and protein assay.....	31
2.5.2 Polyacrylamide Gel Electrophoresis–Sodium Dodecyl Sulphate (SDS–PAGE) and Immunoblotting.....	32

2.6	Proteome profiler antibody array	34
2.7	Statistical Analysis:	35
2.8	Materials:	36
3.	<i>Chapter 3: Computer analysis of ZIP7 protein sequences and analysis of ZIP7 RNA expression and prognosis in different cancer</i>	38
3.1	Introduction	38
3.2	Methods.....	39
3.3	Results	40
3.3.1	Dendrogram of the human SLC39A (ZIP) amino acid sequence	40
3.3.2	Computer analysis of LIV-1 subfamily sequences	41
3.3.3	Identification of potential phosphorylation sites in ZIP7	45
3.3.4	Identification of endoplasmic reticulum retention signals in ZIP7	48
3.3.5	Identification of nuclear localization sequences in ZIP7	49
3.3.6	Analysis the potential phosphorylation sites, ER retention signals, NLS signals in various animal species of ZIP7	53
3.3.7	Elevated transcriptomic levels of ZIP7 associated with cancer	55
3.3.8	Further validation of the relationship between ZIP7 expression and clinical pathological parameters of patients with breast cancer	57
3.3.9	ZIP7 expression predicts the outcome of patient survival in breast cancer	63
3.3.10	The expression of ZIP7 gene in ER ⁺ breast cancer patients receiving Tamoxifen treatment: 67	
3.4	Chapter Summary.....	69
4.	<i>Chapter 4: Investigating ZIP7 activation mechanisms and analysis of endoplasmic reticulum retention signals of ZIP7.....</i>	71
4.1	Introduction:.....	71
4.2	Methods.....	72
4.3	Results:.....	73
4.3.1	Using pZIP7 antibody to examine the timeline of ZIP7 activation after zinc treatment	73
4.3.2	Verification of wild type ZIP7 and mutant constructs	74
4.3.3	Further confirmation by immunofluorescence that pZIP7 antibody only binds to phosphorylated ZIP7.	76
4.3.4	Confirmation of downstream effects of ZIP7 mediated zinc release:.....	79
4.3.5	Effect of ZIP7 S293A and T294A mutants on ZIP7 activation:.....	81
4.3.6	Investigating the endoplasmic reticulum signals of ZIP7:.....	89
4.7	Chapter summary:.....	103
5.	<i>Chapter 5: Discovery the nuclear localization of ZIP7:</i>	105
5.1	Introduction	105
5.2	Methods.....	105
5.3	Results	106
5.3.1	Imaging the localization of ZIP7 in cells	106
5.3.2	Co-localization of ZIP7 with inner nuclear proteins markers:.....	111
5.3.3	Co-localization of pZIP7 with inner nuclear proteins markers:.....	119
5.4	Chapter summary:.....	124
6.	<i>Chapter 6: Investigation the nuclear localization signals (NLS) of ZIP7</i>	126
6.1	Introduction	126

6.2	Methods.....	127
6.3	Results	127
6.3.1	Mutagenesis of the potential NLSs of ZIP7:	127
6.3.2	The role of predicted nuclear localization signals in targeting ZIP7 to the INM:.....	128
6.3.3	Colocalization of ZIP7 NLS mutants with inner nuclear protein markers:	130
6.3.4	Effect the removal of nuclear localization signals on ZIP7 activation:.....	131
6.3.5	Using phospho-kinase arrays to investigate the effect of NLS mutants on ZIP7 activation and downstream signaling:	135
6.3.6	Western blotting to confirm the kinases activated by ZIP7 and downregulated in cells transfected with NLS3 mutant:	148
6.4	Chapter Summary.....	156
7.	<i>Chapter 7: Discussion.....</i>	<i>157</i>
7.1	Overexpression of ZIP7 is a prognostic biomarker in human breast cancer	158
7.2	Analysis of ER retention signals in the ZIP7 sequence.....	163
7.3	The long cytoplasmic/nucleoplasm domain of ZIP7 contains multiple nuclear localization signals.....	166
7.4	Zinc and its role in the nucleus	172
7.5	ZIP7 signaling is involved in diverse kinase signaling pathways.....	174
7.6	ZIP7-mediated zinc release causes AKT and CREB phosphorylation	175
7.7	Removal of the nuclear localization motifs from ZIP7 reduces the activation of AKT and CREB	178
7.8	ZIP7 overexpression activates ERK1/2.....	181
7.9	Decreased ERK1/2 activation in cells overexpressing ZIP7 NLS3.....	182
7.10	Decreased activation of p70S6 Kinases in cells overexpressing the ZIP7 NLS3 mutant	183
7.11	Activation of WNK1 (T60) in cells overexpressing WT ZIP7.....	186
7.12	How to target ZIP7	187
7.13	Summary.....	188
8	<i>References.....</i>	<i>190</i>
9.	<i>Appendices:.....</i>	<i>225</i>

List of Figures

Figure 1.1 Zinc in diet and its distribution in the body.	2
Figure 1.2 Effect of zinc imbalance on human health.	5
Figure 1.3 Zinc homeostasis is regulated by ZIP and ZnT transporter.	6
Figure 1.4: The Phylogenetic tree of human LIV-1 family members	7
Figure 1.5: Predicted structure of the ZIP transporters.	9
Figure 1.6 : Schematic showing ZIP7-mediated zinc handling in cells	11
Figure 1.7: α and β clusters of metallothionein (MT).....	11
Figure 1.8: Downstream pathway of ZIP7 mediated zinc release.	13
Figure 1.9: Schematic Showing Nuclear Envelop.	14
Figure 2.1 DNA sequences of ZIP7 S293A and T294A mutants.....	26
Figure 2.2: DNA sequencing of ZIP7 ER retention signals of ZIP7.....	26
Figure 2.3 DNA sequencing of ZIP7 NLS mutants.	27
Figure 2.4: Schematic representation of "sandwich" gel and membrane setup for electrophoretic protein transfer.....	33
Figure 2.5 Human phosphokinase arrays.	35
Figure 3.1 Phylogenetic tree of human ZIP channels.....	41
Figure 3.2 Alignment of all human LIV-1 subfamily sequences (part A)	43
Figure 3.3 Alignment of all human LIV-1 subfamily sequences (part B).....	44
Figure 3.4 TM5 of the human LIV-1 family of ZIP transporters	45
Figure 3.5 Cellular localization of wild type ZIP7 in MCF-7 cells.....	48
Figure 3.6 Schematic diagram that shows the location of ER retention signals in the ZIP7 sequence.	49
Figure 3.7 : Schematic diagram that shows the location of NLS on ZIP7 sequences.	51
Figure 3.8 The amino acid sequence of ZIP7 zinc transporter.....	52
Figure 3.9 Alignment of ZIP7 in various animal species	54
Figure 3.10 The GEPIA boxplot of ZIP7 gene expressions in common cancers versus paired normal tissues.	56
Figure 3.11 The transcriptional levels of ZIP7 in different subtype of breast cancer in GEPIA database.....	57
Figure 3.12 Relative expression of ZIP7 gene in normal tissues and breast cancer tissues.	59
Figure 3.13 Box plot showing the expression of ZIP7 in subgroups of breast invasive carcinoma samples (BRCA) from UALCAN database.	60
Figure 3.14 Differential expression of ZIP7 in patients with different type of breast cancer using bc-GenExMiner.	61
Figure 3.15 Immunohistochemistry of ZIP7 gene in breast cancer and normal breast tissue from the Human Protein Atlas (HPA).	62
Figure 3.16 Kaplan-Meier survival plots show that higher expression of SLC39A7 lead to worse survival.....	66
Figure 3.17 Kaplan-Meier survival plots show that higher expression of SLC39A7 leads to worse survival in tamoxifen treated ER+ breast cancer patients	68
Figure 4.1: Binding site of pZIP7 antibody.....	73
Figure 4.2 Gradual increase of pZIP7 level after zinc treatment.....	74
Figure 4.3: Transfection efficiency of WT ZIP7, S275A/S276A and S275D/S276D mutants	75
Figure 4.4 pZIP7 activation increased after zinc treatment in cells overexpress WT ZIP7.	77

Figure 4.5 pZIP7 activation increased after zinc treatment in cells overexpress ZIP7 S275D/S276D.....	78
Figure 4.6 Characterization of ZIP7 S275A/S276A after zinc treatment.....	79
Figure 4.7 Downstream effect of ZIP7 mediated zinc release	81
Figure 4.8: Transfection efficiency of WT ZIP7, S293A, and T294A constructs.	83
Figure 4.9 pZIP7 antibody ability to detect ZIP7 activation in cells transfected with WT ZIP7.....	85
Figure 4.10 pZIP7 antibody ability to detect ZIP7 activation in cells transfected with ZIP7 S293A constructs.....	86
Figure 4.11 pZIP7 antibody ability to detect ZIP7 activation in cells transfected with ZIP7 T294A constructs.....	87
Figure 4.12 Activation of the ZIP7 S293A and T294A mutants by zinc	88
Figure 4.13 Schematic diagram that shows the location of ER mutant sites in the ZIP7	90
Figure 4.14: Transfection efficiency and localization of ER ZIP7 mutants.....	92
Figure 4.15: Transfection efficiency and localization pattern of different ZIP7 ER mutants' constructs.....	93
Figure 4.16: Co-localization of ER retention signals mutants with PDI.....	94
Figure 4.17: Co-localization of ER retention signals mutants of ZIP7 with PDI.....	95
Figure 4.18 pZIP7 antibody detect ZIP7 activation in cells transfected with WT ZIP7.	97
Figure 4.19 pZIP7 antibody detect ZIP7 activation in cells transfected with ZIP7 ER1A.....	98
Figure 4.20 pZIP7 antibody detect ZIP7 activation in cells transfected with ZIP7 ER1B.....	99
Figure 4.21 pZIP7 antibody detect ZIP7 activation in cells transfected with ZIP7 ER2.....	100
Figure 4.22 pZIP7 antibody detect ZIP7 activation in cells transfected with ZIP7 ER3.....	101
Figure 4.23 pZIP7 antibody detect ZIP7 activation in cells transfected with ZIP7 ER4.....	102
Figure 5.1 Cellular localization of wild type ZIP7 in MCF-7 cells.....	108
Figure 5.2: Active ZIP7 (pZIP7) localize in ER and nuclear membrane	109
Figure 5.3: Protein Disulfide Isomerase (PDI) localization in cells.....	109
Figure 5.4 ZIP7 and actin localization in cells.....	110
Figure 5.5: Testing overlap of ZIP7 with mitochondria.....	110
Figure 5.6 Topology of the nuclear envelop.....	111
Figure 5.7: ZIP7 Co-localises with Lamin B in MCF-7 cells	113
Figure 5.8: ZIP7 Co-localises with Lamin A/C in MCF-7 cells.....	114
Figure 5.9: ZIP7 Co-localises with NUP98 in MCF-7 cells.....	116
Figure 5.10: ZIP7 Co-localises with Lamin B receptor in MCF-7 cells.....	118
Figure 5.11: ZIP7 Co-localises with emerin in MCF-7 cells.....	119
Figure 5.12: pZIP7 Co-localises with NUP98 in MCF-7 cells.....	121
Figure 5.13: pZIP7 Co-localises with Lamin B receptor in MCF-7 cells.....	123
Figure 6.1 Schematic diagram that shows the alanine mutation in the predicted NLSs	128
Figure 6.2: Transfection efficiency of NLS ZIP7 mutants.....	129
Figure 6.3 Colocalization of NLS mutants with Lamin B:	130
Figure 6.4: Increase ZIP7 activation in the cells transfected with NLS ZIP7 mutant constructs.....	133

Figure 6.5: Effect of zinc treatment on activation of ZIP7 NLS mutants.	134
Figure 6.6 Confirmation of the expression of recombinant ZIP7 constructs.	137
Figure 6.7 Human phospho-kinase array coordinates	137
Figure 6.8 Phosphokinase arrays in MCF-7 cells transfected with WT ZIP7 and ZIP7 NLS mutants with zinc stimulation	138
Figure 6.9 Densitometric analysis of phospho-kinase arrays in MCF-7 cells transfected with WT ZIP7 and stimulated with zinc.	139
Figure 6.10 Densitometric analysis of phospho-kinase arrays in MCF-7 cells transfected with ZIP7 NLS1 with zinc stimulation.	140
Figure 6.11 Densitometric analysis of phospho-kinase arrays in MCF-7 cells transfected with ZIP7 NLS2 with zinc stimulation.	141
Figure 6.12 Densitometric analysis of phospho-kinase arrays in MCF-7 cells transfected with ZIP7 NLS3 plus zinc stimulation.....	142
Figure 6.13 Cells transfected with NLS3 mutant shows less kinase activation than WT ZIP7, NLS1, and NLS2.	147
Figure 6.14 ERK1/2 activation downstream of ZIP7-mediated zinc release.	149
Figure 6.15 AKT activation upon ZIP7 mediated zinc release.	150
Figure 6.16 CREB activation upon ZIP7 mediated zinc release	152
Figure 6.17 p70S6 Kinase (T421/S424) upon ZIP7 mediated-zinc release.	154
Figure 6.18 p70S6 Kinase (T389) upon ZIP7 mediated zinc release.....	155
Figure 7.1 Proposed ZIP7 translocation mechanism into the nucleus.....	169
Figure 7.2 Downstream signalling pathways of ZIP7 mediated zinc release.....	178

List of Tables:

Table 2.1 DNA sequences of ZIP7 mutants used in this project.....	25
Table 2.2: Primary Antibodies	30
Table 2.3: Secondary Antibodies	31
Table 2.4 Recipe of stacking gel	32
Table 2.5 recipe of resolving gel	32
Table 2.6 Materials.....	36
Table 3.1: Predicted phosphorylation sites of ZIP7 and their predicted kinases.....	47
Table 3.2 Predicted endoplasmic retention signals of ZIP7.	49
Table 3.3 Online databases used to detect NLS and ER retention signals	50
Table 3.4: Predicted nuclear localization sequences of ZIP7	51
Table 3.5 Relationship between ZIP7 expression and patients with breast cancer.	65
Table 4.1 Plasmid DNA concentration.....	72

List of Abbreviations:

AKT: Protein Kinase B
BSA: Bovine Serum Albumin
BRCA: breast invasive carcinoma samples
CK2: Protein Kinase 2
CDF : Cation Diffusion Family
Cys: Cysteines
CI: Confidence intervals
CREB: cAMP response element-binding protein
KDa: (unit) KiloDalton
DAPI: 4,6-diamino-2-phenylindol
dH₂O: Distilled water
DMFS: Distant metastasis-free survival
ER: Endoplasmic reticulum
EGFR: Epidermal Growth Factor Receptor
FBS: Foetal bovine serum
HER2: Human epidermal growth factor receptor 2
HR: Hazard ratio
LB: Luria-Bertani
LZT: LIV-1 Subfamily of ZIP transporter
LN: Lymph nodes
NCBI: National Centre for Biotechnology Information
°C: Degree Celsius
OD: Optical density
ONM: Outer nuclear membrane
OS: Overall survival
INM: Inner nuclear membrane
IF: Immunofluorescence
MAPK: Mitogen activated protein kinase
MRE: Metal response element
MTF-1: Metal-regulatory transcription factor-1
MTs: Metallothioneins
MCF-7: Michigan Cancer Foundation–7 cells
NE: Nuclear envelope
NPCs: Nuclear pore complexes
NUPs: Nucleoporins
NLS: Nuclear localisation signals
PBS: Phosphate buffered saline
PKA: Protein kinase A
PDI: Protein Disulfide Isomerase
pZIP7: Phospho-ZIP7 antibody

RFS: Relapse-free survival

SDS-PAGE: Sodium dodecyl sulphate-polyacrylamide gel electrophoresis

TBST: Tris-buffered saline with Tween-20

TE buffer: Tris-EDTA buffer

TM: Transmembrane domain

TamR: Tamoxifen-resistant breast cancer cell

WB: Western blot

Zn: Zinc

1 Chapter 1: Introduction:

1.1 The Important of Zinc in the Body:

Zinc is a biologically essential micronutrient trace element that has a crucial role in human health and disease. Zinc exists as a divalent cation (Zn^{2+}), and it is the second most abundant intracellular metal in the human body (second only to iron)^{1,2}. Dietary zinc is absorbed in the small intestine (duodenum and jejunum) and then is distributed to the circulation through zinc family transporters^{1,3} (**Figure 1.1**). Serum zinc is only ~0.1 % of the total body zinc^{1,4}. Zinc is mainly bound to proteins, including albumin (80%)⁵. The remaining zinc in serum is bound to transferrin, α -macroglobulin and others⁵. The adult human body is estimated to have approximately 2-4 g or 30 mmole of zinc present in all body fluids and tissue¹. Most of the total body zinc is found in the skeleton muscles (60%) and bone (30%), with the highest concentrations in the prostate fluid and eye^{6,7}.

Zinc was identified as an essential micronutrient element in 1961, and its deficiency leads to a wide variety of diseases, so zinc deficiency is considered a global health crisis⁸. Zinc is necessary for the normal metabolism of nucleic acids, proteins, carbohydrates, and lipids⁹ as well as for maintaining proper immune function, defence against free radicals, growth, the wound healing process, and preventing age-related degenerative diseases^{10,11}. Zinc deficiency is a significant public health problem worldwide, and it is the fifth leading cause of morbidity and mortality in developing countries¹. Renal insufficiency patients, premature infants, seniors, pregnant and breastfeeding women, and vegetarians are at a higher risk of zinc deficiency¹². Malnutrition children under five years old have higher rates of death due to severe diarrhea and lower respiratory tract infection (pneumonia) as a result of zinc deficiency^{1,13}. Zinc supplementation in young children is recommended as an adjunct to diarrhea treatment to decrease diarrhea mortality and boost the immune function^{1,13}. The recommended daily allowance (RDA) of zinc that protects us from having signs and symptoms of zinc deficiency varies from 5 mg for the infant to 15 mg for adults¹³. Zinc is available in a wide variety of foods. Oysters and red meats have the highest zinc levels, 20-150mg/100g and 3.6mg/100g, respectively¹⁴ (**Figure 1.1**). Nuts, dairy products, fortified breakfast cereals, potatoes, vegetable oil, lobster, and fruits are also other suitable

sources of zinc¹⁴. The bioavailability of zinc is lower in vegetarian food than from meat sources because phosphate and phytate (phytic acid) is present in vegetable chelate zinc, leading to inhibition of its absorption^{15,16}.

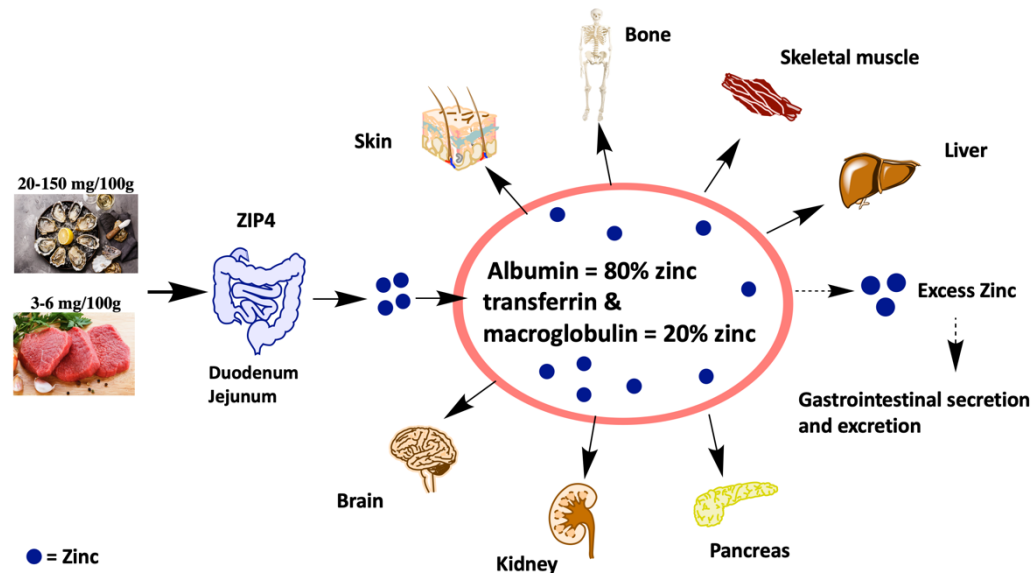


Figure 1.1 Zinc in diet and its distribution in the body.

Zinc is one of the most important trace elements in the human body, and it is available in a wide variety of foods. Oysters and red meats have the highest zinc levels. Dietary zinc is absorbed in the small intestine and then is distributed to the circulation through zinc family transporters

1.2 Biological and Physiological Function of Zinc:

Zinc is a non-redox active ion essential for biochemical and physiological intracellular function. Zinc homeostasis controlled by zinc transporters is crucial for numerous biological processes, including; catalytic, structural function, and regulatory components in a few hundred enzymes, many of which are involved in cancer growth and metastasis⁹. **First**, zinc is the only metal required for catalysis in more than 300 enzymes^{3,17}. In 1939, erythrocyte carbonic anhydrase was the first zinc-dependent enzyme identified, which is essential for the metabolism of carbon dioxide¹⁸. After that, zinc was recognized as a cofactor in all six classes of enzymes (transferase, oxidoreductase, hydrolases, lyases, isomerase, and ligase) and transcription factors containing zinc finger motifs¹⁴. Zinc is essential for many fundamental cellular processes such as DNA synthesis, growth, and

wound healing¹¹. Zinc removal from zinc metalloenzymes such as RNA polymerases, alcohol dehydrogenase, and alkaline phosphatases results in loss of their enzyme activity³. **Second**, zinc has been recognised as essential for the structural arrangement and stability of essential antioxidant defence proteins such as CuZn superoxide dismutase (SOD) to protect and prevent protein oxidation against reactive oxygen species (ROS) by the formation of thiolate complexes². Also, zinc binds up to 10% of all proteins in the mammalian genome, essential for DNA repair, replication and translation¹⁹. Zinc finger proteins contain a functional motif stabilised by a zinc ion that has extraordinarily diverse functions involved in protein folding and assembly, signal transduction, cellular differentiation or proliferation, and lipid binding²⁰. **Third**, zinc has a regulatory role in gene expression. Zinc is necessary to maintain the structural integrity and DNA binding of more than 2000 transcription factors to regulate gene expression⁹. To stimulate transcription, zinc in the cytosol or nucleus must bind to metal-regulatory transcription factor-1 (MTF-1), which contains six Cys₂His₂ zinc fingers, and then interacts with the metal response element (MRE) in the promoter of the regulated gene²⁰⁻²³. The expression of MT, which is responsible for zinc trafficking, is regulated by the metal response element (MRE)³. Alteration in the cellular zinc level by adding extracellular zinc or chelating agent can affect many downstream signalling pathways that need zinc to be activated²⁴.

1.3 Zinc Signaling:

Zinc has been shown to act as an intracellular second messenger in the cytosol that can potentially impact a spectrum of cellular signalling^{25,26}. In mast cells, zinc was able to transduce an extracellular stimulus into an intracellular signalling cascade within two minutes²⁵. Stimulation of the high-affinity immunoglobulin E receptor (Fcε receptor I [Fcε RI]) in mast cells facilitated zinc release from the endoplasmic reticulum (ER) in the form of a “zinc wave” on a timescale of minutes in contrast to transcription factor effect, which would take many hours^{25,27}. This intracellular zinc release resulted in phosphatase inhibition and downstream activation of MAP kinases^{25,27}. This zinc wave from the ER was also shown to depend on Ca²⁺ influx and the activation of mitogen-activated protein kinase activation^{25,27}. FluoZin-3 was used to detect the increase of intracellular zinc after 20 mins of Fcε RI stimulation²⁵. Also, zinc has been shown to act as a neurotransmitter and carry information between cells in synaptic vesicles along with glutamate²⁸. High zinc

level has been observed to induce neuronal death²⁹. Zinc homeostasis is vital to maintaining the proper formation of the nervous system because excess zinc is toxic to neurons and has been implicated in human neurodegenerative diseases such as Alzheimer's and Parkinson's diseases^{30,31}. Zinc has been detected in amyloid plaques in Alzheimer's patients, which is a typical hallmark of this disease³².

On a cellular level, the amount of zinc ions must be strictly regulated by zinc transport and binding proteins such as metallothionein (MTs) to maintain the proper biological function essential for cell growth, differentiation, proliferation, migration, and cell division, DNA synthesis, and RNA transcription³³. In cells, 50% of zinc is in the cytoplasm, 40% in the nucleus, and 10% in the membrane^{1,4}. Excess zinc can be toxic to cells, resulting in apoptosis and leading to cancer development such as breast and lung cancer. Zinc is essential for the function of many cyclins that involve in the cell cycle progression (G1 and G2 phases)^{34,35}, which suggest that cancer cells need more zinc for their survival and proliferation. On the other hand, a low zinc level causes DNA damage due to impairing DNA binding activity of p53 which results in genomic instability³⁶, impairment of the immune system (immune dysfunction)³⁷, increase in susceptibility to infection³⁷, loss of appetite, alopecia, depression, persistent diarrhoea³⁸, increase in oxidative stress³⁹, growth retardation and mental retardation³⁸, delayed wound healing³⁷, glucose intolerance, abnormal pregnancy⁶, increase in bone fragility⁶, and skin diseases, including Acrodermatitis Enteropathica (AE)⁴⁰ (**Figure 1.2**). Acrodermatitis Enteropathica is a rare lethal genetic disease with an estimated frequency of approximately 1 per 500,000 children³. Acrodermatitis Enteropathica patients have zinc deficiency due to a mutation in the ZIP4/SLC39A4 gene, a zinc importer responsible for zinc uptake from dietary food in the intestine by enterocytes. This disease is characterised by diarrhea, alopecia, and eczematous pink dermatitis on acral areas, anogenital, and periorificial areas³. These conditions are reversible with pharmacological zinc supplementation^{1,6,36,37,41,42}. Also, in vivo study in rats have reported that severe zinc deficiency can cause DNA damage via increased oxidative stress and impairments in the DNA repair response, suggesting a significant zinc role in maintaining DNA integrity³⁹. Zinc deficiency could occur due to poor zinc diets or secondary to some conditions such as chronic renal diseases, sickle cell diseases, diabetes, cirrhosis of the liver and also with some drug therapy such as ethambutol, anticonvulsants, and penicillamine⁴³. Knowing that zinc excess and zinc

deficiency impact human health highlights the importance of tightly regulating the zinc level to maintain its homeostatic balance.

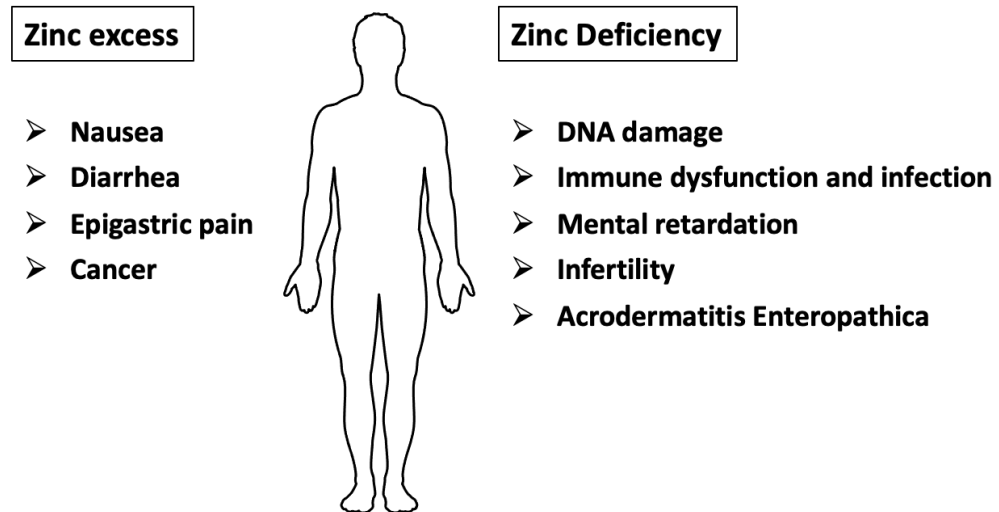


Figure 1.2 Effect of zinc imbalance on human health.

Alterations in zinc homeostasis result in cellular dysfunctions. Therefore, it is necessary for cells to tightly regulate the cellular free zinc level. (Plum, Rink & Haase, 2010).

1.4 Zinc Transporters:

Zinc cannot diffuse passively through cell membranes. Therefore it requires the help of zinc transporter proteins to cross the biological layer and contribute to a wide variety of cellular and physiological functions^{1,44}. Two groups of proteins mediate the cellular homeostasis of zinc: Znt (formally called Cation Diffusion Family (CDF); SLC30A) and ZIP (Zrt, Irt-Like proteins, SLC39A), which have different roles in maintaining cellular zinc homeostasis⁴⁵. *Arabidopsis thaliana* IRT1 gene (iron-regulated transporter) and *Saccharomyces cerevisiae* Zrt protein were the first ZIP family members to be identified⁴⁶⁻⁴⁸. The ZnT transporters (ZnT1 to ZnT10) lower the intracellular zinc level by either promoting zinc efflux from the cytoplasm to the extracellular space or influx into the lumen of intracellular compartments for detoxification and/or storage. In contrast, the ZIP transporters (ZIP1 to ZIP14) replenish the cytosolic zinc by promoting zinc transport from the extracellular space or the intracellular compartments during adaptation to zinc deficiency^{33,49,50} (**Figure 1.3**). ZIP7 has been shown to reside on the ER, ZIP8, ZIP13, and

ZIP14 on intracellular storage vesicles, ZIP9 and ZIP13 on Golgi apparatus⁵¹. Moreover, metallothionein, a zinc-binding protein and binds to the most intracellular zinc, has a role in maintaining the cellular zinc hemostasis^{52,53}. This project focuses mainly on the ZIP transporters. No crystal structure has been known for all zinc transporters; however, only Yipp, a bacterial membrane transporter that is equivalent to the human ZnT transporters, has a known crystal structure⁵⁴. ZnT is predicted to have six transmembrane domains with short cytosolic NH₂ and long COOH termini. All ZnT is present on the intracellular membrane; however, only ZnT1 is located on the plasma membrane⁵⁵. ZnT transporter work as Zn²⁺/H⁺ exchangers⁵⁶.

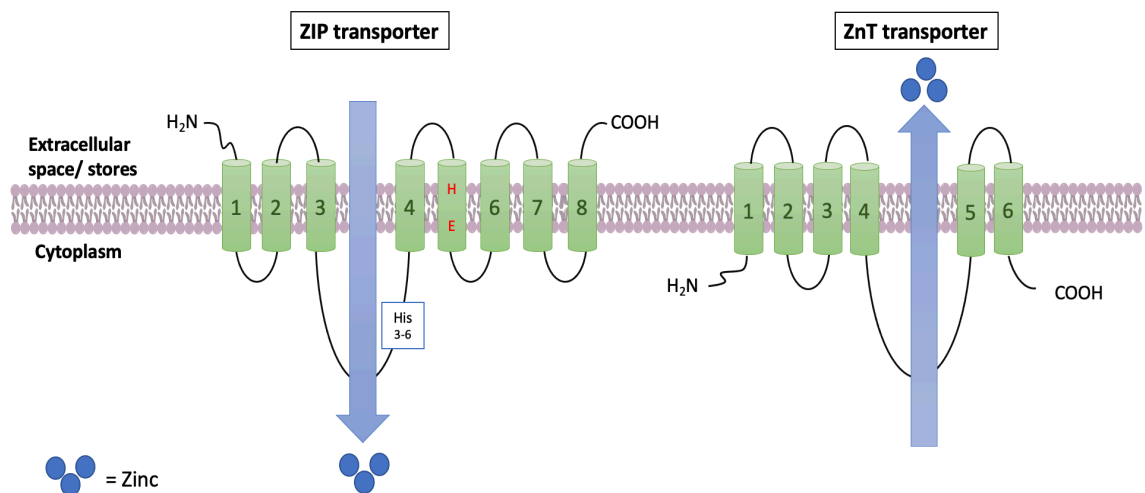


Figure 1.3 Zinc homeostasis is regulated by ZIP and ZnT transporter.

ZIP transporters are zinc export consist of 6 transmembrane domain and responsible for zinc influx into the cytoplasm while the ZnT transporter are zinc imports.

1.5 Structure of ZIP Family of Zinc Transporters:

According to the phylogenetic tree, the human ZIP transporters can be categorised into 4 subfamilies; subfamily I (hZIP9), *gufA* subfamily (hZIP11), subfamily II (hZIP2, hZIP1, hZIP3), and LIV-1 subfamily, also called LZT for the LIV-1 subfamily of ZIP zinc Transporter (hZIP4, hZIP5, hZIP6, hZIP7, hZIP8, hZIP10, hZIP12, hZIP13, and hZIP14)^{44,45,57} (Figure 1.4).

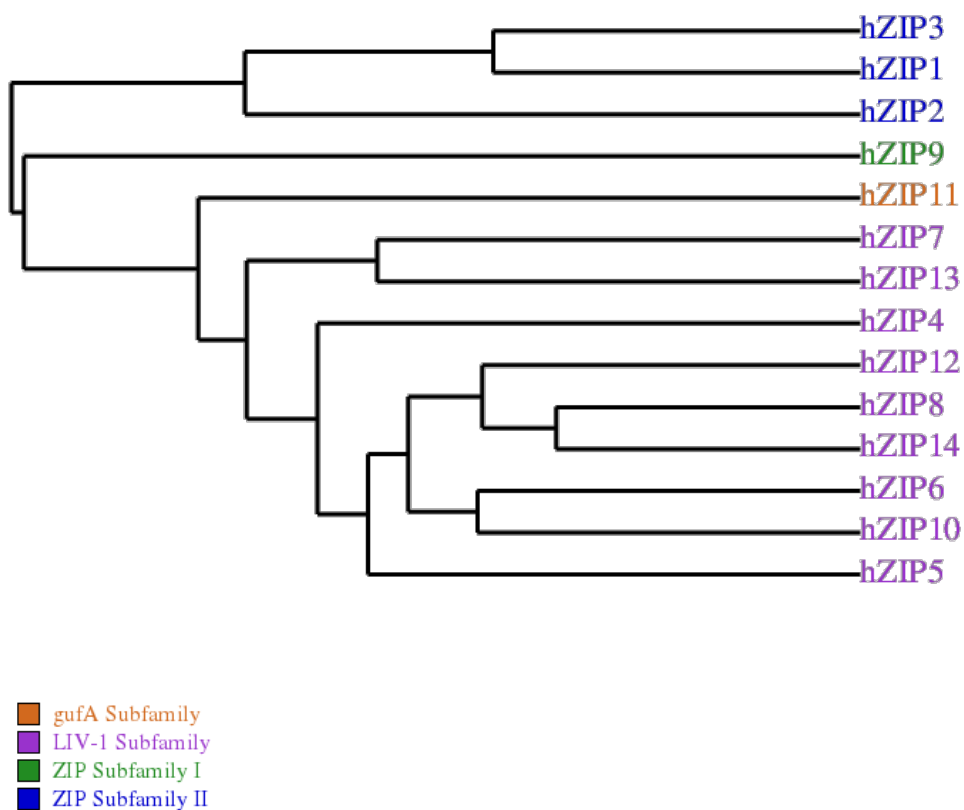


Figure 1.4: The Phylogenetic tree of human LIV-1 family members

To show the relationship among the LIV-1 subfamily, this phylogram was generated using the Phylogeny.fr web service. The amino acid sequences of the human ZIP transporter were retrieved from the NCBI database in the text-based FASTA format and then aligned with the CLUSTAL W (1.83) multiple sequence alignment program. The ZIP family of zinc transporter divided into 4 group.

ZIP transporters are predicted to have eight transmembrane spanning domains (TM) with an extracellular N and C termini⁵⁸ (**Figure 1.5**). There is an extended cytoplasmic variable region between TM3 and TM4 which contains multiple histidine residues^{33,44,45}, which is predicted to be involved in zinc binding and transport^{59,60}. Also, ZIP transporters have histidine-rich regions in TM4 and 5⁵⁹. Those multiple histidine regions are predicted to be involved in zinc transport as the ability of histidine to bind to zinc⁵⁹. The LIV-1 subfamily has some unique features. First, it contains a highly conserved metalloprotease motif HEXPHEXGD (where H=histidine; E=glutamate; P=proline; D=aspartate; G=glycine; X=any amino acid) in TM 5, which is not seen in any other subfamily of the ZIP transporters. This motif has been shown to match the catalytic binding site, which is HEXXH of two members of the zinc metalloprotease^{61,62}. Second, there are additional histidine-rich regions in the long extracellular N terminus and in the extracellular loop between TM2 and 3. The histidine is known to have a high affinity to bind to zinc, and that confirms the strong ability of LIV-1 members to transport zinc. Third, long extracellular N terminus that contains a unique CPALLY (C=cystine, P=proline, A=alanine, L=leucine, Y=tyrosine) motif immediately before the first TM, except for ZIP13 and ZIP7^{44,63}. This motif is predicted to support the tertiary structure of proteins and pore control to regulate zinc transport by forming a disulfide bond with the first conserved cysteine in the metalloprotease-like motif (CHEXPHEXGD)⁴⁴. It is predicted that the N-terminus would sit over the top of the transmembrane domain to regulate zinc transport. Mutation in the C309T in the ZIP4 gene, the third cysteine residue in the CPALLY motif, has been observed in Acrodermatitis Enteropathica patients^{44,64}. Also, The long extracellular N termini are highly glycosylated in most LIV-1 subfamily⁶⁵.

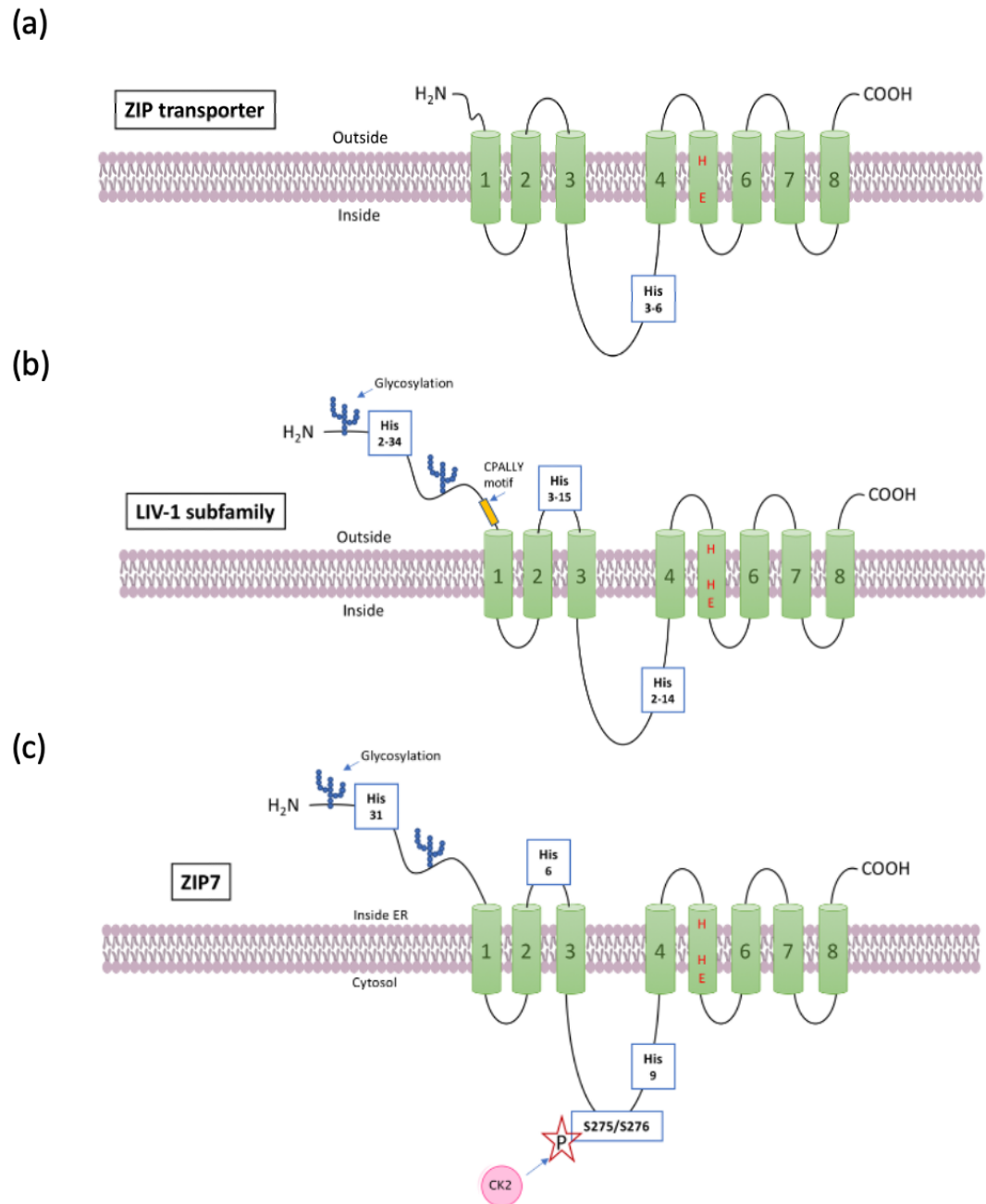


Figure 1.5: Predicted structure of the ZIP transporters.

(a) The ZIP transporters are predicted to have eight transmembrane domains with an extracellular N and C termini and a long cytoplasmic loop between TM3 and TM4 which contains between 3 and 6 histidine residues. (b) LIV-1 subfamily is characterized by a long extracellular N terminus containing a CPALLY motif and metalloprotease motif (CHEXPHEXGD) in TM5, similar to the zinc-binding site of the metalloproteinases⁶¹. They also have an additional histidine-rich motif between TM2 and 3, and in the long cytoplasmic loop between TM3 and 4. (c) ZIP7 is located in the endoplasmic reticulum (ER) and mediates a “zinc wave” in response to phosphorylation by protein kinase 2 (CK2) at residues S275 and S276¹⁶⁹ in the histidine-rich cytoplasmic loop between TM3 and TM4.

1.6 Handling of Zinc in Cells:

The intracellular trafficking and storage of zinc are also regulated by metal-binding proteins such as metallothioneins (MTs) and/or glutathione⁶⁶ under a process called the “muffler reaction”, which essentially buffers the zinc and compartmentalizes it into an intracellular store such as the ER before releasing into the cytosol by a ZIP7-mediated zinc wave^{63,67,68}(**Figure 1.6**). The Free “labile” cytosolic zinc concentration is very low, ranging from picomolar to a very low nanomolar range¹⁷ Zinc release from the ER, resulting in inhibition of many tyrosine phosphatases, leads to uncontrolled cell proliferation and an increase in the growth rate and invasion of tamoxifen-resistant (TamR) breast cancer^{63,69}.

MTs are ubiquitous intracellular proteins characterised by low molecular weight (6-7 kDa)^{30,70}. They are composed of 61-68 amino acids, twenty conserved cysteines (Cys) residues that can bind to seven zinc atoms, no aromatic amino acids, and an ability to complex 20% of intracellular free zinc decrease its level to Nanomolar or less concentrations^{30,70}. MT expression is controlled by metal-responsive-element-binding transcription factor-1 (MTF-1)²². MTs can bind to copper and zinc through their thiol group in the cysteine residues and promote their detoxification to prevent cell death by apoptosis⁷¹. Four mammalian MT isoforms have been detected and investigated: MT-I, MT-II, MT-III, and MT-IV⁷². MTs are mainly distributed in the cytoplasm and bind up to seven zinc ions in two separated zinc/thiolate clusters, Zn_4Cys_{11} (α) and Zn_3Cys_9 (β)^{71,72}. Each zinc binds to four sulfurs from the cysteines (**Figure 1.7**). MT-I and MT-II are located throughout the body, with the highest concentration in the kidney, liver, pancreas, and intestine, whereas MT-III is located mostly in the brain and MT-IV in stratified tissues²⁸.

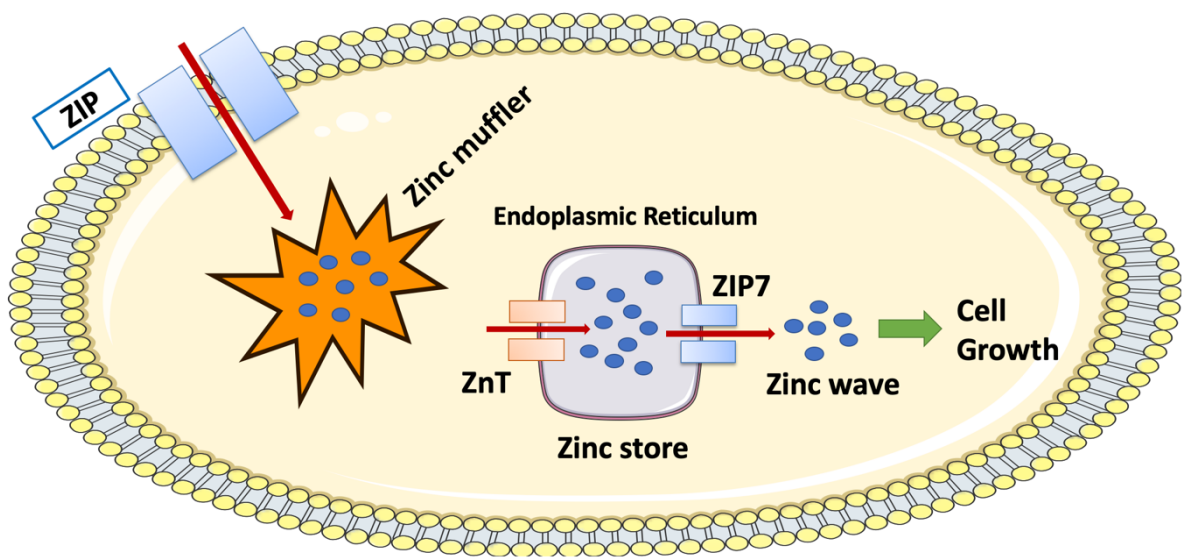


Figure 1.6 : Schematic showing ZIP7-mediated zinc handling in cells

ZIPs in the plasma membrane mediate zinc entrance into cells while is immediately buffered by metallothionein and glutathione in a zinc muffler. ZnTs are responsible for storing zinc in the ER/ Golgi. ZIP7 mediates zinc release in response to phosphorylation by protein kinase CK2, which generate “zinc wave” released from endoplasmic reticulum store^{63,74,75}. The released zinc ions promote the inhibition of multiple tyrosine phosphatases leading to cell proliferation and metastasis^{63,74,75}.

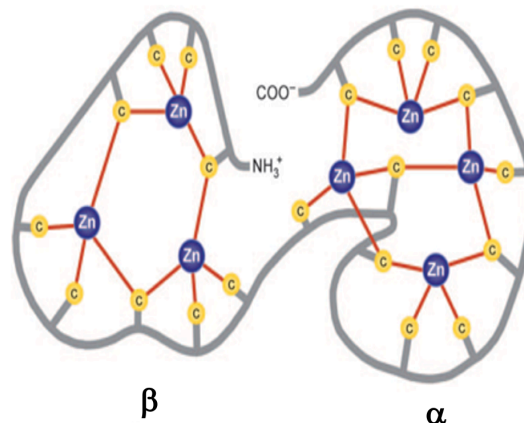


Figure 1.7: α and β clusters of metallothionein (MT).

The N terminal β cluster of metalothionein binds to three zinc atoms utilisis nine cysteins, while the C terminal α cluster binds to four zinc atoms utilising eleven cysteines. Source(B.Vallee and S.Bell, 2009)²⁸

1.7 ZIP Cellular Location and Phosphorylation Site:

ZIP transporters are responsible for increasing cytosolic zinc by promoting zinc transport from either the extracellular fluid or the lumen of the intracellular compartments into the cytosol¹⁷. Most ZIP transporters are located in the plasma membrane except for ZIP7 and ZIP13, which are found on the endoplasmic reticulum and Golgi membranes, respectively^{58,73}.

Zinc transporter ZIP7, also known as SLC39A7 (solute carrier family 39 zinc transporter member 7), contains eight transmembrane domains, with a more extended extracellular N termini domain than other types of ZIP family⁵⁸. ZIP7 has been reported on the membrane of the ER by using fluorescent microscopy^{58,73}. ZIP7 is proposed to be a gatekeeper for intracellular zinc release from the ER, named a “zinc wave” in response to phosphorylation by protein kinase 2 (CK2) at residues S275 and S276 in the histidine-rich intracytoplasmic loop between TM3 and TM4^{63,74,75}. This phosphorylation is activated approximately 2 minutes after exposure to extracellular stimulation such as zinc or epidermal growth factor (EGF)⁷⁵.

ZIP7-mediated zinc release from intracellular stores promotes the inhibition of multiple tyrosine phosphatases, which in turn prevents dephosphorylation of many receptor tyrosine kinases (RTK) such as Epidermal Growth Factor Receptor (EGFR), ErbB2, and Insulin-like Growth Factor Receptor 1 (IGF1-R), which are highly expressed and activated in cancer and play an essential role in the development of tamoxifen-resistant breast cancer⁶³. Downstream activation of receptor tyrosine kinases leads to activation of mitogen-activated protein kinases (MAPKs) and AKT (**Figure 1.8**)^{69,75}. Activation of these tyrosine kinases drives cell survival and proliferation^{63,74–76}. This mechanism explains how zinc was classified as a second messenger because extracellular stimulus resulting in release zinc within a few minutes, leading to activation of many downstream signalling pathways²⁵. CK2 inhibition has been shown to cause cell death in anti-estrogen resistance MCF7 cell line⁷⁷. In addition, CK2 inhibition has been shown to be a potential therapeutic target for different cancers such as glioblastoma, bladder cancer, and leukemia^{78–81}. Taken together, the data imply the critical role of downstream signalling pathways of the ZIP7

transporter in anti-hormone breast cancer, and the CK2 inhibitor is a promising target in resistance breast cancer-suffering patients.

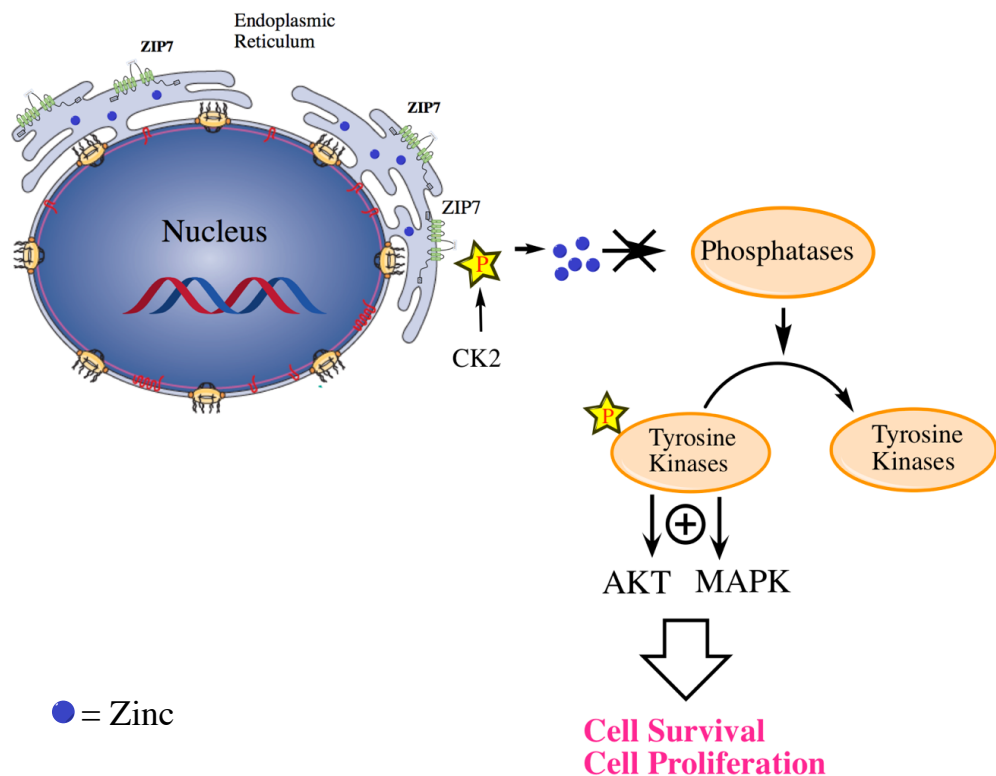


Figure 1.8: Downstream pathway of ZIP7 mediated zinc release.

Upon activation with an extracellular stimulus, protein kinase CK2 phosphorylates ZIP7 at residues S275 and S276 in the histidine-rich cytoplasmic loop between TM3 and TM4, resulting in zinc release from the endoplasmic reticulum as a “zinc wave”^{63,74,75}. The released zinc ions promote the inhibition of multiple tyrosine phosphatases, which in turn prevents dephosphorylation of many receptor tyrosine kinases (RTK), which leads to cell survival and proliferation^{63,74,75}

1.8 Nuclear Membrane:

The nuclear envelope (NE) is composed of two lipid bilayers: the inner nuclear membrane (INM) and the outer nuclear membrane (ONM), which are separated by a 30-50 nm perinuclear space (PNS)^{82,83} (**Figure 1.9**). The nuclear pore complex (NPCs), which serve as a transport hub and regulate the macromolecule trafficking across the nuclear envelope, is embedded in the nuclear membrane⁸². The Inner nuclear membrane (INM) faces the nucleoplasm, containing integral membrane proteins such as lamin B receptor, LEM domain-containing proteins (for lamina-associated protein 2 (Lap2)-emerin-MAN1), and SUN domain-containing proteins (for Sad-Unc-84 homology), which link the INM to

chromatin and nuclear lamina via their nucleoplasm domains⁸³⁻⁸⁵. The outer nuclear membrane (ONM) continuity with the rough endoplasmic reticulum^{83,84}. The integral membrane proteins bind to the nuclear lamina and connect the nuclear envelope to chromatin to maintain the nuclear envelope's structural integrity⁸⁵. In mitosis, the nuclear lamina, nucleoporin, and inner nuclear protein all undergo phosphorylation by mitotic kinases resulting in their depolymerisation and detachment from the nuclear envelope (NE), causing a breakdown of nuclear envelope^{85,86}.

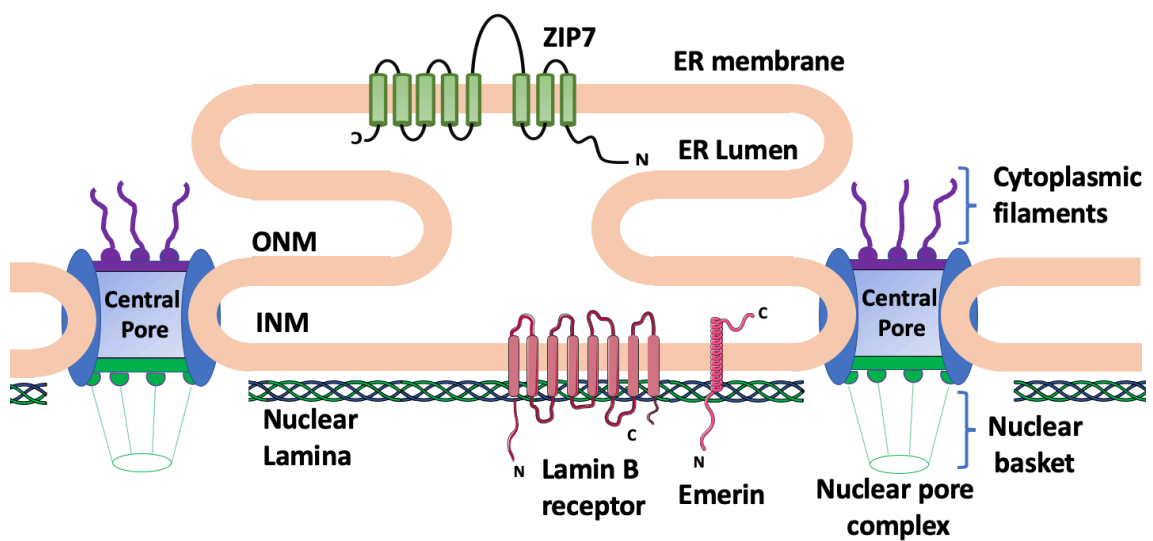


Figure 1.9: Schematic Showing Nuclear Envelop.

The nuclear envelop composed of two separated membrane: the inner nuclear membrane (INM) and the outer nuclear membrane (ONM) which fused at nuclear pore. The outer nuclear membrane (ONM) is continuous with endoplasmic reticulum. The inner nuclear membrane (INM) contains integral membrane proteins such as Lamin B receptor and emerlin.

The nuclear face of the inner nuclear membrane is covered by alpha-helical rod-shaped proteins called nuclear lamina⁸⁵ (**Figure 1.9**). The nuclear lamina is a nuclear intermediate filament protein composed of (B-type and A/C type) with ~10 to 20 nm diameter⁸⁷. This filament meshwork has a role in binding and supporting the inner nuclear membrane proteins and plays an essential role in sustaining the nuclear envelope structure, helping to protect the chromatin, and maintaining the normal cellular physiology⁸⁸. The endoplasmic

reticulum (ER) is the most abundant organelle in the cell and is responsible for various of cellular functions⁸⁹. The ER is an essential and primary site for integral proteins synthesis, protein folding, protein translocation, and protein post-translational modifications⁸⁹. Newly synthesized proteins are generated in the ER. Some proteins can be selectively retained in the INM by moving through the nuclear pore complex, and others translocate to the plasma membrane or Golgi⁸⁵. ZIP7 act as a gatekeeper to release zinc from the ER after phosphorylation by protein kinase CK2^{63,74,75}.

Nuclear pore complexes (NPCs) are an aqueous multi-subunit protein embedded throughout the nuclear envelope and connects the inner and outer nuclear membrane⁹⁰ (**Figure 1.9**). NPCs act as transport channels that control the nucleocytoplasmic trafficking of macromolecules such as proteins and RNA that affect gene expression, growth and proliferation, signalling, cell cycle control, and death^{84,91}. The nuclear pore complex is composed of 3 subunits: cytoplasmic filaments, a central core, and the nuclear basket⁹¹. Each nuclear pore complex contains multiple copies of approximately 30 proteins subunits termed nucleoporins (Nups)⁹², which weigh more than 60 megadaltons (MD) and play an essential role in NPC assembly and function^{93,94}. The NPC allows two types of pathways via its central channel or peripheral channel⁹⁵. Small metabolites, proteins, and ions that are smaller than 40 kDa can diffuse passively through the central channel of the nuclear pore with the assistance of nuclear transport receptors^{96,97}. However, larger molecules such as proteins and RNA molecules are actively transported and require specific targeting signals (nuclear localization sequences NLSs) to enter the nucleus through the central and peripheral channel of NPC⁸⁴. The active transport of cargo greater than 40 kDa needs soluble receptors known as karyopherin in yeast and importins and exportins in mammals that recognise nuclear localisation and export signals (NLSs and NESs), respectively. Karyopherin is a member of the importin β family that acts as transporter factors for shuttling macromolecules through the nuclear pore complex⁹⁸. Importin- α is an adapter molecule that recognises the nuclear localisation signals (NLS) part of the cargo to link it to the β -Karyopherins (importin- β), facilitating the nuclear internalisation through the central channel of the nuclear pore complex. Importin α and β must work together to dock protein through NPC efficiently⁹⁹.

1.7 Integral membrane protein targeting to the inner nuclear membrane:

A previous study has proposed that the integral INM proteins are synthesized in the ER¹⁰⁰. Then they diffuse through the peripheral channel of NPC to be retained in the inner membrane through interactions with nuclear components such as lamins and chromatin¹⁰⁰. Few studies showed that Lamin B receptors bind to the nuclear lamins via its long nucleoplasm NH2-terminal domain, keeping it INM^{101–103}. It is essential to understand the way of ZIP7 trafficking and its function in the nuclear membrane, which could play crucial roles in the nuclear zinc level resulting in cancer developments through activation of many transcription factors that have zinc finger domain. This project aims to determine the nuclear localization sequence of ZIP7 to address the ZIP7 translocation mechanism into the nucleus.

Studies have been shown that the nucleoplasm domains of nuclear proteins contain potential sorting signals called nuclear localization signals (NLS) which are necessary and sufficient short stretches of basic amino acids (lysine-rich) to destine those proteins to the nucleus¹⁰⁴. The classical or the importin α/β pathways which mediate through the recognition of nuclear localization sequences (NLSs) by an adaptor protein called importin- α (karyopherin- α) to form a trimeric complex composed of NLS-protein/Imp- α .Imp- β ¹⁰⁵. Importin- α recognizes and binds to NLS¹⁰⁵. Importin- β translocate the complex through interaction with the FXFG domain of nucleoporin in the nuclear side of the nuclear pore through its FXFG domain binding site¹⁰⁵. The classical NLS could be monopartite or bipartite. The monopartite NLSs contain a single cluster of 4-6 positively charged amino acids (arginine or lysine) in a formula of K-R/K-X-R/K or four consecutive basic amino acids like in Simian virus 40 (SV40) large tumour antigen NLS (¹²⁶PKKKRRV¹³²)¹⁰⁶. Substitution of the critical residue Lys 128 (K¹²⁸) with Asparagine (N)¹⁰⁷ or threonine (T)¹⁰⁸ leads to stopping the function of NLS, resulting in accumulating the protein in the cytoplasm rather than nucleus¹⁰⁹. Bipartite NLSs have two stretches of basic amino acids separated by 10-12 amino acid linker exemplified by the *Xenopus* phosphoprotein nucleoplasmin (¹⁵⁰KRPAATKKAGQAKKKKLDK¹⁷⁰)⁸, which was characterized more than 20 years ago¹¹⁰. Nucleoplasmin is the most abundant protein in the nucleus of *Xenopus* oocyte¹¹¹. It participates in a wide variety of essential cellular activities, and one

of them is nucleosome assembly¹¹². Nucleoplasmin is an acidic factor that binds to histone H2A and H2B and transfer them to DNA to form nucleosome¹¹². A recent study has discovered novel tripartite NLSs consisting of three basic amino acid clusters (⁶⁴⁵RRRHIVRKRTLRR⁶⁵⁷) in the juxtamembrane region of EGFR, and mutation in any of these basic amino acids affected the nuclear localization of EGFR¹¹³.

1.9 Role of Zinc in Oncogenesis:

Zinc has been shown to inhibit protein tyrosine phosphatases¹¹⁴, resulting in inhibiting the dephosphorylation of many tyrosine kinase receptors, which are overexpressed in cancer⁶⁹. Moreover, zinc activates EGF receptor and MAPK molecules, which both have an essential role in breast cancer¹¹⁵. Matrix metalloproteases (MMPs) are proteins responsible for tissue matrix degradation surrounding the cells and allowing the cancer cells to spread from the original cancer (metastatic). Zinc has been shown to have a role in regulating the function of MMP as it is a zinc-binding motif¹¹⁶. This highlights the role of zinc in cancer development and progression.

Breast cancer is one of the most common cancers among women, and it is the primary cause of mortality in females around the worlds¹¹⁷. According to the World Health Organization (WHO), the early detection of breast cancer improves the outcome and survival of the patients. The women with breast cancer are treated with a combination of surgery, chemotherapy, and radiotherapy¹¹⁸. However, making the treatment more personalized will decrease the side effect and improve the overall survival rates.

Breast cancers are different compared to each other due to their receptor status and gene expression¹¹⁹. Breast cancer has three immunohistochemical biomarkers, which are: PR (progesterone receptor), oestrogen receptor and HER2 (human epidermal growth factor receptor 2)¹²⁰. Doing biomarker analysis to know the hormone receptor status in breast cancer patients is necessary to establish the proper therapy. Also, knowing histologic grade, lymph vascular spread, and patient age is important¹²¹. In general, 70-75% of invasive breast carcinomas express oestrogen receptor, and these breast cancers depend on oestrogen signalling for their growth and survival^{120,122}. Patients with breast cancer express estrogen receptor responded well to the endocrine therapy¹²³. Oestrogens have an essential

role in the growth and development of breast cancer by their direct inhibitory effect on the apoptotic machinery in breast cancer cells^{124,125}. Oestrogen receptor positive breast cancer patients are treated with selective estrogen receptor modulators (SERMs), such as tamoxifen to prevent cell proliferation and induce cell death^{126,127} or with the aromatase inhibitor, such as anastrozole, exemestane and letrozole to prevent oestrogen production^{128,129}. Tamoxifen is used as the first line of endocrine therapy, and it acts as a partial oestrogen receptor agonist¹³⁰. Fulvestrant (Faslodex®) is also used in endocrine therapy. It is an oestrogen receptor antagonist that prevents oestradiol binding to the oestrogen receptor^{130,131}. Fulvestrant is a valuable second-line treatment in patients who developed tamoxifen resistance¹³⁰. HER2 is the most important prognostic and predictive marker as it is overexpressed in the aggressive type of breast cancer¹³². Trastuzumab, lapatinib, and pertuzumab are mainly used to treat HER2 positive breast cancer¹²⁰.

Unfortunately, most patients treated with anti-oestrogen therapy develop resistance¹³³, which allows the cancer regrowth and progression and highlights the importance of developing new potential targets. Our lab has generated a unique antihormonal resistance cell line to tamoxifen¹³⁴ and Faslodex®¹³⁵ to understand their aggressive behaviour mechanism better. Tamoxifen resistance cell line has been shown to have a high zinc level⁶⁹ and high ZIP7 gene expression⁵⁷. Knockdown of ZIP7 inhibits the activation of epidermal growth factor receptor (EGFR) and insulin-like growth factor receptor (IGF-1R)⁶⁹ both known to drive the growth of TamR cell line¹³⁶. Zinc level is significantly increased in tumour areas with oestrogen-receptor positive compared to oestrogen-receptor negative area¹³⁷, suggesting that zinc could have a role in regulating oestrogen in breast tissue. Also, zinc concentration in breast cancer was found to correlate to the histological malignancy grade, suggesting that zinc could be a potential marker for breast cancer¹³⁸.

Many studies have shown that intracellular zinc homeostasis is altered in cancer cells, which could be explained by changes in the expression of zinc transporters, especially the ZIP family members¹³⁹. Higher zinc level is associated with breast cancer progression¹⁴⁰ and malignancy¹⁴¹. Zinc may trigger cancer development by a direct regulatory role on gene expression and/or cell survival or indirectly affecting the activity, function, and/or survival of immune cells that attack tumour cells²⁷. The zinc level in breast and lung cancer patients is significantly elevated compared to normal human tissue using atomic emission

spectroscopy and mass spectrometry¹⁴². Also, the N-methyl-N-nitrosourea (MNU)-induced rat mammary tumorigenesis model has shown the zinc level to be 12 fold higher in a mammary tumour than a healthy mammary glands¹⁴³. Several studies have been shown that the level of zinc in tumour breast tissues is higher than normal breast tissue^{144,145}.

Measuring the serum zinc level in patients with breast cancers was very low compared to healthy person¹⁴⁵⁻¹⁴⁷, while other study observed that the serum zinc level in patients with breast cancer is increase¹⁴⁸ and other study showed no changes in serum zinc level¹⁴⁹. In addition, measuring the zinc level in the hair showed that the zinc level is decreased compared to healthy person¹⁵⁰ or no change in hair zinc level¹⁴⁹. Another study confirmed the relationship between low serum and hair zinc levels and the risk of breast cancer¹⁴⁴. Further study showed the association between serum zinc and breast cancer as the serum zinc in patients with breast cancer has not changed, but their hair zinc level is low¹⁵⁰. A meta-analysis study showed that serum zinc is low in most cancers type¹⁴⁵. Interestingly, measuring the zinc level from breast cancer tumours showed a significantly high level compared to normal breast tissue^{141,142,150}. Those results are also confirmed in the N-methyl-N-Nitrosourea (MNU) rat model, where the zinc concentration in the mammary tumour was observed to be a 19 fold increase compared to normal mammary tissue¹⁵¹. Another study has supported this data showed a 12 fold increase in zinc level in mammary tumours of MNU rat model compared to normal mammary tissue¹⁵². It is worth noting that zinc has a high ability to bind to albumin in the blood, which could be one reason why zinc is lower in serum¹⁵³. Zinc is well known to associate cell cycle progression as G1, and G2 phases depend on zinc³⁴. So, another reason why serum zinc is lower compared to tumour zinc level, that the cancer cells may need more zinc during their uncontrolled growth, and this cause a decrease in zinc from plasma. So many factors have been shown to affect the serum zinc level, either physiological or pathological²⁰. That suggests that measuring the zinc level directly from breast tumour tissue is more accurate to determine zinc content. Knowing that the zinc level is high in breast tumour tissue, especially the aggressive type, suggest that zinc have a role in breast cancer. So, by further investigating the exact role of zinc and downstream pathways in breast cancer, we could discover a new therapeutic target.

1.10 Zinc Transporters and Cancer

It is clear from the studies above that zinc has a significant role in cancer, and its level is different in each cancer type. It is essential to examine the mechanism of action of zinc in cancer to know the appropriate clinical target. It is complicated to study zinc itself. To overcome this issue, the research has begun to explore the zinc transporter's location and expression to know how they alter zinc status. Alteration in the expression levels of ZIP transporters and malfunction of intracellular zinc homeostasis can contribute to the onset and severity of various cancers^{49,154}.

ZIP1, ZIP2, and ZIP3 have been reported to be downregulated in prostate cancer¹⁵⁵. As a result of the dysregulation of those ZIP transporters, the zinc level is very low in prostate cancer compared to normal prostate tissue¹⁵⁶. ZIP6 is the first member of the LIV-1 subfamily overexpressed in breast cancer¹⁵⁷. ZIP7, ZIP6 and ZIP10 are reported to be overexpressed in breast cancer and associated with metastasis of cancers to the lymph nodes^{50,158,159}. The expression of ZIP4 has been reported to be five times higher in pancreatic cancer than in normal tissue, contributing to higher proliferation, migration, and progression¹⁶⁰. ZIP4 increases IL-6, which activates STAT3 and leads to increased cell proliferation by increasing cyclinD1¹⁶¹. ZIP4 silencing in different pancreatic cancer cell lines decreased the cell migration and proliferation¹⁶⁰. ZIP4 also has been implicated in the zinc level of hepatocellular carcinoma¹⁶². Zinc level has been shown to significantly decrease in hepatocellular cancer resulting from the downregulation in the expression of ZIP4¹⁶³ and ZIP14¹⁶³. ZIP14 expression also is used as a potential biomarker¹⁶⁴ or a therapeutic target in colorectal cancer¹⁶⁵.

Those evidence showed the sequences of zinc transporter dysregulation in cancer. Most zinc transporters are upregulating in cancer, which suggests the need for zinc in cell proliferation and metabolism. Knowing the mechanism of ZIP transporters and zinc signalling in different carcinomas will open the door to potential clinical biomarkers and/or treatments for a wide variety of cancers.

1.11 ZIP7 and breast cancer:

ZIP7 plays an essential role in regulating zinc release from the intracellular store, resulting in the activation of tyrosine kinases that are required for cell growth and migration⁶³. ZIP7 has been reported to be overexpressed in tamoxifen-resistant (TamR) breast cancers leading to an increase in tumour cell invasion and growth^{63,69}. The intracellular zinc level in TamR is double compared to MCF7 breast cancer cells⁶⁹, which suggests that zinc level is higher in the aggressive form of diseases. Zinc level has been reported to be a useful biomarker for breast cancer, and its concentration correlates to the histological malignancy grade¹³⁸.

ZIP7-mediated zinc release in the form of a zinc wave caused activation of ErbB2, EGFR, IGFI-R, Src, Map Kinase and serine/threonine protein-kinase, which are highly expressed in breast cancer and have been contributing to tumour cell proliferation, invasion and growth rate^{63,69}. This effect was eliminated when ZIP7 was removed using small interfering RNA technology (siRNA)⁶⁹. Also, recently ZIP7 knockdown shown to inhibit cell growth and induce apoptosis in human colorectal cancer cells¹⁶⁶. The growth of the Tamoxifen-resistant (TamR) breast cancer cell line mainly relies on the EGFR/MAPK pathway, which is a potential therapeutic target for antihormone-resistant tumors^{64,134}. A recent study developed an immunostaining test that detected pZIP7 in breast cancer clinical samples and showed a higher pZIP7 level in antihormonal resistance samples, especially tamoxifen resistance¹⁶⁷. This evidence suggests that the phosphorylated ZIP7 could be a potential biomarker in the aggressive type of cancer cells and could be a targeted therapy.

1.12 Hypotheses, aims and objectives of this project

Our group were the first to discover that ZIP7, located on the endoplasmic reticulum, is the hub of zinc release from stores within cells^{57,63,158}. ZIP7 needs phosphorylation by CK2 on residues S275 and S276 to release zinc from ER store, which activates PI3K, AKT, mTOR, MAPK, and other important signalling pathways known to drive cancer progression⁷⁴. Knowing the importance of phosphorylation in the regulation of ZIP transporters, this project further investigates the new potential phosphorylation sites of ZIP7, which will help us understand how ZIP7 is activated and regulated. A recent study in our group demonstrated that ZIP7 expression is elevated in anti-hormone resistance breast cancer, suggesting the importance of ZIP7-mediated zinc release in driving the growth of these cells¹⁶⁷. Knowing the role of ZIP transporters and zinc in the progression of many carcinomas¹⁶⁸, especially breast cancer, highlights the potential therapeutic zinc signalling target treatment. So, this project expanded the previous work in our group to assess the role of ZIP7-mediated signalling in driving the growth of different cancer, which will provide new cancer targets. Probing for ZIP7 in cells showed ZIP7 location on the ER, and it always appears to be located on the nuclear membrane. This is the first time any zinc transporter has been found around the nucleus, which could have a role in transporting the zinc to the nucleus that is essential for gene transcription, especially in cancer. This project is to investigate the nuclear localization of ZIP7 further and determine whether it has a critical role in cancer development.

1.12.1 Hypothesis

The hypotheses of the current project are:

1. Gate release from ZIP7 is influenced by phosphorylation sites additional to those previously.
2. ZIP7 levels are increased in different cancers.
3. ZIP7 is located in the inner nuclear membrane resulting in the activation of nuclear pathways leading to cancer development.

1.12.2 Aims and objectives:

The aims for this project were:

Aim 1: To predict phosphorylation motifs within the LIV-1 subfamily that contribute to gated release, and to investigate the expression level of ZIP7 in different cancers.

Objectives for Aim 1

- a. Informatic and metadata analysis were used to investigate the amino acid sequences of the LIV-1 subfamily to enable comparison between family members.
- b. Search for any predicted phosphorylation sites of ZIP7 using multiple online database sites to investigate whether S275 and S276 were the only functional sites in ZIP7.
- c. Identify ZIP7 localization motifs such as for the endoplasmic reticulum and nucleus using different online prediction databases.

Aim 2: Investigate the potential role for ZIP7 in breast cancer progression.

Objectives for Aim 2

- a. Gene expression and survival analysis web tools were used to investigate ZIP7 gene expression in different cancers and to document the role of ZIP7 in breast cancer survival outcome.

Aim 3: Confirm the nuclear localization of ZIP7 and investigate the mechanism of the nuclear translocation.

Objectives for Aim 3

- a. Determine the nuclear localization of ZIP7 and pZIP7 by colocalization analysis using inner nuclear membrane markers and high-resolution microscopy.
- b. Generate ZIP7 mutants lacking the potential nuclear targeting signals and investigate their effect on cellular location and function.
- c. Use phospho-kinase arrays to examine changes to the ZIP7 downstream pathways according to cellular location of ZIP7 that may lead to cancer progression.

2. Chapter 2: Materials and Methods

2.1 Cell Preparation and Treatment

2.1.1 Cell Culture

MCF-7 (human breast carcinoma) cells were grown in Roswell Park Memorial Institute (RPMI) medium (Gibco, UK) that was supplemented with 5% foetal bovine serum (FBS), 200mM L-glutamine, antibiotics (10 IU/mL Penicillin, 10 µg/mL Streptomycin), and fungizone (2.5 µg/mL Amphotericin B) (Gibco) and incubated at 37°C with 5% CO₂. The medium was changed every three to four days. For experiments, cells in a T25 flask were trypsinised when they reached 90% confluence by using 5 mL of trypsin for 3-5 minutes at 37°C or until cells were in suspension. Then, cells suspension was neutralised using an equal amount of medium with serum. After re-suspending the cell pellet in medium with serum, 100 µL of the cell suspension was added to 10 mL Isoton II balanced electrolyte solution (Beckman Coulter). The number of cells present was determined using a Coulter counter (Beckman Coulter) at least twice, and 1-3x10⁵ cells were seeded into 35 mm dishes with 22x22 mm ultra-thin glass coverslips (0.17 mm thick) for immunofluorescence or without coverslips for western blotting.

2.1.2 Transfection

MCF-7 cells at 60 -90 % confluence were transfected with plasmid DNAs of wild-type ZIP7 or mutant constructs by using Lipofectamine-3000 transfection reagent (Invitrogen). The C-terminal of the recombinant DNA contained a V5 tag which allowed visualisation with a V5 antibody by immunofluorescence. 4µg of plasmid DNA was diluted in a 188 µL serum-free phenol-red-free RPMI medium (Gibco). Likewise, 7.5 µL Lipofectamine 3000 was diluted in a 188 µL serum-free phenol-red-free RPMI medium (Gibco). Subsequently, the plasmid DNA and Lipofectamine 3000 was mixed within 5 minutes. Then the mixture was further incubated at room temperature for at least 20 minutes, while the medium in each dish was replaced with 1015 µL medium with serum. After 20 minutes of incubation, 380 µL of Lipofectamine and DNA mixture was added to the cells. The cells were incubated in the transfection mixture at 37°C for 18 hours before being harvested with or without zinc treatment.

2.1.3 Zinc Treatment

The transfected MCF-7 cells were treated with 20 μ M zinc in the presence of 10 μ M sodium pyrithione (zinc ionophore) in phenol–red–free RPMI medium with glutamine, but without serum at 37°C, before being fixed for immunofluorescence, or lysed for protein assay.

2.2 Site-directed mutagenesis

Site-directed mutagenesis was performed by Mutagenex Inc. to generate mutant ZIP7 constructs. The DNA of wild type ZIP7 and mutant constructs was inserted into the ampicillin-resistant plasmid vector, which has a V5 tag at the carboxyl-terminus. The mutations were confirmed by DNA sequencing (**Figure 2.1, 2.2, and 2.3**). In the phospho-null mutants (inactive mutant), the serine residues were mutated to alanine (**Table 2.1**). The alanine contains a methyl group (-CH₃) in the lateral chair which prevents its phosphorylation. However, the serine contains a hydroxyl (-OH) group which are often phosphorylated. While the phospho-mimetic mutants (constitutively active mutant), the serine mutated to aspartate. In the endoplasmic retention signals, ZIP7 mutants and nuclear localization signals ZIP7 mutants, all the basic residues were mutated to alanine. ZIP7 mutants that have been used in this project are listed in **Table 2.1**.

Table 2.1 DNA sequences of ZIP7 mutants used in this project

Construct	Wild-type DNA sequence	Mutant DNA sequence
ZIP7 S275A S276A	CAG AGCTCAGAG	CAG gCgCAGAG
ZIP7 S275D S276D	CAG AGCTCAGAG	CAG gaCgacGAG
ZIP7 S293A	GGAGGG AGC ACAGTA	GGAGGG gC ACAGTA
ZIP7 T294A	GGAGGGAG C ACAGTA	GGAGGGAG gC AGTA
ER1A	TCT CCCCGGCATCGCTCT	TCT gCCgCgCgTgcCTCT
ER1B	CCCCGGCATCGCTCT	CCgCgCgTgcCTCT
ER2	AG ACATGTGAAAGGA	AG gCgTGCgCgCAGGA
ER3	ACC AAGGAGAAGCAG	ACC gCgCgCgCAG
ER4	TGC AGCAAAAAGCAG	TGC gCgCgCgCAG
NLS1	CAG AAGAGGCGAGGA	CAG gCgCgCgCAGGA
NLS2	AG AAAAAAGAGGC	GA gCgCgCAGGC
NLS3	NLS1 and NLS2 in the same sequence	

The letters in bold represents the DNA bases of the wild type ZIP7 sequence that were mutated by site-directed mutagenesis. The mutated bases are indicated on the right by lower case letters in bold.

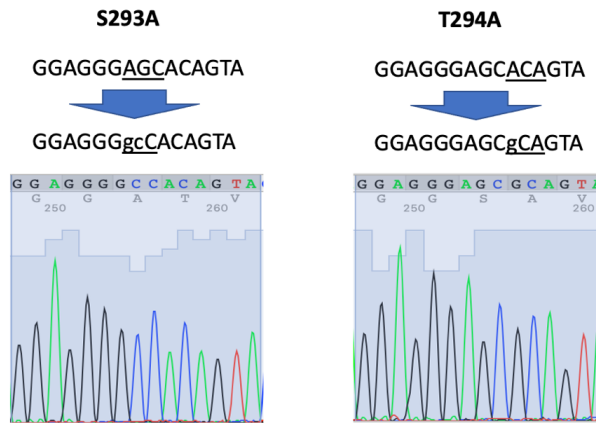


Figure 2.1 DNA sequences of ZIP7 S293A and T294A mutants.

The schematic shows that underlined individual serine (codon AGC) or threonine (codon ACA) at the predicted nuclear localization signals in WT-ZIP7 were successfully mutated to alanine (codons GCC, GCA).

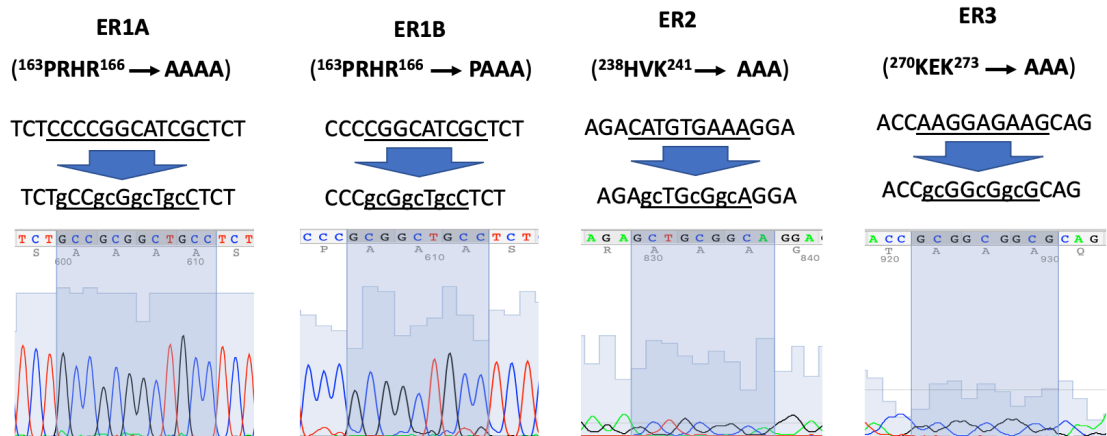


Figure 2.2: DNA sequencing of ZIP7 ER retention signals of ZIP7.

The schematic shows that underlined individual lysine (codons AAG, AAA) or arginine (codons CGG, CGC, AGG, CGA, AGA) or histadine (codon CAT) at the predicted endoplasmic retention signals in WT-ZIP7 were successfully mutated to alanine (codons GCG, GCA).

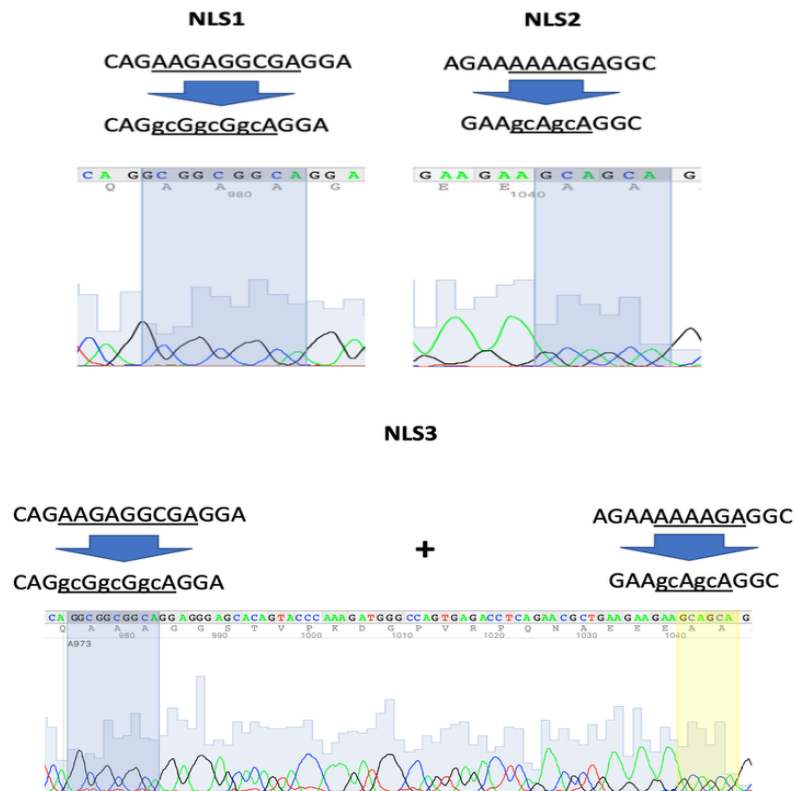


Figure 2.3 DNA sequencing of ZIP7 NLS mutants.

The schematic shows that underlined individual lysine (codons AAG, AAA) or arginine (codons AGG, CGA, AGA) at the predicted nuclear localization signals in WT-ZIP7 were successfully mutated to alanine (codons GCG, GCA).

2.3 Plasmid Preparation:

The transformation was performed by inserting recombinant WT ZIP7 or mutant ZIP7 DNA constructs containing a C-terminal V5 tag into an ampicillin-resistant cDNA3.1/V5-His-TOPO plasmid vector and amplified by transformation in JM-109 *E. coli* competent cells. The instructions from EndoFree Plasmid Maxi Kit (Qiagen) protocol were followed for DNA purification. Briefly, to grow the colony, bacteria were plated on 15 mL agar plates containing 30 μ L (100 μ g/mL) ampicillin (1:500) overnight at 37°C. The next day, a single colony was selected and placed in 5 mL Luria-Bertani (LB) medium with 100 μ g/mL ampicillin (1:500) and placed in a shaker 200 rpm at 37°C for 8 hours of vigorous shaking. The starter culture was diluted 1/500 into 150 ml LB medium containing 100

$\mu\text{g/ml}$ ampicillin and further cultured with vigorous shaking for 8 hours at 37 °C. Bacterial cells were harvested by centrifugation at 6500 rpm at 4 °C for 15 minutes and the bacterial pellet was resuspended in 10 ml Buffer P1, containing 100 $\mu\text{g/mL}$ RNase and 1x lyseBlue. Then 10 mL of Buffer P2 was added to the cells and incubated at room temperature for 5 minutes. To enhance precipitation of lysate, 10 mL of chilled Buffer P3 was added and cleared by filtration using a QIAfilter Cartridge. Then, 2.5 mL of Buffer ER was added to the filtrated lysate and incubated for 30 minutes on ice to remove the endotoxin. QIAGEN -tips were used to purify the plasmid DNA and DNA was eluted with 15 mL buffer QN. The resulting DNA was precipitated by 10.5 mL isopropanol and centrifuged for 30 minutes. The pellet was washed with 5 mL endotoxin-free 70% ethanol and left to air dry for 10 minutes. Finally, the DNA was dissolved in 300 μL of endotoxin-free Buffer TE. DNA concentration and purity were determined by UV spectrophotometry at 260 nm (OD260).

2.4 Immunofluorescence:

The cells were 70-80% confluence on the coverslips when harvested for the best imaging results using fluorescence microscopy. Before harvesting, some of the coverslips were treated with zinc at different time points, as described in section 2.1.3. The coverslips were loaded into a rack to fixing with 3.7 % formaldehyde (Sigma Aldrich) for 15 minutes, then washed in Phosphate Buffered Saline (PBS) twice for 5 minutes each time. The fixing step was necessary to preserve the structure of the cells and to immobilise antigens. In the meantime, the dishes were washed three times with permeabilisation buffer to remove all the medium in which the cells had been seeded. The cells were then permeabilised using permeabilisation buffer with 1% bovine serum albumin (BSA) (Sigma Aldrich) to block the non-specific binding sites of the antibodies, and 0.4% saponin (Sigma Aldrich) made up in PBS for 15 minutes. Saponin is a detergent to permeabilise the cell membrane allowing the primary antibodies to detect the antigens inside the cells. The coverslips were then blocked with 10% normal goat serum (DAKO, UK) made up in permeabilisation buffer for 15 minutes to block the non-specific binding of the secondary antibodies. After that, the cells were incubated with the two primary antibodies (**Table 2.2**); one mouse and one rabbit, to detect two different antigens at the same time, for at least 1 hour in a moisture chamber followed by washing three times with permeabilisation buffer. After washing, the cells were incubated with fluorescent secondary antibodies (**Table 2.3**), usually a

combination of anti-rabbit Alexa Fluor-488 (green) and anti-mouse Alexa fluor-594 (red) (Molecular Probes, Invitrogen, USA) for 30 mins, with light protection. After the secondary antibody, Alexa Fluor-488 phalloidin (green) (1:5) was added for 20 minutes. In Mito-tracker experiments, 100 nM MitoTracker™ Red CMXRos (M7512, Invitrogen™) in medium without serum was added for 30 minutes at 37°C, followed by a 30-minute recovery in the dye-free medium at 37°C. The coverslip was mounted on a microscope slide with VECTASHIELD Mounting Media (Vector Laboratories, USA) containing 1.5 µg/mL 4,6-diamidino-2-phenylindole (DAPI) and sealed with nail varnish. DAPI is a fluorescent dye that binds to nucleus DNA (blue). The stained slides were visualised on a Leica RPE automatic microscope using a 63x oil immersion lens with a multiple bandpass filter for DAPI, Texas Red and fluorescein. Images were acquired using Openlab modular imaging software for Macintosh operating system with one-level deconvolution. Brightness and contrast adjustments were performed using Fiji Image J. The coverslips were also evaluated with a Zeiss LSM 880 with Airyscan Microscope, using a 63x Zeiss oil immersion lens and Zeiss's ZEN software for the Microsoft Operating system. Images were processed using ImageJ. The 'RGB profiler' plugin from ImageJ was used to plot co-localisation.

Table 2.2: Primary Antibodies

Antibody	Supplier	Species	Dilution	
			IF	WB
V5	Abcam (Ab15828)	Rabbit	1:1000	1:1000
V5	Invitrogen (R960-25)	Mouse	1:1000	-
tZIP7	ProteinTech (19429-1-AP)	Rabbit	-	1:1000
pZIP7 ¹ (TKEKQ-pS ²⁷⁵ -pS ²⁷⁶ -EEEEK)	In house	Mouse	1:100	1:1000
NUP98	CST (C39A3)	Rabbit	1:50	-
Lamin A/C	CST (4C11)	Mouse	1:100	-
Lamin B	CST (D8P3U)	Rabbit	1:50	-
Lamin B Receptor	Abcam (Ab32535)	Rabbit	1:50	-
Protein disulfide isomerase (PDI)	CST (C81H6)	Rabbit	1:100	-
Emerin	Abcam (Ab204987)	Mouse	1:50	-
pAKT (S473)	CST (9271)	Rabbit	-	1:1000
pAKT (S473)	CST (4051)	Mouse	-	1:1000
GAPDH–peroxidase	CST (SC32233)	Mouse	-	1:50000
p44/42 MAPK (ERK1/2)	CST (9102)	Rabbit	-	1:1000
p-GSK-3 α/β (S21/9)	CST (9331)	Rabbit	-	1:1000
P70S6 Kinase (T389)	CST (9234)	Rabbit	-	1:1000
P70S6 Kinase (T421/S424)	CST (9204)	Rabbit	-	1:1000

The table indicates the supplies, species, and dilution at which antibody was used in this project. ¹ **pZIP7 (S275/S276)**. The epitope is TKEKQ pS pS EEEEEK (residues 270–281, in the cytoplasmic loop between TM3 and TM4). **IF**, immunofluorescence; **WB**, Western blot; **CST**, Cell Signalling Technologies.

Table 2.3: Secondary Antibodies

Antibody	Supplier	Species	Dilution	
			IF	WB
Alexa Fluor 488	Invitrogen (A11034)	Goat anti-Rabbit	1/1000	-
Alexa Fluor 488	Invitrogen (A10684)	Goat anti-mouse	1:1000	-
Alexa Fluor 594	Invitrogen (A11032)	Goat anti-mouse	1/1000	-
Alexa Fluor 594	Invitrogen (A11072)	Goat anti-rabbit	1:1000	-
HRP-linked IgG	Fisher (10094724)	Goat anti-mouse	-	1:10000
HRP-linked IgG	CST (7074)	Goat anti-rabbit	-	1:10000
Alexa Four 488 phalloidin	CST(A12379)	-	1:5	-

The table indicates the supplies, species, and dilution at which antibody was used in this project. **IF**, immunofluorescence; **WB**, Western blot; **CST**, Cell Signalling Technologies.

2.5 Western Blot

2.5.1 Cell lysis and protein assay

For western blot, the cells were grown in 35 mm dishes until they reached 80-90% confluence. After transfection with wild type or mutant ZIP7 constructs, the cells were treated with zinc at different time points as described in section 2.1.3. The medium was removed with an aspirator, and the cells were washed three times with 100 mL ice-cold PBS to stop the temperature-dependent zinc signalling cascades. The cells were harvested with 100 mL pre-prepared lysis buffer (**Appendix**). 50 mL of protease cocktail inhibitor (Sigma) was added to the lysis buffer just before use. After scraping, the cells were harvested into cold Eppendorf tubes on ice and left for at least one hour to release the proteins of interest from membranes. Next, the cells were centrifuged at 12,000 rpm (13684 x g) at 4°C for 12 minutes. The pellet was discarded, and the supernatant was transferred to clean Eppendorf tubes. The protein concentration of the lysate was determined using a BioRad Microassay procedure, and the absorbance was measured at 595nm. The samples were diluted with laemmli buffer (loading buffer) containing 0.2 M Dithiothreitol (DTT) (Roche;10708984001) and bromophenol blue (Merch;108122) (**Appendix**), to make a final concentration of 1 µg/µL. Then, the protein was denatured by

heating at 100°C for 5 minutes and then centrifuged briefly (~ 20 seconds) at 12,000 rpm to deposit the condensate formed during heating.

2.5.2 Polyacrylamide Gel Electrophoresis–Sodium Dodecyl Sulphate (SDS–PAGE) and Immunoblotting

SDS–PAGE was used to separate proteins according to their molecular weight. The concentration of resolving gels used in this project was either 7.5% or 10% with either a 10 or 15 well comb, depending on the size of the protein of interest, and the number of samples being tested (Table 2.4 and 2.5).

Table 2.4 Recipe of stacking gel

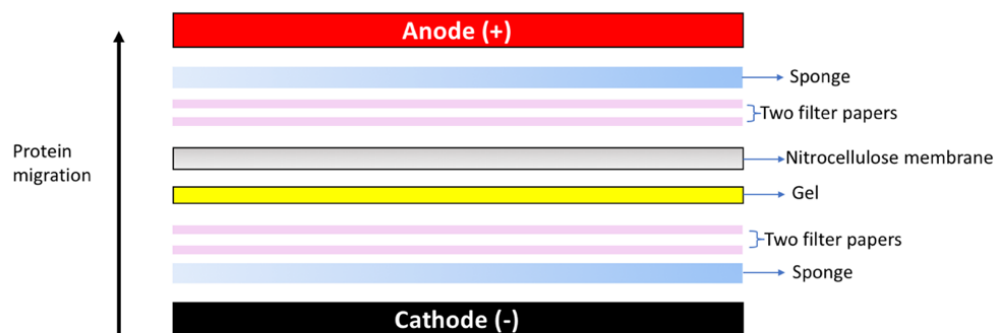
Reagent (stacking gel)	units	5% (3 x 1.5 mm gel)
Distilled H ₂ O	ml	6.1
TRIS-HCl buffer, pH 6.8	ml	2.5
30% Acrylamide	ml	1.3
10% Sodium dodecylsulfate (SDS)	μl	100
10% Ammonium persulfate (APS)	μl	50
Tetramethylethylenediamine (TEMED)	μl	10

Table 2.5 recipe of resolving gel

Reagent (resolving gel)	units	7.50%	10%
Distilled H ₂ O	ml	9.6	8
TRIS-HCl buffer, pH 8.8	ml	5	5
30% Acrylamide	ml	5	9.52
10% Sodium dodecylsulfate (SDS)	μl	200	200
10% Ammonium persulfate (APS)	μl	200	200
Tetramethylethylenediamine (TEMED)	μl	12	12

Casting stand assembly was set up to prepare the gel with 1.5 mm thickness. The resolving gel mixture was prepared and mixed gently then poured immediately by using 5 mL pipette between the two plates. After that, the gels were immediately overlay with 200 μ L isopropyl alcohol to get a sharp interface between the resolving gel and stacking gel. The gel was left to polymerise for at least 30 minutes. After 30 minutes, the isopropyl alcohol was poured away, and the stacking gel was made as described above and poured onto the resolving gel. The desired comb was inserted between the spacers at the top of the spacer plate immediately after pouring the stacking gel, which was left to polymerize for at least 30 minutes. The gel cassette sandwich was placed into the Electrode Assembly with the short plate facing inward. 20 μ g of each sample were loaded into the wells and 3 μ L of ladder. The cassette was filled with 1x running buffer (**Appendix**). The proteins in the samples were separated by SDS-PAGE at 120 V for 90 minutes. After the electrophoresis was completed, the gel, nitrocellulose membrane (GE Life Science; 1060002), filter papers, and sponge were soaked in transfer buffer (**Appendix**) and then the “sandwich” (**Figure 2.4**) was made according to the following schematic:

Figure 2.4: Schematic representation of "sandwich" gel and membrane setup for electrophoretic protein transfer.



The sandwich was added in a blotting cassette in a Trans-Blot Module with an ice pack to prevent overheating and a magnetic stirring bar in the bottom to maintain uniform buffer temperature and ion distribution in the tank. The transfer of proteins onto the nitrocellulose membrane was performed at 100 V for 60 minutes. The proteins on the membrane were reversibly stained with 0.1% (w/v) Ponceau S (Sigma) in 5% acetic acid to check that the

transfer was successful and that each lane was evenly loaded. Then, the membrane was washed with 1x Tris-buffered saline containing 0.05% Tween-20 (TBST) three times to remove the Ponceau S staining. The non-specific proteins were blocked with 5% non-fat dried milk (Marvel) in TBST for 1 hour at room temperature, followed by a 30-minute wash in 1x TBST (**Appendix**). The membrane was incubated in 5mL primary antibodies overnight at 4°C on a roller-bed. The primary antibody solution was made with TBST 1X containing 1 mM sodium azide (NaN₃), 5% Western Blocking reagent (Roche), and the primary antibody at the required concentration (**Table 2.2**). The following day, the membrane was washed for 15 minutes with TBST at room temperature and then incubated with horseradish-peroxidase (HRP)-labelled goat secondary antibodies (**Table 2.3**) at room temperature for 1 hour on a roller-bed. The secondary antibody solution was made up with 1% Marvel in TBST 1X. Following a further 30-minute wash, Pierce® ECL Western Blotting Substrate (Thermo Scientific;), Clarity™ Western ECL Substrate (BioRad;), or SuperSignal® West Femto Maximum Sensitivity Substrate (Thermo Scientific) chemiluminescent substrates were used to detect the densities of protein bands on the blot. To visualize the protein bands, the blot was exposed to X-ray film in a dark room or G:BOX system were used. The densitometry data were acquired using Fiji Image J and analyzed using the Microsoft Excel program. The results were normalized to the expression of V5 for cells expressing recombinant ZIP7 or GAPDH for cells expressing the only endogenous protein.

2.6 Proteome profiler antibody array

The human phospho-kinases (R&D Systems, ARY003B) antibody arrays were used according to the manufactures instructions. The strategies of array signal detection are illustrated in (**Figure 2.5**). In brief, the cells were lysed in lysis buffer 6 (R&D Systems; 895561) with Protease Inhibitor Cocktail (1:50) (Sigma, P8340). Membranes were blocked in arrays buffer 1 at room temperature for 1 hour, 380 µg of lysate were diluted with arrays buffer 1 to a final volume of 2 mL. The prepared samples were incubated with membranes overnight at 4°C. The membranes were washed with 1X wash buffer and then incubated with detection cocktail antibody for 2 hours at room temperature. Next, the membranes were washed three times and then incubated with Streptavidin-HRP (1:2000) in 1X arrays buffer 2/3 at room temperature for 30 minutes. Then, the membranes were washed before adding chemiluminescent reagent mix. G:BOX system were used to detect the signals on

the membrane over a 10-minute period. The density of the dots was measured using Quick Spot Imaging Analysis Software, and the results were analysed using Microsoft® Excel for Mac. Heat maps were generated using the GENE-E matrix visualisation and analysis platform (The Board Institute).

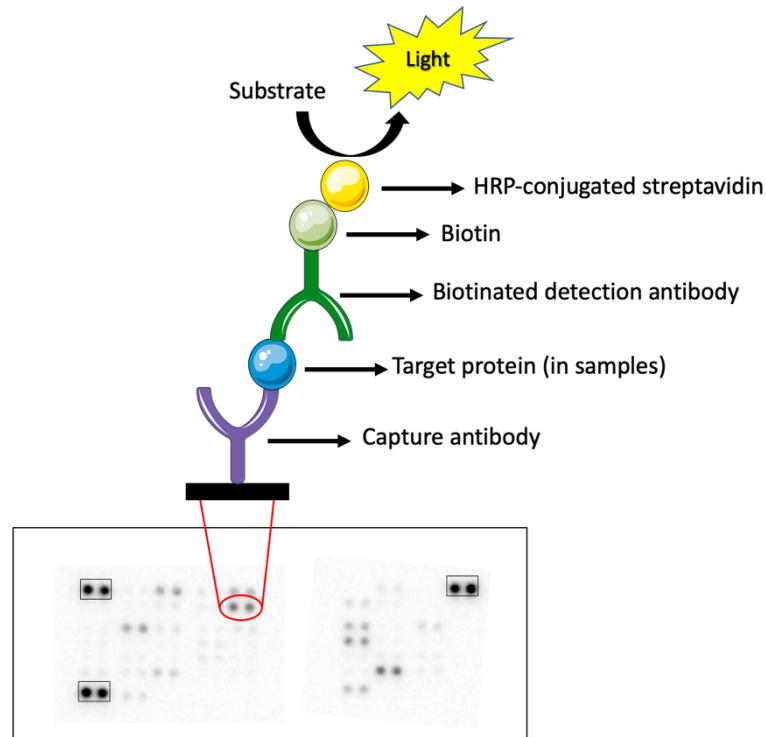


Figure 2.5 Human phosphokinase arrays.

This schematic illustrates the signal detection strategy for phospho-kinase arrays. Three pairs of reference spots are present on the left upper, right upper and left lower corners of each array. Capture antibodies are blotted on the membrane in duplicate and bind to proteins that are present in the cell lysates. Presence of particular proteins is determined by application of biotin-conjugated detection antibodies and HRP-conjugated streptavidin. Signals are detected using a standard chemiluminescence procedure.

2.7 Statistical Analysis:

Statistical analysis was performed by using a Paired t-test or analysis of variance (ANOVA) with Dunnett's test. The difference was considered significant when the p-value less than 0.05 ($p < 0.05$). Statistical analysis was performed using IBM SPSS or GraphPad (Prism) software. Results are displayed at mean \pm standard error of the mean from at least three biological replicates.

2.8 Materials:

All the materials that were used in this project are shown in Table 2.6

Table 2.6 Materials

Reagent/material	Manufacturer	Catalogue number
Acrylamide/bis-acrylamide 30% solution, 37.5:1	Sigma Aldrich, USA	A3699
Agarose	Bioline Ltd, UK	BIO-41025
Ammonium persulfate (APS)	Sigma Aldrich, USA	A3678
Amphotericin B (fungizone)	Invitrogen, UK	15290
Bio RAD Protein Assay Dye Reagent Concentrate	Bio-Rad, USA	#500-0006
Blue sensitive X-ray film	Photon Imaging Systems	FM024
Bovine Serum Albumin	Sigma Aldrich, USA	A7030
Bromophenol Blue	Merck, USA	L54971322
Cell scraper	Greiner Bio-one Ltd, UK	
Coulter Counter counting cups and lids	Sarstedt AG and Co., Nümbrecht, Germany	
Clarity, Western ECL substrate	Bio-Rad, USA	#170-5061
Dimethyl sulphoxide (DMSO)	Sigma Aldrich, USA	D8418
1,4-Dithiothreitol (DTT)	Sigma Aldrich, USA	10708984001
Dulbecco's Modified Eagle Medium (DMEM)	Fisher Scientific, UK	11960044
Ethanol	Fisher, UK	E/0650DF/17
Foetal bovine serum (FBS)	Invitrogen, UK	26140
Formaldehyde 37-41%	Fisher Scientific, UK	10041040
Glass coverslips	BDH Chemicals Ltd, Poole, Dorset, UK	
Hydrochloric acid 5M	Fisher, UK	J/4310/17
Immersol oil	Carl Zeiss, Germany	150925
Isopropanol	Fisher Scientific, UK	10723124
Isoton azide-free balanced electrolyte solution	Beckman, UK	8448011
L-glutamine 200 mM (100X)	Life Technologies Europe Ltd, UK	25030-024
Lipofectamine 3000	Life Technologies Europe Ltd, UK	L3000001
Marvel Dried Skimmed Milk	Premier Internationals Foods, UK	3023034
Methanol	Fisher Chemical, UK	10284580
Mounting Medium with DAPI	Sigma Aldrich, USA	DUO82040
Nitrocellulose membrane	GE Healthcare Life Sciences, UK	10600002
Penicillin/Streptomycin	Invitrogen, UK	15140
Pierce ECL Western Blotting Substrate	Thermo Scientific, USA	#32209
Ponceau S	Sigma Aldrich, USA	P-3504

Reagent/material	Manufacturer	Catalogue number
Precision plus Protein All-Blue Standards	Bio-Rad, USA	#161-0373
Propidium iodide solution	Sigma Aldrich, USA	P4864
Proteome Profiler Human Phospho-Kinase Array Kit	R&D system europe, Abingdon, UK	ARY003B
Protease Inhibitor Cocktail, animal component free in DMSO	Sigma Aldrich, USA	P8340-5ml
Resolving gel buffer, 1.5 M Tris-HCl pH 8.8	Bio-Rad, USA	#161-0798
RPMI (Roswell Park Memorial Institute)	Life Technologies Europe Ltd, UK	21875-034
Saponin from quillaja bark	Sigma Aldrich, USA	S7900
Sodium azide (NaN ₃)	Sigma Aldrich, USA	S-8032
Sodium butyrate	Sigma Aldrich, USA	B5887
Sodium chloride (NaCl)	Sigma Aldrich, USA	S6191
Sodium chloride (NaCl) 99.5%	Fisher, UK	S/3161/60
Sodium dodecylsulfate (SDS)	Sigma Aldrich, USA	L4390
Sodium fluoride (NaF)	Sigma Aldrich, USA	S-1504
Sodium orthovanadate (Na ₃ VO ₄)	Sigma Aldrich, USA	S5608
Sterile phosphate buffered saline (PBS)	Invitrogen, Paisley, UK	
Restore PLUS Western Blot Stripping Buffer	Thermo Scientific, USA	#46430
SuperSignal West Femto Maximum Sensitivity Substrate	Thermo Scientific, USA	#34095
Tetramethylethylenediamine (TEMED)	Fisher Scientific, UK	10549960
Tris Base	Fisher Scientific, UK	10103203
Trypsin-EDTA 0.5% (10X)	Life Technologies Europe Ltd, UK	15400-054
Tween 20	Sigma Aldrich, USA	P2287
Whatman filter paper	GE Healthcare Life Sciences, UK	3030-917
Western Blocking reagent	Roche, Germany	11921673001
Vectashield with DAPI	Vector Laboratories, Inc, UK	H-1200

3. Chapter 3: Computer analysis of ZIP7 protein sequences and analysis of ZIP7 RNA expression and prognosis in different cancer

3.1 Introduction

Zinc is essential for living cells, and two families of zinc transporters control cellular zinc levels. The ZIPs family of zinc transporter have a critical function in maintaining normal cell growth by controlling the cellular zinc level. Dysregulation in the level of the LIV-1 family, which is a subfamily of ZIP transporters, could cause cancer or apoptosis⁴⁴. This project focuses on ZIP7, which is uniquely placed on the ER, while the other ZIPs are located on the plasma membrane. ZIP7 is a gatekeeper of zinc release from the ER, which leads to inhibition of many receptor tyrosine kinases, which has been implicated in the growth of tamoxifen-resistant (TamR) breast cancer⁶⁹. Downregulation of ZIP7 in TamR cells by siRNA has been shown to prevent the zinc-stimulated activation of the receptor and nonreceptor tyrosine kinases⁶⁹. This evidence suggests that ZIP7 could be a potential clinical target for diseases such as cancer. Our group has discovered that ZIP7 is phosphorylated on S275 and S276 by CK2, which opens the zinc channel to allow the release of zinc from stores¹⁶⁹. This data highlights the importance of phosphorylation in the regulation of zinc transporters. ZIP7 S275 and S276 are the only residues that have been experimentally confirmed to be phosphorylated by CK2, resulting in zinc release from the ER and promotion of cell proliferation and migration⁷⁵. Furthermore, ZIP7 gene expression is associated with the poor outcome of breast cancer patients, according to the Oncomine database⁵⁷. Therefore, ZIP7 and zinc are considered to be cancer-promoting and contribute to malignant behaviour.

Breast cancer incidence has been increasing for many years, and currently, it is the most commonly diagnosed cancer in females with a higher mortality rate¹⁷⁰. Screening and early breast cancer diagnoses are crucial to reducing morbidity and mortality^{171,172}. Several therapies are now available to treat breast cancer patients; however, the development of resistance is a considerable problem. Finding a biomarker for the detection of early-stage breast cancer is vital in breast cancer research¹⁷³. Therefore, it is essential to identify prognostic markers for the disease progression and resistance to treatment and predict the

patient's outcome. Gene expression and survival analysis web tools were used to analyse the association of ZIP7 gene expression with cancer type and survival outcome.

Knowing that ZIP7 is functionally controlled by phosphorylation, it was hypothesized that there could also be other phosphorylation sites in ZIP7 that could play a role in its function. This chapter aims to analyse the protein sequence of the LIV-1 subfamily and further investigating ZIP7 sequences to explore any additional potential phosphorylation sites and the candidate kinases. The second aim is to identify ZIP7 NLS motifs and ER motifs using different online prediction databases. The third aim is to investigate the expression level and survival outcome of ZIP7 in breast cancer clinical samples.

3.2 Methods

To investigate the sequences of ZIP transporters, the amino acid sequences of all human ZIP transporters (ZIP1 to ZIP14) were retrieved from the National Centre for Biotechnology Information (NCBI) gene database in a text-based FASTA format from the Uniprot page. The FASTA format was then aligned using the CLUSTAL O multiple sequence alignment program and shaded using the Boxshade online program (Swiss Institute of Bioinformatics). The phylogenetic tree was generated using the Phylogeny.fr web service. The potential transmembrane (TM) domains of the LIV-1 subfamily were identified by using a combination of DAS¹⁷⁴, CCTOP¹⁷⁵, LOCATE¹⁷⁶, Predict protein¹⁷⁷, SOPMA¹⁷⁸, PSORT¹⁷⁹, and TMPred¹⁸⁰.

To detect the potential phosphorylation sites in ZIP7, the following websites were used: PhosphoNET (Kinexus Bioinformatics Corporation), PHOSIDA (Max Planck Institute of Biochemistry)¹⁸¹, PhosphoSitePlus (PSP)¹⁸², and NetPhorest 2.1. The amino acid sequences indicated for the phosphorylation sites and their locations were confirmed with those retrieved from the UniProtKB/Swiss-Prot database (The European Bioinformatics Institute). Predicted kinases with the highest prediction scores were selected, and their functions were searched for in the UniProt Knowledgebase (UniProtKB).

To investigate the expression patterns and survival outcome of ZIP7 in breast cancer patients, various online databases were used. GEPIA server¹⁸³ was used to analyse the

expression of ZIP7 in common cancer types and different subgroups of breast cancer which also was confirmed by using UALCAN server¹⁸⁴ and bc-GenExMiner (v4.4) online tool¹⁸⁵. The protein expression level of ZIP7 in normal breast tissues and cancer breast tissues was determined using Human Protein Atlas (HPA)¹⁸⁶. Also, an online survival analysis tool, Kaplan Meier¹⁸⁷⁻¹⁸⁹ was used to evaluate the effect of ZIP7 expression on the survival outcome of breast cancer patients.

3.3 Results

3.3.1 Dendrogram of the human SLC39A (ZIP) amino acid sequence

Fourteen human proteins have been identified as ZIP channels. The amino acid sequences of the human ZIP family members were retrieved from the NCBI database in the text-based FASTA format. According to the sequence similarity of the phylogenetic tree, the human ZIP transporters can be categorized into four subfamilies: subfamily I (hZIP9), GufA subfamily (hZIP11), subfamily II (hZIP2, hZIP1, hZIP3), and the LIV-1 subfamily (hZIP4, hZIP5, hZIP6, hZIP7, hZIP8, hZIP10, hZIP12, hZIP13, and hZIP14) (**Figure 3.1**). Each pair in the same branch has been shown to share some common features and are more related to each other than pairs in other branches. Both ZIP6 and ZIP10 are grouped together and have both been reported to undergo an N-terminal cleavage upon activation and play an essential role in breast cancer growth^{159,190}. Most ZIP transporters are on the plasma membrane and are responsible for increasing cytosolic zinc by promoting zinc transport from the extracellular fluid into the cytoplasm. In contrast, ZIP7 and ZIP13 were grouped together and are reported to be the only two intracellularly located in the ER and Golgi, respectively, rather than plasma membrane^{58,73}. Additionally, ZIP8 and ZIP14 are grouped because they can transport other metals such as manganese and cadmium¹⁹¹⁻¹⁹³ as well as iron¹⁹⁴.

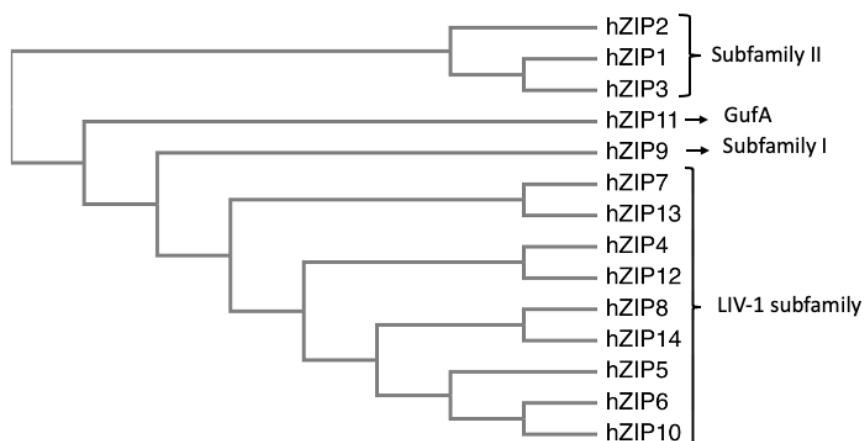


Figure 3.1 Phylogenetic tree of human ZIP channels.

The amino acid sequences of the human ZIP transporters were retrieved from the NCBI database in the text-based FASTA format, and then aligned with the CLUSTAL O (Maderia et al, 2019) program to generate the phylogenetic tree.

3.3.2 Computer analysis of LIV-1 subfamily sequences

The protein sequences of all human LIV-1 subfamily were aligned using the CLUSTAL O multiple sequence alignment program and shaded using the Boxshade online program. All the TM regions were identified according to previous computer sequence analysis¹⁵⁸. All ZIP transporters have an eight TMs domain, a long cytoplasmic loop between TM3 and TM4, and a very short C-terminus^{33,44,45}.

The LIV-1 subfamily is distinguished by some unique features compared with other ZIP transporters. **First**, they have additional histidine-rich regions in the long N-terminus and in the loop between TM2 and TM3, which suggest the higher binding capacity of the LIV-1 subfamily to zinc compared to the other subfamily as histidine is known to be a zinc-binding amino acid (**Figure 3.2 and 3.3**). **Second**, they have a longer N-terminus with a maximal 408 amino acid as in ZIP10, while the maximal number of amino acids in the other ZIPs is 31 amino acids as in ZIP1. The longer N terminus in the LIV-1 subfamily suggests a more complex post-translation mechanism of the LIV-1 subfamily as the signal's sequences are contained in the N-terminus¹⁹⁵ and the post-translation modification in the N-terminus have been shown to participate in the functional control of protein¹⁹⁶. **Third**, they also contain a highly conserved potential metalloprotease HEXPHEXGD motif within TM5 (H=histidine, E=glutamate, P=proline, G=glutamine, D=aspartate,

X=any amino acid) which form the conserved motif for recognition of this family of protein (**Figure 3.3**). This highly conserved motif is predicted to be a catalytic zinc-binding site because it is similar to the zinc-binding region of the zinc metalloproteinases⁶¹. **Fourth**, they contain a CPALLY motif (C=cysteine, P=proline, A=alanine, L=leucine, Y=tyrosine). The CPALLY motif is present in the majority of the LIV-1 subfamily, except in ZIP7 and ZIP13 (**Figure 3.2**), and it is located in the long extracellular N terminus immediately before the first TM helix^{44,63}.

ZIP8 and ZIP14 transporters are not strict about transporting zinc only. However, they can also transport other metals across cell membranes such as manganese, iron, copper, and cadmium¹⁷. The first conserved histidine residue in TM 5 (HEXPHEXGD) may play an important role in zinc transport specificity⁴⁴. ZIP8 and ZIP14 have a glutamic acid (E) instead of the first histidine (H) in this motif (**Figure 3.4**), which have been shown the ability to transport/bind to several divalent metal ions other than zinc such as manganese, iron, copper, and cadmium^{17,191–193}.

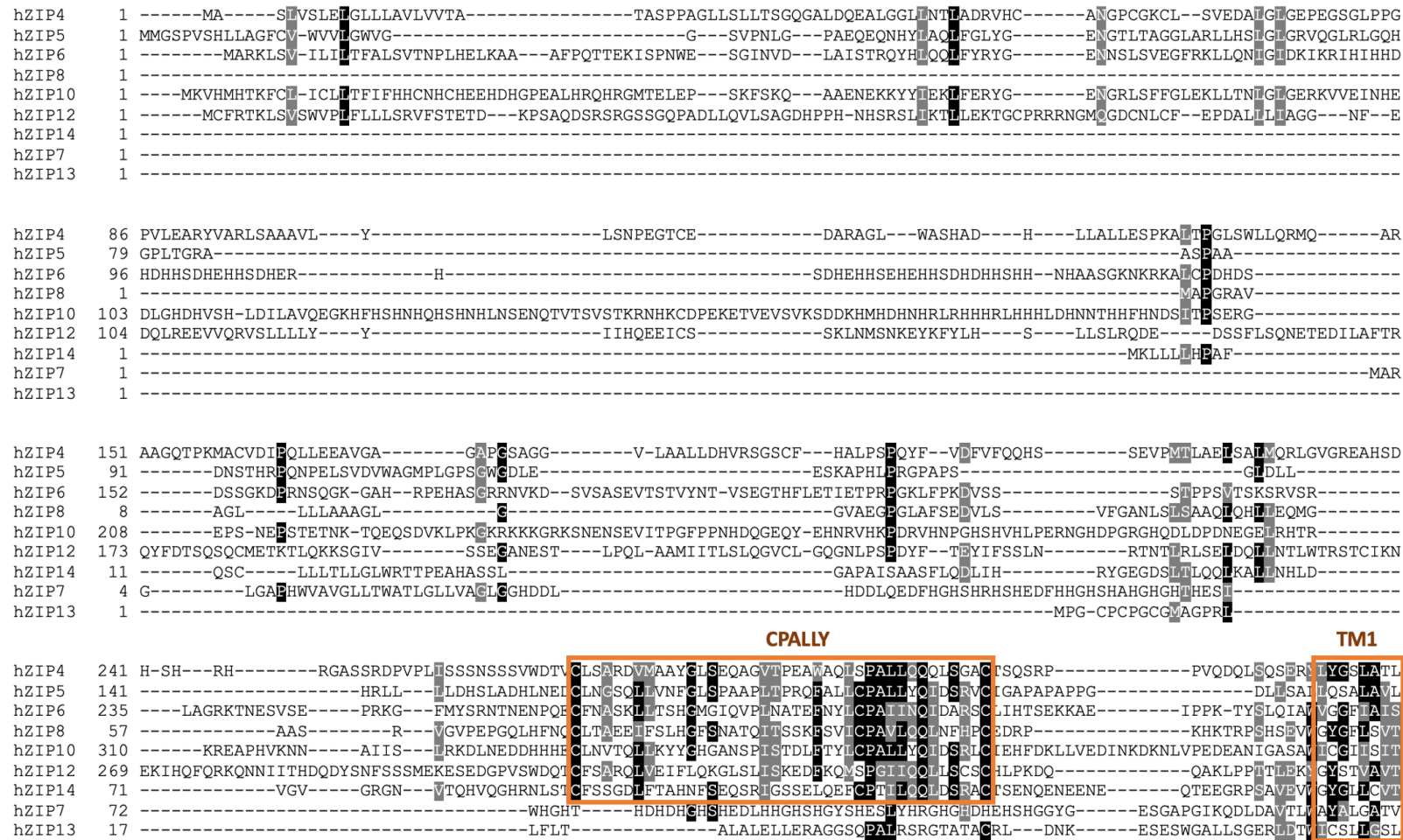


Figure 3.2 Alignment of all human LIV-1 subfamily sequences (part A)

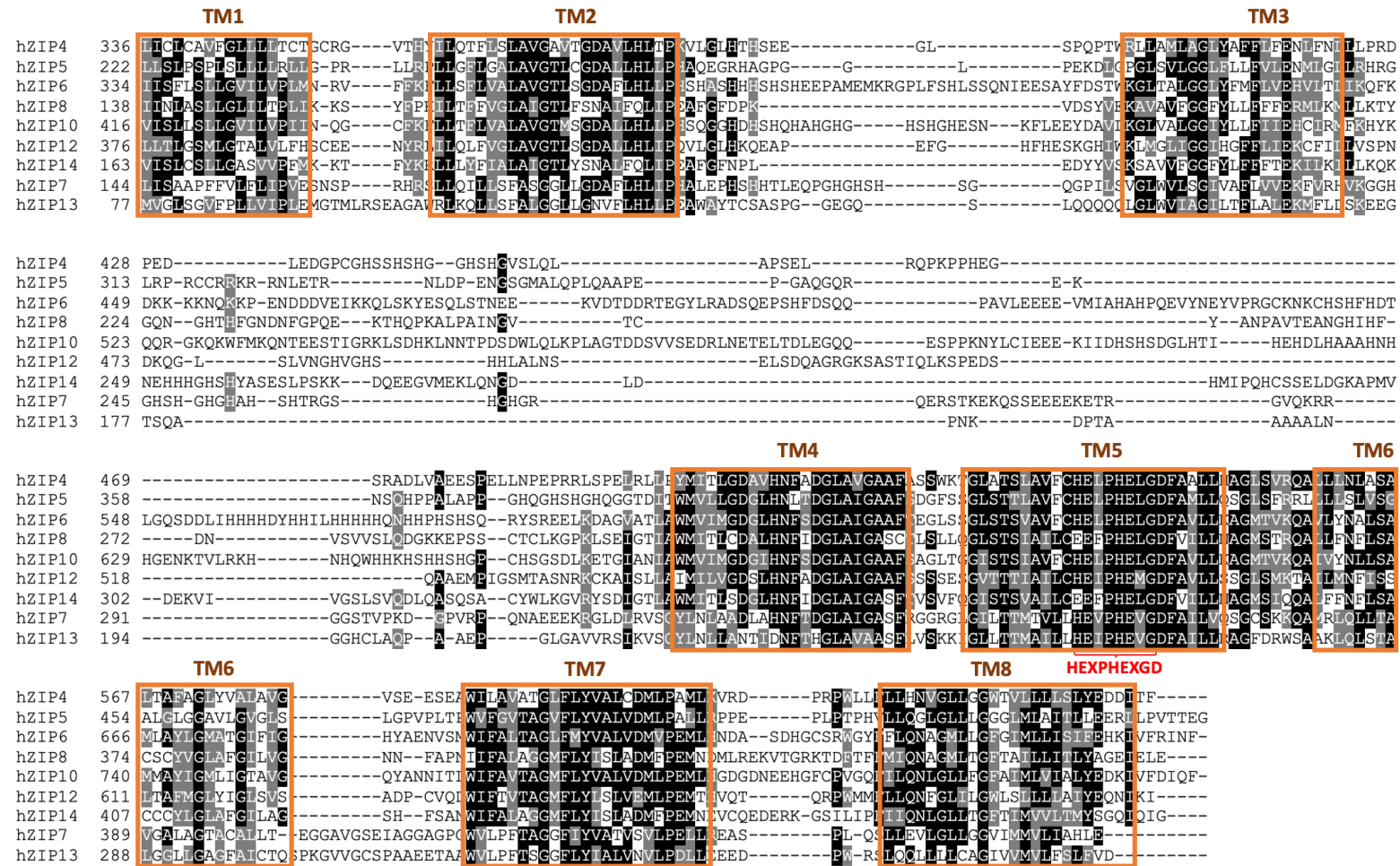


Figure 3.3 Alignment of all human LIV-1 subfamily sequences (part B).

Amino acid sequences of the human LIV-1 subfamily were aligned using CLUSTAL O (Maderia et al, 2019). Residues were shaded using the BoxShade online program. The CPALLY motif, which contains three conserved cysteine residues, is indicated in a box. This motif is seen in the N-terminus of the LIV-1 subfamily, except ZIP7 and ZIP13. The predicted TM regions are also indicated with a box. The metalloprotease motif (CHEXPHEXGD) in TM5 is indicated in red.



Figure 3.4 TM5 of the human LIV-1 family of ZIP transporters

The protein sequences of the LIV-1 subfamily were retrieved from NCBI and then aligned using the CLUSTAL O alignment program (Maderia et al, 2019) and shaded by using Boxshade. The metalloprotease motifs are indicated. The glutamic acid (E) in ZIP8 and ZIP14 are indicated in red.

3.3.3 Identification of potential phosphorylation sites in ZIP7

ZIP7 has been shown to release zinc after phosphorylation by protein kinase CK2 at residues S275 and S276^{63,74,75}. To explore the other potential phosphorylation sites of ZIP7 and their predicted kinases, five websites were used. These were PhosphoSitePlus (PSP)¹⁸², NetPhos¹⁹⁷ PhosphoNET, NetPhorest¹⁹⁸, and PHOSIDA¹⁸¹. Thirty predicted phosphorylation sites of ZIP7 were either predicted from amino acid sequences or experimentally confirmed by mass spectrometry; listed in **Table 3.1**. The majority of the predicted phosphorylation residues in ZIP7 are either serine or threonine. This is expected because 90% of cellular protein is expected to be phosphorylated in serine/threonine by cellular kinases and reversed by phosphatase^{199,200}.

Interestingly S275, S276, S293, and T294 are the only residues predicted to be phosphorylated by all five-phosphorylation prediction software. Also, they are all confirmed by mass spectrometry and share the location in the long cytoplasmic loop between TM3 and TM4. This location implicates this domain as functionally significant

in the regulation of ZIP7. S275 and S276 are predicted to be phosphorylated by CK2, which has been experimentally confirmed as a key mechanism for ZIP7 activation^{74,75}. S293 and T294 are interesting, predicted phosphorylation sites that will be further investigated experimentally in the next chapter. S293 and T294 are adjacent residues and are predicted to be phosphorylated by the same kinase, PIM2/3, which is known to have a role in cell survival and proliferation. The double phosphorylation of adjacent residues in the cytoplasmic loop between TM3 and TM4 is a potentially significant modification in the regulation of ZIP transporters.

In addition to identifying ZIP7 phosphorylation sites, many databases were used to identify potential kinases that may phosphorylate these residues. Interestingly, the predicted kinases that phosphorylate ZIP7 have a role in cancer progression. ZIP7 was predicted to be phosphorylated by CK2 on residues S273 and S276, which regulates many cellular processes such as apoptosis, cell cycle progression, and transcription^{201–203}. MAPKAPK3-2 and PKC are also predicted to phosphorylate ZIP7, which are known to promote cell migration, proliferation, and survival²⁰⁴ and PIM1-3 is a proto-oncogenesis serine/threonine kinase, have a role in cell survival, differentiation, proliferation, and tumorigenesis²⁰⁵. Also, ZIP7 is predicted to be phosphorylated by mTOR, which regulates cell proliferation and apoptosis²⁰⁶. Cyclin-dependent kinase (CDK) regulates the cell cycle, and it is frequently overexpressed or mutated in cancer²⁰⁷. These kinases and their roles in the process of carcinogenesis and tumour progression were obtained from the UniProt page. Interestingly, all these predicted kinases of ZIP7 have cancer-promoting properties suggesting a role for ZIP7 in driving cancer growth.

Position	Sequences	Phosphosite	NetPhos	Kinexus	NetPhorest	Phosida	No. of rec.
S46	QEDFHGHSHRHSHE		Y		PKC		
S47	HGHSRHSHEDFHH		Y		PKA		
S48	HDHDHGHSHEDLHH		Y		CK2		
S93	EDLHHGSHGYSHES	Y		MAPKAPK2/3			1
Y96	HHGSHGYSHESLYH			EPHA1-JAK2			
S97	HGSHGYSHESLYHR	Y					1
S100	SHGYSHESLYHRGHG			mTOR-CK1	Y		
Y102	GYSHESLYHRGHGHD			FRK			
Y117	HEHSHGGYGESGAPG		Y	SYK			
S120	SHGGYGESGAPGIKQ			mtTOR-PIM3			
T142	WAYALGATVLISAAP	Y					1
S160	LFLIPVESNSPRHRS			ERK2/1-MAPKAPK2/3			
S162	LIPVESNSPRHRSLL		Y	ERK2/1-JNK1/3	CDK1/2/3/5		
S167	SNSPRHRSLLQILLS			MAPKAPK2/3	PKA		
S176	SNSPRHRSLLQILLS		Y				
S197	PHALEPHSHHTLEQP		Y	mTOR-ERK2			
T200	LEPHSHHTLEQPGHG			mTOR-CK1			
S209	EQPGHGHSHSGQGPI		Y	mTOR-PIM3/1			
S211	PGHGHSHSGQGPILS			mTOR-PIM3/1			
S255	HGHGHAHSHTRGSHG		Y	mTOR-PIM3/1	Y		
T257	HGHASHTRGSHGHG			mTOR-PIM3/1	Y		
S260	AHSHTRGSHGHGRQE		Y	mTOR-PIM3/1			
S269	GHGRQERSTKEKQSS		Y	AKT1/2/3	PKC/CK2		
T270	HGRQERSTKEKQSSE			PIM1/3	CLK		
S275	RSTKEKQSSEEEKE	Y	Y	CK2	CK2	CK2	26
S276	STKEKQSSEEEKET	Y	Y	CK2	CK2	CK2	26
S293	VQKRRGGSTVPKDGDP	Y	Y	MAPKAPK2/3-PIM3/2	CLK	Y	3
T294	QKRRGGSTVPKDGVP	Y	PKC	PIM1/2/3	CLK	Y	2
S376	VQSGCSKKQAMRLQL		PKC		PKC		1
S444	PELLREASPLQSLLE			MAPKAPK2/3			

Table 3.1: Predicted phosphorylation sites of ZIP7 and their predicted kinases.

ZIP7 phospho-sites were predicted using PhosphoSitePlus (PSP) (Hornbeck et al, 2014), NetPhos (Blom et al, 2004), PhosphoNET, NetPhorest (Miller et al, 2008), and PHOSIDA (Gand et al, 2011). Analysis was completed using the human ZIP7 protein sequence in FASTA format. Highlighted in orange are residues that were positive for mass spectrometry data and located within the cytoplasmic loop between TM3-4. S, serine; T, threonine; Y, tyrosine. Blank spaces indicate no kinase prediction. No. of rec., number of records. representing the number of proteomic studies that detected phosphorylation at the individual residues using mass spectrometry.

3.3.4 Identification of endoplasmic reticulum retention signals in ZIP7

The endoplasmic reticulum (ER) is the largest intracellular compartment and consists of tubules and flattened sacs that extend throughout the cytosol. Membrane protein synthesis, folding, assembly, and degradation occurs in the ER²⁰⁸. The ER acts as a quality control compartment for proteins because misfolded proteins will be retained in the ER to be degraded²⁰⁸. The correctly folded and assembled proteins are rapidly transported out of the ER to reside in the plasma membrane or the membrane of other organelles. For a protein to remain in the ER, ER-resident proteins require a specific signal composed of a short amino acid motif located in the cytoplasmic domain of the protein, responsible for their ER retention²⁰⁹. The immunofluorescence picture of ZIP7 always has ER staining and a perinuclear ring (**Figure 3.5**), which suggests that ZIP7 is located in the ER and the nuclear envelope. To identify the sequence of ZIP7, which could have a role in ZIP7 retention in the ER, different online databases were used, showing that ZIP7 is predicted to have four ER retention motifs (**Table 3.2, Figure 3.6**).

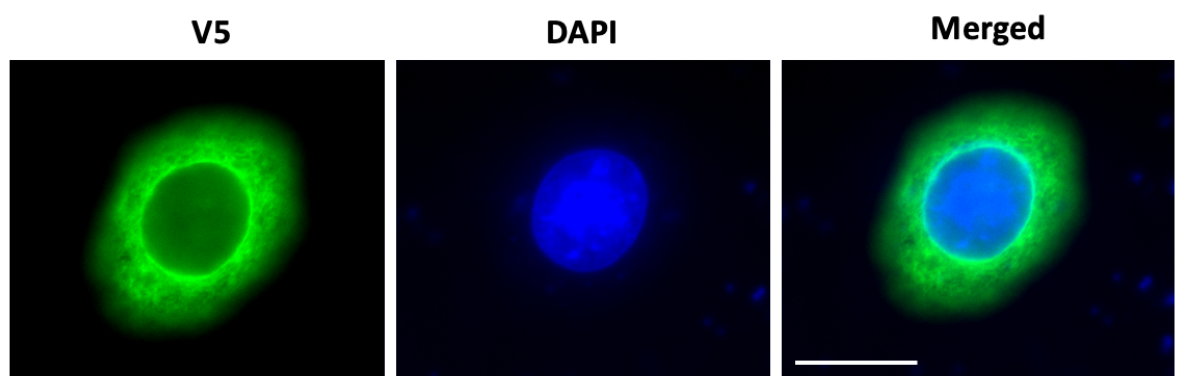


Figure 3.5 Cellular localization of wild type ZIP7 in MCF-7 cells

MCF-7 cells were transfected with WT-ZIP7 for 18 hours. The cells were fixed and permeabilized before probing with rabbit V5 conjugated Alexa Fluor 488 (Green), and nuclei were stained blue with DAPI. These images were captured with a Leica RPE automatic microscope using a 63x magnification lens. Scale bar, 10 μ m

ER retention motifs	Position
PRHR	163-166 (between TM1 and TM2)
HVK	238-241 (between TM3 and TM4)
KEK	270-273 (between TM3 and TM4)
SKK	375-378 (between TM5 and TM6)

Table 3.2 Predicted endoplasmic retention signals of ZIP7.

ZIP7 is predicted to have a four endoplasmic reticulum signals as shown in the table above.

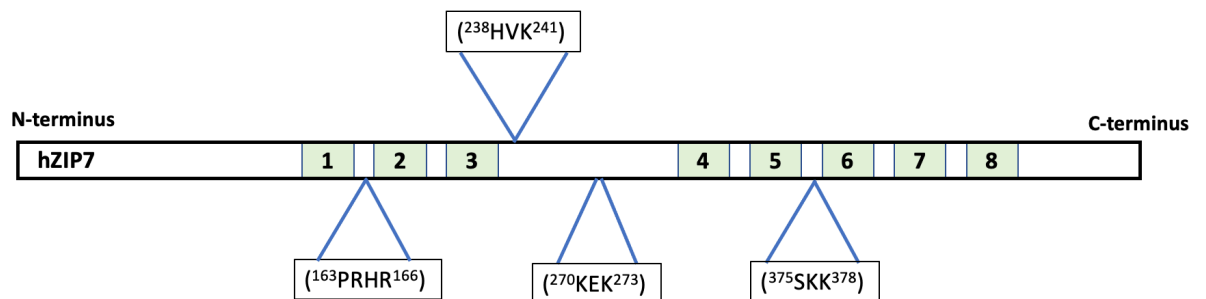


Figure 3.6 Schematic diagram that shows the location of ER retention signals in the ZIP7 sequence.

ZIP7 was predicted have four endoplasmic reticulum retention signals.

3.3.5 Identification of nuclear localization sequences in ZIP7

Imaging ZIP7 in MCF7 cells has suggested that not only is ZIP7 present in the ER, but it always stains a strong perinuclear ring, indicating the potential for ZIP7 to be located on the inner nuclear membrane (**Figure 3.5**). Several online databases were searched to detect predicted nuclear localization signals of ZIP7 (**Table 3.3**). The amino acid sequence of ZIP7 that was used for searching was a text-based FASTA format, retrieved from the gene database of the National Centre for Biotechnology Information (NCBI). Computer analysis of the ZIP7 sequence revealed two monopartite NLS motifs, which contain only one cluster of basic amino acids, RGVQKRRGGST (amino acids 288-290) between TM3 and TM4 and EEKRGGL (amino acids 310-311). Both sequences are located between TM3 and TM4.

ZIP7 is also predicted to have bipartite NLSs, consisting of two clusters of basic amino acids starting at residue 288 and ending at residue 311 (RGVQ**KRR**GGSTVPKDGVPVRPQN**AEEEEKR**GLD). The predicted NLS motifs, which have been named NLS1-3 (Table 3.4), are detected based on the significant similarity of the ZIP7 sequence with already known nuclear proteins. All three nuclear localisation sequences are located in the long cytoplasmic loop between TM3 and TM4 (Figure 3.7), which is predicted to be a nucleoplasm domain when ZIP7 is on the INM. This suggests that ZIP7 could rely on its nuclear localization signals for transport through the nuclear pore complex. Figure 3.8 shows ZIP7 predicted phosphorylation sites, NLS, and ER retention signals on the amino acid sequence of ZIP7, which will be mutated to alanine and further investigated in the following chapters.

Table 3.3 Online databases used to detect NLS and ER retention signals

Predictor	Web address	Reference
PSORT	https://psort.hgc.jp	Gardy et al. 2003 ²¹⁰
cNLS Mapper	http://nls-mapper.iab.keio.ac.jp/cgi-bin/NLS_Mapper_form.cgi	Kosugi et al. 2009 ²¹¹
PredictNLS	https://rostlab.org/services/nlsdb/	Cokol et al.2000 ²¹²
NLStradamus	http://www.moseslab.csb.utoronto.ca/NLStradamus/	Nguyen et al. 2009 ²¹³
NucPred	https://nucpred.bioinfo.se/cgi-bin/single.cgi	Brameier et al. 2007 ²¹⁴
SeqNLS	http://mleg.cse.sc.edu/seqNLS/	Lin et al. 2013 ²¹⁵
ELM	http://elm.eu.org	Diella et al. 2009 ²¹⁶
LocSigDB	http://genome.unmc.edu/LocSigDB/index.html	Negi et al. 2015 ²¹⁷
LOCATE	http://locate.imb.uq.edu.au/	Sprenger et al. 2008 ¹⁷⁶

	NLS motif	NLS Class	Position
NLS1	RGVQ KRR GGST	monopartite	288-290
NLS2	EE KR GL	monopartite	310-311
NLS3	RGVQ KRR GGSTV PKDGPV RPQNA EEEK RGL	bipartite	288-311

Table 3.4: Predicted nuclear localization sequences of ZIP7

Characterization of the nuclear localization signals of ZIP7. Predicted basic amino acid residues are indicated in bold.

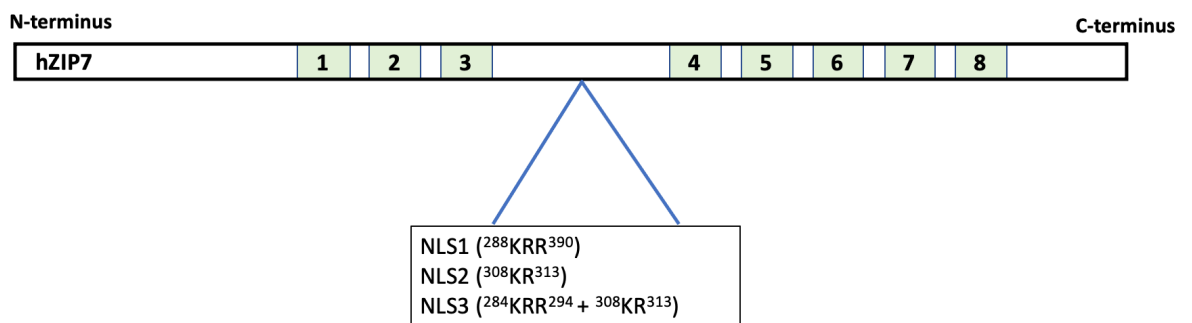


Figure 3.7 : Schematic diagram that shows the location of NLS on ZIP7 sequences.

Schematic of the three nuclear localization signals in the long cytoplasmic loop between TM 3 and TM 4.

MARGLGAPHWVAVGLLTWATLGLLVAGLGGHDDLHDDLQEDFHGHSHRHSHEDFHGHSH
 AHGHGHTHESIWHGHTHDHDHGHSHEDLHHGHSHGYSHESLYHRGHGHDEHSHGGYGES
 GAPGIKQDLDAVTLWAYALGATVLI SAAPFFVLFLIPVESNS **PRHR** SLLQILLSFASGGL
 LGDAFLHLI PHALEPHSHHTLEQPGHGHSHSGQGPILSVGLWVLSGIVAFLLVVEKFVR **HV**
KGGHGHSHGHGHAHSHTRGSHGHGRQERST **KEKQ** **SS** EEEEEKETRGVQ **KRRGG** **ST** VPKDGP
 VRPQNAEEEE **KR** GLDLRVSGYLNLAADLAHNFTDGLAIGASFRGGRGLGILTTMTVLLHEV
 PHEVGDFAILVQSGC **SKK** QAMRLQLLTAVGALAGTACALLTEGGAVGSEIAGGAGPGWVL
 PFTAGGFIYVATVSVLPELLREASPLQSLLEVLGLLGGVIMMVLI AHLE

469

Figure 3.8 The amino acid sequence of ZIP7 zinc transporter.

The predicted phosphorylation site of ZIP7 were highlighted in red. The predicted ER retention signals were highlighted in green, and the predicted NLS were highlighted in blue.

3.3.6 Analysis the potential phosphorylation sites, ER retention signals, NLS signals in various animal species of ZIP7

To determine evolutionary conservation of the predicted phosphorylation sites, ER retention signals, and nuclear localization signals, which might imply the potential importance of these residues in ZIP7 post-translational control and localization, ZIP7 amino acid sequences in different animal species were aligned. ZIP7 sequence alignment was performed in human, chimpanzee, gorilla, cat, rhesus monkey, dog, rabbit, bovine, rat, pig, sheep, panda, mouse, and horse (**Figure 3.9**). Evolutionary conservation of the protein sequences was clearly seen across these species. Importantly, the four consecutive predicted phosphorylation residues, ER retention signals and NLS were highly conserved across the mammalian species. The predicted NLSs are in the long cytoplasmic loop between TM3 and TM4 close to the predicted phosphorylation sites. ER retention signals are located between (TM1 and TM2), (TM3 and TM4), and between (TM5 and TM6). Also, the four predicted phosphorylation sites were conserved in different species, which imply these phosphorylation sites could play an essential role in ZIP7 regulation.

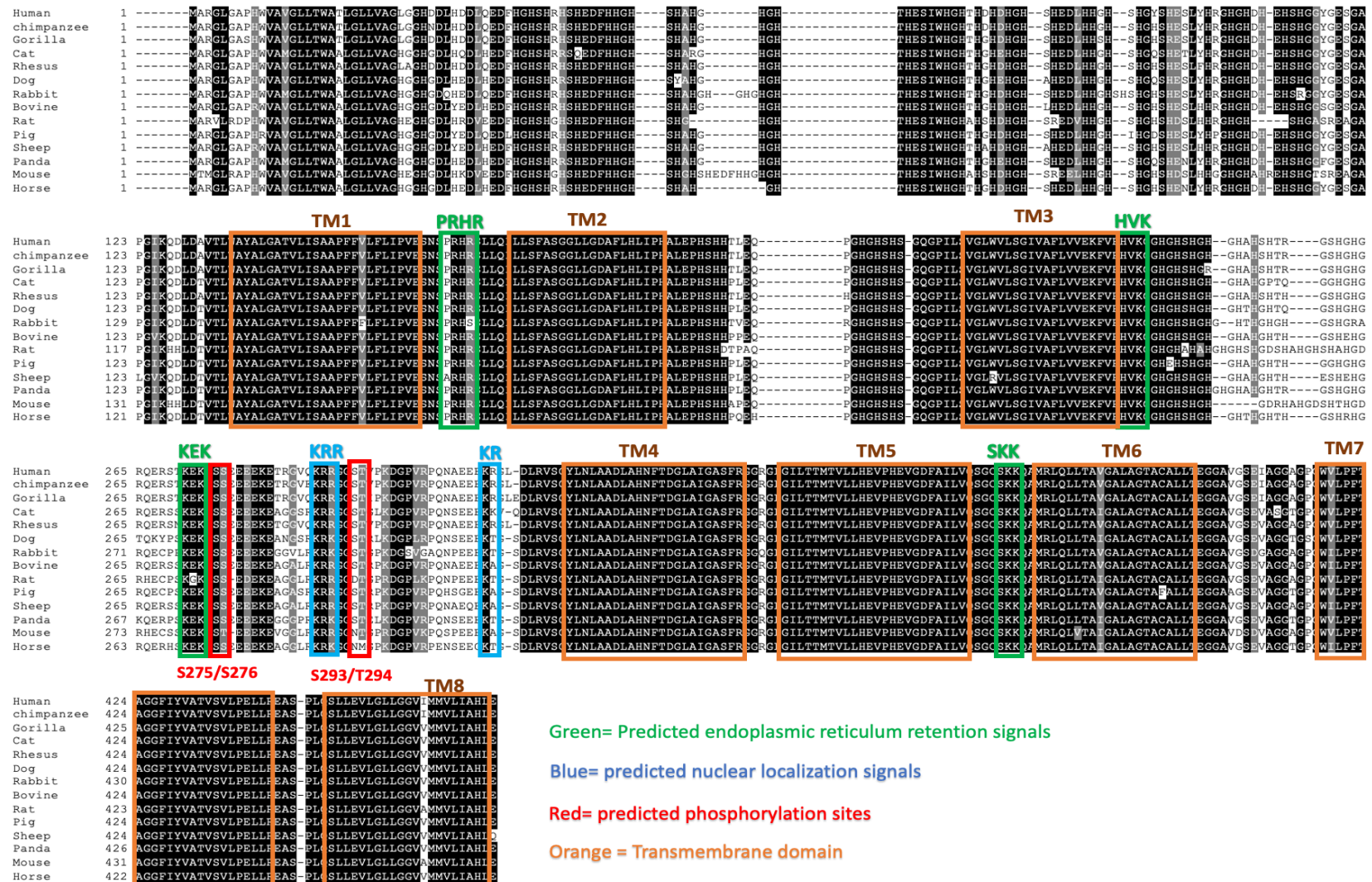


Figure 3.9 Alignment of ZIP7 in various animal species

Amino acid sequences of ZIP7 from human, chimpanzee, gorilla, cat, rhesus monkey, dog, rabbit, bovine, rat, pig, sheep, panda, mouse, and horse were aligned using the Clustal O multiple sequence alignment program (Maderia et al, 2019). Residues were shaded using the BoxShade 3.21 online program. The regions equivalent to the TM regions (orange box) and predicted phosphorylation sites (red box), predicted endoplasmic reticulum signals (green box), predicted nuclear localization sequence (blue box) in hZIP7 are indicated.

3.3.7 Elevated transcriptomic levels of ZIP7 associated with cancer

To explore the prognostic and potential therapeutic values of ZIP7 in different cancers, GEPIA (Gene Expression Profiling Interactive Analysis; <http://gepia.cancer-pku.cn>) was used to compare the mRNA expression level of ZIP7 in multiple tumour types with normal healthy samples. GEPIA is a web-based tool to deliver fast and customizable functionalities based on The Cancer Genome Atlas (TCGA) and Genotype Tissue Expression project (GTEx) data, which scientists of Peking university developed²¹⁸. TCGA and GTEx contain a large number of RNA sequence data of normal and cancer samples^{219,220}. As shown in the GEPIA boxplots, there was a significant difference in ZIP7 expression between normal and cancer tissues (**Figure 3.10**). The red and grey boxes represent cancer and normal tissues, respectively. The expression of ZIP7 in tumour tissues was significantly higher than those in normal tissues ($P < 0.01$), which suggests that ZIP7 may represent a potentially viable therapeutic target.

The correlation between the mRNA expression levels of ZIP7 and the clinical-pathological parameter of breast cancer were further investigated; ZIP7 transcriptional levels of ZIP7 in different molecular subtypes of invasive breast carcinoma were analysed using the GEPIA2 database²²¹. ZIP7 overexpression was observed to be high in all invasive breast carcinoma subtypes compared with normal breast groups with a significant difference in basal-like and HER2 subtypes (**Figure 3.11**). In contrast, in luminal A and luminal B cancer, the ZIP7 level is increased but not statistically significant (**Figure 3.11**). These results suggest that ZIP7 is a potential biomarker for aggressive breast cancer.

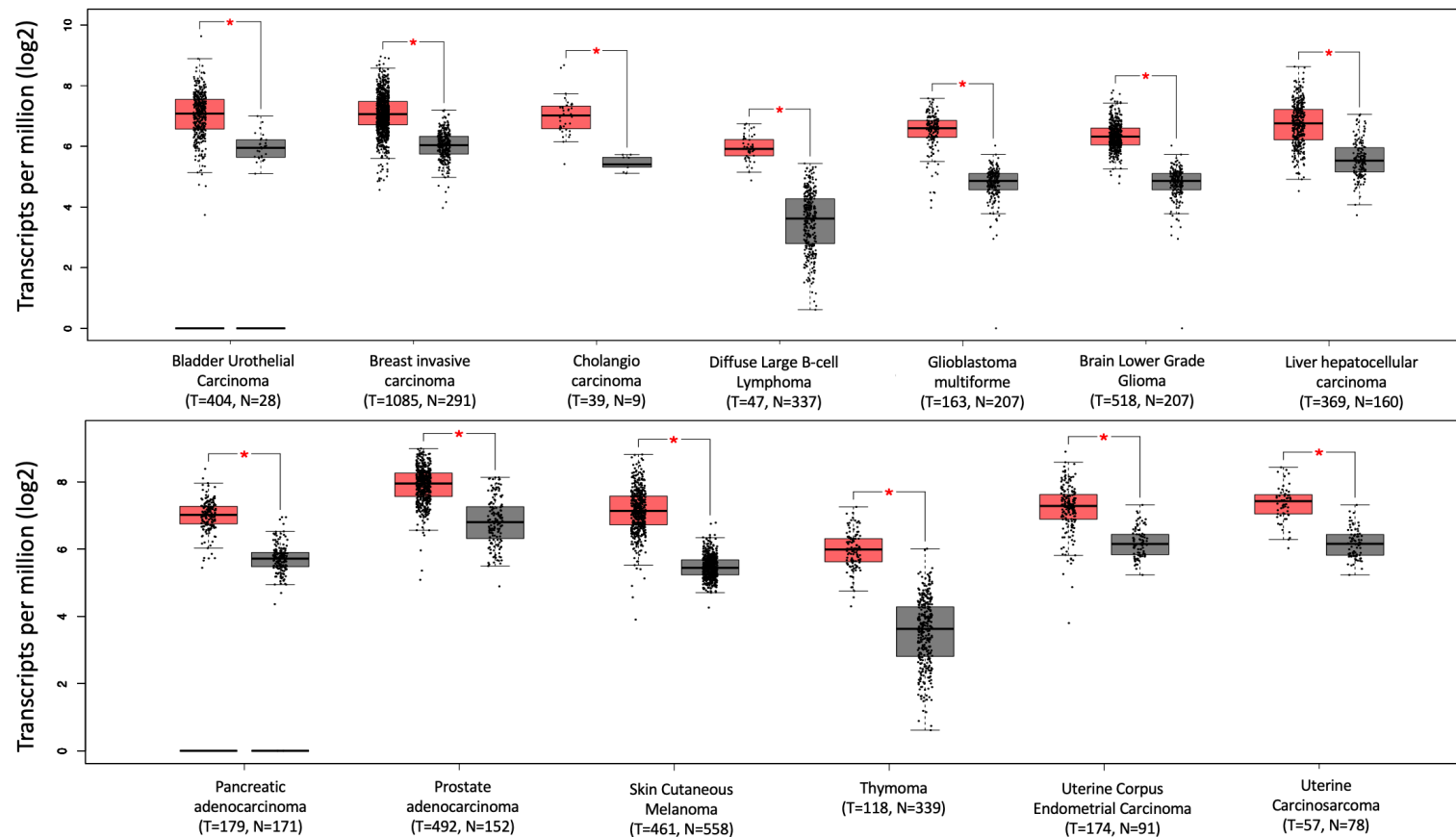


Figure 3.10 The GEPIA boxplot of ZIP7 gene expressions in common cancers versus paired normal tissues.

Boxplots describing differential ZIP7 expression between normal and cancerous tissues, represented by grey and red boxes, respectively. All plots were produced by GEPIA server (Tang et al. 2017) and describe matched gene expression data derived from TCGA and GTEx databases. Data was filtered to show only differential expression relationships significant at a P -value cut-off of 0.01. X-axes are annotated sizes of normal (N) and tumour (T) sample cohorts.

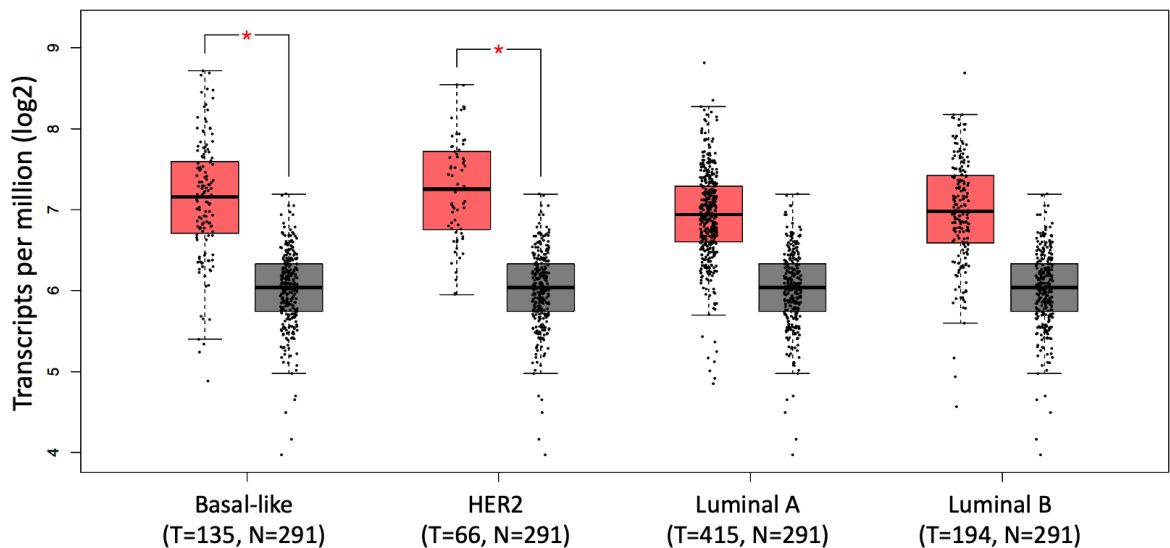


Figure 3.11 The transcriptional levels of ZIP7 in different subtype of breast cancer in GEPIA database.

Boxplots describing differential ZIP7 expression between normal and cancerous tissues in different breast cancer subtype. All plots were produced by GEPIA2 server (Tang et al. 2019) and describe matched gene expression data derived from TCGA and GTEx databases. The red and grey boxes represent cancer and normal tissues, respectively. *P*-value cutoff 0.01 were defined. X-axes are annotated sizes of normal (N) and tumour (T) sample cohorts.

3.3.8 Further validation of the relationship between ZIP7 expression and clinical pathological parameters of patients with breast cancer

The expression analysis of the ZIP7 gene was further verified using UALCAN (<http://ualcan.path.uab.edu/index.html>), a data platform based on the TCGA database, the world's largest and most comprehensive gene chip database²²². One of the portal's user-friendly features is that it analyses relative expression of a query gene(s) across tumour and normal samples and various tumour molecular subtypes such as the individual age, gender, and tumour stages or other clinicopathological features. The mRNA information was unified as transcripts per million (TPM) reads for data comparison from different sources. Therefore, the correlation between the mRNA expression level of ZIP7 and the clinicopathological stage of patients with invasive breast carcinoma were explored via the UALCAN database. *P*-values < 0.05 were considered statistically significant.

The mRNA expression levels of ZIP7 were significantly higher in tumour breast tissue than those in normal breast tissue (**Figure 3.12**). Further subgroup analysis of multiple clinical and pathological features of breast cancer samples consistently showed high-expression levels of ZIP7. The tumour stages and subclass boxplots of ZIP7 genes are shown in **Figure 3.13a** and **Figure 3.13b**, respectively. The results demonstrated that expression levels of the ZIP7 genes were significantly associated with all stages and subclasses of breast cancer compared to normal breast cancer tissues. In addition, the expression levels of the ZIP7 gene are significantly elevated in breast cancer samples than adjacent normal samples in subgroup analyses based on nodal metastasis status, menopause status, age, and gender of patients (**Figure 1.13 c,d,e,f**). These results suggest that ZIP7 expression may serve as a potential diagnostic indicator in breast cancer.

To further evaluate the diagnostic potential of ZIP7 as a biomarker in breast cancer patients, bc-GenExMiner (v4.4) online tool¹⁸⁵ (<http://bcgenex.ico.unicancer.fr/BC-GEM/GEM-Accueil.php?js=1>) was used to assess the relationship between mRNA ZIP7 expression level and various clinical features of breast cancer patients. Box plots are provided to visualize output results. ZIP7 gene expression was explored in healthy tissue, a mammary tissue without any link with cancer, or adjacent tumour tissue that is more or less influenced by cancer cells or tumour tissues¹⁸⁵. Welch's t-test was performed to compare the transcription levels of ZIP7 among groups of patients based on different clinicopathological parameters¹⁸⁵.

ZIP7 overexpression was significantly higher in tumour breast cancer tissue than healthy normal breast cancer tissue (**Figure 3.14a**), which is consistent with GEPIA (**Figure 3.11**) and UALCAN database (**Figure 3.14**). The overexpression of ZIP7 was observed to be significantly higher in basal-like, human epidermal growth factor receptor 2 (HER2)-enriched, and luminal A and B subtypes than healthy tissues (**Figure 3.14b**). In addition, ZIP7 expression was significantly higher in the oestrogen receptor and HER2 group than in normal tissues (**Figure 3.14c and d**). Moreover, ZIP7 overexpression is significantly elevated in triple-negative breast cancer (**Figure 3.14e**). According to HER2 immunohistochemistry data, ZIP7 was significantly higher in the HER2+ group than the HER2- group (**Figure 3.14f**). The

results implied that ZIP7 were positively correlated with the types of high malignancy and poor prognosis breast cancer, which have a feature of high invasiveness, metastasis, and relapse. These results suggest further confirm that ZIP7 expression may serve as a potential diagnostic indicator in breast cancer.

After examining the mRNA expression of ZIP7 in invasive breast carcinoma, the protein expression levels of ZIP7 were explored using the Human Protein Atlas (HPA) database¹⁸⁶ (<https://www.proteinatlas.org>). Human Protein Atlas, a website that contains immunohistochemistry-based expression data for approximately 20 most common types of cancers²²³. The ZIP7 antibody used for the Human Protein Atlas database was HPA053999, an antibody against human SLC39A7. The protein level of ZIP7 was a low expression in normal breast tissue (**Figure 3.15**). In contrast, high expression in breast cancer tissue (**Figure 3.15**) suggests that ZIP7 is a potential biomarker in breast cancer patients.

In summary, these results indicated that ZIP7 is more highly expressed at the transcriptional and proteomic level in breast cancer tissue than normal breast tissue. The higher expression pattern of ZIP7 revealed that ZIP7 might be a new biomarker and maybe a potential target therapy for patients with breast cancer.

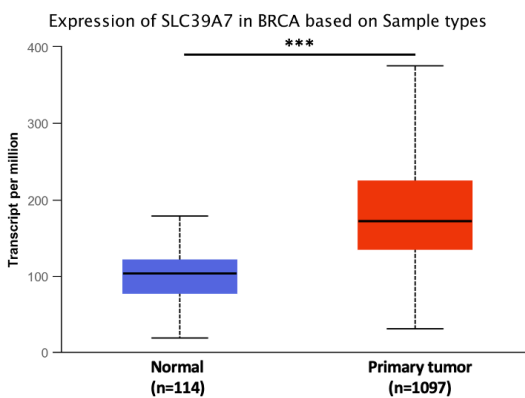


Figure 3.12 Relative expression of ZIP7 gene in normal tissues and breast cancer tissues.

The box plot was obtained from UALCAN database (Chandrashekar et al.2017). Data are mean \pm SE. *** $P < 0.001$. BRCA= breast invasive carcinoma samples. n= number of samples

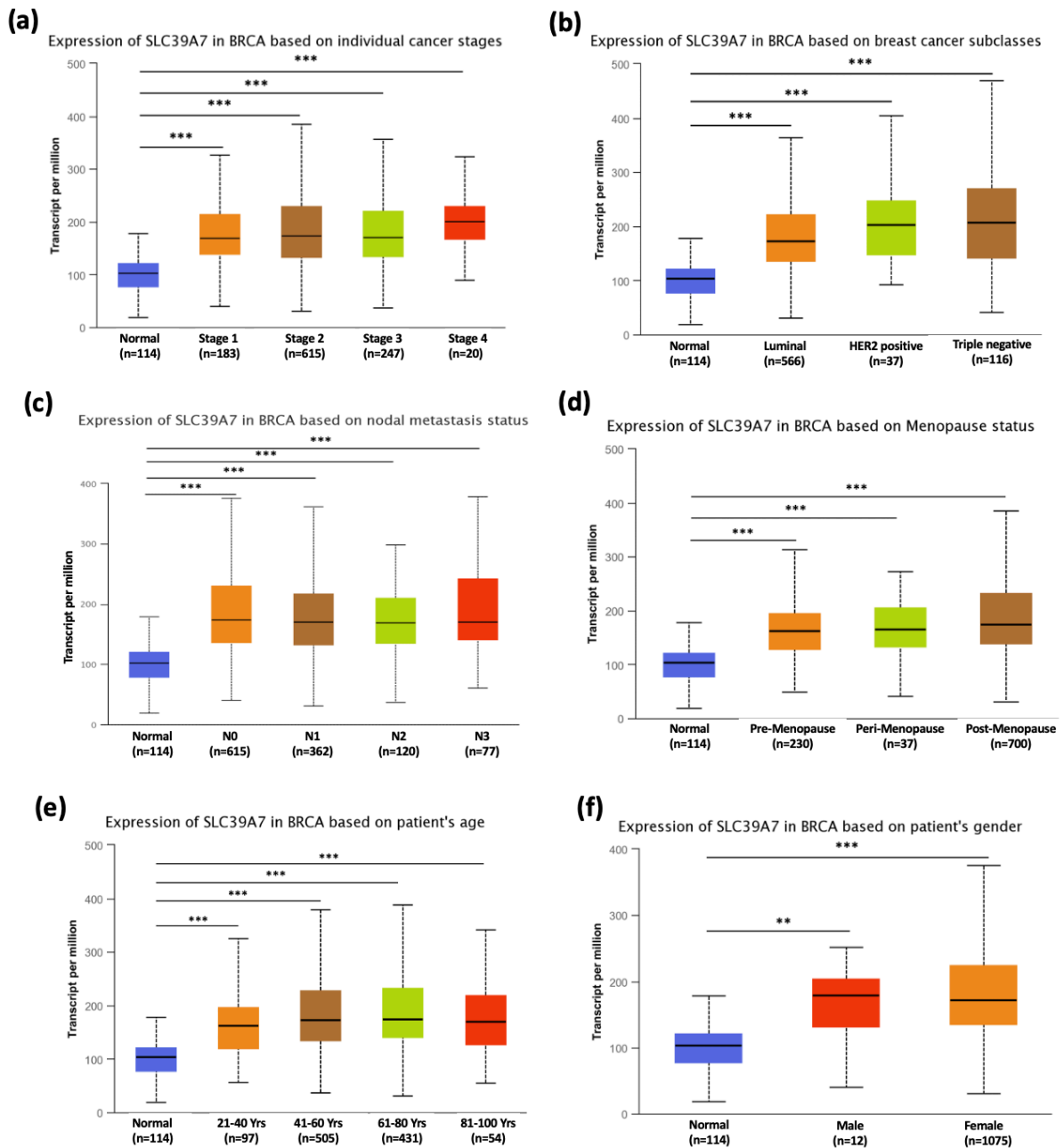


Figure 3.13 Box plot showing the expression of ZIP7 in subgroups of breast invasive carcinoma samples (BRCA) from UALCAN database.

Box plots showing ZIP7 expression according to **(a)** tumour stage. **(b)** subclasses. **(c)** nodal metastasis status. N0=no regional lymph node metastasis, N1=metastases in 1 to 3 axillary lymph nodes, N2= Metastases in 4 to 9 axillary lymph nodes, N3= metastases in 10 or more axillary lymph node. **(d)** menopause status. **(e)** patient's age. **(f)** gender. Data obtained from UALCAN database (Chandrashekar et al.2017). Data are mean \pm SE. ** $P < 0.01$, *** $P < 0.001$. BRCA= breast invasive carcinoma samples.

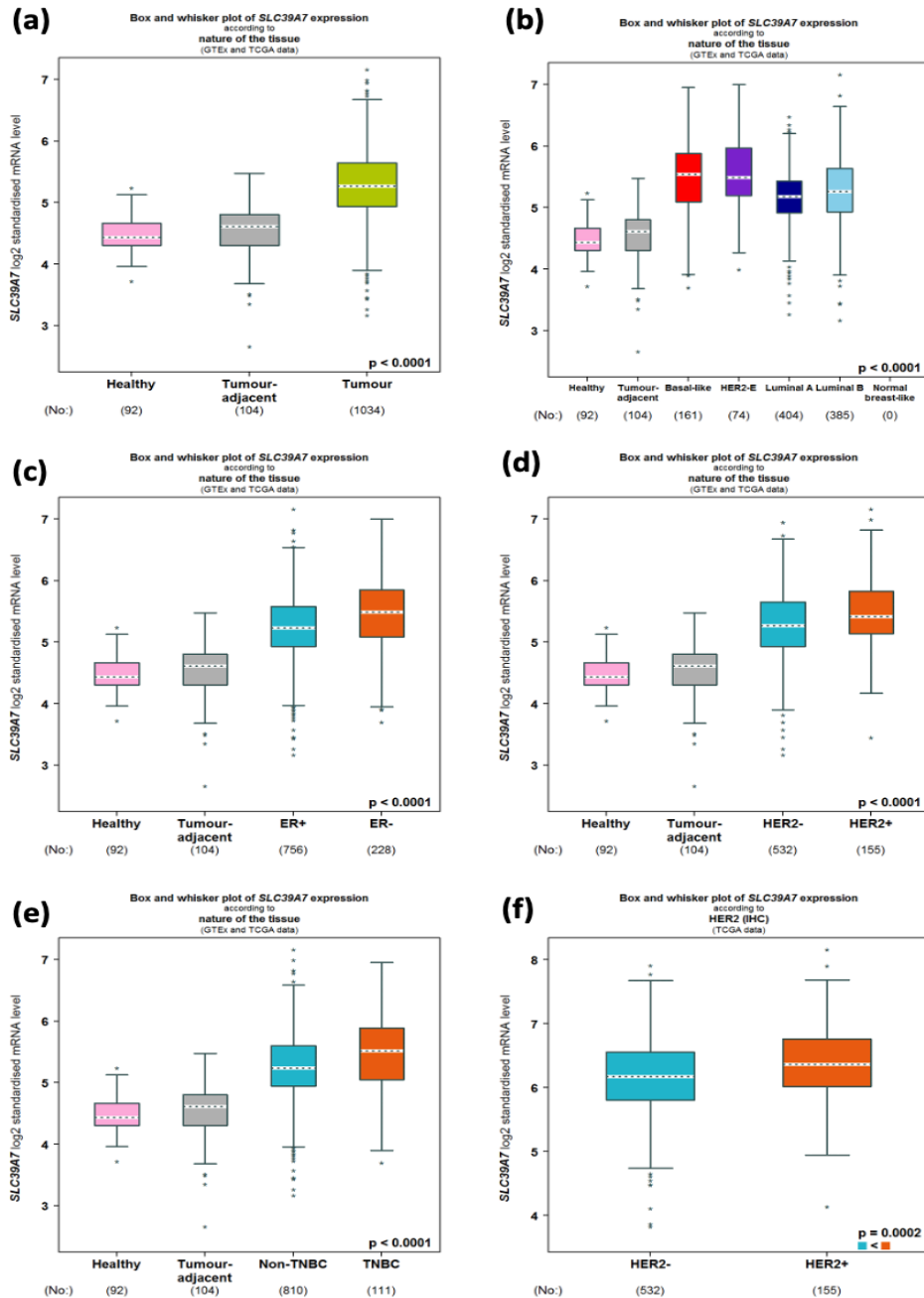


Figure 3.14 Differential expression of ZIP7 in patients with different type of breast cancer using bc-GenExMiner.

(a) ZIP7 expression in breast cancer tissue compared to normal tissue. (b) ZIP7 expression according to different breast cancer subtypes. (c) ZIP7 expression in ER positive and ER negative breast cancer tissue. (D) ZIP7 expression in HER negative breast cancer and HER2 positive breast cancer tissue. (E) ZIP7 expression in patients with non-triple negative breast cancer (non-TNBC) and TNBC. (F) ZIP7 expression in HER2 negative breast cancer and HER2 positive breast cancer tissue according to immunohistochemistry data. These data were obtained from bc-GenExMiner (Jezequel et al, 2012).

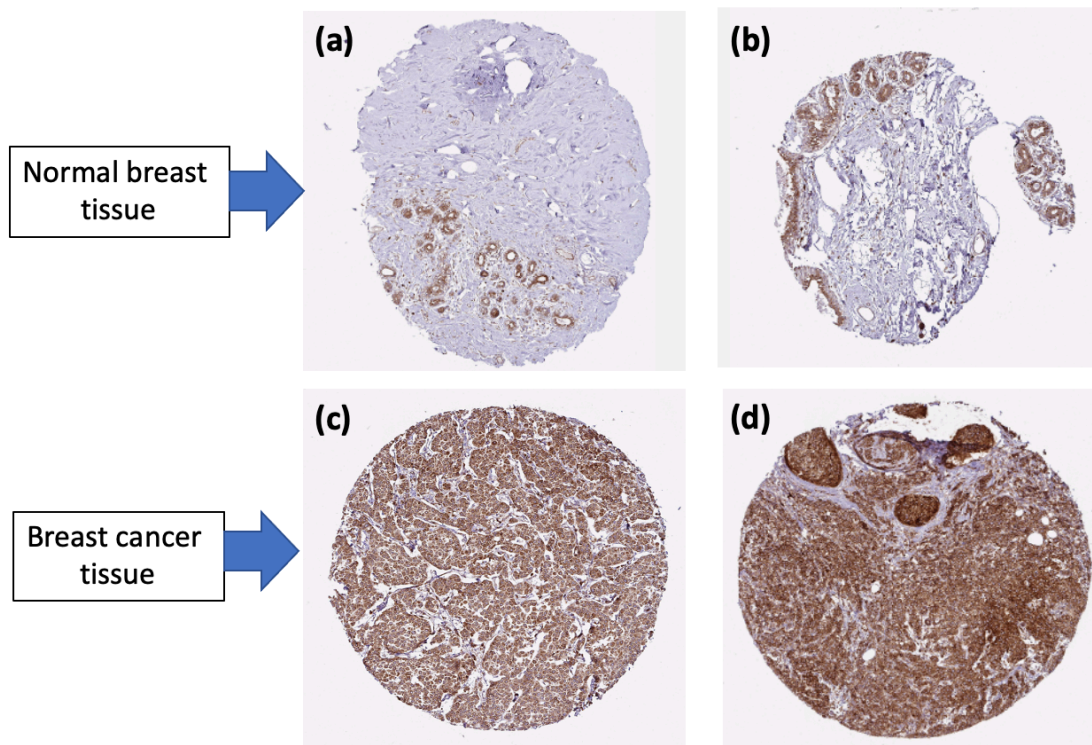


Figure 3.15 Immunohistochemistry of ZIP7 gene in breast cancer and normal breast tissue from the Human Protein Atlas (HPA).

(a) Protein level of ZIP7 in normal breast tissue was from a 27 years-old female (antibody, HPA053999; patient ID, 3856; staining, medium; intensity, moderate). **(b)** Protein level of ZIP7 in normal breast tissue was from a 45 years-old female (antibody, HPA053999; patient ID, 3544; staining, medium; intensity, moderate). **(c)** The protein level of ZIP7 in breast cancer tissue was from a 55 years-old female (antibody, HPA053999; patient ID, 1775; staining, high; intensity, strong). N=normal, T=tumour. **(d)** The protein level of ZIP7 in breast cancer tissue was from a 59 years-old female (antibody, HPA053999; patient ID, 2805; staining, high; intensity, strong).

3.3.9 ZIP7 expression predicts the outcome of patient survival in breast cancer

To evaluate the clinical significance of ZIP7, Kaplan Meier Plotter tools were used to explore the correlation between ZIP7 expression and the survival of breast cancer patients with different molecular subtypes. Kaplan–Meier Plotter (<http://www.kmplot.com>) is an online public database evaluating the effect of 54,000 genes on the clinical outcome of patients with 21 different types of cancer, including 7.830 samples of breast^{187–189}. This online tool is handled by a PostgreSQL server that can simultaneously integrate gene expression and clinical data^{187,224}. Gene expression data and the survival information are derived from the Gene Expression Omnibus (GEO), The Cancer Genome Atlas (TCGA) and European Genome-phenome Atlas (EGA). The primary purpose of the tool is the meta-analysis-based discovery and validation of survival biomarkers.

For the prognostic value of the SLC39A7 gene (ZIP7), the Kaplan–Meier curves were plotted for SLC39A7 (Affymetrix ID: 202667_s_at) in different breast cancer subtypes. The cut-off value of gene expression was chosen as auto select best cut-off, which split the patient samples into two groups and plots generated accordingly. A collection of clinical data, including human epidermal growth factor receptor 2 (HER2) status and lymph node status, were collected. The Kaplan-Meier survival plots with number at risk, hazard ratio (HR), 95% confidence intervals (CI) and log-rank P-values were obtained using the Kaplan-Meier plotter website. *P*-value < 0.05 was considered to be a statistically significant difference between high and low ZIP7 expression. The horizontal axis represents the time of the event, and the vertical axis shows the estimated probability of survival. The log-rank test compares the survival of two groups, giving a *p*-value to know the statistically significant difference between the two groups²²⁵. The HR will show the increased rate of having an event in one curve versus the other²²⁶. Every time an event occurs, the survival probability drops until the end of the study period or when the number of patients at risk is 0. The number of patients at risk are listed below the time axis. Evaluation the association of SLC39A7 gene (ZIP7) with relapse-free survival (RFS), overall survival (OS) and distant metastasis-free survival (DMFS) was performed. The event of interest in OS curves is death. The vertical dash in the survival

curve represents the censored observations when the information about patient survival time is incomplete either for a patient who does not experience the event of interest for the duration of the study, or a patient drops out of the study before the end of the study observation and did not experience the event. So, in other words, the censored data is a type of missing data.

To identify the clinical relevance of ZIP7 expression in breast cancer, the correlation between ZIP7 expression and clinic pathological parameters such as HER status and lymph node status were examined. Kaplan Meier survival curves for ZIP7 expression were plotted using the website. The results showed that higher expression of ZIP7 displayed a poor RFS (n=4929, HR=1.39, 95% CI 1.25-1.55, P-value =9.3e-10), OS (n=1879, HR=1.26, 95% CI 1.03-1.55, P-value =0.026), DMFS (n=2765, HR=1.24, 95% CI 1.05-1.46, P-value =0.01) than patients with low ZIP7 expression. **Figure 3.16 a,b,c** and **Table 3.5** present the prognostic effect of the expression of ZIP7 in breast cancer.

Lymph nodes (LN) have an important role in the staging and treatment of breast cancer. The lymph node called lymph node positive if it has some cancer cells²²⁷. Breast cancer cells in the lymph nodes under arm suggests an increased risk of cancer spreading. Survival analysis showed that LN positive patients with high ZIP7 overexpression displayed worse RFS (n=1656, HR=1.43, 95% CI 1.2-1.7, P-value =5.3e-05), OS (n=452, HR=1.75, 95% CI 1.22-2.5, P-value =0.002), and DMFS (n=889, HR=1.4, 95% CI 1.03-1.88, P-value =0.029) than low ZIP7 expression. **Figure 3.16 d,e,f** and **Table 3.5** present the prognostic effect of the expression of ZIP7 in relation to lymph node involvement.

Human epidermal growth factor receptor 2 (HER2) plays a pivotal function in breast cancer development and progression. To confirm the key role of ZIP7 in the presence of HER2, Kaplan-Meier survival analysis was conducted, as shown in **Figure 3.16 g,h,i**. High ZIP7 expression was associated significantly with poor survival in HER2+ patients RFS (n=882, HR=1.92, 95% CI 1.44-2.54, P-value =4.40e-06), OS (n=420, HR=2.1, 95% CI (1.28-3.42), P-value =0.0025), and DMFS (n=451, HR=1.62, 95% CI (1.06-2.49), P-value =0.024) compare to low ZIP7 expression. These results suggest that ZIP7 is significantly associated with poor prognosis in breast cancer patients who are HER2 positive.

In summary, as a cancer-progression driving oncogene, ZIP7 overexpression is associated with disease progression and malignant prognosis of LN+ and HER2+ breast cancer patients. So ZIP7 could be used as a predictive biomarker that might have clinical utility and act as a therapeutic target for breast cancer.

Breast cancer subtypes	RFS			OS			DMFS		
	N	HR	P-value	N	HR	P-value	N	HR	P-value
Total	4929	1.39 (1.25-1.55)	9.30E-10	1879	1.26 (1.03-1.55)	0.026	2765	1.24 (1.05-1.46)	0.01
LN+	1656	1.43 (1.2-1.7)	5.30E-05	452	1.75 (1.22-2.5)	0.002	889	1.4 (1.03-1.88)	0.029
HER2+	882	1.92 (1.44-2.54)	4.40E-06	420	2.1 (1.28-3.42)	0.0025	451	1.62 (1.06-2.49)	0.024
ER+	3768	1.38 (1.21-1.57)	8.80E-07	1309	1.32 (1.05-1.67)	0.018	2016	1.32 (1.08-1.62)	0.0063
Tamoxifen treated ER+ patients	725	1.66 (1.2-2.31)	0.0022	108	1.79 (0.83-3.84)	0.13	547	1.82 (1.18-2.81)	0.0061

Table 3.5 Relationship between ZIP7 expression and patients with breast cancer.

P-value < 0.05 was considered to be statistically significant difference. Abbreviations: *OS*; overall survival, *RFS*; relapse-free survival, *DMFS*; distant metastasis-free survival, N; number of patients, LN+; lymph node positive. HER2+; Human epidermal growth factor receptor 2 positive. ER+; estrogen receptor positive.

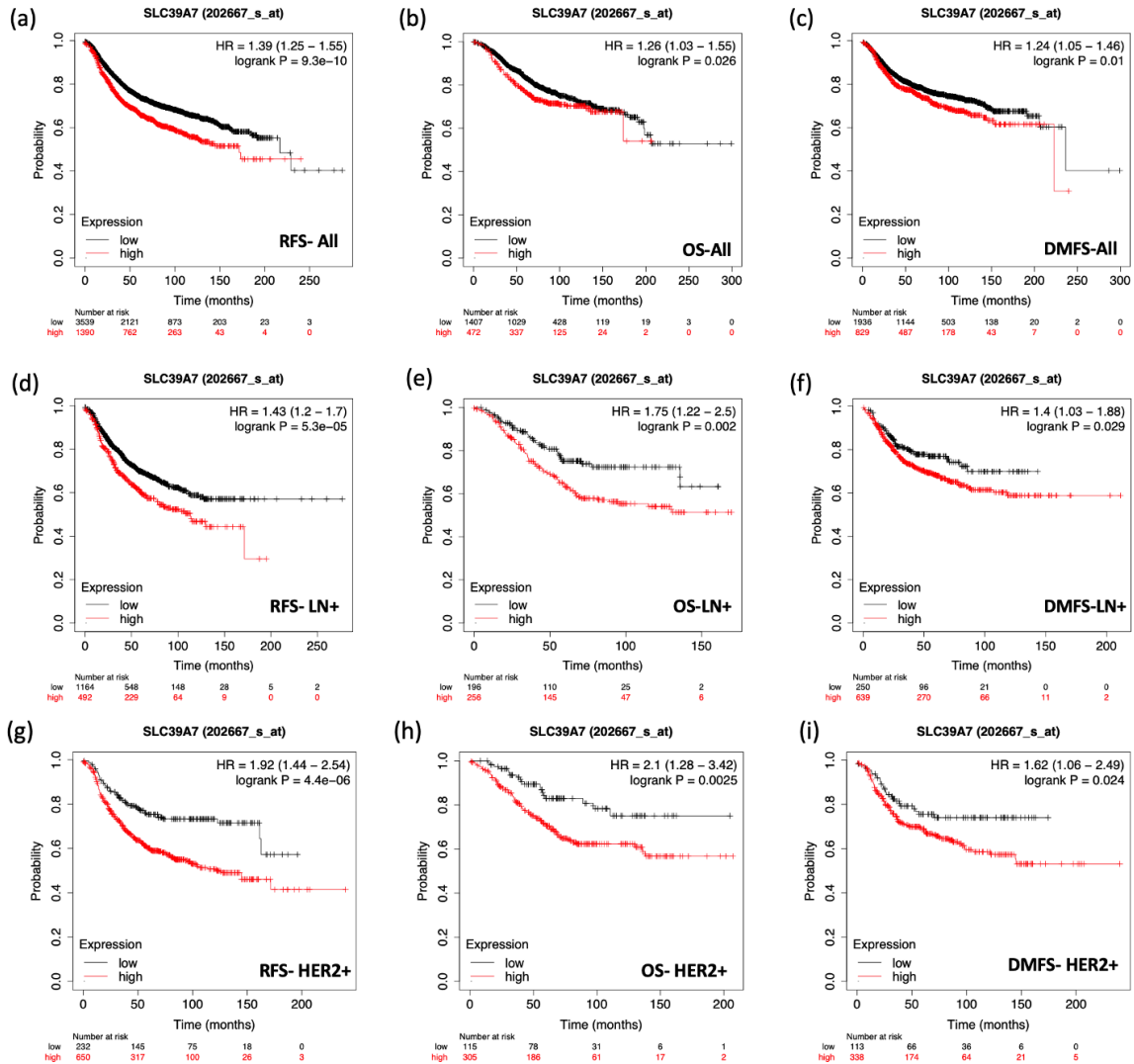


Figure 3.16 Kaplan-Meier survival plots show that higher expression of SLC39A7 lead to worse survival

Kaplan-Meier survival curves of breast cancer patients based on ZIP7 expression status (black lines indicate patients with low ZIP7 expression; red lines indicate patients with high ZIP7 expression). **(a)** RFS curve of breast cancer with ZIP7 status of 4929 breast cancer patients ($p=9.3e-10$). **(b)** OS curve of breast cancer with ZIP7 status of 1879 breast patients ($p=0.026$). **(c)** DMFS curve of breast cancer with ZIP7 status of 2765 breast patients ($p=0.01$). **(d)** RFS curve according to ZIP7 expression status of 1656 LN-positive breast cancer patients ($p=5.3e-05$). **(e)** OS curve according to ZIP7 expression status of 452 LN-positive breast cancer patients ($p=0.002$). **(f)** DMFS curve according to ZIP7 expression status of 889 LN-positive breast cancer patients ($p=0.029$). **(g)** RFS curve according to ZIP7 expression status of 882 HER2-positive breast patients ($p=4.40e-06$). **(h)** OS curve according to ZIP7 expression status of 420 HER2-positive breast patients ($p=0.0025$). **(i)** DMFS curve according to ZIP7 expression status of 451 HER2-positive breast patients ($p=0.024$). Kaplan-Meier survival plots show that higher expression SLC39A7 leads to worse survival. The p-values were calculated using the log-rank test. Vertical hash marks indicate censored data. Abbreviations: *OS*; overall survival, *RFS*; relapse-free survival; *DMFS*, distant metastasis-free survival; *LN*, lymph node; *HER2*, Human epidermal growth factor receptor 2.

3.3.10 The expression of ZIP7 gene in ER⁺ breast cancer patients receiving

Tamoxifen treatment:

Breast cancer is the second most diagnosed cancer worldwide and the most common among women²²⁸. The most common type of breast cancer is oestrogen receptor-positive breast cancer (ER⁺), targeted with endocrine therapy, including tamoxifen²²⁹. Unfortunately, some patients treated with endocrine agents develop a resistance resulting in disease relapse and cancer recurrence during treatment^{229,230}. So, it is essential to discover a new target to control the aggressive type of breast cancer. Tamoxifen resistance breast cancer model (TamR) has a higher zinc level⁶⁹ and ZIP7 gene expression⁵⁷ compared to MCF-7. ZIP7 activates downstream tyrosine kinases pathways such as EGFR and IGF-1R, which drive tamoxifen resistance breast cancer growth⁶⁹. Kaplan-Meier survival curves were plotted to assess the association of ZIP7 gene expression with the survival of tamoxifen-treated ER⁺ patients.

High ZIP7 expression in breast cancer patients with oestrogen receptor positive displayed worse RFS (n=3768, HR=1.38, 95% CI 1.21-1.57, P-value =8.8e-07), OS (n=1309, HR=1.32, 95% CI 1.05-1.67, P-value =0.018), and DMFS (n=2016, HR=1.32, 95% CI 1.08-1.62, P-value =0.0063) than low ZIP7 expression. **Figure 3.17 a,b,c** and **Table 3.5** present the prognostic effect of the expression of ZIP7 in relation to oestrogen receptor positive breast cancer.

Tamoxifen is the most common drug used in hormonal therapy²²⁹. Kaplan Meier analysis revealed ZIP7 expression was significantly associated with worse RFS (n=725, HR=1.66, 95% CI 1.2-2.31, P-value =0.0022), OS (n=108, HR=1.79, 95% CI 0.83-3.84, P-value =0.13), and DMFS (n=547, HR=1.82, 95% CI 1.18-2.81, P-value =0.0061) in tamoxifen-treated ER⁺ patients than low ZIP7 expression (**Figure 3.17 d.e.f**). These results show that ZIP7 expression is significantly associated with poor survival in tamoxifen-treated ER⁺ patients, suggesting that ZIP7 is a potential prognostic biomarker in tamoxifen-treated patients.

In summary, high ZIP7 expression is associated with an increased risk of cancer mortality, especially in ER⁺ breast cancer patients with tamoxifen resistance. So, the results of this study

further indicate the importance of ZIP7 expression level in the prognosis of breast cancer, and ZIP7 represents a potential therapeutic target to circumvent endocrine resistance.

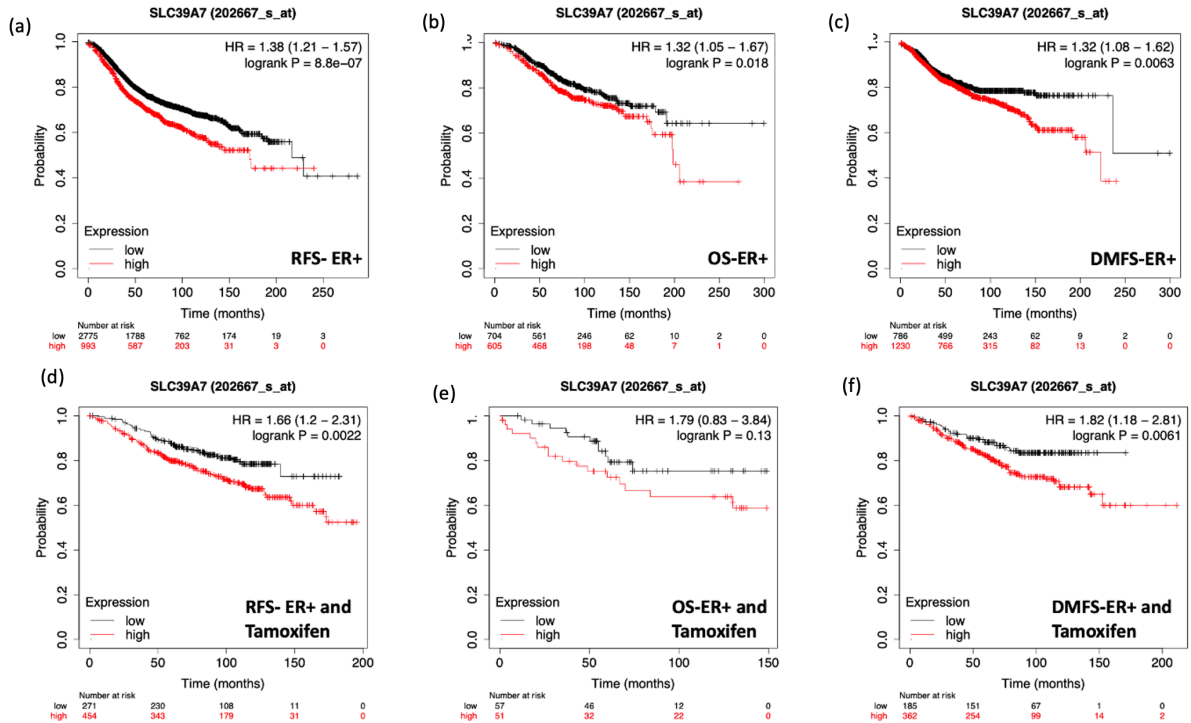


Figure 3.17 Kaplan-Meier survival plots show that higher expression of SLC39A7 leads to worse survival in tamoxifen treated ER+ breast cancer patients

Kaplan-Meier survival curves of breast cancer patients based on ZIP7 expression status (black lines indicate patients with low ZIP7 expression; red lines indicate patients with high ZIP7 expression). **(a)** RFS curve according to ZIP7 expression status of 3768 ER-positive breast cancer patients ($p=8.80e-07$). **(b)** OS curve according to ZIP7 expression status of 1309 ER-positive breast cancer patients ($p=0.018$). **(c)** DMFS curve according to ZIP7 expression status of 2016 ER-positive breast cancer patients ($p=0.0063$). **(d)** RFS curve according to ZIP7 expression status of 725 tamoxifen-treated ER+ patients ($p=0.0022$). **(e)** OS curve according to ZIP7 expression status of 108 tamoxifen-treated ER+ patients ($p=0.13$). **(f)** DMFS curve according to ZIP7 expression status of 547 tamoxifen-treated ER+ patients ($p=0.0061$). The p-values were calculated using the log-rank test. Vertical hash marks indicate censored data. Abbreviations: OS; overall survival, RFS; relapse-free survival, DMFS; distant metastasis-free survival, LN; lymph node. HER2; Human epidermal growth factor receptor 2.

3.4 Chapter Summary

The computer analysis of the LIV-1 subfamily showed that all members contain eight transmembrane domains with an extended N-terminus containing the CPALLY motif except for ZIP7 and ZIP13. Also, a metalloprotease motif (HEXPHEXPHGD) is in TM5, and uniformly presented in the LIV-1 subfamily. ZIP7 is known to be phosphorylated by CK2 on the two adjacent serine residues S275 and S276¹⁶⁹. Exploring other phosphorylation sites of ZIP7 showed that S293 and T294 are interesting, predicted phosphorylation sites, which will be further investigated experimentally in the next chapter. Furthermore, ZIP7 is predicted to have three nuclear localization signals suggesting that these signals have a role in ZIP7 nuclear localization. ZIP7 show a clear nuclear ring around the nucleus under the microscope which suggest nuclear localization of ZIP7. This hypothesis will be further investigated experimentally in this thesis.

Breast cancer is the most common cause of cancer-related death among all human cancers²²⁸. This chapter aimed to characterize ZIP7 gene expression and survival outcome in different subtype of breast cancer tissue samples. Bioinformatic analysis of ZIP7 with different clinical parameters and survival data was performed to investigate the ZIP7 expression in breast cancer patients using several online tools. Genome-wide profiling offers insights into tumorigenesis and proves to be an efficient way to identify pathogenic genes thoroughly²³¹. For the first time, a large cohort of human breast cancer samples was investigated to understand the role of ZIP7 in breast cancer. The current study investigated the mRNA expression pattern and survival outcome through large databases, including GEPIA, UALCAN, bc-GenExMiner, Human Protein Atlas (HPA), and Kaplan–Meier Plotter. ZIP7 expression was explored as a prognostic biomarker for breast cancer and correlated with various clinical factors of breast cancer samples such as cancer stage, tumour grade, subtype, and nodal metastases status. ZIP7 expression was significantly higher in breast tumour samples than the normal breast by GEPIA, UALCAN, and bc-GenExMiner, which suggests that ZIP7 may play an essential role in the progression of breast cancer. Also, ZIP7 expression is associated with tumour stages, and aggressive types of breast cancer, suggesting ZIP7 is associated with breast cancer tumorigenesis and progression and can be a promising biomarker for breast cancer. ZIP7

overexpression was associated with poor survival in breast cancer patients, suggesting that ZIP7 may have a “driver” function in breast cancer progression.

In conclusion, in this chapter, we determined that ZIP7 may be a critical gene in the development and prognosis of breast cancer through bioinformatic analysis. The data represented here is mainly focused on the mRNA expression level of ZIP7 which showed the possible role of ZIP7 in aggressive breast cancer. It would be valuable to analyse the protein expression level to see if it will mirror what have been represented here of ZIP7 RNA level. The rest of this thesis will attempt to investigate the protein level of ZIP7 and its cellular localization to understand its relevance in breast cancer. These data will provide a better understanding the molecular biology of potential drug targets in breast cancer.

4. Chapter 4: Investigating ZIP7 activation mechanisms and analysis of endoplasmic reticulum retention signals of ZIP7

4.1 Introduction:

Zinc is an essential trace element that has been implicated in many diseases, including breast cancer. ZIP7 is involved in the development of tamoxifen resistance in breast cancer and contributes to the aggressive behaviour of tamoxifen resistant cells⁶⁹. The bioinformatics data in the previous chapter showed that higher ZIP7 gene expression is associated with poor clinical outcomes of breast cancer. ZIP7 is known to be phosphorylated on S275 and S276 by CK2¹⁶⁹. Staining with our pS²⁷⁵S²⁷⁶ZIP7 antibody, which only recognizes ZIP7 when activated by phosphorylation, showed considerable increases in our tamoxifen resistant breast cancer cell line (TAMR), suggesting that pZIP7 could be used as a biomarker in this aggressive type of breast cancer¹⁶⁷. The previous study showed that this pZIP7 antibody was specific to ZIP7 when it was phosphorylated on S275 and S276⁷⁴, which will be further explored in this chapter.

Previous work in our group has confirmed that the phosphorylation of both S275 and S276 is needed to activate ZIP7¹⁶⁹. Database searching in an earlier chapter has predicted other phosphorylation sites on ZIP7. These are residues S293 and T294 and they are positioned in the same cytoplasmic loop as S275 and S276. This chapter will examine the role of these residues by using two ZIP7 mutations, namely S293A and T294A, where the active site residue has been replaced with an alanine, which will prevent phosphorylation. The role of these residues in ZIP7 activation will be examined using immunofluorescence and western blot techniques. ZIP7, located on the ER, is the hub for zinc release into the cytoplasm, which directly activates AKT, MAPK, and mTOR, all known to drive cell survival and proliferation⁷⁴. Using different online databases, it was discovered that ZIP7 is predicted to have four endoplasmic reticulum retention signals. Alanine mutations were generated to remove these sites in order to assess the function of these motifs on ZIP7 ER localisation and ZIP7 phosphorylation status. Immunofluorescence was performed to confirm the transfection

efficiency and the cellular localisation of the mutants. Colocalisation of all these mutants was examined with specific ER located proteins and was investigated by immunofluorescence.

4.2 Methods

DNA constructs of all ZIP7 mutant constructs have been inserted into an ampicillin-resistant plasmid vector and were amplified by the transformation of the single-use JM109 *E.coli* component cells (Promega). The plasmids of ZIP7 mutant constructs were purified using the EndoFree Plasmid Maxi Kit (Qiagen). A UV spectrophotometer was used to determine the DNA concentration at 260 nm (OD260) (**Table 4.1**). Please refer to Chapter 2 for the methods of transfection (Section 2.1.2) and zinc treatment (Section 2.1.3), site-directed mutagenesis (2.2), plasmid preparation (Section 2.3), immunofluorescence (Section 2.4), and western blotting (Section 2.5).

Table 4.1 Plasmid DNA concentration

Construct	Concentration ($\mu\text{g}/\mu\text{L}$)
WT ZIP7	3.656
ZIP7 S275A S276A (ZIP7AA)	2.6
ZIP7 S275D S276D (ZIP7 DD)	2.912
ZIP7 S293A	0.324
ZIP7 T294A	1.475
ZIP7 ER1A	1.777
ZIP7 ER1B	1.717
ZIP7 ER2	1.551
ZIP7 ER3	1.618
ZIP7 ER4	1.673

4.3 Results:

4.3.1 Using pZIP7 antibody to examine the timeline of ZIP7 activation after zinc treatment

The pZIP7 antibody has been developed in our group, and has been confirmed to only binds to ZIP7 when phosphorylated on residues S275 and S276, resulting in zinc release from the ER store to the cytosol¹⁶⁹. The epitope of pZIP7 consists of 12 amino acids with two phosphorylated sites TKEKQ pS pS EEEEEK (position 270-281) (**Figure 4.1**). To investigate the timeline of ZIP7 activation, western blot was performed on MCF-7 cells transfected with WT-ZIP7 and treated with zinc at different time points. A previous study observed that pZIP7 level increased from 2 minutes after zinc treatment in cells transfected with WT-ZIP7⁷⁴. The western blot showed a gradual increase of pZIP7 level after zinc treatment for only 2 minutes and with a significant increase after a 10 minutes of zinc treatment (**Figure 4.2**), which further confirmed the previous observation that zinc treatment of ZIP7 transfected cells increases ZIP7 mediated zinc release within 5 minutes as judged by AKT activation¹⁶⁹. According to these results, 10 minutes of zinc treatment was used in the following sections to investigate the downstream effect of different ZIP7 mutant constructs as that represented the significant response.

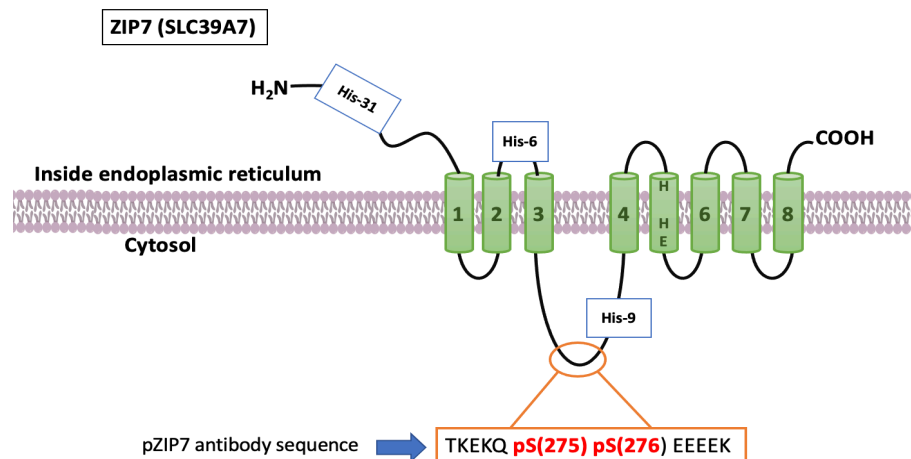


Figure 4.1: Binding site of pZIP7 antibody

pZIP7 is a monoclonal antibody consisting of 12 amino acids with two phosphorylated serine residues TKEKQ pS pS EEEEEK (position 270-281). His, Histidine Rich Repeat; SLC39A7, Solute carrier family 39 member 7

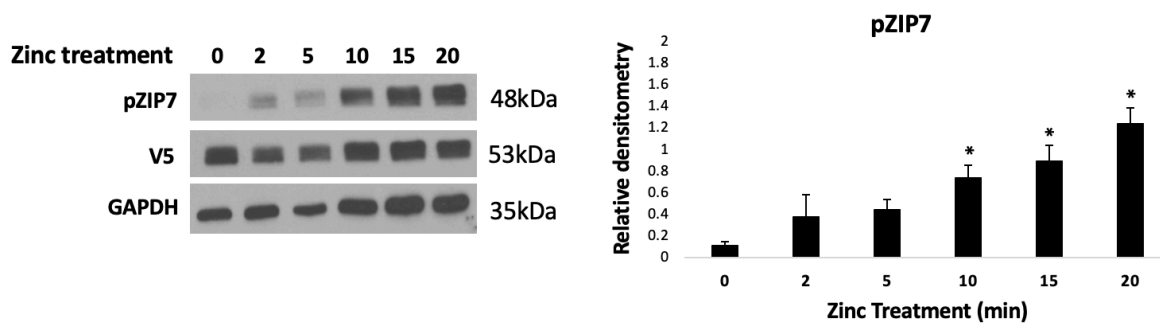


Figure 4.2 Gradual increase of pZIP7 level after zinc treatment.

Immunoblotting was performed in MCF7 cells transfected with WT-ZIP7 and treated with zinc at different time points. pZIP7 antibody, V5 antibody, and GAPDH were used to probe the membrane and protein bands of pZIP7 (48kDa), V5 (53kDa), and GAPDH (35kDa) were obtained. Densitometric data was normalised to V5 expression. ZIP7 phosphorylation levels are represented as a mean value of $n = 4 \pm$ standard error. The statistical significance was compared to time zero and is indicated by * ($p < 0.05$).

4.3.2 Verification of wild type ZIP7 and mutant constructs

To investigate the role of ZIP7 in cancer, recombinant constructs of wild-type ZIP7 and mutant ZIP7 have been made, as shown in the methods chapter. The recombinant constructs of WT-ZIP7 and ZIP7 mutants were tested for their transfection efficiency and to verify that the mutants were located in the same cellular location as WT ZIP7. Immunofluorescence was performed by using a V5 tag antibody in MCF-7 cells transfected with WT-ZIP7 and mutant constructs. The V5 antibody binds to the carboxyl terminal V5 tag of plasmid constructs. **Figure 4.3** shows that MCF7 cells transfected with WT ZIP7 and ZIP7 mutants express the recombinant protein well (green) and clearly showed the ER localization pattern of ZIP7, which was consistent with the previous study that showed ZIP7 colocalization with the ER marker (Calreticulin) in CHO cells⁵⁸. The proportion of positive cells for the V5 tag in four random visual fields was calculated to measure the transfection rate. The transfection rates are 53% in cells overexpressing WT ZIP7, 46% in cells overexpressing ZIP7 AA, and 58% in cells overexpressing ZIP7 DD (**Figure 4.3**), therefore confirming they are equivalent.

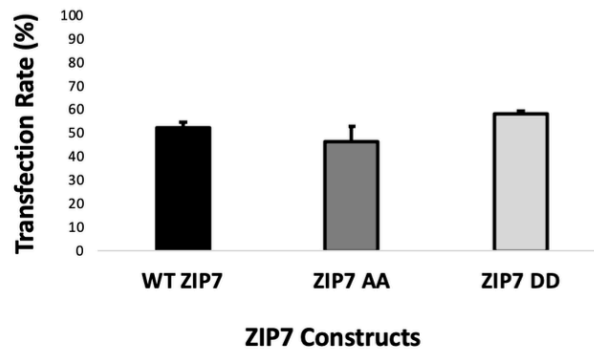
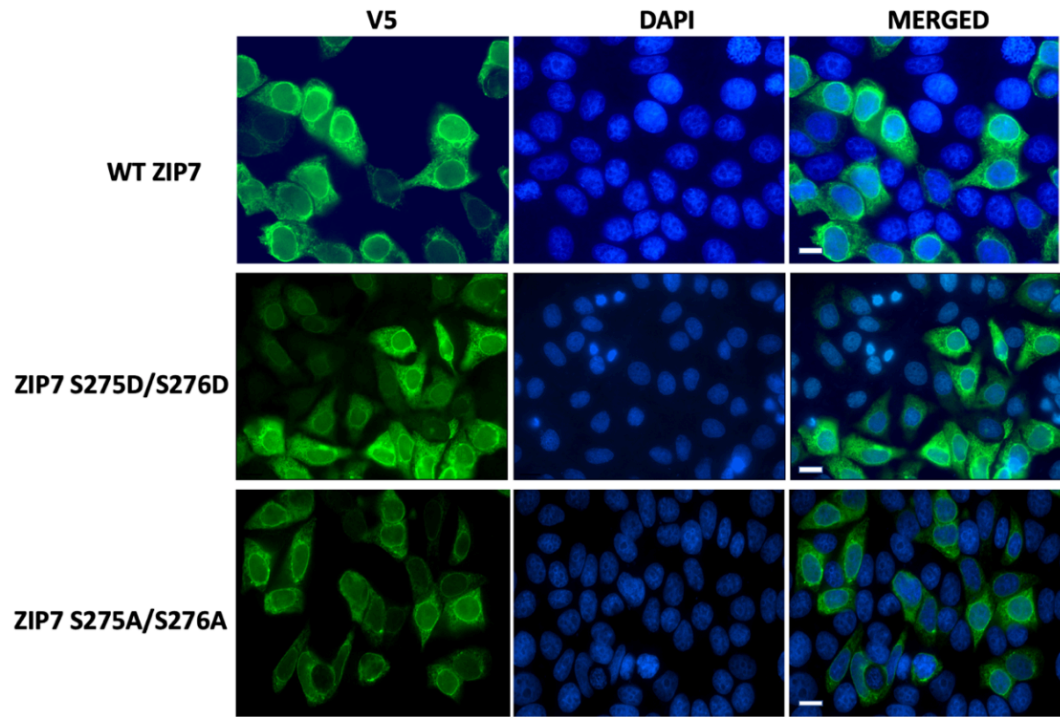


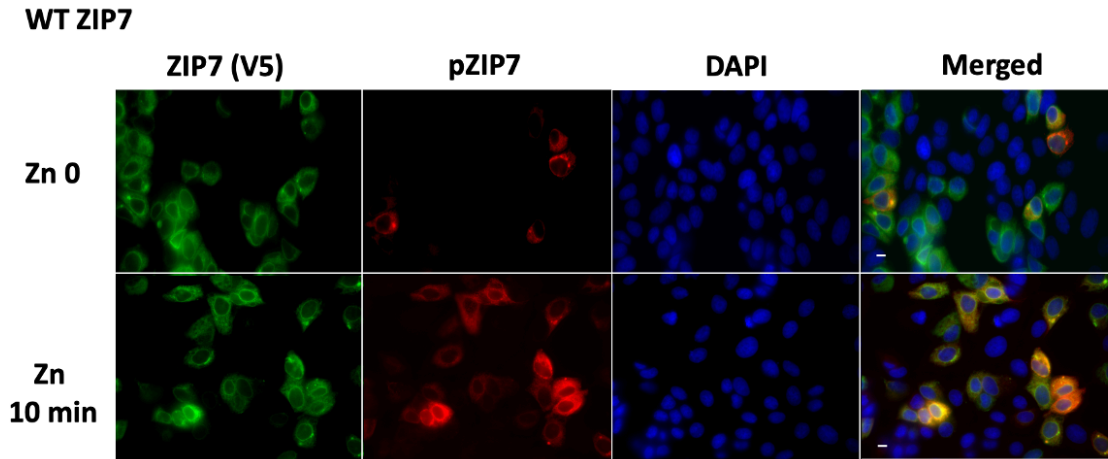
Figure 4.3: Transfection efficiency of WT ZIP7, S275A/S276A and S275D/S276D mutants

MCF-7 cells were transfected with wild-type and mutant ZIP7 for 18 hours. The cells were fixed and permeabilized before probing with rabbit V5 conjugated to Alexa Fluor 488 (green) and the nuclei were stained blue with DAPI. These images were captured with a Leica RPE Automatic Microscope using a 63x magnification lens. The transfection rates are demonstrated in a bar graph as the mean of four represented fields \pm standard error. Scale bar, 10 μ m.

4.3.3 Further confirmation by immunofluorescence that pZIP7 antibody only binds to phosphorylated ZIP7.

Cells transfected with either WT ZIP7 or different ZIP7 mutants were stained with our pZIP7 antibody to confirm the previous observation that this pZIP7 antibody only recognizes S275/S276 when they are phosphorylated⁷⁴. The mutants included a phospho-ablative (inactive) mutant (ZIP7 S275A/S276A) in which both serine 275 and serine 276 were replaced with alanine and a phospho-mimetic (constitutively active) mutant (ZIP7 S275D/S276D) in which the two serine residues were replaced with aspartate. Immunofluorescence results confirmed the ability of the pZIP7 antibody to recognize the cells transfected with WT ZIP7 and ZIP7 S275D/S276D mutants in basal conditions with no zinc treatment (**Figure 4.4 and 4.5**). To test the ability of the pZIP7 antibody to recognise the ZIP7-mediated zinc wave after zinc treatment, the cells transfected with WT ZIP7, ZIP7 S275D/S276D or ZIP7 S275A/S276A mutants were treated for 10 minutes. A significant increase in pZIP7 level was observed after 10 minutes of zinc treatment in cells transfected with both WT ZIP7 and ZIP7 S275D/S276D mutants (**Figure 4.4b and 4.5b**). These results further confirm that the monoclonal antibody pZIP7 can recognize a phosphorylated ZIP7^{74,169}. For the phospho-mimetic mutant, the pZIP7 level were expected to be high even at time zero because the antibody is able to bind to ZIP7 DD constructs without actual phosphorylation. However, the pZIP7 level in cells transfected with ZIP7 DD at time zero almost similar to cells transfected with WT ZIP7(**Figure 4.4 and 4.5**). In contrast, the pZIP7 antibody did not recognise any cells transfected with ZIP7 S275A/S276A mutants, confirming no pZIP7 staining was observed in basal conditions or after 10 minutes of zinc treatment (**Figure 4.6**). These results further confirm the previous results that showed the removal of two serine residues (S275/S276) prevented ZIP7 phosphorylation by CK2, and the pZIP7 antibody recognizes ZIP7 only when residues S275 and S276 are phosphorylated.

(a)



(b)

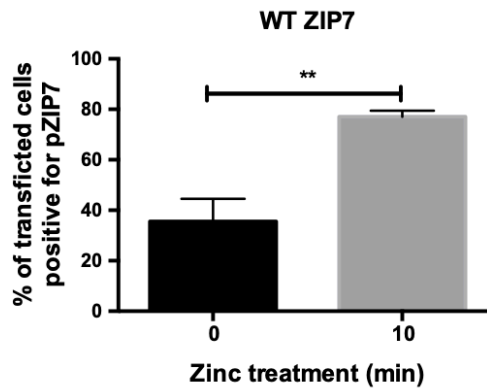


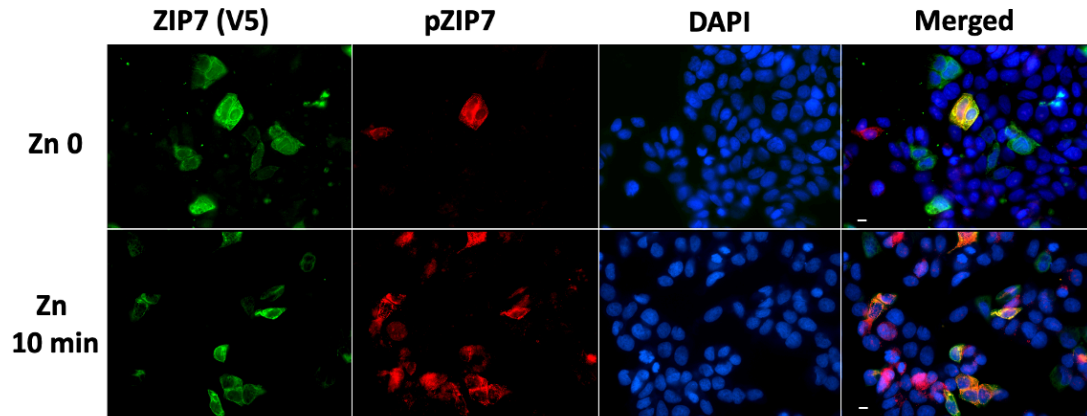
Figure 4.4 pZIP7 activation increased after zinc treatment in cells overexpress WT ZIP7.

(a) MCF-7 cells were transfected with WT ZIP7 for 18 hours. The cells were fixed and permeabilized before being probed with mouse pZIP7 antibody and rabbit V5 antibody conjugated to Alexa Fluor 594 (red) and Alexa Fluor 488 (green) respectively, and the nuclei were stained blue with DAPI. These images were captured with a Leica RPE automatic microscope using a 63x magnification lens. Scale bar, 10 μ m.

(b) This bar graph shows the percentage of transfected cells that are positive for pZIP7 as a mean of four different fields of view \pm standard error. ** = $p < 0.01$

(a)

ZIP7 S275D/S276D



(b)

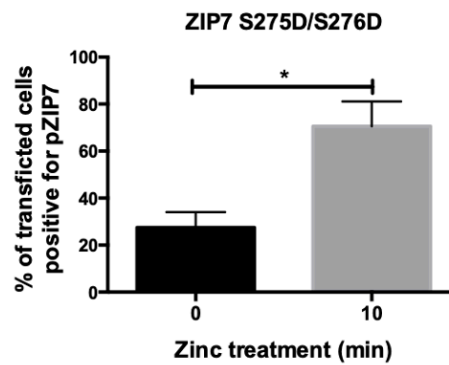


Figure 4.5 pZIP7 activation increased after zinc treatment in cells overexpress ZIP7 S275D/S276D.

(a) MCF-7 cells were transfected with ZIP7 S275D/S276D for 18 hours. The cells were fixed and permeabilized before being probed with mouse pZIP7 antibody and rabbit V5 antibody conjugated to Alexa Fluor 594 (red) and Alexa Fluor 488 (green) respectively, and the nuclei were stained blue with DAPI. These images were captured with a Leica RPE automatic microscope using a 63x magnification lens. Scale bar, 10 μ m.

(b) This bar graph shows the percentage of transfected cells that are positive for pZIP7 as a mean of four different fields of view \pm standard error. * $p < 0.05$

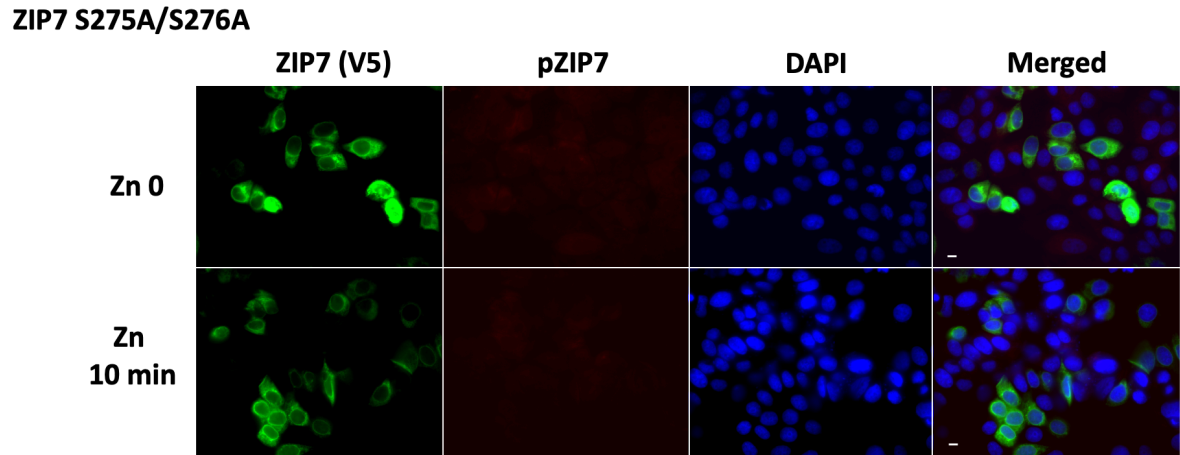


Figure 4.6 Characterization of ZIP7 S275A/S276A after zinc treatment.

MCF-7 cells were transfected with ZIP7 S275D/S276D for 18 hours. The cells were fixed and permeabilized before being probed with mouse pZIP7 antibody and rabbit V5 antibody conjugated to Alexa Fluor 594 (red) and Alexa Fluor 488 (green) respectively, and the nuclei were stained blue with DAPI. These images were captured with a Leica RPE automatic microscope using a 63x magnification lens. Scale bar, 10 μ m.

4.3.4 Confirmation of downstream effects of ZIP7 mediated zinc release:

ZIP7 phosphorylation by protein kinase CK2 leads to zinc release from intracellular stores, resulting in the activation of tyrosine kinases by inhibition of tyrosine phosphatases¹⁶⁹, which play an essential role in cancer growth and metastasis. To further confirm the previous observation that zinc treatment of ZIP7 transfected cells increases ZIP7 mediated zinc release, which in turn activates AKT¹⁶⁹, MCF7 cells were transfected with WT ZIP7, phospho-null ZIP7 (ZIP7 S275A/S276A), and phospho-mimetic ZIP7 (ZIP7 S275D/S276D) then treated with zinc for different time points to measure the level of activated pS⁴⁷³AKT. AKT is a

serine/threonine protein kinase involved in several cellular pathways of proliferation, growth, and invasion²³².

As expected, the cells that had not been transfected with ZIP7 showed no pS⁴⁷³AKT until 15 minutes after zinc treatment (**Figure 4.7A**). In contrast, cells transfected with WT ZIP7 showed increased pS⁴⁷³AKT, which was detected as soon as 2 minutes and significantly increased at 15 minutes after zinc treatments (**Figure 4.7B**). ZIP7 activation results in zinc release from the ER store, which inhibits protein tyrosine phosphatases and promotes activation of AKT⁶⁹. pS⁴⁷³AKT level in the cells transfected with the phospho-ablative mutant ZIP7 S275A/S276A does not respond in the same way as in the cells transfected with WT-ZIP7 did and only shows an increase after 20 minutes of zinc treatment when compared to time zero (**Figure 4.7C**), similarly to the un-transfected cells, confirming that this mutant does not activate ZIP7 mediated zinc release. This confirms that ZIP7 needs to be phosphorylated on S275 and S276 before it can release zinc. Cells transfected with the phospho-mimetic mutant ZIP7 (S275D S276D) showed a substantial increase in pS⁴⁷³AKT at 5 minutes after zinc treatment and a significant increase after 20 minutes of zinc treatment (**Figure 4.7D**), consistent with a fully active ZIP7 as expected. These results further confirm that AKT phosphorylation at residue S473 appears to be an immediate response to ZIP7-mediated zinc release from the cellular store.

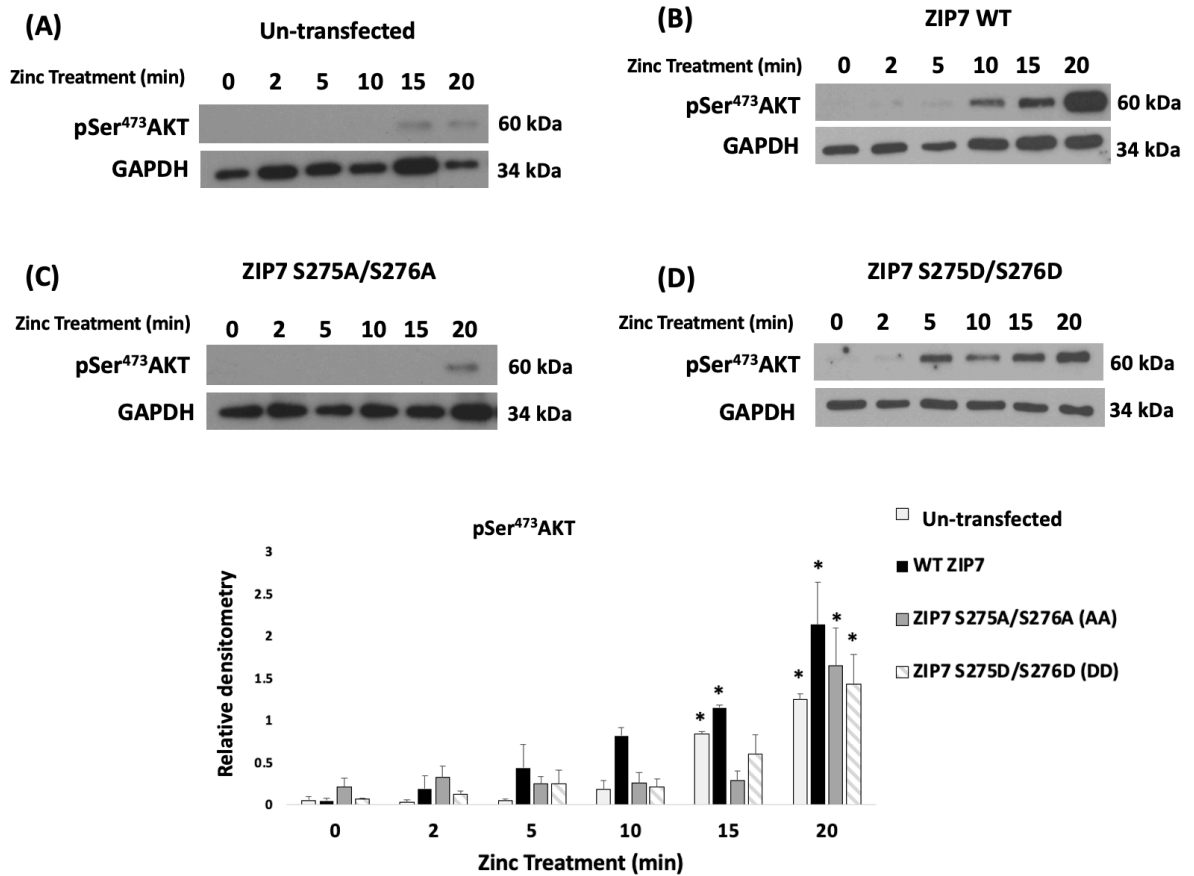


Figure 4.7 Downstream effect of ZIP7 mediated zinc release

Immunoblotting was performed in MCF7 cells transfected with WT-ZIP7 and ZIP7 mutant constructs and treated with zinc at different time points. pS⁴⁷³AKT antibody, and GAPDH were used to probe the membrane. Protein bands of pS⁴⁷³AKT (60 kDa), and GAPDH (35 kDa) are demonstrated. Densitometric data are normalised to GAPDH and demonstrated in relative density unit as mean values of $n = 3 \pm$ standard error. The statistical significance compared to the samples without zinc treatment, is indicated by * ($p < 0.05$)

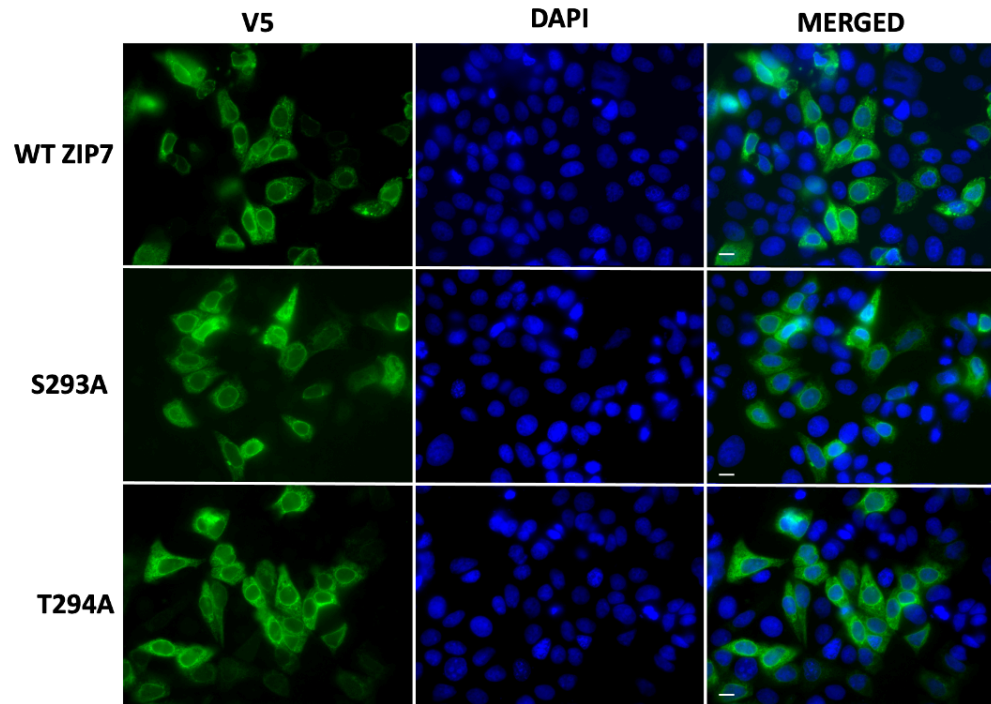
4.3.5 Effect of ZIP7 S293A and T294A mutants on ZIP7 activation:

The computer analysis in chapter 3 shows that ZIP7 is predicted to be phosphorylated on S293 and T294 in addition to S275 and S276. To investigate the effect of these sites on ZIP7 activation, these residues were individually removed by replacing them with alanine to prevent

phosphorylation. To verify the transfection efficiency and cellular localization of the mutants, immunofluorescence was performed by staining cells with a V5 tag antibody in MCF-7 cells transfected with WT-ZIP7 and mutant constructs. **Figure 4.8a** shows that MCF7 cells transfected with WT-ZIP7, S293A ZIP7, and T294A ZIP7 mutant constructs all express the recombinant protein well (green). The cells transfected with ZIP7 S293A and ZIP7 T294A show a 48% and 46% transfection rate, respectively, while cells transfected with WT-ZIP7 show a 51% transfection rate (**Figure 4.8b**). The transfection rate was calculated by counting the proportion of positive cells for the V5 tag in six random visual fields. There was no statistical difference between the transfection rate of WT ZIP7 and S293A and T294A mutant constructs (**Figure 4.8b**).

To investigate whether the S293A and T294A mutations altered the ZIP7 activation and the ability of the pZIP7 antibody to bind to ZIP7, immunofluorescence was performed in cells transfected with ZIP7 S293A and T294A with or without 10 minutes of zinc treatment. A V5 antibody was used to stain the transfected cells. For the cells transfected with WT ZIP7, the percentage of pZIP7 increased significantly from 20% to 92% after 10 minutes of zinc treatment (**Figure 4.9**). For ZIP7 S293A, the percentage of the positively transfected cells for pZIP7 increased from 43% before zinc treatment to 74% after zinc treatment (**Figure 4.10**). In cells transfected with ZIP7 T294A, the pZIP7 level was 45% before zinc treatment and increased to 78% after 10 minutes of zinc treatment (**Figure 4.11**). ZIP7 S293A and T294A have high pZIP7 level without zinc treatment suggesting that those mutants could have an inhibitory role on ZIP7. Also, these data suggested that the pZIP7 antibody could recognize ZIP7 S294A and T293A mutants, and these mutations may not interfere with the zinc -induced CK2-mediated phosphorylation on residues S275 and S276 of ZIP7.

(a)



(b)

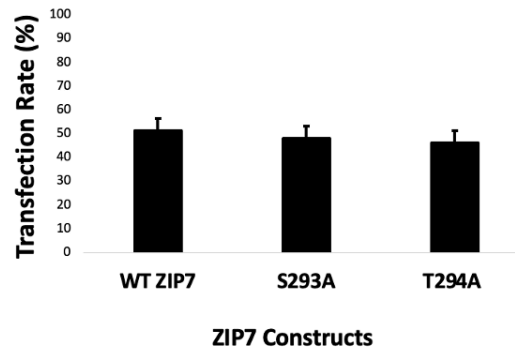
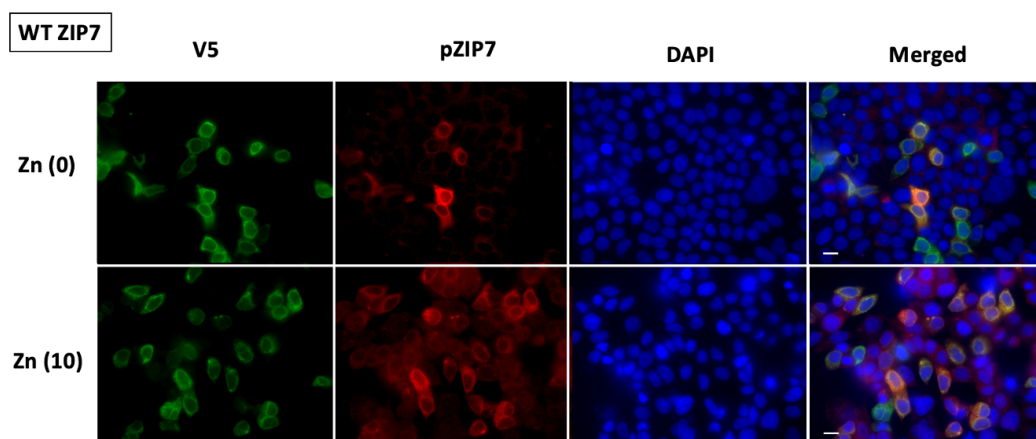


Figure 4.8: Transfection efficiency of WT ZIP7, S293A, and T294A constructs.

(a) MCF-7 cells were transfected with WT ZIP7 and mutant ZIP7 for 18 hours. The cells were fixed and permeabilized before probing with rabbit V5 antibody conjugated to Alexa Fluor 488 (green) and the nuclei were stained blue with DAPI. These images were captured with a Leica RPE automatic microscope using a 63x magnification lens. Scale bar, 10 μm **(b)** The transfection rate demonstrated in a bar graph as mean of six represented fields \pm standard error.

To confirm the immunofluorescence results, western blot was performed in the cells transfected with WT-ZIP7, ZIP7 S293A mutant or ZIP7 T294A mutant. The cells transfected with WT ZIP7 showed a significant increase in pZIP7 level after 10 minutes of zinc treatment (**Figure 4.12a**), leading to zinc release into the cytoplasm and tyrosine kinase activation. Also, the cells transfected with ZIP7 T294A mutant demonstrates a significant increase of pZIP7 after zinc treatment (**Figure 4.12c**), which suggests this construct's ability to be activated by zinc addition. On the contrary, cells transfected with the ZIP7 S293A mutant showed an increase of pZIP7 after 10 minutes of zinc treatment, but no significant difference compared to the time zero (**Figure 4.12b**), which suggests that S293A is required for ZIP7 maximal activation. The results were represented as a percentage of the untreated control state to understand how ZIP7 S293A and T294A mutant response differently to zinc stimulation. This showed that the WT ZIP7 and T294A were statistically increased after 10 minutes of zinc treatment while the S293A mutant showed an increase in the level of pZIP7 after zinc treatment but not statistically significant compared to the time zero (**Figure 4.12D**), suggesting that residue S293 may play a role in ZIP7 activation.

(a)



(b)

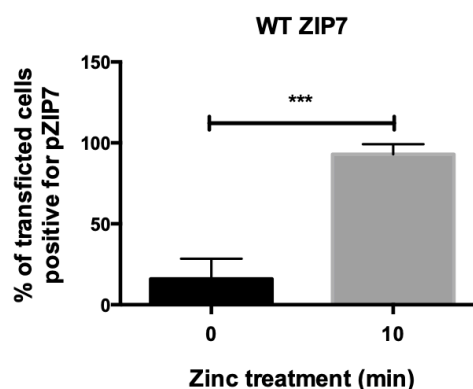
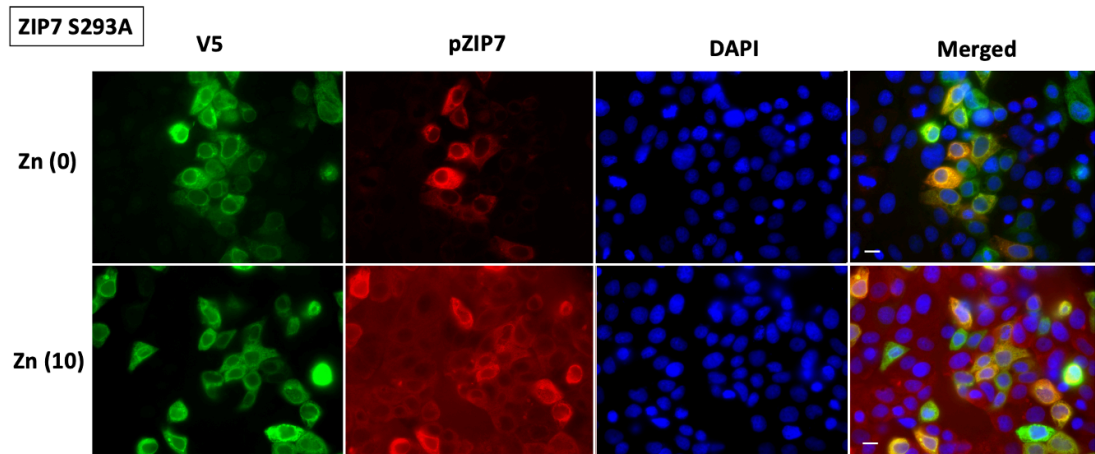


Figure 4.9 pZIP7 antibody ability to detect ZIP7 activation in cells transfected with WT ZIP7.

(a) MCF-7 cells were transfected with WT ZIP7 for 18 hours. The cells were fixed and permeabilized before probing with mouse pZIP7 antibody and rabbit V5 antibody conjugated to Alexa Fluor 594 (Red) and Alexa Fluor 488 (Green) respectively, and the nuclei were stained blue with DAPI. These images were captured with a Leica RPE automatic microscope using a 63x magnification lens. Scale bar, 10 μ m. **(b)** The transfection rate demonstrated in a bar graph as mean of three represented fields \pm standard error.

(a)



(b)

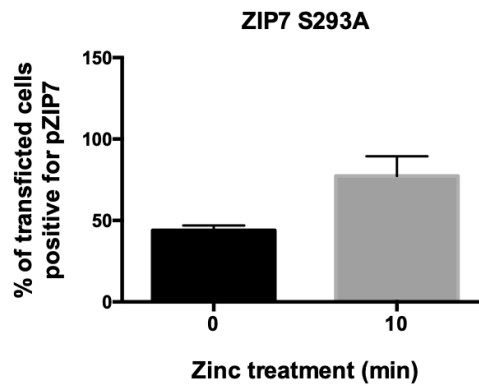
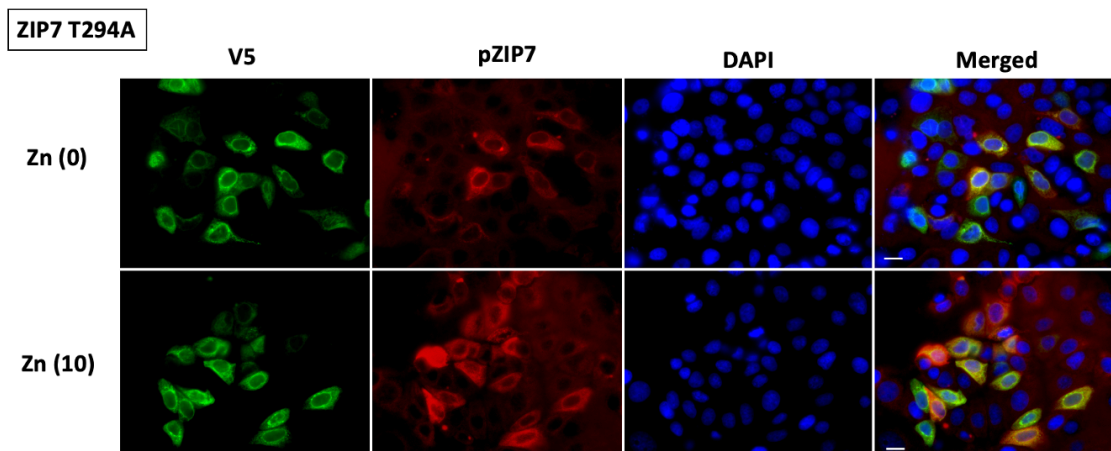


Figure 4.10 pZIP7 antibody ability to detect ZIP7 activation in cells transfected with ZIP7 S293A constructs

(a) MCF-7 cells were transfected with ZIP7 S293A for 18 hours. The cells were fixed and permeabilized before probing with mouse pZIP7 antibody and rabbit V5 antibody conjugated to Alexa Fluor 594 (Red) and Alexa Fluor 488 (Green) respectively, and the nuclei were stained blue with DAPI. These images were captured with a Leica RPE automatic microscope using a 63x magnification lens and the images were proceeded with one round of deconvolution. Scale bar, 10 μ m. **(b)** The transfection rate demonstrated in a bar graph as mean of three represented fields \pm standard error.

(a)



(b)

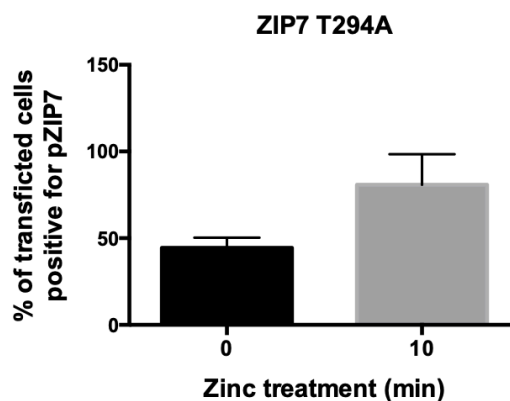


Figure 4.11 pZIP7 antibody ability to detect ZIP7 activation in cells transfected with ZIP7 T294A constructs

(a) MCF-7 cells were transfected with ZIP7 T294A for 18 hours. The cells were fixed and permeabilized before probing with mouse pZIP7 antibody and rabbit V5 conjugated to Alexa Fluor 594 (Red) and Alexa Fluor 488 (Green) respectively, and the nuclei were stained blue with DAPI. These images were captured with a Leica RPE automatic microscope using a 63x magnification lens and the images were proceeded with one round of deconvolution. Scale bar, 10 μ m. **(b)** The transfection rate demonstrated in a bar graph as mean of three represented fields \pm standard error.

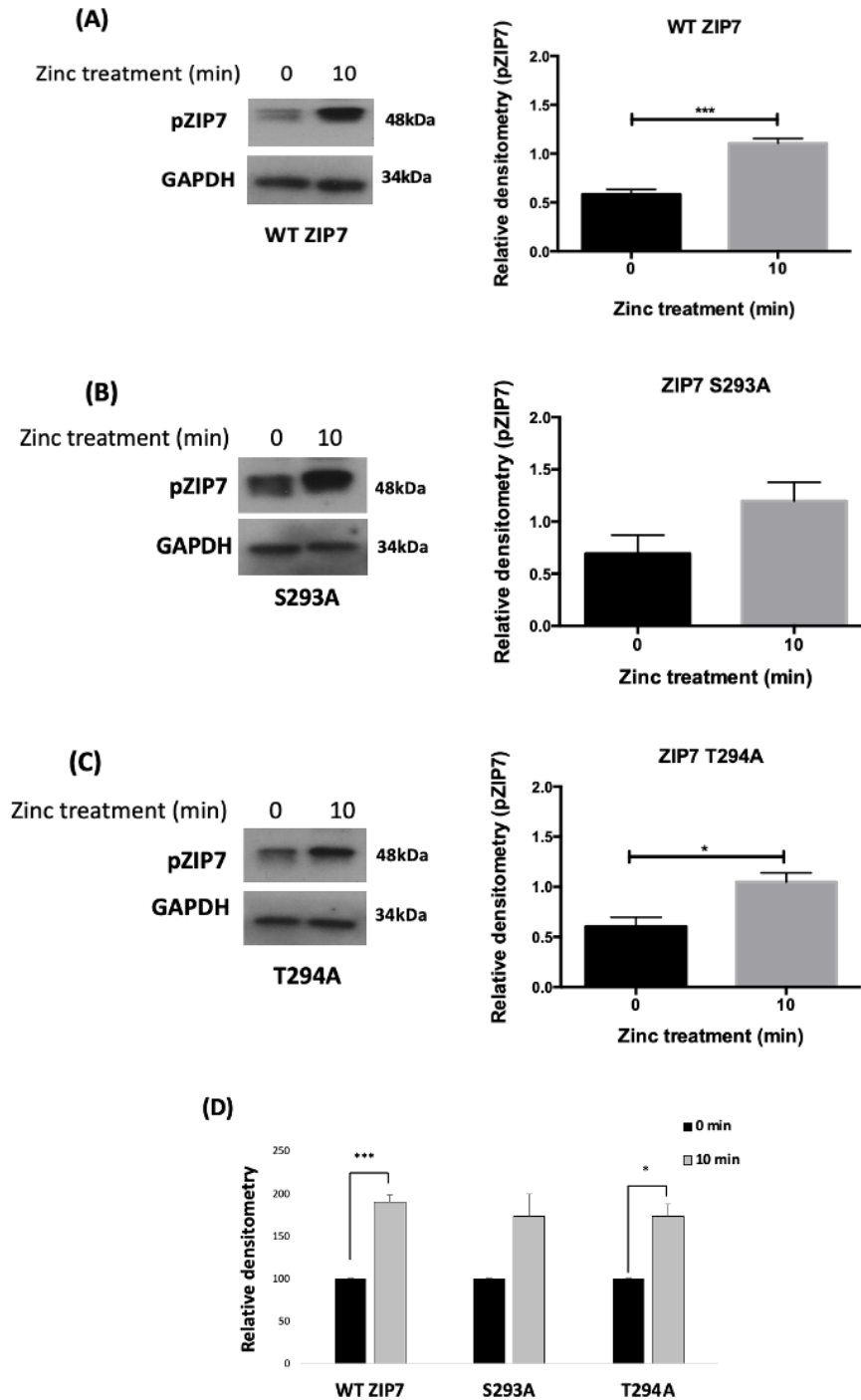


Figure 4.12 Activation of the ZIP7 S293A and T294A mutants by zinc

MCF7 cells transfected with (A) wild type ZIP7, (B) S293A ZIP7, and (C) T294A ZIP7 and then treated with zinc for 0 or 10 minutes. pZIP7 antibody, and GAPDH were used to probe the membrane. Protein bands of pZIP7 (48kDa) and GAPDH (35kDa) are demonstrated. Densitometric data normalised to GAPDH expression and demonstrated in relative density units as mean values of $n = 4 \pm$ standard error. The statistical significance was compared to the samples with no zinc treatment. (D) Graph represents the results expressed as percentage of the untreated WT ZIP7 constructs.

4.3.6 Investigating the endoplasmic reticulum signals of ZIP7:

ZIP7 is located in the endoplasmic reticulum and is essential for zinc release from this intracellular stores⁵⁸. This ZIP7-mediated zinc release requires phosphorylation by protein kinase CK2 on two serine residues (S275 and S276) on the long intracellular loop of ZIP7 between TM3 and TM4¹⁶⁹. The previous chapter showed that ZIP7 is predicted to have four ER retention signals, which could have a role in ER localization of ZIP7. In this chapter, the endoplasmic reticulum signals were investigated further by immunofluorescence.

4.3.6.1 Exploring mutagenesis of the potential ER retention signals of ZIP7:

To study the critical residues that are essential for the endoplasmic reticulum retention of ZIP7, specific alanine mutations were made by site-directed mutagenesis. Four separate sites were located in ZIP7 as having potential ER retention motifs (**Figure 4.13**) and these were then mutated out to allow investigation. The ER1A mutant (¹⁶³PRHR¹⁶⁶ to ¹⁶³AAAA¹⁶⁶) has a mutation in the four basic amino acids whereas the ER1B mutant (¹⁶³PRHR¹⁶⁶ to ¹⁶³PAAA¹⁶⁶) has the first proline intact and a mutation in the three basic amino acids. In the other mutants, ER2, ER3 and ER4, the 3 basic amino acids were all substituted with alanine. The predicted ER retention signals of ZIP7 located in the cytoplasmic domains of ZIP7. ER1 is located between TM1 and TM2. ER2 and ER3 are located between TM3 and TM4. ER4 is located between TM5 and TM6 (**Figure 4.13**).

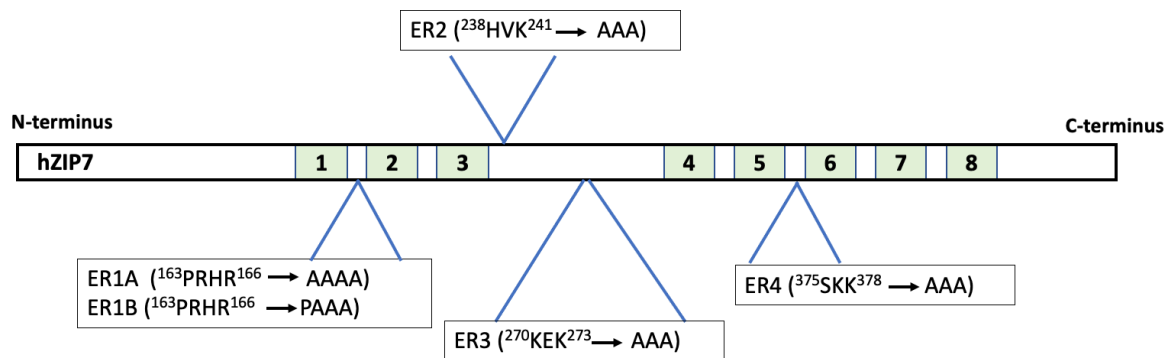


Figure 4.13 Schematic diagram that shows the location of ER mutant sites in the ZIP7

ZIP7 is predicted have four ER retention signals. Alanine mutations were generated (as indicated) to study the effect on ZIP7 endoplasmic reticulum localization.

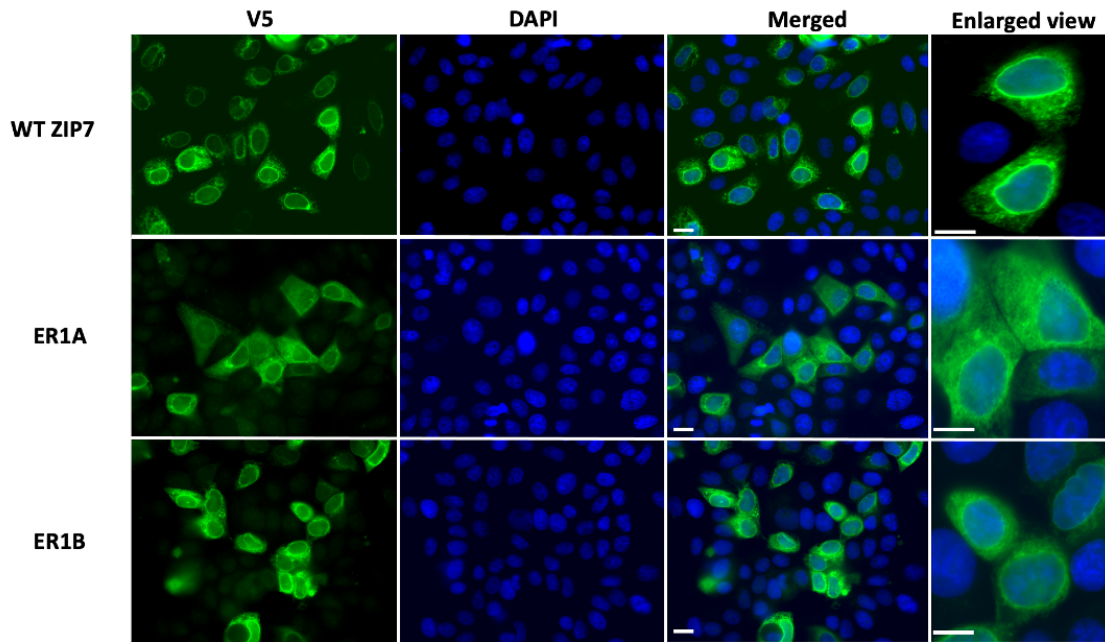
4.3.6.2 Transfection efficiency and cellular localization of ZIP7 ER mutants:

To investigate the transfection efficiency of the ZIP7 endoplasmic reticulum retention signals mutants and the localization patterns, they were assessed by immunofluorescence using a V5 antibody. The immunofluorescence images of all five total mutants are shown in **Figures 4.14** and **4.15**. The V5 antibody targets the C-terminal V5 tag of the plasmid constructs. By counting the cells that were positive for the V5 tag, the transfection rate was assessed. This transfection rate varied from 31% in cells overexpressing WT ZIP7 to 25% in cells transfected with ER1A mutant constructs (**Figure 4.14b**). The enlarged images show a clear ER localization pattern of the recombinant mutant proteins, exactly the same as for the cells transfected with WT ZIP7 (**Figure 4.14a**). Those results suggest that ZIP7 ER1A mutants and ER1B mutants do not disrupt ZIP7 endoplasmic reticulum retention.

Immunofluorescence was also performed on the cells transfected with the other ZIP7 ER mutants to investigate whether the mutation altered the transfection efficiency and whether the ZIP7 ER2, ER3, and ER4 mutants would have a different location. The transfection rates

were between 39% to 34% for these ZIP7 mutants (**Figure 4.15b**). The cells transfected with ER2, ER3, and ER4 showed the same localization pattern as those transfected with WT ZIP7 (**Figure 4.15a**). Both have endoplasmic reticulum staining as well as perinuclear ring staining. The transfection rate was calculated by counting the proportion of positive cells for the V5 tag in six random visual fields. No statistically significant difference was observed between WT ZIP7 and any of the ZIP7 ER mutant constructs. These results suggest that those stretches of basic amino acids might not be critical for ZIP7 endoplasmic reticulum retention and ZIP7 may have a different mechanism for its ER localization which are still not clearly understood.

(a)



(b)

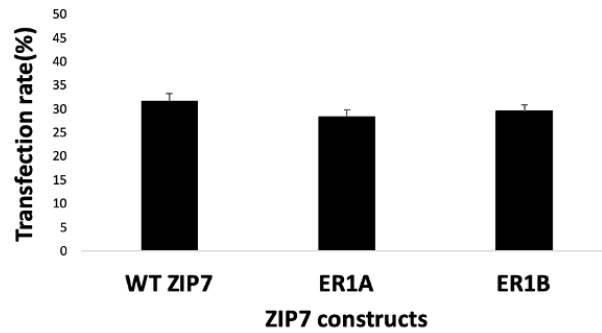


Figure 4.14: Transfection efficiency and localization of ER ZIP7 mutants.

(a) MCF-7 cells were transfected with wild-type, ER1A, and ER1B mutants of ZIP7 for 18 hours. The cells were fixed and permeabilized before probing with V5 antibody conjugated to Alexa Fluor 488 (green) and the nuclei were stained blue with DAPI. These images were captured with a Leica RPE automatic microscope using a 63x magnification lens. Scale bar, 10 μ m. **(b)** The transfection rate is demonstrated in a bar graph as mean of nine represented fields of view \pm standard error.

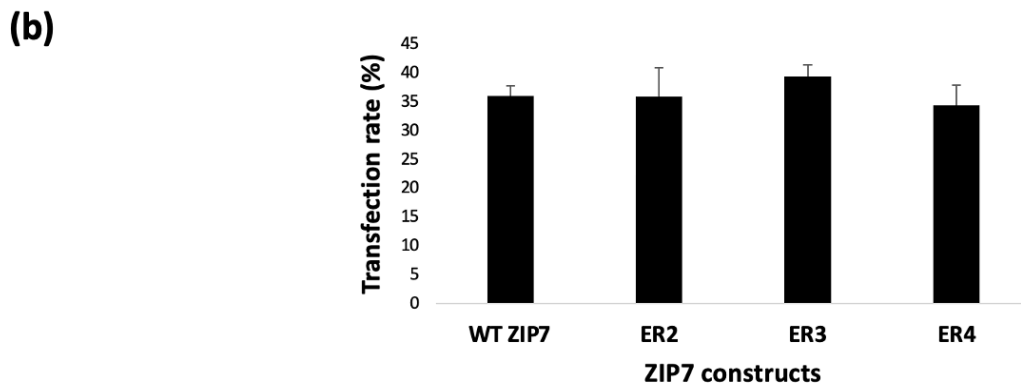
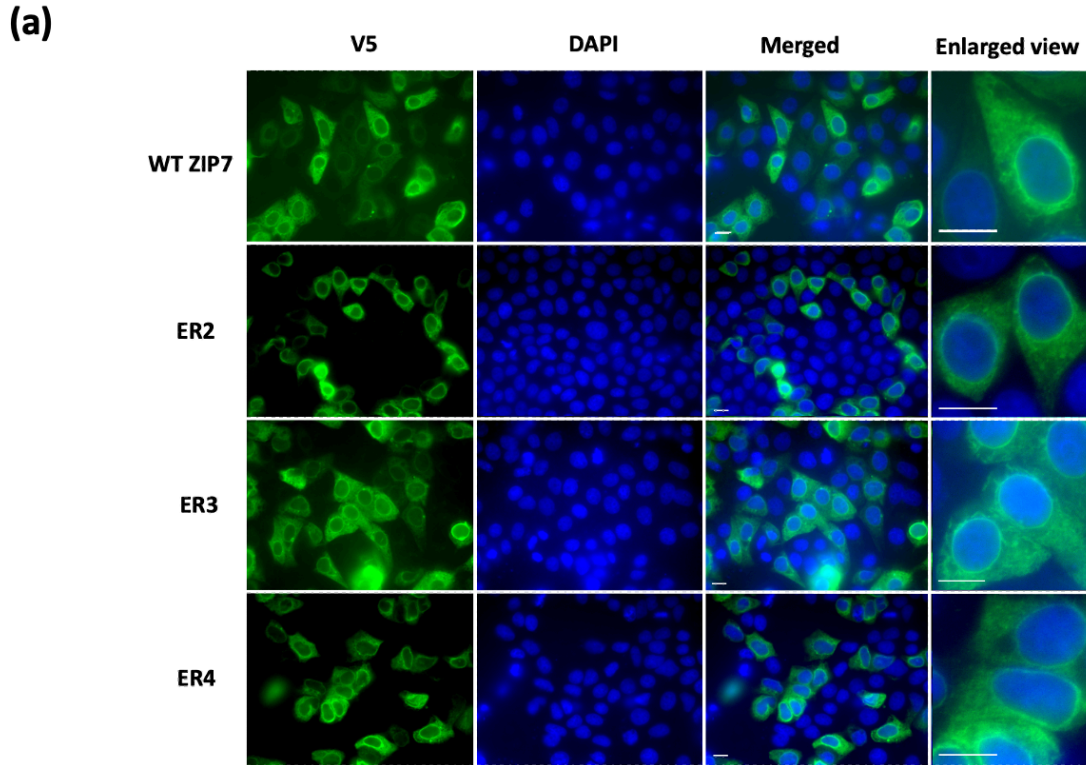


Figure 4.15: Transfection efficiency and localization pattern of different ZIP7 ER mutants' constructs.

(a) MCF-7 cells were transfected with WTZIP7, ER2, ER3, or ER4 mutants of ZIP7 for 18 hours. The cells were fixed and permeabilized before probing with V5 antibody conjugated to Alexa Fluor 594 (red) and the nuclei were stained blue with DAPI. These images were captured with a Leica RPE automatic microscope using a 63x magnification lens. Scale bar, 10 μ m **(b)** The transfection rate is demonstrated in a bar graph as mean of six represented fields of view \pm standard error.

4.3.6.3 Colocalization of ZIP7 ER mutants with Protein Di-sulfide Isomerase:

Protein Disulfide Isomerase (PDI) is a protein located in the ER and have a role in formation of disulfide bonds between cysteine residues within proteins as they fold^{233–235}. To further characterise the cellular location of the ZIP7 ER retention signals mutant, cells were transfected with the different ZIP7 mutants, and they were stained for Protein Disulfide Isomerase (PDI). The V5 tag was used to visualize the ZIP7 ER mutants. PDI showed red staining in the endoplasmic reticulum with no perinuclear ring (**Figure 4.16**). The merged figure showed a yellow colour around the nucleus as well as in the endoplasmic reticulum due to the higher background of the PDI. Immunofluorescence was repeated with the other mutants to investigate the colocalization of ER2, ER3, and ER4 ZIP7 mutants with PDI. Although the PDI produced quite a lot of background staining it was clear that is only showed traditional endoplasmic reticulum staining without any perinuclear staining at all as was always seen with ZIP7. The PDI staining pattern was compared to V5, which showed a clear perinuclear ring as well as the traditional endoplasmic reticulum staining (**Figure 4.17**). These results suggest that the mutated sequences do not alter the ability of ZIP7 to be retained in the endoplasmic reticulum.

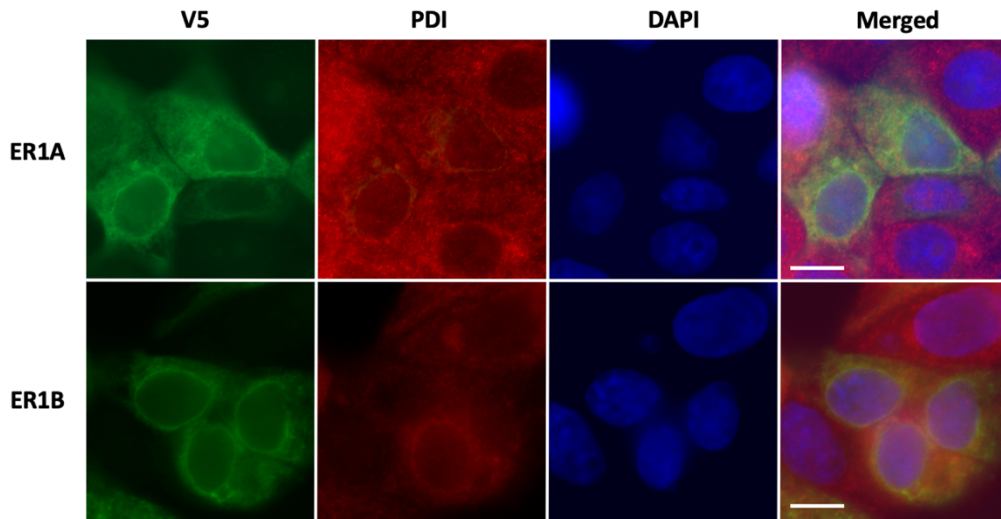


Figure 4.16: Co-localization of ER retention signals mutants with PDI.

MCF-7 cells were transfected with ZIP7 ER1A and ER1B mutants of ZIP7 for 18 hours. The cells were fixed and permeabilized before being probed with mouse V5 conjugated to Alexa Fluor 488 (green) and rabbit PDI antibody conjugated to rabbit Alexa Fluor 594 (red), and nuclei were stained blue with DAPI. This image was captured with a Leica RPE Automatic Microscope using a 63x magnification lens. Scale bar, 10 μ m

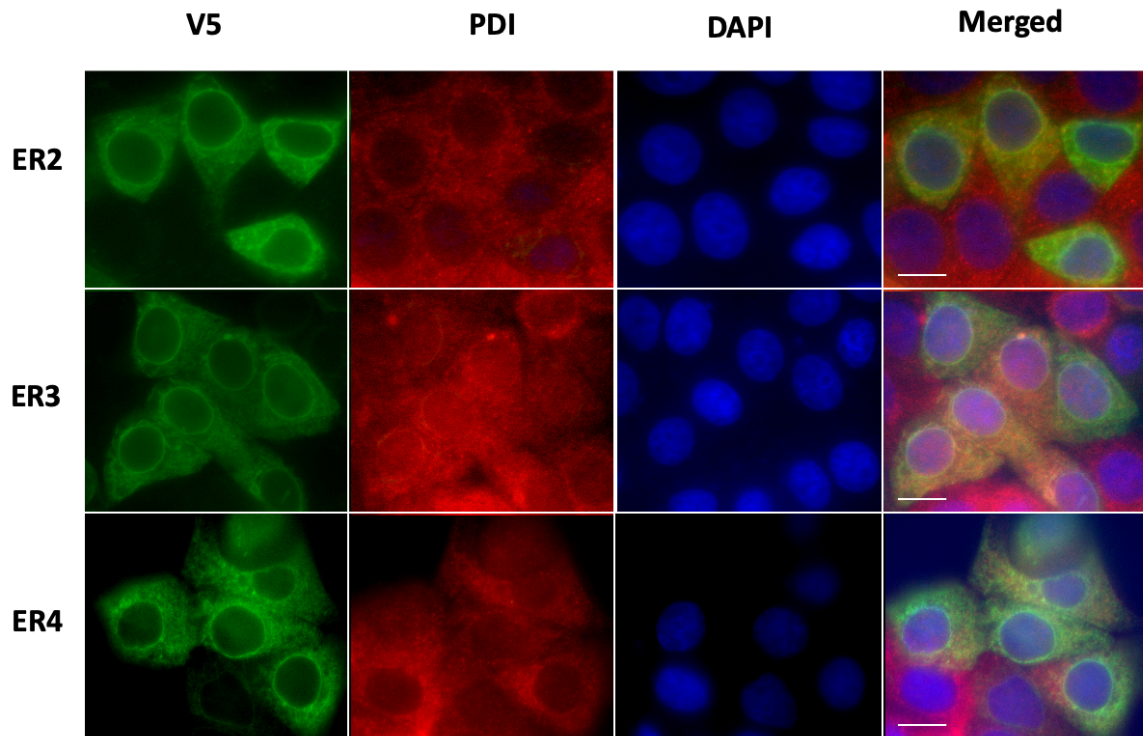


Figure 4.17: Co-localization of ER retention signals mutants of ZIP7 with PDI.

MCF-7 cells were transfected with ZIP7 ER2, ER3, and ER4 mutants for 18 hours. The cells were fixed and permeabilized before being probed with mouse V5 and rabbit PDI antibodies before being conjugated to Alexa Fluor 594 (red) and Alexa Fluor 488 (green) respectively, and the nuclei were stained blue with DAPI. This image was captured with a Leica RPE Automatic Microscope using a 63x magnification lens. Scale bar, 10 μ m

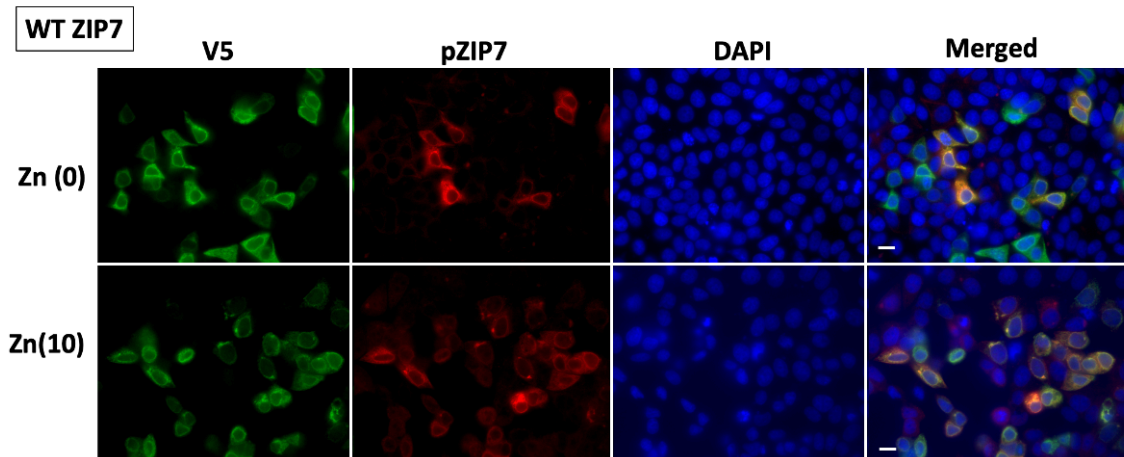
4.6.3.4 Effect of the removal of endoplasmic retention signals on ZIP7 activation:

To investigate whether ZIP7 ER retention signal mutants adversely affected ZIP7 phosphorylation after 10 minutes of zinc treatment, immunofluorescence was performed using our purified pZIP7 antibody, which has previously been verified in Chapter 3 as capable of recognising activated ZIP7. The V5 antibody was used to identify the cells that were transfected with the different ZIP7 constructs. By counting the number of cells that were positive for pZIP7, the proportion of cells that were positive for ZIP7 activation was calculated.

The cells overexpressing WT ZIP7 showed 42% of cells positive for pZIP7 before zinc treatment and this significantly increased to 85% after stimulation with zinc for 10 minutes (**Figure 4.18**). Probing for V5 and pZIP7 both showed an ER staining as well as a ring around the nucleus. For the ER mutants, 21% of cells overexpressing the ER1A mutants and 24% of cells overexpressing ER1B mutants were positive for pZIP7 before zinc treatment (**Figure 4.19 and 4.20**). After 10 minutes of zinc treatment, the percentage of pZIP7 significantly increased to 70% in ER1A and 88% in ER1B ZIP7 mutants (**Figure 4.19 and 4.20**). Both mutants were transfected comparably to WT ZIP7. Probing for V5 and pZIP7 gave an ER staining just as observed for WT ZIP7, which suggests that these mutations did not alter ZIP7 ER localization and did not alter ZIP7 activation on residues S275 and S276. The percentage of cells positive for pZIP7 before zinc treatment were 43%, 31% in cells overexpressing ER2 and ER4, respectively. This percentage significantly increased after 10 minutes of zinc treatment to 70% and 69% in cells overexpressing ER2 and ER4, respectively (**Figure 4.21 and 4.23**), which suggest the ability of these constructs to be activated by zinc addition. They all have the same ER staining as WT ZIP7, confirming that these mutants do not affect ZIP7 ability to be retained in the ER. These data suggested that the pZIP7 antibody could recognize ZIP7 ER1A, ER1B, ER2, and ER4, and these mutations do not interfere with the zinc-induced CK2-mediated phosphorylation on residues S275 and S276 of ZIP7.

Interestingly, the cells overexpressing ER3 do not show any cells positive for pZIP7 either before or after zinc treatment (**Figure 4.22**). The construct of ER3 had an alanine mutation on residues 270 to 273, and those residues were extremely close to residues S275 and S276, which are the binding sites of the pZIP7 antibody. This data suggests that the ER3 mutation interferes with pZIP7 antibody binding on residues S275 and S276, implying that these residues are important for ZIP7 function.

(a)



(b)

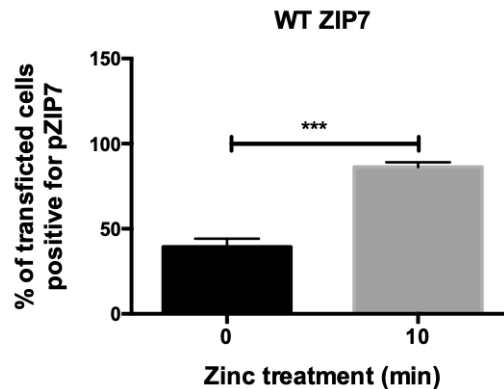
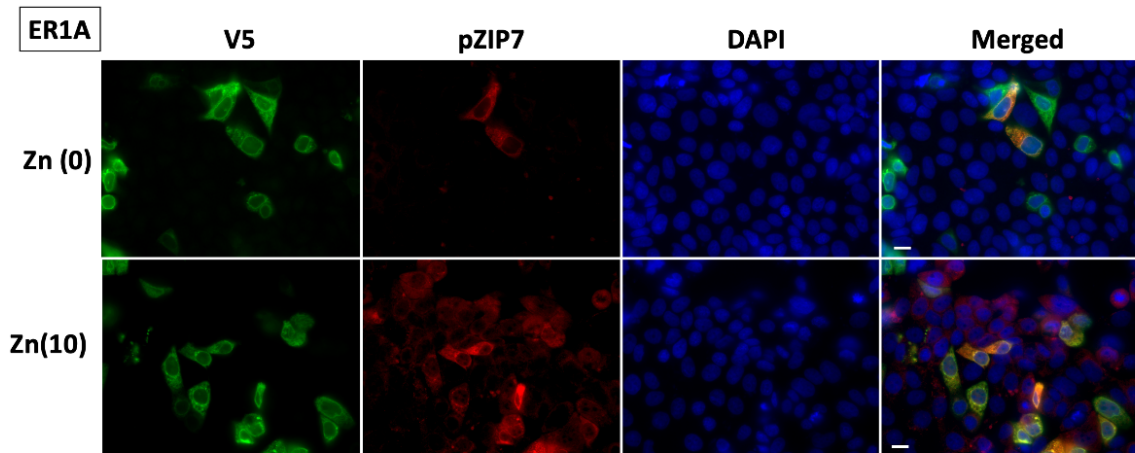


Figure 4.18 pZIP7 antibody detect ZIP7 activation in cells transfected with WT ZIP7.

(a) MCF-7 cells were transfected with WT ZIP7 for 18 hours. The cells were untreated or treated with zinc for 10 minutes before being fixed and permeabilized. The coverslips were probed with mouse pZIP7 antibody and rabbit V5 conjugated to Alexa Fluor 594 (red) and Alexa Fluor 488 (green) respectively and the nuclei were stained blue with DAPI. Images were captured with a Leica RPE automatic microscope using a 63x magnification lens. Scale bar, 10 μ m. **(b)** The bar graph shows the percentage of transfected cells that are positive for pZIP7 as a mean of five different fields of view \pm standard error. *** = $p < 0.001$

(a)



(b)

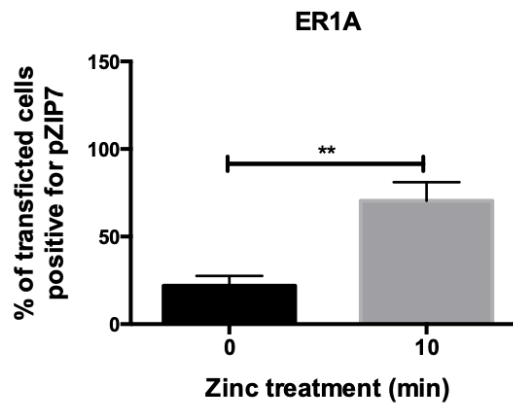
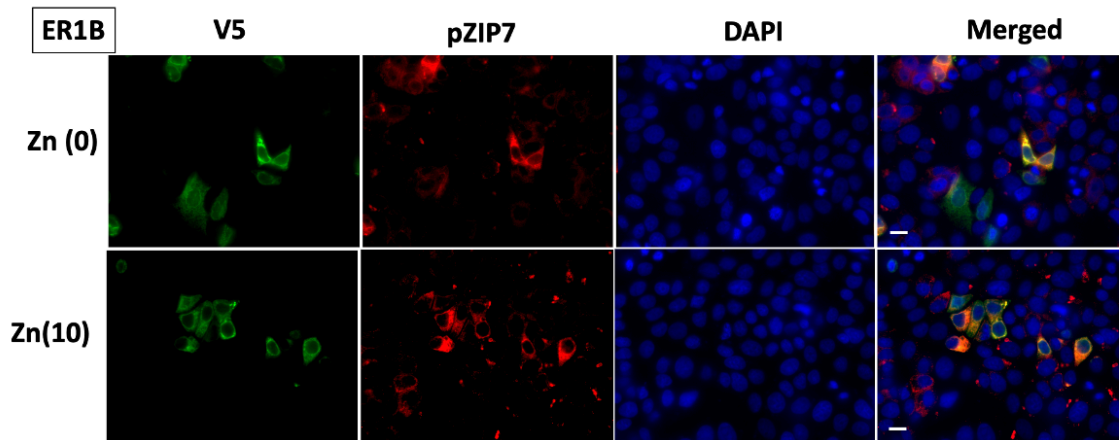


Figure 4.19 pZIP7 antibody detect ZIP7 activation in cells transfected with ZIP7 ER1A.

(a)MCF-7 cells were transfected with ZIP7 ER1A mutant for 18 hours. The cells were untreated or treated with zinc for 10 minutes before being fixed and permeabilized. The coverslips were probed with mouse pZIP7 antibody and rabbit V5 conjugated to Alexa Fluor 594 (red) and Alexa Fluor 488 (green) respectively and the nuclei were stained blue with DAPI. Images were captured with a Leica RPE automatic microscope using a 63x magnification lens. Scale bar, 10 μ m. **(b)**The bar graph shows the percentage of transfected cells that are positive for pZIP7 as a mean of five different fields \pm standard error. ** = $p < 0.01$

(a)



(b)

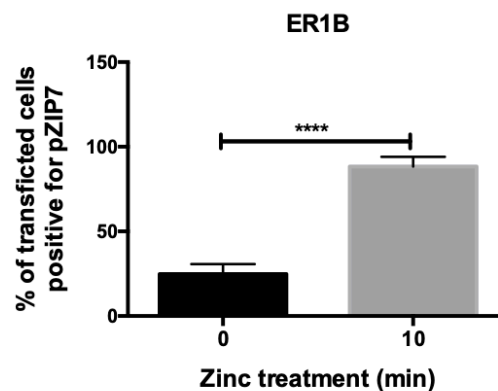
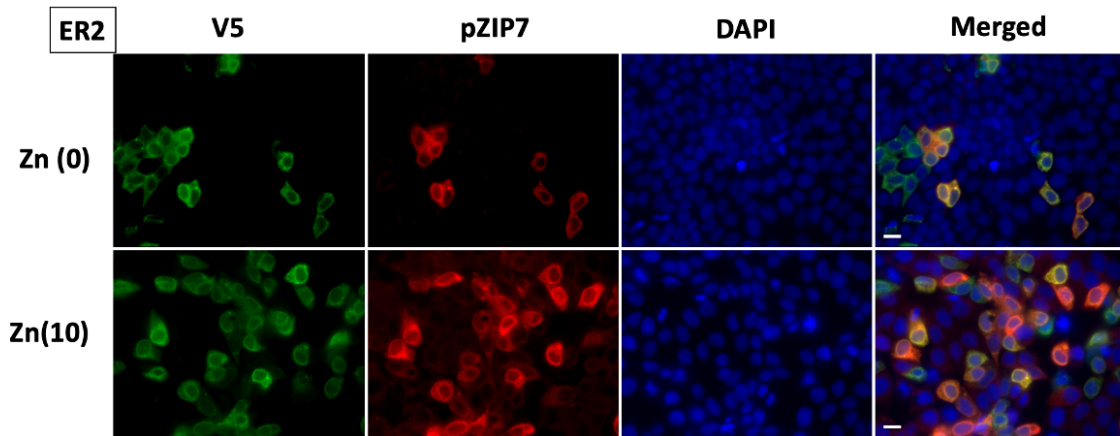


Figure 4.20 pZIP7 antibody detect ZIP7 activation in cells transfected with ZIP7 ER1B.

(a)MCF-7 cells were transfected with ZIP7 ER1B mutant for 18 hours. The cells were untreated or treated with zinc for 10 minutes before being fixed and permeabilized. The coverslips were probed with mouse pZIP7 antibody and rabbit V5 conjugated to Alexa Fluor 594 (red) and Alexa Fluor 488 (green) respectively and the nuclei were stained blue with DAPI. Images were captured with a Leica RPE automatic microscope using a 63x magnification lens. Scale bar, 10 μ m. **(b)**The bar graph shows the percentage of transfected cells that are positive for pZIP7 as a mean of five different fields \pm standard error. **** = $p < 0.0001$

(a)



(b)

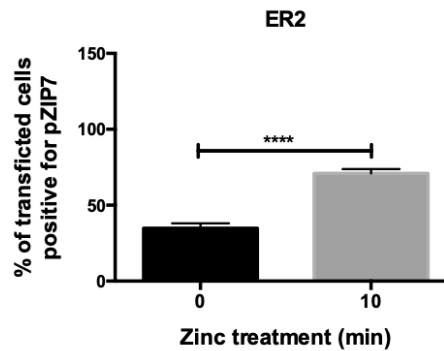


Figure 4.21 pZIP7 antibody detect ZIP7 activation in cells transfected with ZIP7 ER2.

(a) MCF-7 cells were transfected with ZIP7 ER2 mutant for 18 hours. The cells were untreated or treated with zinc for 10 minutes before being fixed and permeabilized. The coverslips were probed with mouse pZIP7 antibody and rabbit V5 conjugated to Alexa Fluor 594 (Red) and Alexa Fluor 488 (Green) respectively and the nuclei were stained blue with DAPI. Images were captured with a Leica RPE automatic microscope using a 63x magnification lens. Scale bar, 10 μ m. **(b)** The bar graph shows the percentage of transfected cells that are positive for pZIP7 as a mean of four different fields \pm standard error. **** = $p < 0.0001$

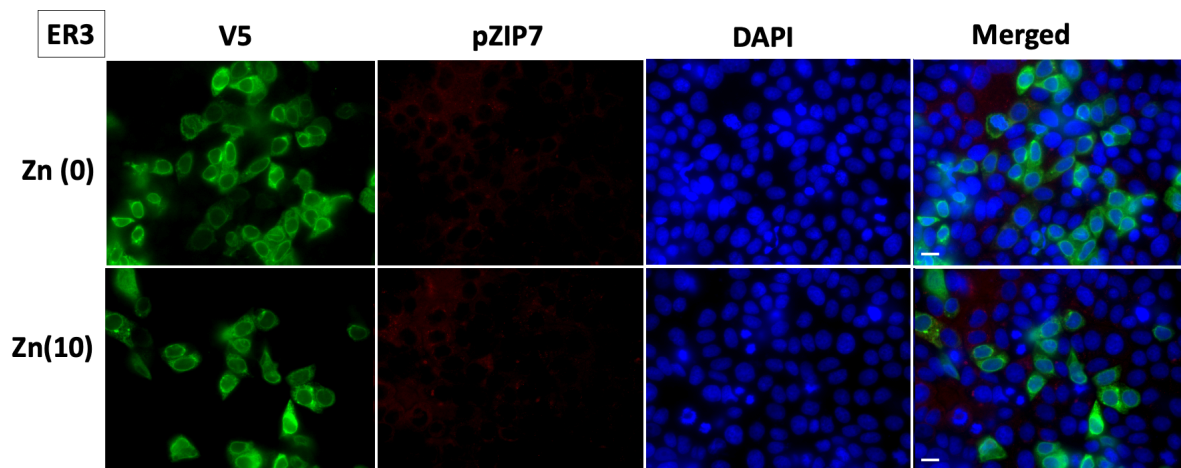
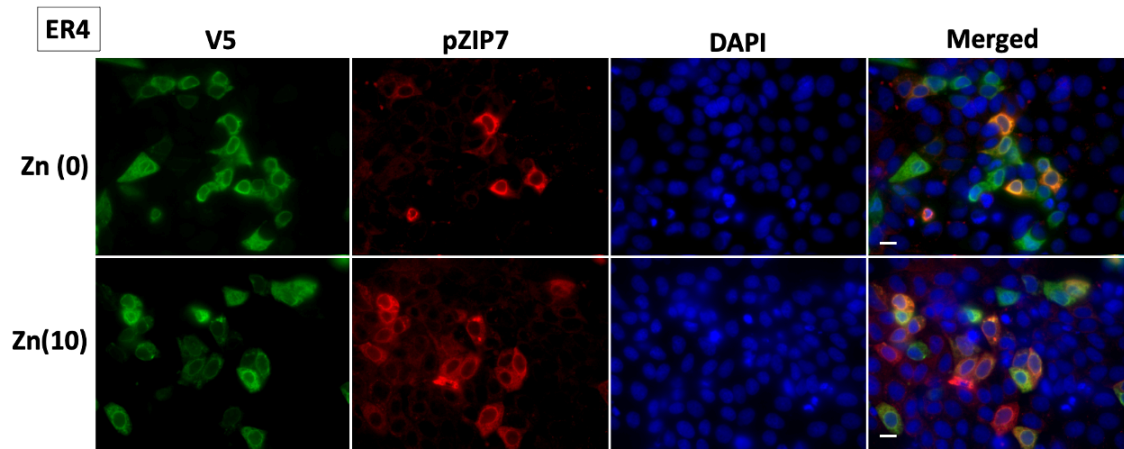


Figure 4.22 pZIP7 antibody detect ZIP7 activation in cells transfected with ZIP7 ER3.

(a) MCF-7 cells were transfected with ZIP7 ER3 mutant for 18 hours. The cells were untreated or treated with zinc for 10 minutes before being fixed and permeabilized. The coverslips were probed with mouse pZIP7 antibody and rabbit V5 conjugated to Alexa Fluor 594 (red) and Alexa Fluor 488 (green) respectively and the nuclei were stained blue with DAPI. Images were captured with a Leica RPE automatic microscope using a 63x magnification lens. Scale bar, 10 μ m.

(a)



(b)

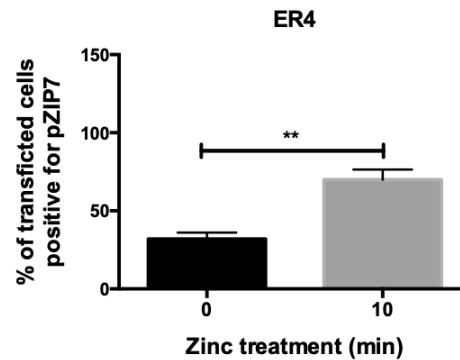


Figure 4.23 pZIP7 antibody detect ZIP7 activation in cells transfected with ZIP7 ER4.

(a) MCF-7 cells were transfected with ZIP7 ER4 mutant for 18 hours. The cells were untreated or treated with zinc for 10 minutes before being fixed and permeabilized. The coverslips were probed with mouse pZIP7 antibody and rabbit V5 conjugated to Alexa Fluor 594 (Red) and Alexa Fluor 488 (Green) respectively and the nuclei were stained blue with DAPI. Images were captured with a Leica RPE automatic microscope using a 63x magnification lens. Scale bar, 10 μ m. (b) The bar graph shows the percentage of transfected cells that are positive for pZIP7 as a mean of five different fields \pm standard error. ** = $p < 0.01$

4.7 Chapter summary:

This chapter has provided further confirmation that our pZIP7 antibody is bound explicitly to ZIP7 when it is phosphorylated on residues S275 and S276⁷⁴ (**Figure 4.1**). Using an immunofluorescence technique confirmed the specificity of the pZIP7 antibody for activated ZIP7, which was verified further by its ability to recognize ZIP7 when residues S275 and S276 were mutated to aspartate (DD), which structurally mimics phosphoserine (**Figure 4.5**). In contrast, the mutation of these residues to alanine prevents the binding of the pZIP7 antibody even after 10 minutes of zinc treatment (**Figure 4.6**). The presence of alanine (AA) instead of serine prevents the phosphorylation of ZIP7 by the CK2 because the alanine is a hydrophobic amino acid with a methyl in its side chain, while the serine is a hydrophilic amino acid with a hydroxyl group on its side chain. Immunofluorescence technique showed also a significant increase of pZIP7 antibody after 10 minutes of zinc treatment in cells transfected with WT ZIP7 and ZIP7 S275D/S276D (**Figure 4.4 and 4.5**), confirming the previous results⁷⁴. These results further confirm the ability of pZIP7 antibody to bind to the phosphorylated form of WT ZIP7 or the phospho-mimetic ZIP7 S275D/S276D) mutants but not recognize phospho-ablative mutant (ZIP7 S275A/S276A).

Phospho-mimetic ZIP7 DD should be constitutively active due to its molecular structure. The aspartic acid in ZIP7DD mutants is similar to the structure of serine in WT ZIP7 when the channel is phosphorylated. So ZIP7 DD would be expected to have a higher zinc level at time 0 and the pZIP7 antibody able to detect this mutant. The immunofluorescence results showed a similar pattern of pZIP7 activation as WT ZIP7. The significant increase of AKT in cells transfected with phospho-mimetic ZIP7 DD was at 20 minutes of zinc treatment compared to time zero. These results suggest that ZIP7 DD mutants are able to induce ZIP7 mediated zinc release, but it is delayed because the zinc in ER store is depleted. A possible explanation of these results is that during the 18 hours of the transfection before exogenous zinc treatment, ZIP7 DD mutant constructs have been releasing the zinc from stores leading to store depletion. The cells might muffle this excess zinc by metallothionein^{28,67} or transport it outside the cells through ZnT1²³⁶. Therefore, after exogenous zinc treatment, the cells might have to wait until the store will be refilled with zinc which will be able of ZIP7 to release zinc from store to

cytoplasm. To further investigate ZIP7 DD mutants, measuring the intracellular zinc levels using zinc-specific dyes such as FluoZin-3, Zinquin, and Newport Green Diacetate would be needed to investigate the change in the intracellular zinc homeostasis^{69,237}. Also, zinc could be measured specifically in the ER stores using FRET-based zinc sensors²³⁸⁻²⁴⁰, which will help to support the hypothesis of zinc depletion from ER store. Also, to further investigate the hypothesis that the delayed of zinc related downstream effects because the zinc is depleted from ER storage, the transfected cells with ZIP7 DD mutants could be treated with EGF plus calcium ionophore instead of zinc, which has been known to activate ZIP7¹⁶⁹.

ZIP7 is a gatekeeper for zinc release from the cellular store and a hub for phosphorylation of tyrosine kinases⁶³. ZIP7 activity is regulated by phosphorylation at S275 and S276 by protein kinase CK2 resulting in zinc release from intracellular stores, which inhibit protein tyrosine phosphatase results in AKT activation^{169,241,242}. Database analysis showed that ZIP7 is potentially also predicted to be phosphorylated on S293 and T294. Immunofluorescence and western blot techniques showed the ability of the pZIP7 antibody to bind to ZIP7 S293A and T294A mutants (**Figure 4.10,11,12**). ZIP7 is an ER protein responsible for releasing zinc from the ER store into the cytoplasm. ER-resident proteins generally require specific signals for their retention in the ER. Computer analysis showed that ZIP7 is predicted to have four ER retention signals (**Figure 4.13**). Alanine mutation in all these predicted ER retention signals did not change the ER residency of ZIP7 (**Figure 4.14 and 4.15**), suggesting that these motifs might not be a requirement for ZIP7 to reside in the ER. Furthermore, immunofluorescence results showed that ZIP7 ER1A, ER1B, ER2, and ER4 did not interfere with ZIP7 phosphorylation on S275 and S276 as the pZIP7 antibody recognized ZIP7 activation after zinc treatment in all mutants except ER3. ZIP7 mutant ER3 did not show any positive cells for pZIP7(**Figure 4.18-23**) but this may have been due to its close proximity to residues 275 and 276 and not a functional effect.

5. Chapter 5: Discovery the nuclear localization of ZIP7:

5.1 Introduction

ZIP7 is a zinc transporter that is responsible for zinc release from the ER store. Imaging ZIP7 in MCF7 cells has suggested that not only is ZIP7 present in the ER, but it always stains a strong perinuclear ring, indicating the potential for ZIP7 to be located on the inner nuclear membrane. The previous chapter showed that ZIP7 is predicted to have three nuclear localization signals, suggesting that ZIP7 may reside in the nucleus. If this were the case, the ZIP7 would be expected to be oriented on the inner nuclear membrane to transport zinc from the ER store into the nucleus and lead to cancer development. No ZIP transporter has been located in the nucleus yet, and there is much zinc in the nucleus required for DNA zinc fingers and transcription factors binding to the target gene, especially in cancer. This chapter aim to confirm the nuclear localization of ZIP7 and pZIP7 using inner nuclear membrane markers.

5.2 Methods

MCF-7 cells grown on coverslips were transfected with ZIP7 and harvested after 18 hours. The coverslips were stained for V5 and a variety of known nuclear markers. The primary antibodies were incubated with fluorescent secondary antibodies such as Alexa Fluor 488 and 594, and the nuclei were stained blue with DAPI before imaging on the microscope. The RGB profiler plugin from ImageJ was used to plot co-localization according to fluorescence intensity. Initially, Leica RPE Automatic Microscope was used, which was complemented by Zeiss LSM 880 confocal microscope. Please refer to Chapter 2 for the detailed transfection methods (Section 2.1.2) and immunofluorescence (Section 2.4).

5.3 Results

5.3.1 Imaging the localization of ZIP7 in cells

ZIP7 is a transmembrane protein known to be located in the endoplasmic reticulum (ER) and responsible for zinc release from ER store. Knowing that ZIP7 has three predicted nuclear localization signals suggests its nuclear localization, which will be further investigated in this chapter by immunofluorescence using breast cancer cells transfected with WT ZIP7.

5.3.1.1 Localization of ZIP7 in breast cancer cells

To study the cellular localization of ZIP7, immunofluorescence was performed by using the V5 antibody and total ZIP7 antibody in MCF-7 cells transfected with a WT-ZIP7 construct. It has been documented that ZIP7 was located on the ER^{58,73}, yet there was always obvious perinuclear staining observed as well as the ER (**Figure 5.1a,b**). The V5 staining and the total ZIP7 showed a clear ring around the nuclear and ER staining which further confirm the nuclear and ER ZIP7 location (**Figure 5.1b**). To show that ZIP7 is present in its active form around the nucleus, another experiment was performed to study the co-localization of V5 with phosphorylated ZIP7, which is the active form of ZIP7. The merged picture in **Figure 5.2** showed a bright yellow perinuclear staining as well as the ER. These results suggest that ZIP7 is active around the nucleus and could play a role in transport zinc into the nucleus.

Protein Disulfide Isomerase (PDI) is a specific protein located only on the ER, required for correct disulphide bond formation. To further characterize the perinuclear localization of ZIP7, cells transfected with wild type ZIP7 were stained with Protein Disulfide Isomerase (PDI). **Figure 5.3** shows that Protein Disulfide Isomerase is only located on the ER without any perinuclear ring staining, suggesting that ZIP7 is in the nuclear envelop (NE) and in the endoplasmic reticulum. Actin is a microfilament protein that plays an essential role in the cellular process of maintaining cell structure and shape. Alexa Flour 488® phalloidin was used to label F-actin with a green, fluorescent colour. **Figure 5.4** showed a green actin filament structure on the cellular membrane around all cells. These results confirm that the ZIP7 transporter is located intracellularly as expected and not found on the plasma membrane as other ZIP transporters are.

To investigate the presence of ZIP7 in the mitochondria, the mitochondria were stained using MitoTracker™ Red CMXRos. The cells were transfected with WT ZIP7 and then stained with MitoTracker™. The red images showed a red fluorescence dye that stains the mitochondria around the cells (**Figure 5.5**). In contrast, the green pictures showed a clear ring of ZIP7 around the nucleus and in the ER. The merged image did not show a yellow colour, suggesting that ZIP7 and the mitochondria are not localised.

These data together suggest that not only is ZIP7 localized in the ER but that it is also on the nuclear envelope (NE). This is an important finding and would indicate that it could be capable of transporting zinc into the nucleus and the cytoplasm, adding to its role as a hub of intracellular zinc release. There has been no other zinc transporter localize in the nucleus, yet there is much need for zinc control in the nucleus. Therefore, the next aim was to confirm this observation by co-localizing ZIP7 with known markers of the inner nuclear membrane such as Lamins (Lamin A/C and Lamin B), NUP98 Lamin B receptor, and Emerin.

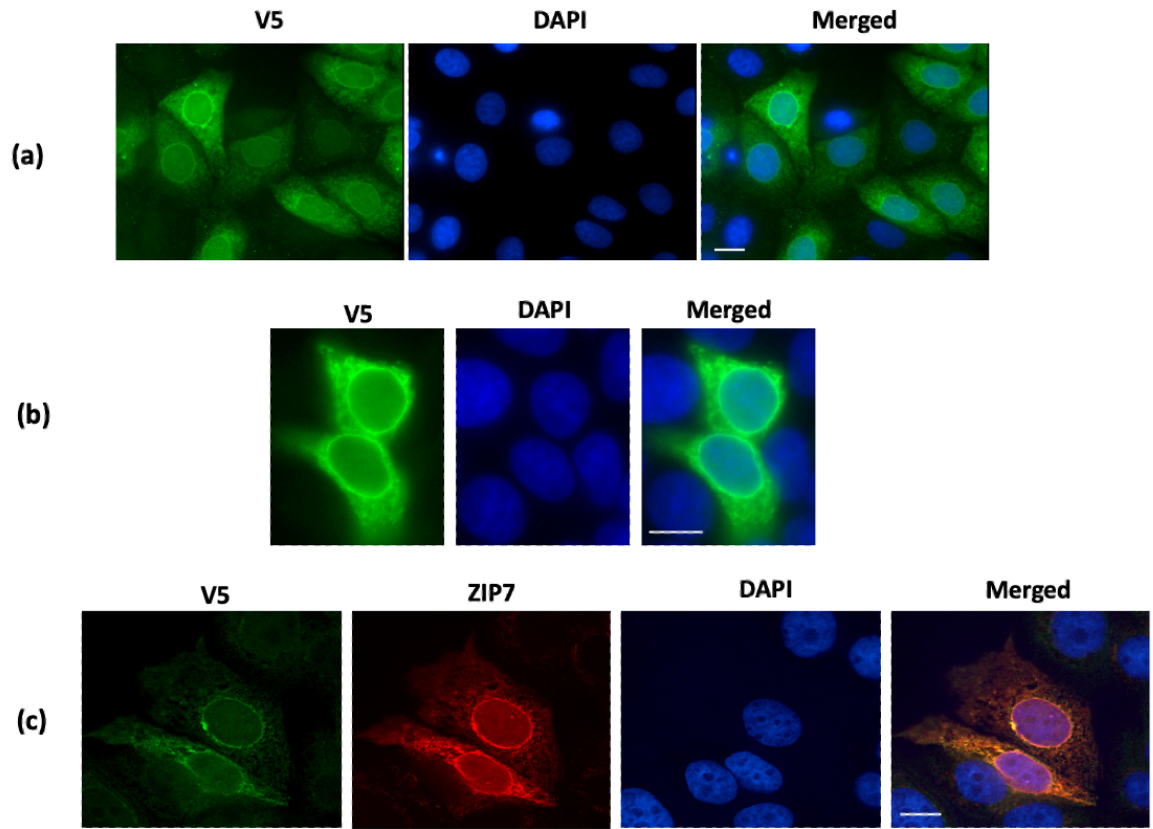


Figure 5.1 Cellular localization of wild type ZIP7 in MCF-7 cells

MCF-7 cells were transfected with WT ZIP7 for 18 hours. The cells were fixed and permeabilized before probing with **(a)** rabbit V5 conjugated Alexa Fluor 488 (Green), **(b)** rabbit total ZIP7 antibody and mouse V5 antibody conjugated to Alexa Fluor 488 (Green) and Alexa Fluor 594 (Red) respectively, and nuclei were stained blue with DAPI. These images were captured with a Leica RPE automatic microscope using a 63x magnification lens. Scale bar, 10 μ m

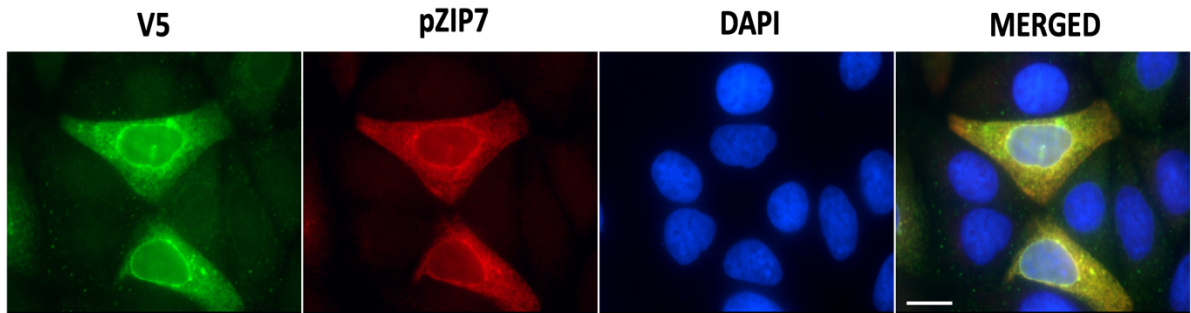


Figure 5.2: Active ZIP7 (pZIP7) localize in ER and nuclear membrane

MCF-7 cells were transfected with WT ZIP7 for 18 hours. The cells were fixed and permeabilized before probing with mouse pZIP7 antibody and rabbit V5 conjugated to Alexa Fluor 594 (Red) and Alexa Fluor 488 (Green) respectively, and nuclei were stained blue with DAPI. These images were captured with a Leica RPE automatic microscope using a 63x magnification lens. Scale bar, 10 μ m

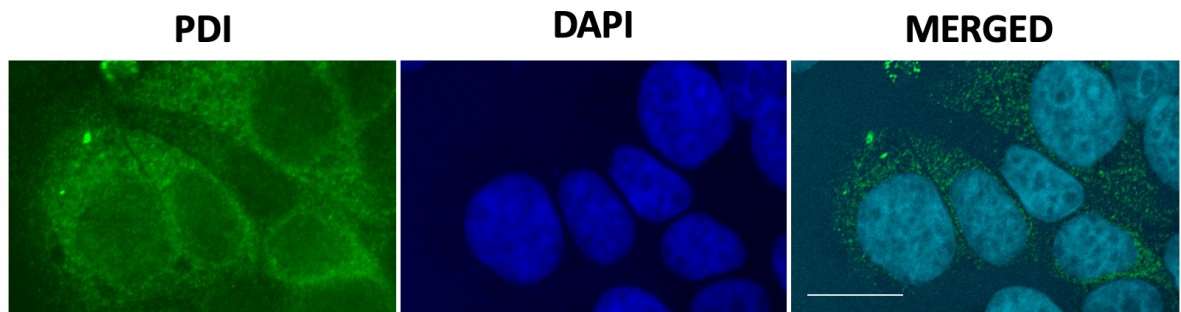


Figure 5.3: Protein Disulfide Isomerase (PDI) localization in cells.

MCF-7 cells were transfected with WT ZIP7 for 18 hours. The cells were fixed and permeabilized before probing with rabbit PDI antibody, and nuclei were stained blue with DAPI. These images were captured with a Leica RPE automatic microscope using a 63x magnification lens. Scale bar, 10 μ m

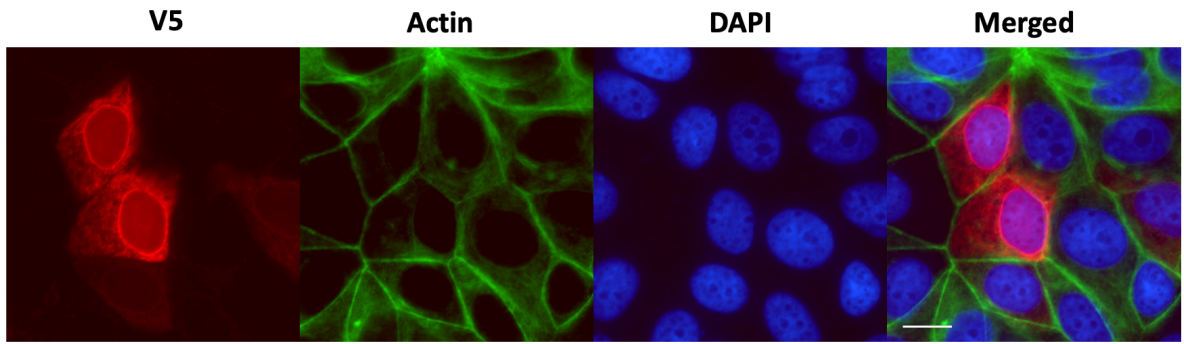


Figure 5.4 ZIP7 and actin localization in cells.

MCF-7 cells were transfected with WT ZIP7 for 18 hours. The cells were fixed and permeabilized before probing with mouse V5 conjugated Alexa Fluor 594 (Red) and (1:5) 488 phalloidin (green), and nuclei were stained blue with DAPI. This image was captured with a Leica RPE Automatic Microscope using a 63x magnification lens. Scale bar, 10 μ m

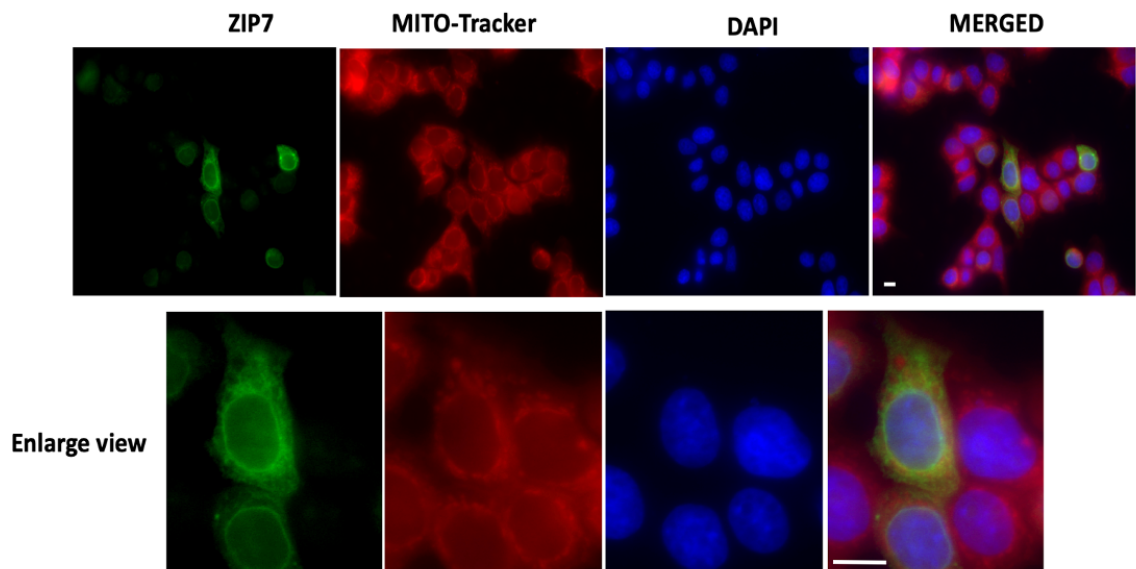


Figure 5.5: Testing overlap of ZIP7 with mitochondria.

MCF-7 cells were transfected with WT ZIP7 for 18 hours. 100 nM MitoTracker™ Red CMXRos in medium without serum were added to the cells for 30 minutes at 37°C, followed by a 30-minute recovery in dye-free medium at 37°C. The cells were fixed and permeabilized before probing with mouse V5 conjugated Alexa Fluor 488 (green), and the nuclei were stained blue with DAPI. These images were captured with a Leica RPE automatic microscope using a 63x magnification lens. A line was drawn across the cell and the colocalization intensity was measured along this line. The RGB profiler plugin from ImageJ was used to plot co-localization. Scale bar, 10 μ m

5.3.2 Co-localization of ZIP7 with inner nuclear proteins markers:

The previous immunofluorescence images showed a unique nuclear localization of ZIP7, which highlighted its role in transporting the zinc into the nucleus. Next, we attempted further to characterize the nuclear localization of ZIP7 by immunofluorescence using specific proteins located in the inner nuclear membrane (INM) such as Lamins (Lamin A/C and Lamin B), NUP98, Lamin B receptor, and Emerin (**Figure 5.6**).

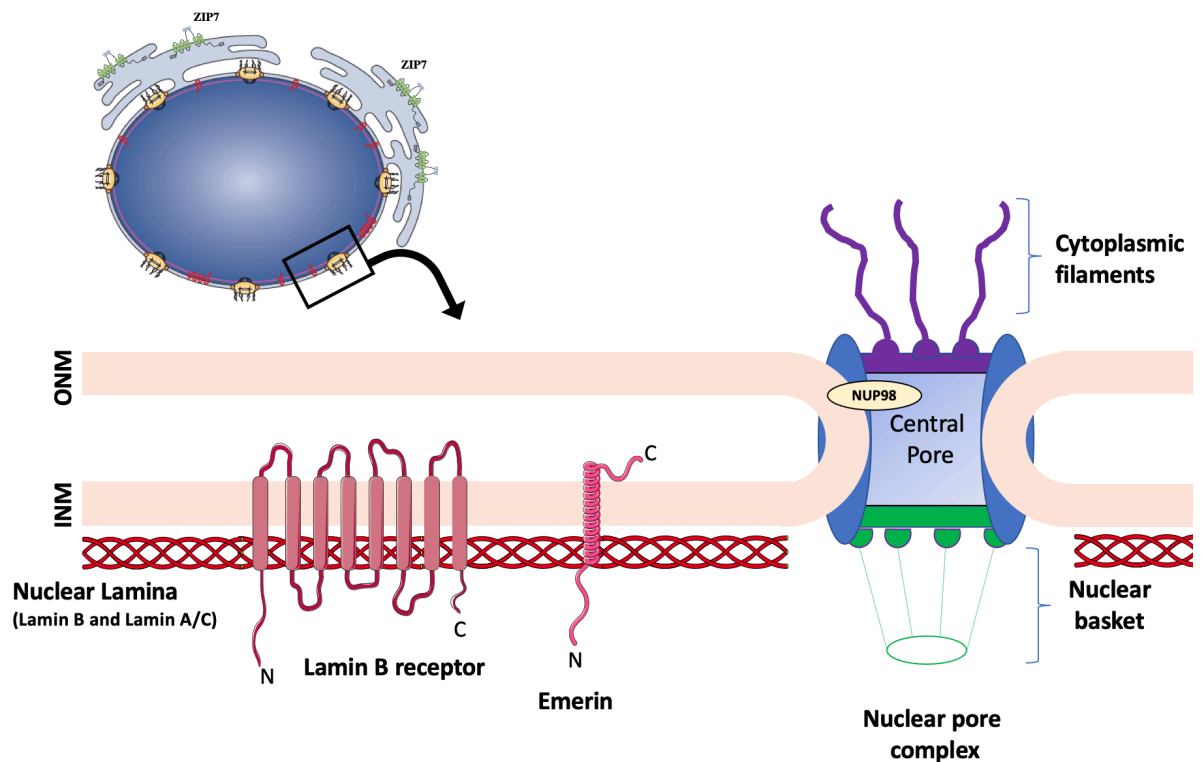


Figure 5.6 Topology of the nuclear envelop.

The nuclear envelop consist of inner and outer nuclear membranes (INM, ONM) which are joined at the nuclear pore complex (NPC). NPCs are built of many nucleoporin proteins including (NUP98). The INM is anchored by transmembrane proteins to the underlying layer of lamina (Lamin B and Lamin A/C).

5.3.2.1 ZIP7 co-localize with Lamins (Lamin B and Lamin A/C)

Lamins are nuclear intermediate filament proteins that are located within the INM²⁴³. The nuclear lamins are named lamin A, B, and C²⁴⁴. Due to their position in the INM, they were chosen to investigate the nuclear localization of ZIP7. Immunofluorescence was performed in cells transfected with WT-ZIP7 and stained with antibodies against Lamin B and Lamin A/C. By using a Lecia RPE Automatic microscope, ZIP7 showed a clear ring around the nuclear as well as in the ER. In contrast, lamin B and lamin A/C showed a circle around the nucleus without any ER staining (**Figure 5.5A and 5.6A**). The merged images stained green and red show a bright yellow colour in the perinuclear region in cells transfected with WT ZIP7 and probed with Lamin B and Lamin A/C (**Figure 5.5A and 5.6A**). These results suggest that ZIP7 co-localizes with lamin B and lamin A/C.

After obtaining impressive results on the Lecia RPE Automatic microscope, the coverslips were used to image them on a Zeiss LSM 880 confocal microscope with the option of higher resolution. The merge images stained green and red showed clear, bright yellow staining around the nucleus in cells transfected with WT ZIP7, suggesting that ZIP7 and Lamin B and Lamin A/C are localized in the same place (**Figure 5.7B and 5.8B**). To confirm that a line was drawn across the cell to measure the fluorescence intensity, which gives us a more confirmation of ZIP7 colocalization with lamin B and Lamin A/C as a clear peak overlay of lamin B Lamin A/C with V5 (**Figure 5.7B and 5.8B**). These results suggest the nuclear localization of ZIP7.

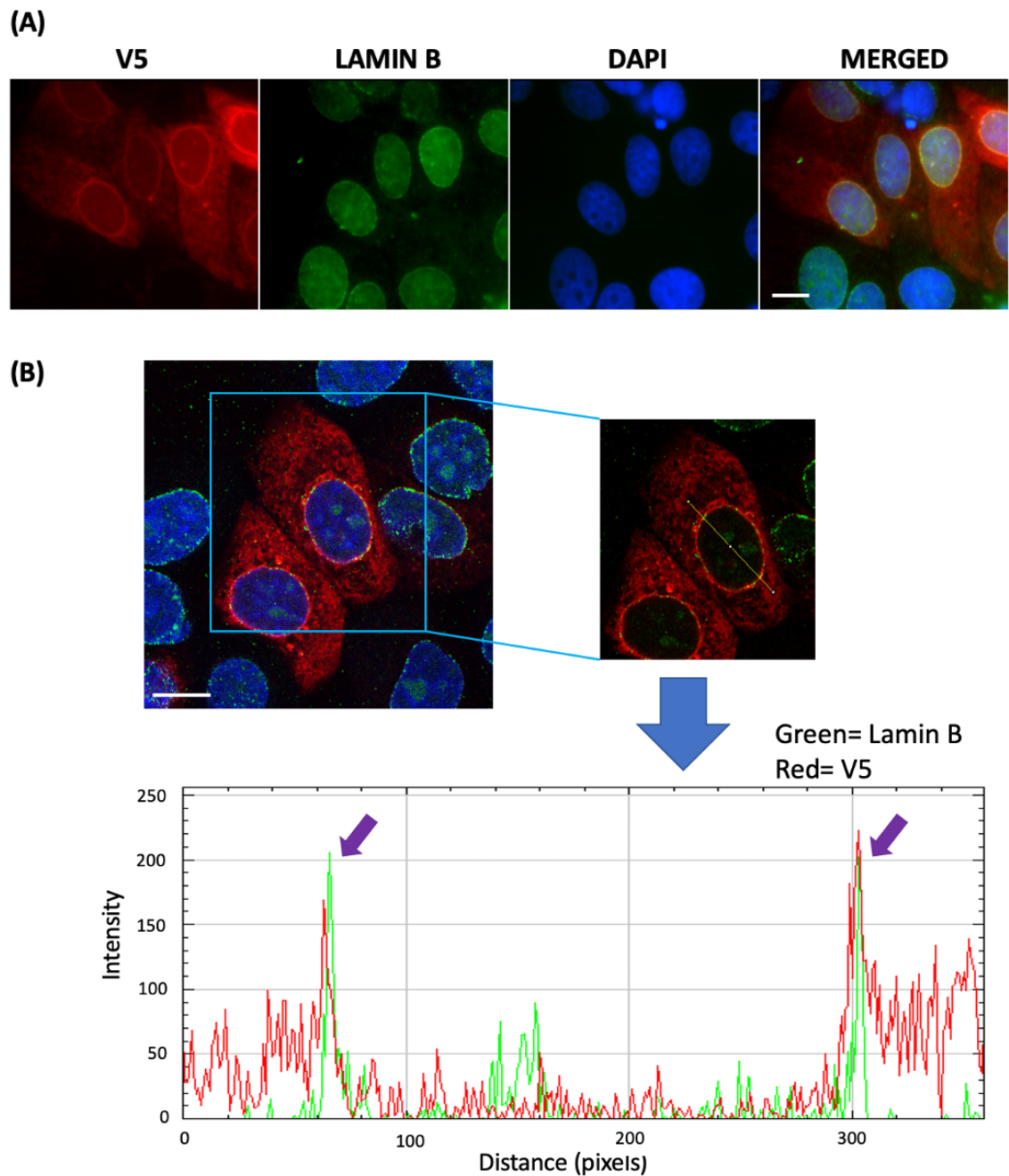


Figure 5.7: ZIP7 Co-localises with Lamin B in MCF-7 cells

MCF-7 cells were transfected with WT-ZIP7 for 18 hours. The cells were fixed and permeabilized before probing with mouse V5 and rabbit Lamin B conjugated to Alexa Fluor 594 (Red) and Alexa Fluor 488 (Green) respectively, and the nuclei were stained blue with DAPI. (A) These images were captured with a Leica RPE automatic microscope using a 63x magnification lens. (B) Image was taken on a Zeiss LSM 880 Microscope using a 63x Zeiss Oil immersion lens and processed using Zeiss's ZEN software for Microsoft Operating system. A line was drawn across the cell and the colocalization intensity was measured along this line. The RGB profiler plugin from ImageJ was used to plot colocalization. Scale bar, 10 μ m

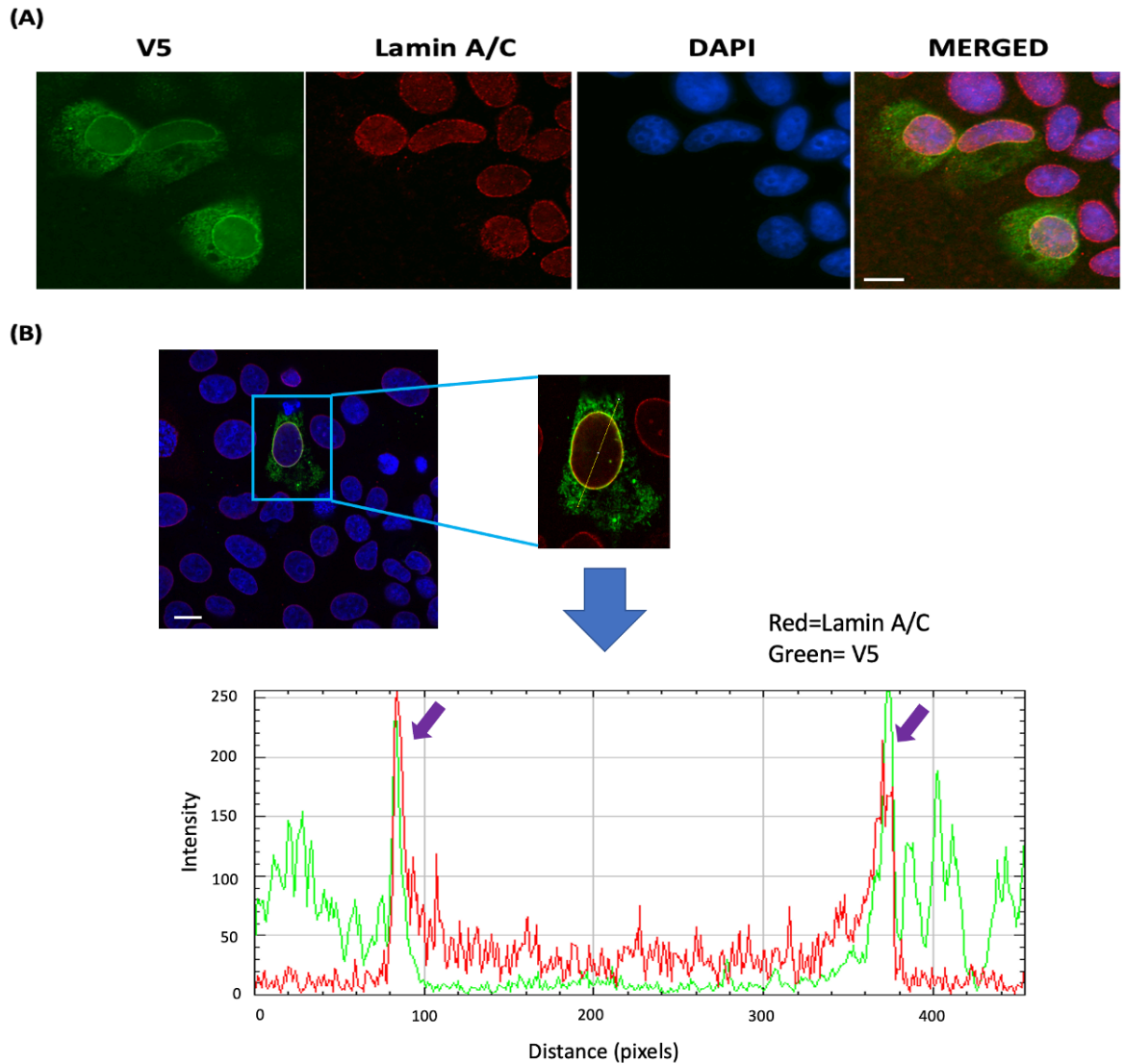


Figure 5.8: ZIP7 Co-localises with Lamin A/C in MCF-7 cells.

MCF-7 cells were transfected with WT ZIP7 for 18 hours. The cells were fixed and permeabilized before probing with rabbit V5 and mouse anti-Lamin A/C conjugated to Alexa Fluor 488 (Green) and Alexa Fluor 594 (Red) respectively, and the nuclei were stained blue with DAPI. (A) These images were captured with a Leica RPE automatic microscope using a 63x magnification lens. (B) Image was taken on a Zeiss LSM 880 Microscope using a 63x Zeiss Oil immersion lens and processed using Zeiss's ZEN software for Microsoft Operating system. A line was drawn across the cell and the colocalization intensity was measured along this line. The RGB profiler plugin from ImageJ was used to plot colocalization. Scale bar, 10 μm

5.3.2.2 ZIP7 colocalizes with component of the nuclear pore complex (NPC).

Having confirmed the colocalization of ZIP7 with Lamin B (**Figure 5.7**) and Lamin A/C (**Figure 5.8**), this investigation was extended further to examine the colocalization of ZIP7 with nuclear pore complex. The nuclear pore complexes (NPCs) are channels that penetrate the nuclear envelope, which connecting the nucleus and the cytoplasm²⁴⁵ (**Figure 5.6**). These structures consist of multiple copies of different proteins known as nucleoporin (NUPs)²⁴⁵. NUP98 is a nucleoporin protein anchored into the inner ring of the nuclear pore complex, which is embedded in the nuclear envelope⁹². The V5 staining (red fluorescent) has been shown to have solid perinuclear staining in addition to endoplasmic reticulum showing in (**Figure 5.9A**). However, NUP98 gives intermittent staining around the nucleus without any endoplasmic reticulum staining as expected because the nuclear pore complex are channels embedded intermittently throughout the nuclear envelope. In the merged picture there is some orange intermittent perinuclear staining in the cells transfected with wild type ZIP7 (**Figure 5.9A**).

To improve the pictures, a high-resolution Zeiss LSM 880 confocal microscope was used to image the coverslips. High-resolution images show a clear yellow intermittent perinuclear ring around the nucleus in cells transfected with wild-type ZIP (**Figure 5.9B**). The peak of V5 (red colour) and NUP98 (green colour) was found to overlap when plotting the colocalization using the RGB profiler plugin from ImageJ and using a line drawn through two nuclear pore complexes. When a line was drawn through only one NPC, there was no colocalize of NUP98 and ZIP7. This colour histogram suggests that ZIP7 is located all over the nuclear membrane, and at any point when it meets the nuclear pore complex, the colour will be yellow, and the peak will appear. These results suggest that ZIP7 is located in the nuclear envelope.

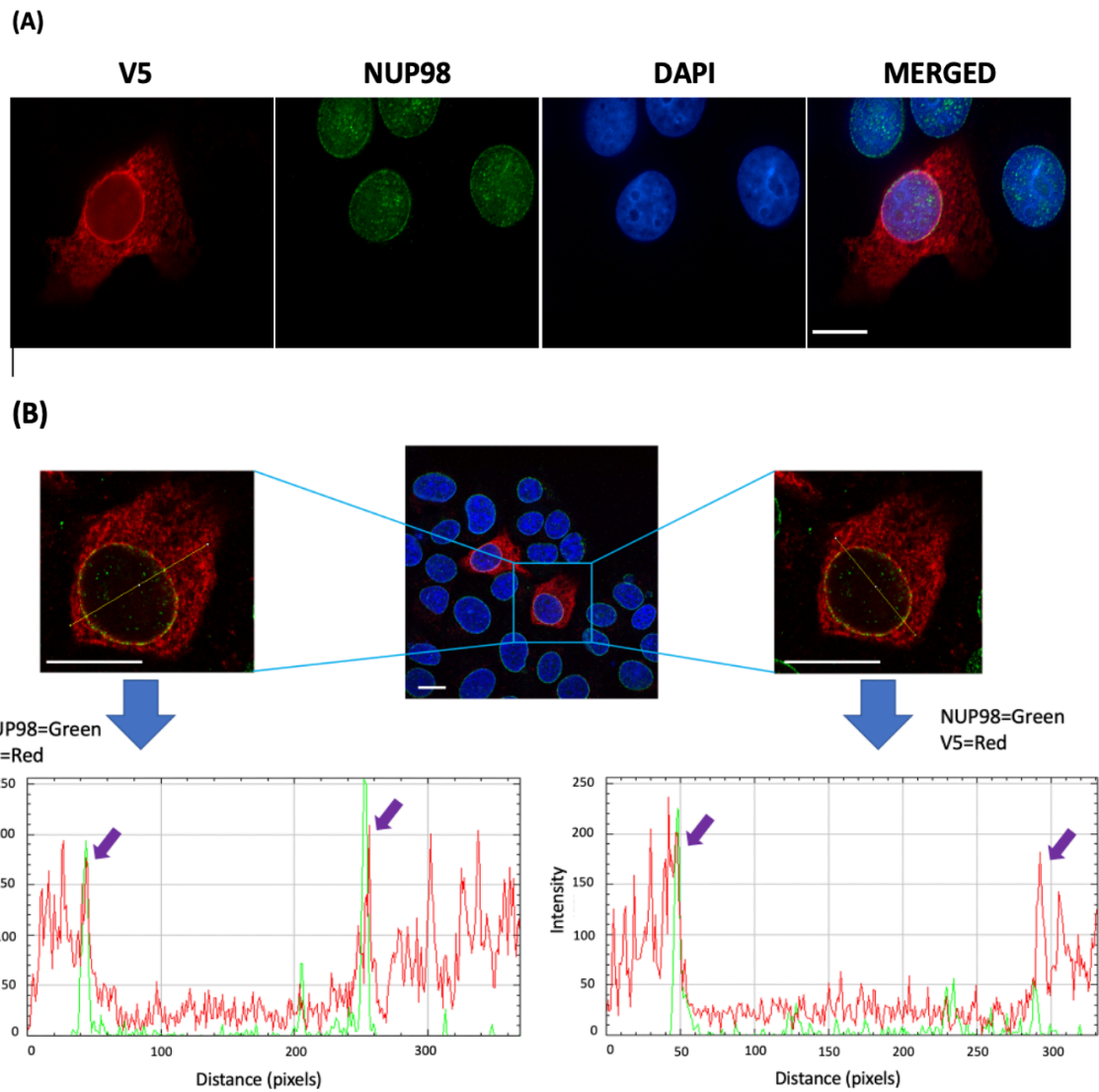


Figure 5.9: ZIP7 Co-localises with NUP98 in MCF-7 cells.

MCF-7 cells were transfected with WT ZIP7 for 18 hours. The cells were fixed and permeabilized before probing with mouse V5 and rabbit NUP98 conjugated to Alexa Fluor 594 (Red) and Alexa Fluor 488 (Green) respectively, and the nuclei were stained blue with DAPI (blue). (A) These images were captured with a Leica RPE automatic microscope using a 63x magnification lens. (B) Image was taken on a Zeiss LSM 880 Microscope using a 63x Zeiss Oil immersion lens and processed using Zeiss's ZEN software for Microsoft Operating system. A line was drawn across the cell and the colocalization intensity was measured along this line. The RGB profiler plugin from ImageJ was used to plot colocalization. Scale bar, 10 μ m

5.3.2.3 ZIP7 co-localizes with inner nuclear transmembrane proteins

The ONM of the nuclear envelope is contiguous with the endoplasmic reticulum, whereas the INM contains several integral membrane proteins, including lamin B receptor and emerin. Having confirmed the colocalization of ZIP7 with Lamins (**Figure 5.7, 5.8**) and NUP98 (**Figure 5.9**), this investigation was extended further to examine the colocalization of ZIP7 with some of the integral membrane proteins which are located in the inner nuclear membrane.

A- ZIP7 co-localizes with Lamin B Receptor

Lamin B receptor is an eight transmembrane integral protein located in the INM and the ER²⁴⁶, and it is expected to be similar to ZIP7. Using a Leica RPE Automatic Microscope shows that the lamin B receptor is located in the ER membrane, and also some of the cells show some perinuclear staining (**Figure 5.10A**). The merged image shows a yellow perinuclear region around the nucleus as well as the ER, which suggests a similar location of the lamin B receptor to ZIP7. This was investigated further using a Zeiss LSM 880 microscope. The enlarged picture of the figure shows clear yellow spotting in the perinuclear region without ER co-localization. By plotting the colour histogram across the yellow line in (**figure 5.10B**), the peak of V5 (red colour) can be seen to colocalize with the peak of the lamin B receptor (green colour). This colour histogram suggests the co-localization of the Lamin B receptor and ZIP7.

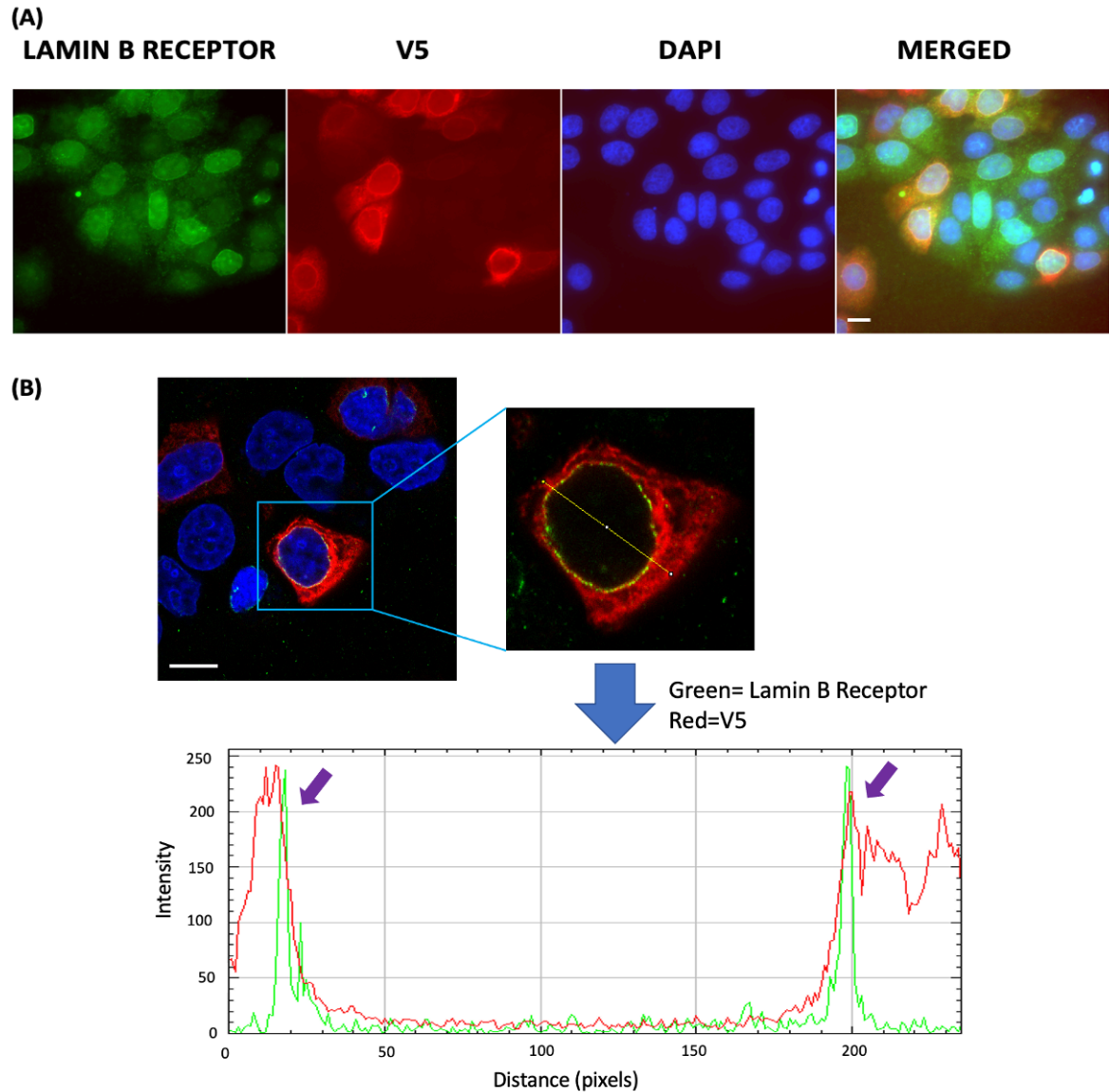


Figure 5.10: ZIP7 Co-localises with Lamin B receptor in MCF-7 cells.

MCF-7 cells were transfected with WT ZIP7 for 18 hours. The cells were fixed and permeabilized before probing with mouse V5 and rabbit Lamin B receptor conjugated to Alexa Fluor 594 (Red) and Alexa Fluor 488 (Green) respectively, and nuclei were stained blue with DAPI (blue). (A) These images were captured with a Leica RPE automatic microscope using a 63x magnification lens. (B) Image was taken on a Zeiss LSM 880 Microscope using a 63x Zeiss Oil immersion lens and processed using Zeiss's ZEN software for Microsoft Operating system. A line was drawn across the cell and the colocalization intensity was measured along this line. The RGB profiler plugin from ImageJ was used to plot colocalization. Scale bar, 10 μ m

B- ZIP7 colocalizes with emerin

Emerin is a single transmembrane protein that resides in the inner nuclear membrane²⁴⁶. Using a Leica RPE Automatic Microscope shows that emerin is located around the nucleus (**Figure 5.11**). The merged image shows a yellow perinuclear region around the nucleus, suggesting a similar location of emerin and ZIP7.

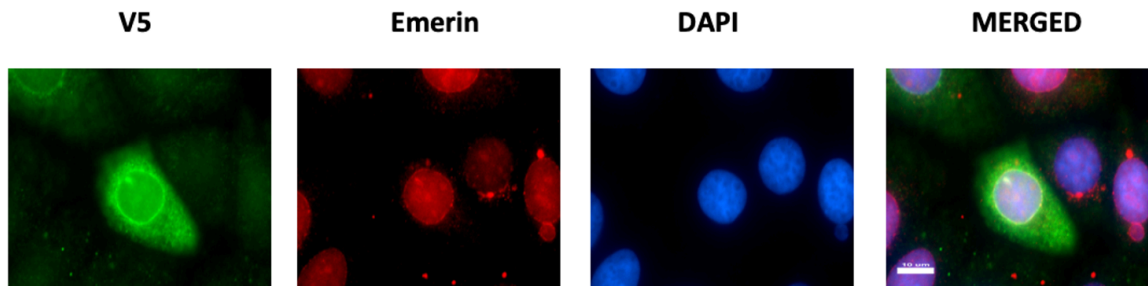


Figure 5.11: ZIP7 Co-localises with emerin in MCF-7 cells.

MCF-7 cells were transfected with WT ZIP7 for 18 hours. The cells were fixed and permeabilized before probing with rabbit V5 and mouse anti emerin conjugated to Alexa Fluor 488 (Green) and Alexa Fluor 594 (Red) respectively, and the nuclei were stained blue with DAPI (blue). (A) These images were captured with a Leica RPE automatic microscope using a 63x magnification lens. (B) A line was drawn across the cell and the colocalization intensity was measured along this line. The RGB profiler plugin from ImageJ was used to plot co-localization. Scale bar, 10 μm

5.3.3 Co-localization of pZIP7 with inner nuclear proteins markers:

After getting the promising results showing that ZIP7 colocalize with lamins (**Figure 5.7 and 5.8**), NUP98 (**Figure 5.9**), Lamin B receptor (**Figure 5.10**), and emerin (**Figure 5.11**), this investigation was extended further to examine the colocalization pZIP7 with markers of the INM. pZIP7 is the active form of ZIP7 when it's phosphorylated on S275 and S276, resulting in zinc release from the ER into cytosol. In this section, we investigate the nuclear localization of pZIP7, which could have a role in transporting the zinc into the nucleus and activate many of the transcription factors that have a role in cancer development.

5.3.3.1 Imaging pZIP7 with the nuclear pore complex

After getting promising results that show that ZIP7 colocalize with NUP98 (**Figure 5.9**), another experiments were performed to investigate the colocalization of NUP98 with the active form of ZIP7. The cells were transfected with WT ZIP7 and probed with pZIP7 antibody, which only binds to the active form of ZIP7. Using Lecia RPE automatic microscope, the pZIP7 image showed a ring around the nucleus and the ER. NUP98 showed clear green staining around the nucleus. The merged figure of cells transfected with wild-type ZIP7 clearly shows a yellow perinuclear ring (**Figure 5.12A**). These results suggest colocalization of the active form of ZIP7 (pZIP7) with NUP98.

Using a Zeiss LSM 880 confocal microscopy to obtain a higher resolution picture, the merged images show a clear yellow intermittent perinuclear ring around the nucleus in cells transfected with WT-ZIP7 (**Figure 5.12B**). The peak of pZIP7 (red colour) and NUP98 (green colour) was found to overlap together by plotting the colocalisation using the RGB profiler plugin from ImageJ. However, in some positions, the NUP98 and pZIP7 are not colocalising, according to the line drawn. This colour histogram suggests that pZIP7 is located all over the nuclear membrane, and when it meets the nuclear pore complex, the colour is yellow, and the peak appears. These results confirm that not only is ZIP7 colocalising with markers of the inner nuclear membrane, the activated form of ZIP7, pZIP7, is as well. These promising results suggest that ZIP7 around the nucleus is active and could actively transport zinc into the nucleus as well as into the cytoplasm from the ER store.

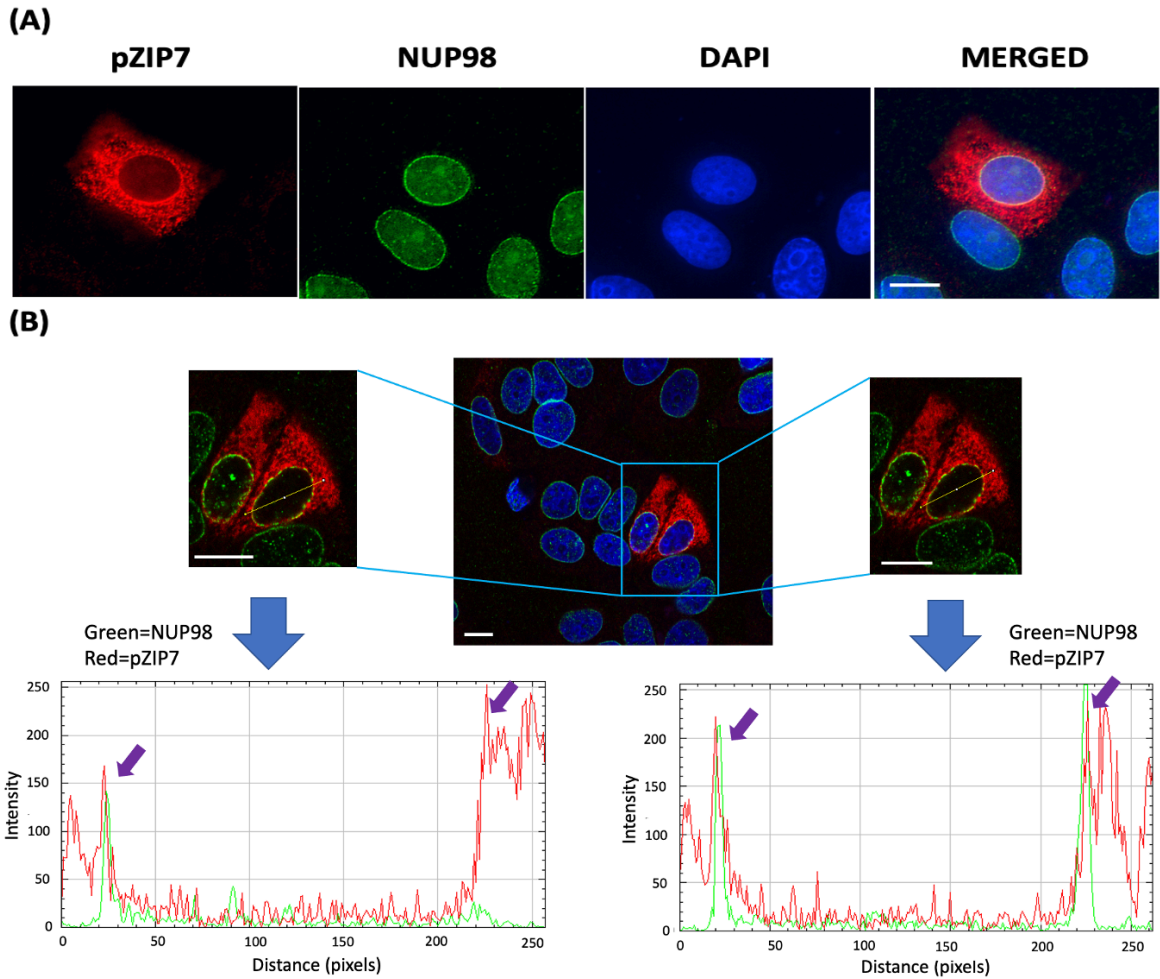


Figure 5.12: pZIP7 Co-localises with NUP98 in MCF-7 cells.

MCF-7 cells were transfected with WT ZIP7 for 18 hours. The cells were fixed and permeabilized before probing with mouse pZIP7 antibody and rabbit NUP98 conjugated to Alexa Fluor 594 (Red) and Alexa Fluor 488 (Green) respectively, and the nuclei were stained blue with DAPI (blue). (A) These images were captured with a Leica RPE automatic microscope using a 63x magnification lens. (B) Image was taken on a Zeiss LSM 880 Microscope using a 63x Zeiss Oil immersion lens and processed using Zeiss's ZEN software for Microsoft Operating system. A line was drawn across the cell and the colocalization intensity was measured along this line. The RGB profiler plugin from ImageJ was used to plot co-localization. Scale bar, 10 μ m

5.3.3.2 Co-localizes of pZIP7 with Lamin B Receptor

To test co-localization of the lamin B receptor with the active form of ZIP7, cells transfected with WT-ZIP7 were probed with antibodies for pZIP7 and Lamin B receptor. With the Leica RPE Automatic Microscope, the Lamin B receptor shows a bright green perinuclear staining with minimal endoplasmic reticulum staining (**Figure 5.13A**). The merged picture shows apparent yellow staining in the perinuclear region and some orange staining in the ER, which suggests the lamin B receptor and pZIP7 are co-localized.

The coverslips were additionally imaged using a Zeiss LSM 880 confocal microscope to see a higher resolution perinuclear image and measure the intensity of fluorescence. **Figure 5.13B** shows a clear intermittent yellow staining in the perinuclear region. Also, the peak overlay in the colour histogram confirms the colocalization of the lamin B receptor with the active form of ZIP7, suggesting that ZIP7 is active on the nuclear envelope, and it is likely to be able to transport zinc into the nucleus.

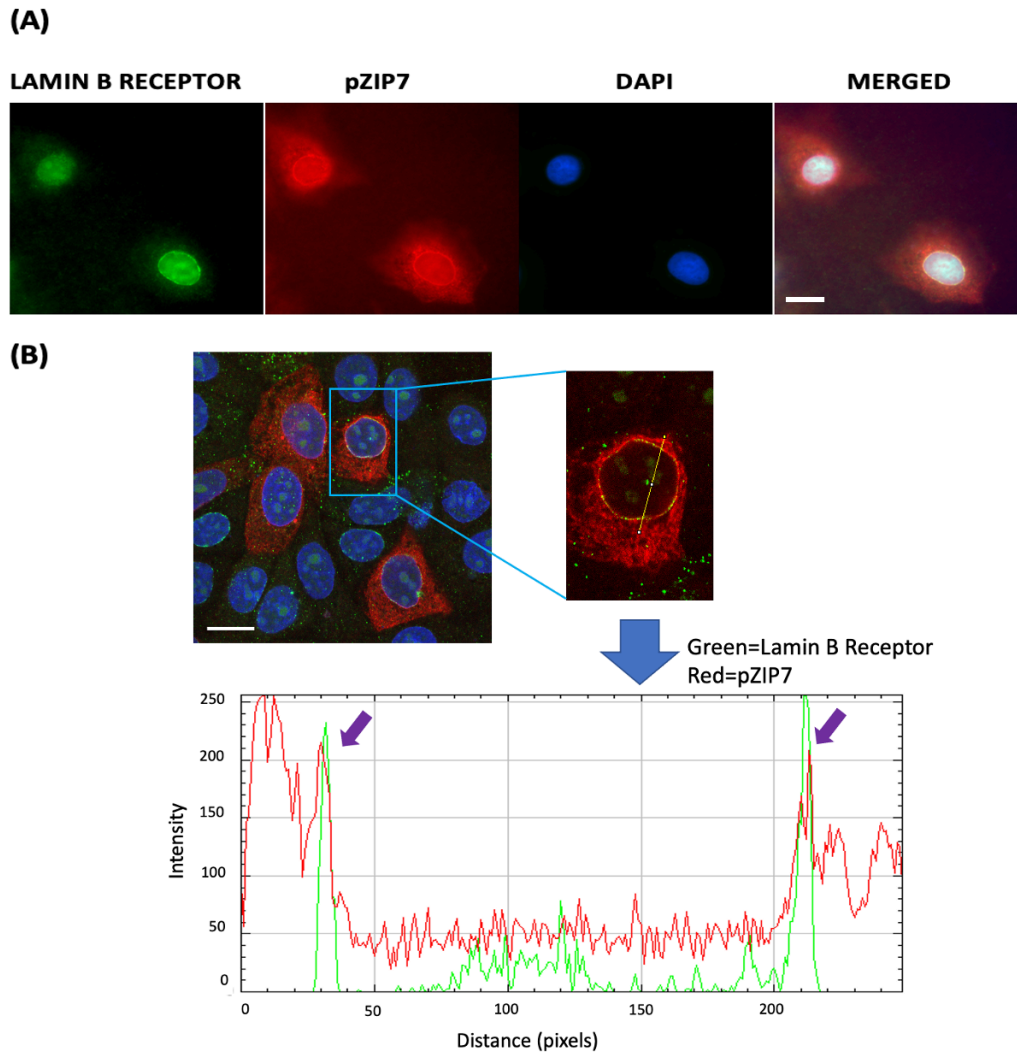


Figure 5.13: pZIP7 Co-localises with Lamin B receptor in MCF-7 cells.

MCF-7 cells were transfected with WT ZIP7 for 18 hours. The cells were fixed and permeabilized before probing with mouse pZIP7 antibody and rabbit Lamin B receptor conjugated to Alexa Fluor 594 (Red) and Alexa Fluor 488 (Green) respectively, and the nuclei were stained blue with DAPI (blue). (A) These images were captured with a Leica RPE automatic microscope using a 63x magnification lens. (B) Image was taken on a Zeiss LSM 880 Microscope using a 63x Zeiss Oil immersion lens and processed using Zeiss's ZEN software for Microsoft Operating system. A line was drawn across the cell and the colocalization intensity was measured along this line. The RGB profiler plugin from ImageJ was used to plot co-localization. Scale bar, 10 μ m

5.4 Chapter summary:

The data shown in this chapter suggest that ZIP7 is located on the nuclear envelope due to its co-localisation with Lamin, NUP98, Lamin B Receptor, and Emerin. Furthermore, the active form of ZIP7 (pZIP7) also colocalises with NUP98 and Lamin B Receptor suggesting the presence of the active form of ZIP7 on the nuclear envelope. This would also mean that ZIP7 could transport zinc into the nucleus as well as into the cytoplasm from its position on the ER membrane and the nuclear envelope. This is an important discovery that now needs further investigation.

The nuclear membrane consists of two separate lipid bilayers, the inner nuclear membrane (INM) and outer nuclear membrane (ONM) which are separated by a perinuclear space of approximately 30-50 nm^{247,248}. Due to the close proximity of the ONM and INM, we need an advanced techniques to further confirm the INM localization of ZIP7. The immunofluorescence microscopy images presented in this chapter suggest that ZIP7 is located in the nuclear envelope at the resolution of light microscopy. The Airyscan confocal microscopy used in this project generate images with a lateral resolution of approximately 140 nm and an axial resolution of approximately 350 nm²⁴⁹⁻²⁵¹. This resolution is not sufficient to differentiate if the protein of interest located in INM or ONM because the distance between them is well below these limits. However, the use of differential labelling of protein located in INM or ONM with a fluorescent protein (mCherry) and a different colour fluorophore (eGFP) will help to overcome this weakness and will allow to study the colocalization^{252,253}.

To further confirm the hypothesis that ZIP7 is located in INM, immunogold-label electron microscopy²⁵⁴⁻²⁵⁶ and proximity ligation assay in combined with super-resolution microscopy is needed. Due to the high resolution of the immunoelectron microscopy, it is considered as a gold standard to study the protein localization^{257,258}. The super-resolution microscopy is capable to provide an image with a resolution between 100 to 20 nm²⁵⁹⁻²⁶¹ and this will overcome the issue of diffraction limit of the light microscope which is approximately 250 nm lateral and 800 nm axial²⁶². Single molecule fluorescence recovery after photobleaching (smFRAP)²⁶³ is a new technique which could be used to understand the dynamic movement

of ZIP7 and its distribution on INM. Metal-Induced Energy Transfer (MIET) is also a new technique with an axial resolution of a few nanometers which allows an accurate differentiation between the INM and ONM^{262,264}. ZIP7 has already been implicated in cancer growth, and proving a role for ZIP7 in nuclear zinc transport could have significant implications for new cancer therapeutics. To build upon this discovery that ZIP7 is located on the NE, the next chapter will focus on investigating the mechanism of ZIP7 trafficking to the inner nuclear membrane.

6. Chapter 6: Investigation the nuclear localization signals (NLS) of ZIP7

6.1 Introduction

The immunofluorescence results in the previous chapter demonstrate that ZIP7 is present on the nuclear membrane as well as on the endoplasmic reticulum (ER) membrane, suggesting ZIP7 can transport zinc from the ER store into the nucleus. It is of fundamental importance to understand how ZIP7 is targeted into the nucleus because it could have a crucial role in many cellular processes such as DNA replication, transcription, and RNA processing²⁶⁵. The nuclear pore complex allows the bidirectional movement of macromolecules between the cytoplasm and the nucleus. Small molecules (<40 kDa) can diffuse passively through the nuclear pore complex; however, larger proteins are transported actively and their NLS is recognized by a specific carrier (importin- α or importin- β)²⁶⁶. There is much less is known about the mechanisms for nucleocytoplasmic transport of ZIP7 and other integral membrane proteins compared to transport of soluble proteins which are well characterized. The aim of this chapter to investigate the nuclear translocation mechanism of ZIP7.

It is not clear how ZIP7 is translocated to the nucleus. Computer analysis of the ZIP7 sequence in chapter 3 revealed that ZIP7 is predicted to have three NLSs, which could have a role in its nuclear localisation. To assess the function of these motifs, ZIP7 mutants, lacking the potential NLS signals, were generated by site-directed mutagenesis. These mutants were assessed to characterise the role of ZIP7-mediated zinc transport from the endoplasmic reticulum and nucleus. Immunofluorescence was performed to confirm the transfection efficiency and the cellular localisation of the mutants. Colocalisation of those mutants with inner nuclear membrane markers was investigated. Furthermore, a western blot was performed to examine the effect of those mutants on ZIP7 activation. The different functions of the ZIP7 NLS mutants were assessed using phospho-kinase arrays to examine the activated downstream pathways.

6.2 Methods

Site-directed mutagenesis was performed by Mutagenex Inc. to generate ZIP7 mutant constructs lacking the predicted NLS. MCF-7 cells grown on coverslips or dishes were transfected with WT-ZIP7 and ZIP7 NLS mutant constructs and harvested after 18 hours. The coverslips were stained for V5 and Lamin B receptor or pZIP7. The human phospho-kinase arrays (R&D system, ARY003B) were used, and according to the arrays, the kinases that markedly increased were further confirmed by western blot. Please refer to Chapter 2 for the methods of cell preparation and treatment (Section 2.1), site-directed mutagenesis (Section 2.2), immunofluorescence (Section 2.4), western blot (Section 2.5), and proteome profiler antibody arrays (Section 2.6).

6.3 Results

6.3.1 Mutagenesis of the potential NLSs of ZIP7:

Confocal microscopy of MCF7 cells (Chapter 5) showed that ZIP7 and its active form (pZIP7) co-localised with Lamin, NUP98, Lamin B Receptor, and emerin, all molecules that are associated with the INM. Since the mechanism of ZIP7 translocation to INM is not known, the potential NLS motifs in ZIP7 were mutated (**Figure 6.1**) to study the effect of each one of these on ZIP7 nuclear targeting. NLS1 has alanine mutation in the three basic amino acids (²⁸⁸KRR³⁰¹ to ²⁸⁸AAA³⁰¹), the NLS2 has alanine mutation in two basic amino acids (³¹⁰KR³¹¹ to ³¹⁰AA³¹¹), and the NLS3 (²⁸⁸AAAGGSTVPKDGPVRPQNAEEEEAA³¹¹) contains both these mutations (**Figure 6.1**).

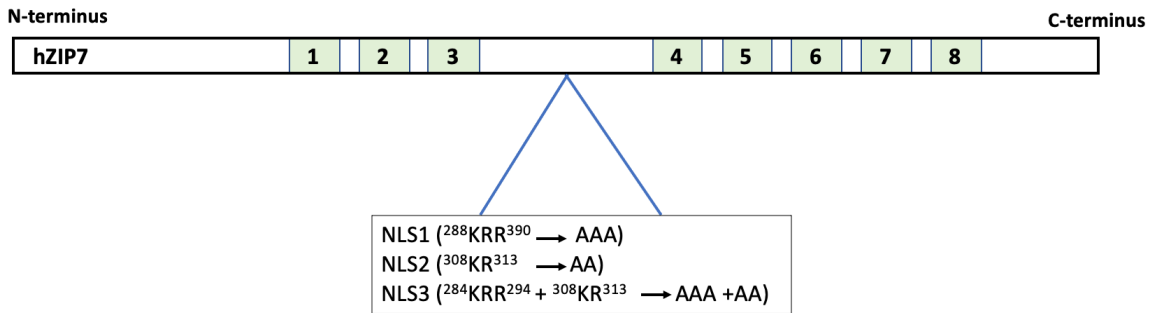


Figure 6.1 Schematic diagram that shows the alanine mutation in the predicted NLSs

ZIP7 is predicted to have three nuclear localization signals. Alanine mutations were performed to study the effect on ZIP7 nuclear localization.

6.3.2 The role of predicted nuclear localization signals in targeting ZIP7 to the INM:

To study the transfection efficiency of the ZIP7 mutant constructs and the role of the basic region of ZIP7 in its nuclear localization, immunofluorescence was performed on the cells transfected with WT-ZIP7, NLS1, NLS2, and NLS3. The immunofluorescence results showed the cells were expressing the recombinant protein well. By counting the number of cells that were positive for V5 in different visual fields, the transfection rates varied from 33%, in cells overexpressing WT ZIP7 to 27%, as in cells overexpressing NLS2 (**Figure 6.2**). This result suggests that all these mutations of ZIP7 were expressed similarly to the WT ZIP7.

The enlarged views were examined to observe any changes in the location of ZIP7. These revealed no or little effect on the nuclear translocation ability of ZIP7 as all the mutants showed a bright nuclear ring around the nucleus (**Figure 6.2**). Furthermore, all mutants appeared to show similar endoplasmic reticulum staining as well, suggesting little or no effect of these mutations on the cellular location of ZIP7 and that ZIP7 may have a different mechanism of nuclear translocation, not involving these motifs which are still not clearly understood.

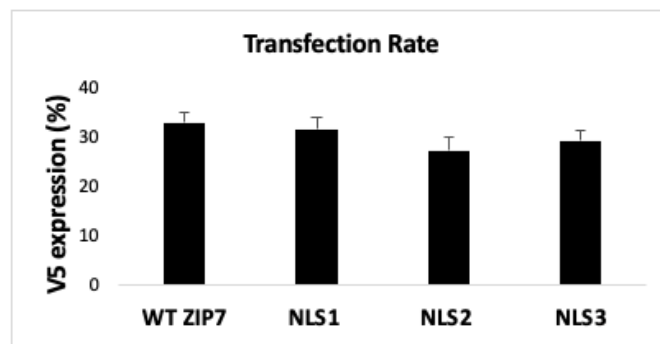
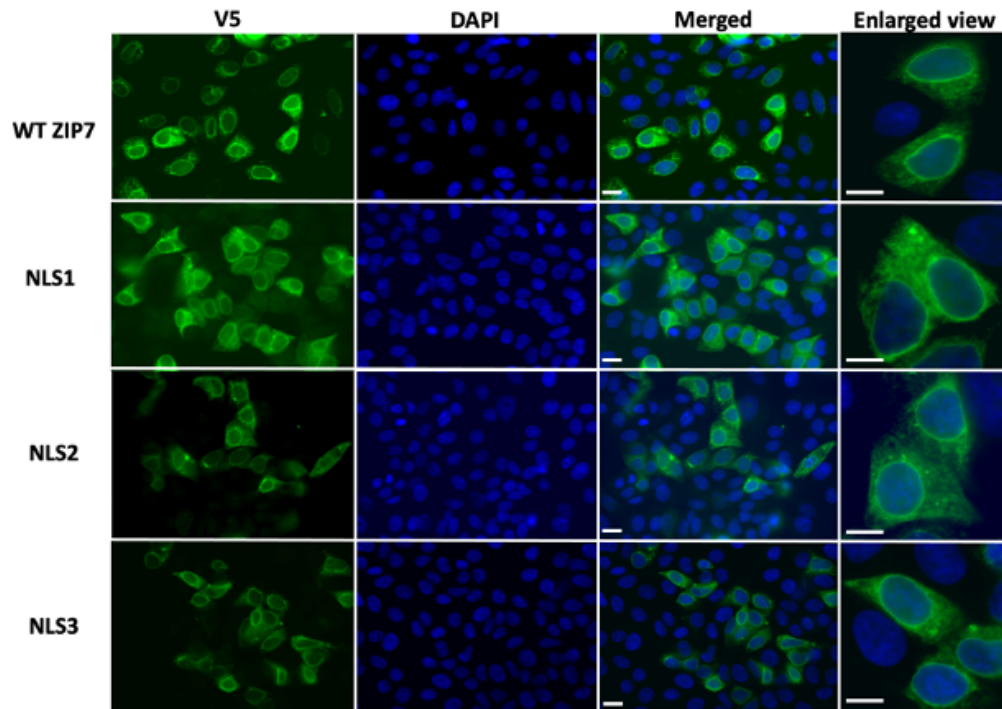


Figure 6.2: Transfection efficiency of NLS ZIP7 mutants.

MCF-7 cells were transfected with wild-type and NLS mutants of ZIP7 for 18 hours. The cells were fixed and permeabilized before being probed for V5 conjugated to Alexa Fluor 488 (green) and the nuclei were stained blue with DAPI. These images were captured with a Leica RPE Automatic Microscope using a 63x magnification lens. Scale bar, 10 μ m. The bar graph represents the percentage of cells positive for the ZIP7 constructs, from seven different fields of view.

6.3.3 Colocalization of ZIP7 NLS mutants with inner nuclear protein markers:

To further characterise the NLS ZIP7 mutants, immunofluorescence was performed using a INM marker such as lamin proteins, lamin B, located close to the inner nuclear membrane. The V5 antibody that recognises the C-terminal V5 tag on the recombinant proteins was used to detect the ZIP7 mutant constructs. The merged images show a bright yellow colour around the nucleus (**Figure 6.3**) which suggests the colocalisation of ZIP7 NLS mutants (V5, green) with lamin B (red) and their location on the inner nuclear membrane. The results, therefore, suggest that these mutations might not affect ZIP7 nuclear translocation.

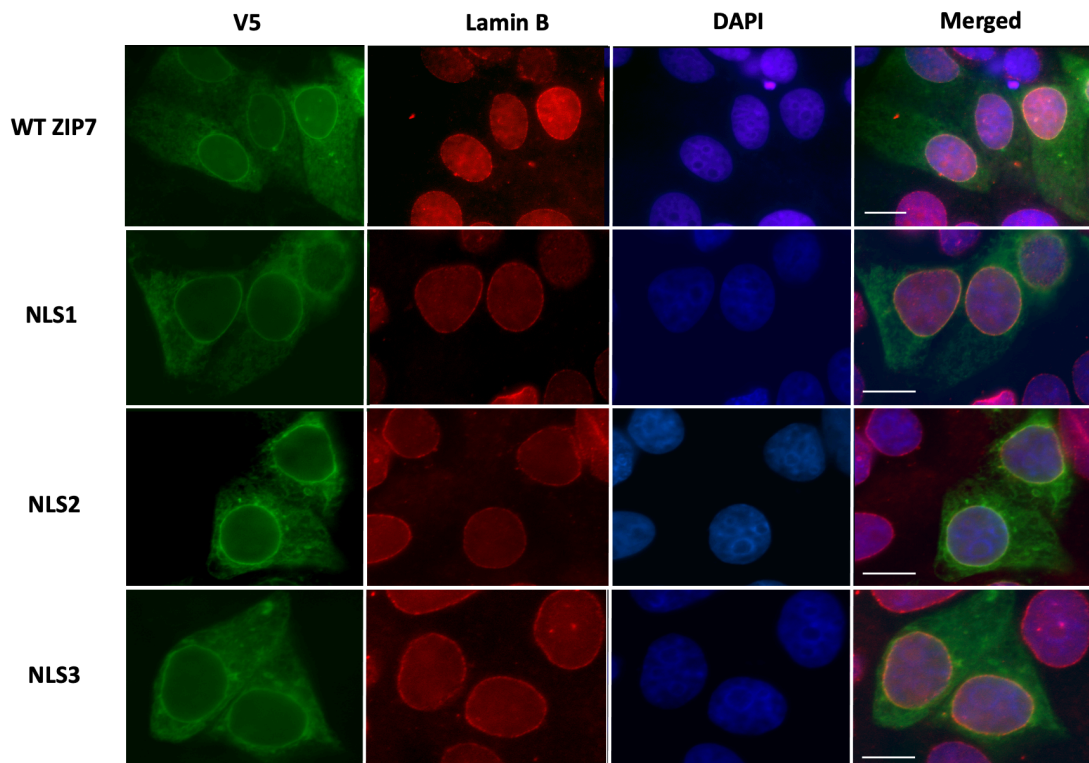


Figure 6.3 Colocalization of NLS mutants with Lamin B:

MCF-7 cells were transfected with NLS ZIP7 mutants for 18 hours. The cells were fixed and permeabilized before being probed with mouse V5 and rabbit LaminB conjugated to Alexa Fluor 594 (red) and Alexa Fluor 488 (green) respectively, and nuclei were stained blue with DAPI. These images were captured with a Leica RPE Automatic Microscope using a 63x magnification lens. Scale bar, 10 μ m

6.3.4 Effect the removal of nuclear localization signals on ZIP7 activation:

To investigate whether ZIP7 phosphorylation after 10 minutes of zinc treatment was adversely effected by mutation of the NLSs, immunofluorescence was performed using a pZIP7 antibody, which has been tested in Chapter 4. The V5 antibody was used to identify the cells transfected with different ZIP7 constructs. The percentage of cells transfected with WT ZIP7 that were positive for pZIP7 has increased significantly from 48% before zinc treatment to 84% after zinc treatment (**Figure 6.4**). The pZIP7 level in cells transfected with mutants NLS1 and NLS2 were 42% and 41% respectively at basal condition. After 10 minutes of zinc treatment, 67% of cells overexpressing ZIP7 NLS1 and 54% of the cells overexpressing NLS2 were positive for pZIP7. Interestingly the cells transfected with NLS3 showed a lower pZIP7 activation at basal condition 38% and after 10 minutes of zinc treatment 41%. All the ZIP7 NLS mutants showed an increase after 10 minutes of zinc treatment; however, none significantly. These results suggest that ZIP7 NLS mutation might interfere with CK2 binding on S275 and S276, resulting in less ZIP7 activation. These results further support the usefulness of the pZIP7 antibody in determining ZIP7 activation.

Western blot was performed in the cells transfected with WT ZIP7, NLS1, NLS2, and NLS3 and treated with zinc for 10 minutes to confirm the immunofluorescence results. Total ZIP7 antibody (proteinTech™) was used due to its ability to bind to both the active and inactive forms of ZIP7, while the pZIP7 antibody only binds to the active form of ZIP7 when it's phosphorylated on residues S275 and S276. Cells transfected with WT ZIP7 showed a similar activation pattern as in Chapter 4 - a significantly increased ZIP7 activation after 10 minutes of zinc treatment (**Figure 6.5 A**). A similar pattern of WT ZIP7 activation showed with cells transfected with NLS mutants, the level of pZIP7 increase after 10 minutes of zinc treatment but with no statistically significant compared to the untreated cells (**Figure 6.5 B-D**).

The results are represented as a percentage of the untreated state to understand how the NLS mutant response performed differently to zinc stimulation. This showed that pZIP7 level is significantly increased after 10 minutes of zinc treatment in cells transfected with WT ZIP7

only while cells transfected with NLS1, NLS2, and NLS3 mutants showed an increase in the level of pZIP7 after zinc treatment, but this was not statistically significant (**Figure 6.5 E**). These results suggest that the predicted NLS is essential for maximal ZIP7 activation as none of the mutants was significantly increased in pZIP7 level after 10 minutes of zinc treatment. NLS mutants might interfere with CK2 binding on S275 and S276, affecting ZIP7 activation and downstream signaling pathways.

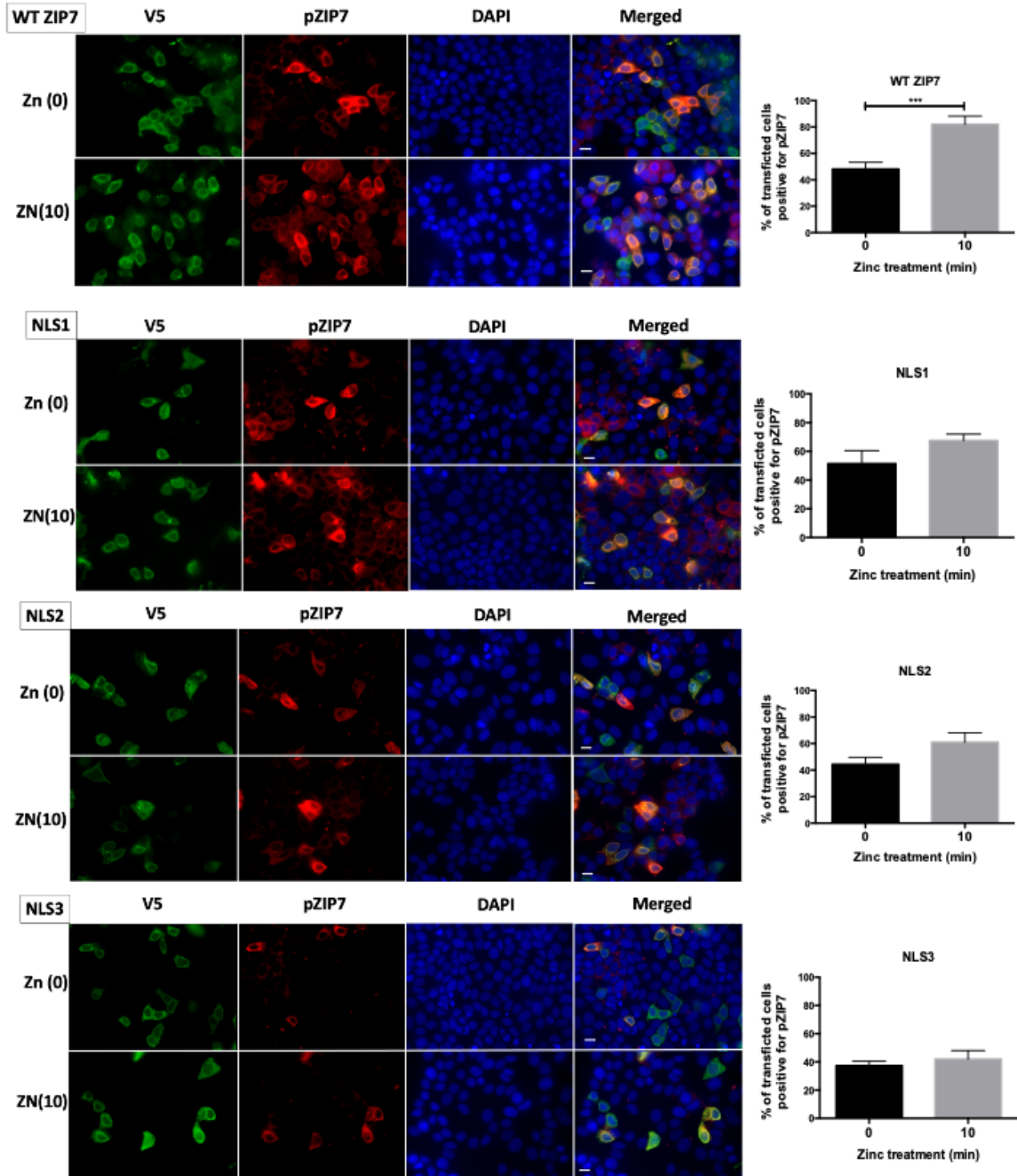


Figure 6.4: Increase ZIP7 activation in the cells transfected with NLS ZIP7 mutant constructs.

MCF-7 cells were transfected with WT ZIP7 or ZIP7 NLS mutants for 18 hours. The cells were untreated or treated with zinc for 10 minutes before being fixed and permeabilized. The coverslips were probed with pZIP7 antibody and V5 conjugated to Alexa Fluor 594 (Red) and Alexa Fluor 488 (Green) respectively and the nuclei were stained blue with DAPI. Images were captured with a Leica RPE automatic microscope using a 63x magnification lens. Scale bar, 10 μ m. Numbers in brackets indicate the length of zinc treatment in minutes. The bar graph shows the percentage of transfected cells that are positive for pZIP7 as a mean of nine different fields of view \pm standard error. *** = $p < 0.001$

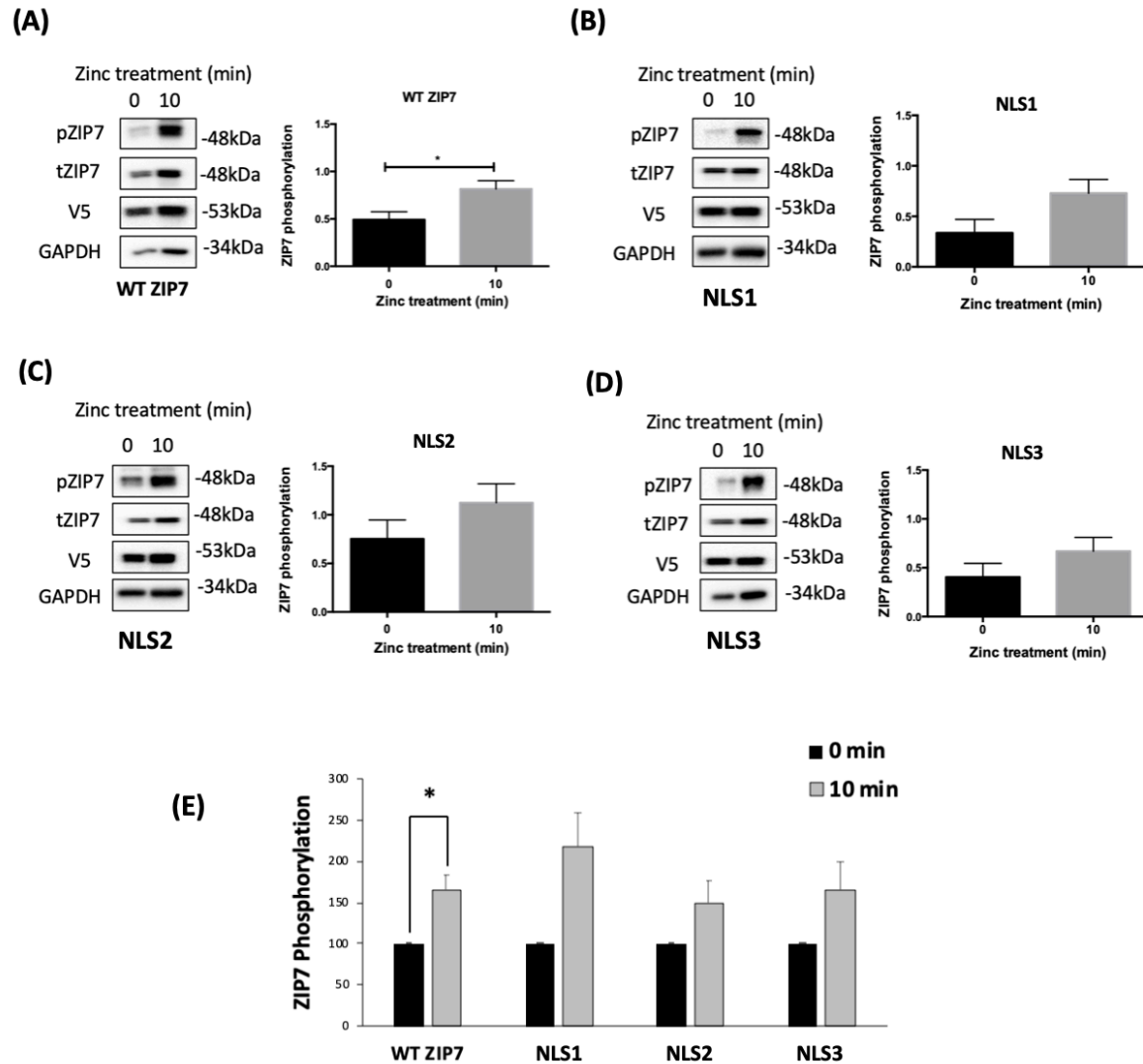


Figure 6.5: Effect of zinc treatment on activation of ZIP7 NLS mutants.

MCF7 cells transfected with wild type ZIP7, NLS1, NLS2, or NLS3, treated with zinc for 10 minutes and the cell lysates were analysed by western blot. The membrane was probed with antibodies to pZIP7 (48 kDa), tZIP7 (48 kDa), V5 (53 kDa) and GAPDH (35 kDa). Densitometric data was normalised to tZIP7 and demonstrated in relative density units as mean values of $n = 4 \pm$ standard error. The statistical significance compared to the samples with no zinc treatment is indicated by * ($p < 0.05$). E, Graph represents the results expressed as percentage of the untreated constructs.

6.3.5 Using phospho-kinase arrays to investigate the effect of NLS mutants on ZIP7 activation and downstream signaling:

ZIP7 is a gatekeeper for zinc release from cellular stores⁶³. Zinc ions released from cellular stores inhibit protein tyrosine phosphatases such as protein tyrosine phosphatase 1B, resulting in activation of many cellular tyrosine kinases^{241,242}. Activation of these tyrosine kinases as a result of ZIP7 activation is responsible for the aggressive behaviour of tamoxifen resistance breast cancer cells⁶⁹. The previous chapter suggested that ZIP7 is located on the nuclear membrane, and by searching different online databases, it was discovered that ZIP7 have 3 predicted NLSs. The western blot results in **Figure 6.5** showed that nuclear localisation signals of ZIP7 are essential for ZIP7 maximal activation. In this study, phospho-kinase arrays were used to analyse any differences between the WT ZIP7 and those mutants with a potential nuclear localisation site removed. Human phospho-kinase arrays are a helpful tool that determines the activation of 43 different cellular kinases with their specific phosphorylated residue in the same samples. The samples used for this analysis were additionally treated with 0, 2, 5, or 10 minutes of zinc to assess response to a zinc stimulus and a direct comparison to the wild-type ZIP7.

Before running cell samples on the array's membranes, western blot analysis was performed to confirm that the expression level of recombinant ZIP7 does not change with zinc treatment by probing the membrane with V5. Western blot results in **Figure 6.6** shows a good transfection level of WT ZIP7 and ZIP7 NLS mutants at different time points of zinc treatment. This result confirms that any change in the downstream signaling pathways of NLS mutants is not due to their expression level and due to their affect on ZIP7 activity.

The phospho-kinases arrays used in this study are based on the analysis of cell lysate samples on nitrocellulose membranes. The cells were transfected with WT ZIP7 or ZIP7 NLS mutants and treated with zinc for up to 10 minutes. The cell lysates were incubated on a membrane containing several antibodies targeted to different kinases. The human phospho-kinase arrays consist of two membranes, part A and part B. Part A consists of two pairs of reference spots on the left corners and one pair of negative control spots on the bottom right corner, as illustrated in **Figure 6.7**. Part B contains one pair of reference spots on the upper right corner

and one pair of negative control spots on the bottom right corner, as illustrated in **Figure 6.7**. The density of the dots was measured using Quick Spot Imaging Analysis Software, and the results were analysed using Microsoft® Excel for Mac. The high density of the spots in the phospho-kinase arrays corresponds to an increased phosphorylation level within the cells. The results obtained from these arrays are shown in **Figure 6.8**.

Assessing the results obtained from the WT ZIP7 blot shows an increase in intensity to many dots, especially after 10 minutes of zinc treatment (**Figure 6.8**). However, some key kinases are also activated by 5 minutes, such as AKT 1/2/3 (S473), ERK1/2 (T202/Y204, T185/Y187), CREB (S133), WNK1 (T60), p70S6 Kinase (T389), and p70S6 Kinase (T421/S424). This is an encouraging result as these kinases are immediately downstream of ZIP7-mediated zinc release^{69,74}. Significant phosphorylation of ZIP7 is detected at 2 minutes of zinc treatment, which is compatible with kinase activation at 5 minutes of zinc treatment¹⁶⁹. Examination of the NLS mutants suggests that NLS1 and NLS2 appear similar to the WT ZIP7. In contrast, the cells transfected with NLS3 appear to have paler dots, suggesting that the important motif has been removed, resulting in decreased phosphorylation of many kinases.

To examine the actual level of each kinase, a bar graph was produced showing densitometric values of the pairs of corresponding duplicate dots for all the kinases detected at 0, 2, 5 and 10 minutes of zinc treatment. The activity of the kinases was divided into two groups according to the signal density: marked increase (> 5000 density units) and mild increase (2000-5000 density units) at 10 minutes of zinc treatment compared with the untreated cells. To reduce false positive results due to the variability of background intensity, differences of less than 2000 units were considered negative.

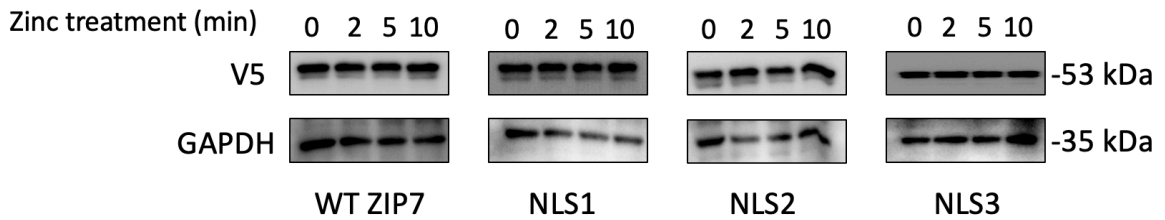


Figure 6.6 Confirmation of the expression of recombinant ZIP7 constructs.

MCF7 cells transfected with wild type ZIP7, NLS1, NLS2, or NLS3 and then treated with zinc for up to 10 minutes. The cell lysates were analysed by western blot. Antibodies against V5 and GAPDH were used to probe the membrane. Protein bands of V5 (53 kDa) and GAPDH (35 kDa) are pictured.

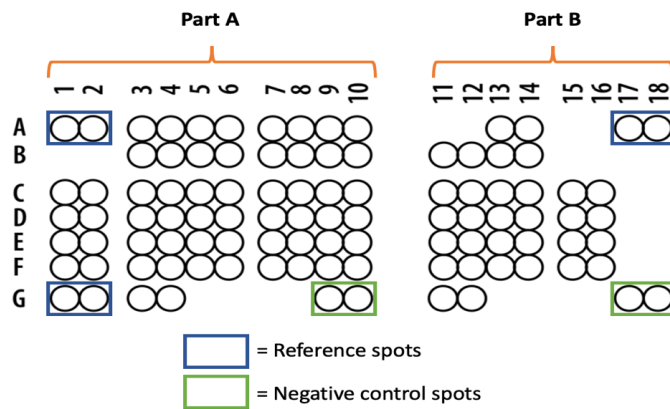


Figure 6.7 Human phospho-kinase array coordinates

The image shows schematic dots in the array's membrane. There are a pair of reference spots in the corner of each membrane. Two pairs on the left side of Part A and one pair on the right side of Part B) which highlighted in blue box. Each membrane also has a negative control spot which is highlighted in green box. The Image sourced from R &D System.

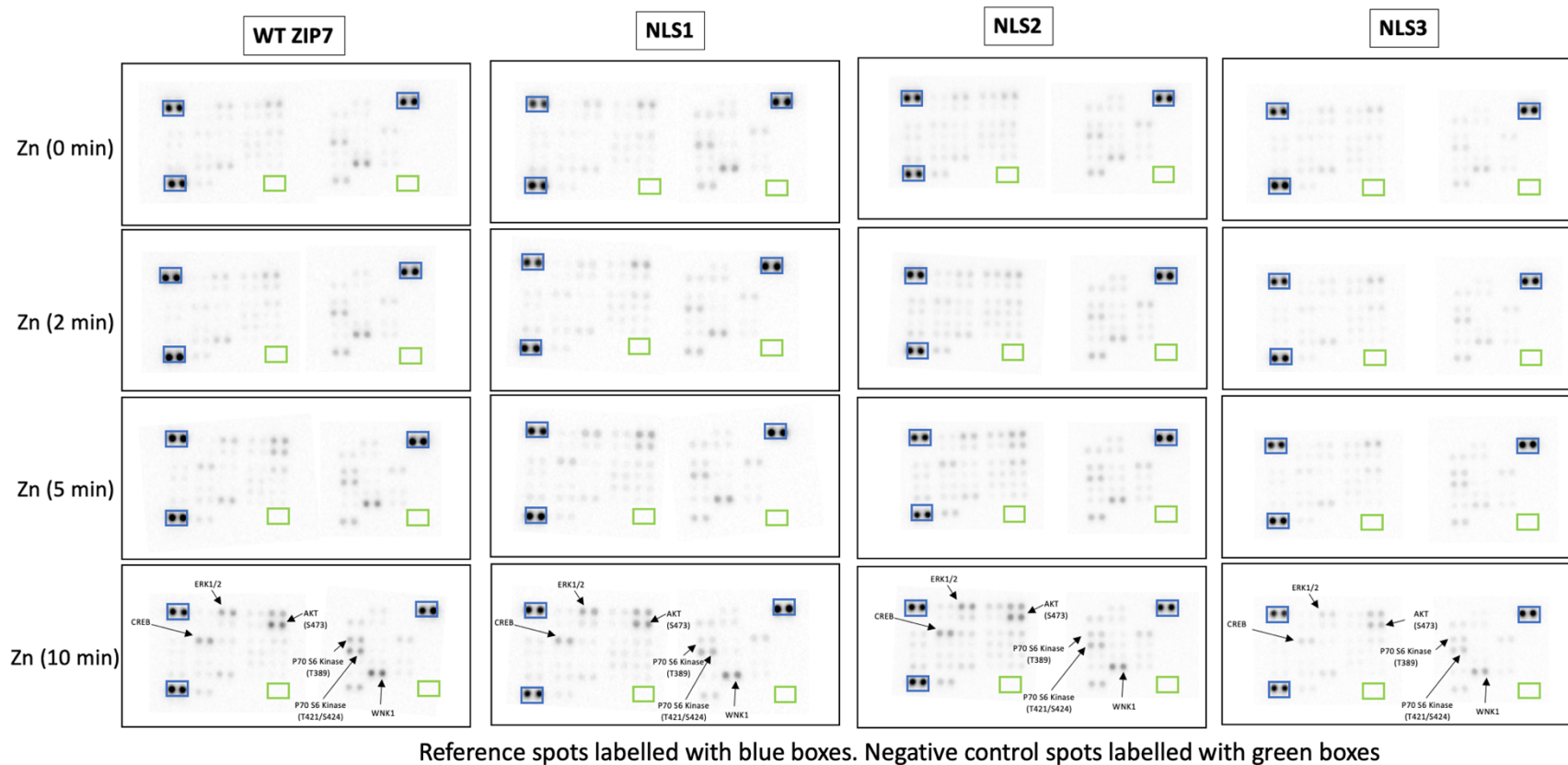


Figure 6.8 Phosphokinase arrays in MCF-7 cells transfected with WT ZIP7 and ZIP7 NLS mutants with zinc stimulation

MCF-7 cells were transfected with WT ZIP7, NLS1, NLS2, or NLS3 and treated with zinc for up to 10 minutes. Phosphorylation of selected kinases was determined using the human phospho-kinase antibody arrays (R&D Systems) according to manufacturer's instructions. Each kinase was detected in duplicate spots. Reference spots are labelled with the blue boxes and the negative control spots are labelled with green boxes. The kinases that show a marked increase (>5000 density units) after 10 minutes zinc treatment, compared with the control samples (no zinc treatment) are indicated.

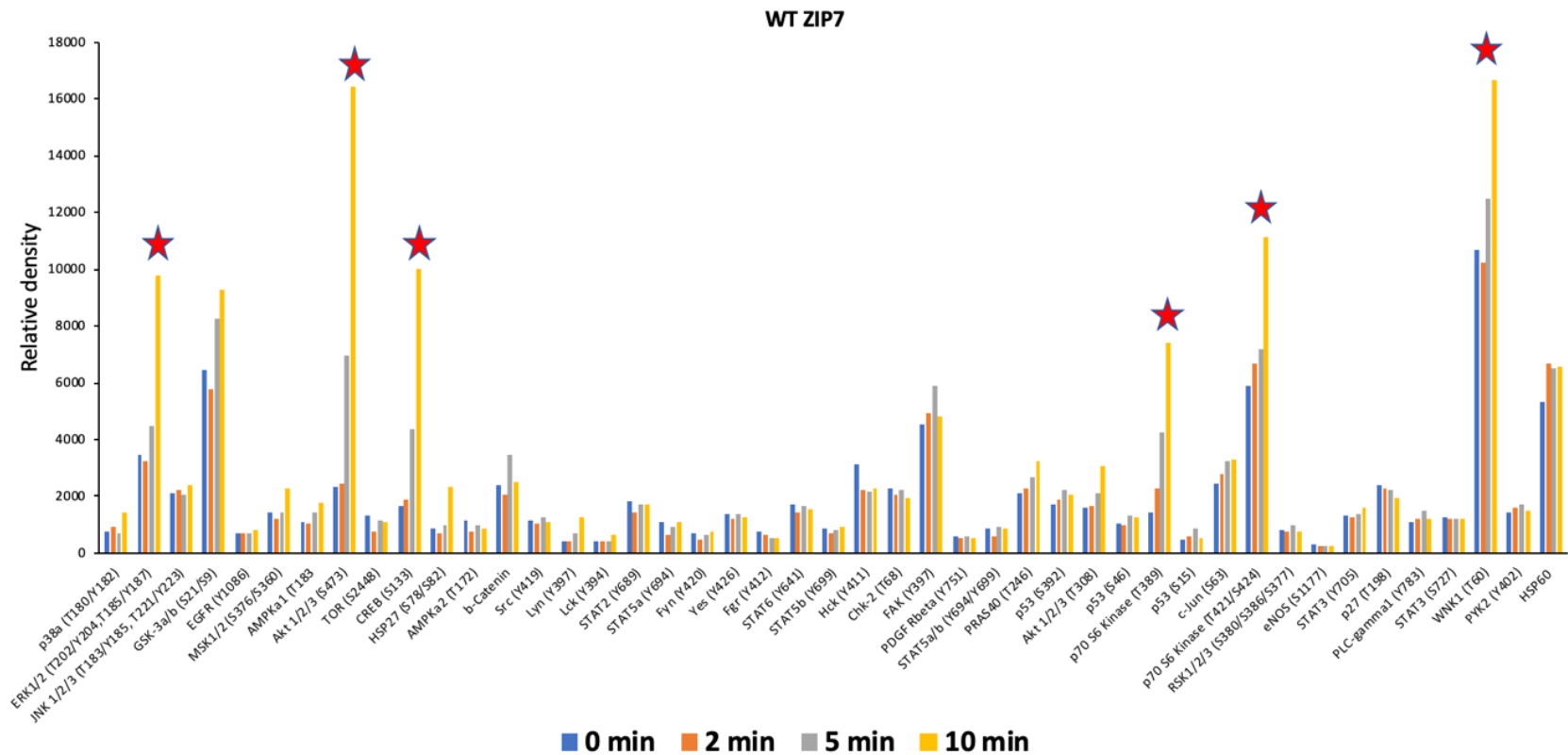


Figure 6.9 Densitometric analysis of phospho-kinase arrays in MCF-7 cells transfected with WT ZIP7 and stimulated with zinc.

MCF-7 cells were transfected with WT ZIP7 for 18 hours. Zinc treatment was performed for 2, 5, and 10 minutes. Phosphorylation of selected kinases at the residues indicated in bracket was determined using the human phospho-kinase antibody arrays (R&D Systems). Densitometric data are presented as mean of the duplicate dots for each kinase \pm standard error (n=2). The kinases that show a marked increase (>5000 density units) after 10 minutes zinc treatment, compared with the control samples (no zinc treatment) are indicated with a red star.

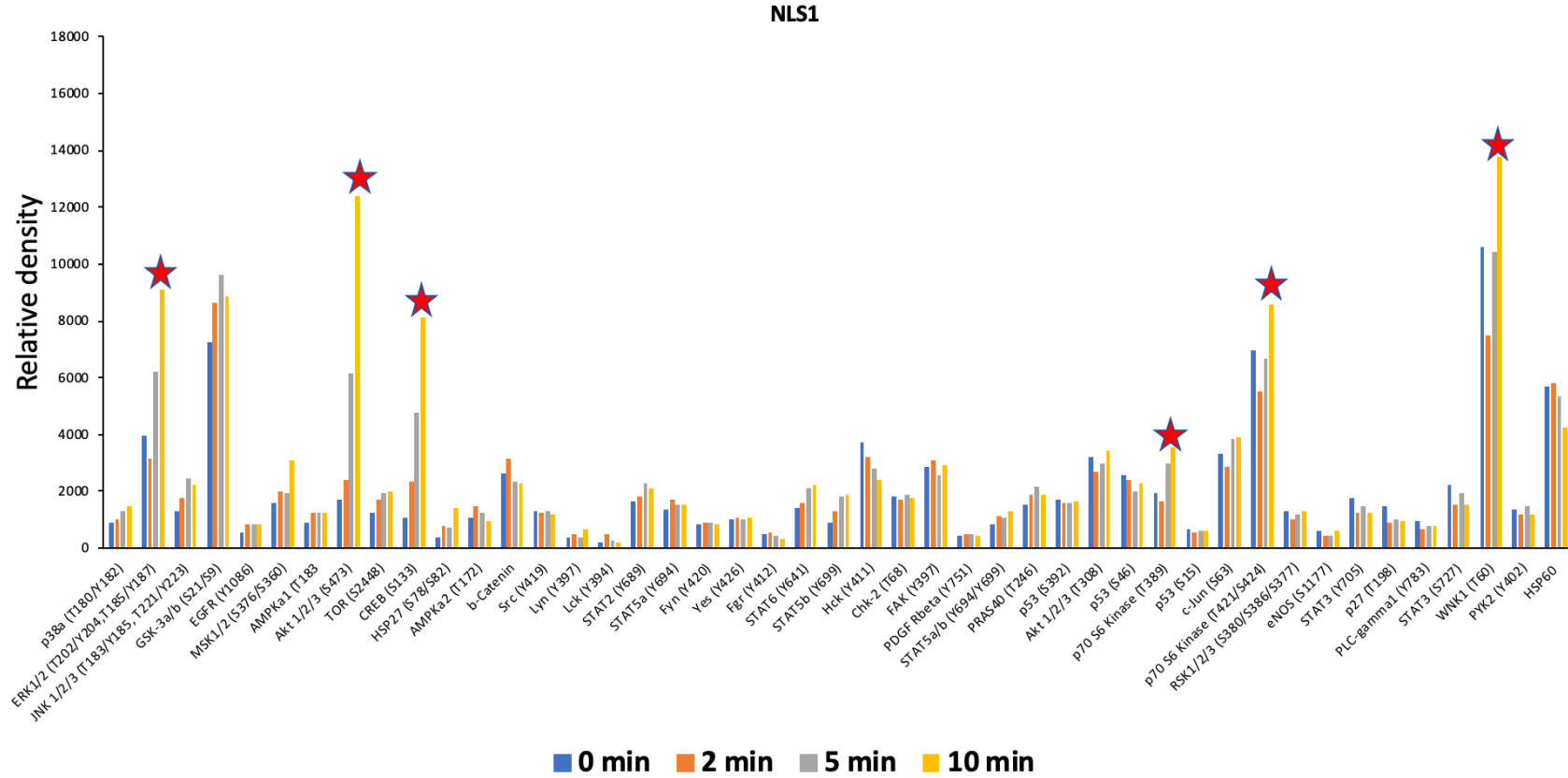


Figure 6.10 Densitometric analysis of phospho-kinase arrays in MCF-7 cells transfected with ZIP7 NLS1 with zinc stimulation.

MCF-7 cells were transfected with NLS1 for 18 hours. Zinc treatment was performed for 2, 5, and 10 minutes. Phosphorylation of selected kinases at the residues indicated in bracket was determined using the human phospho-kinase antibody arrays (R&D Systems). Densitometric data are presented as mean of the duplicate dots for each kinase \pm standard error ($n=2$). The kinases that show a marked increase (>5000 density units) after 10 minutes zinc treatment, compared with the control samples (no zinc treatment) are indicated with a red star.

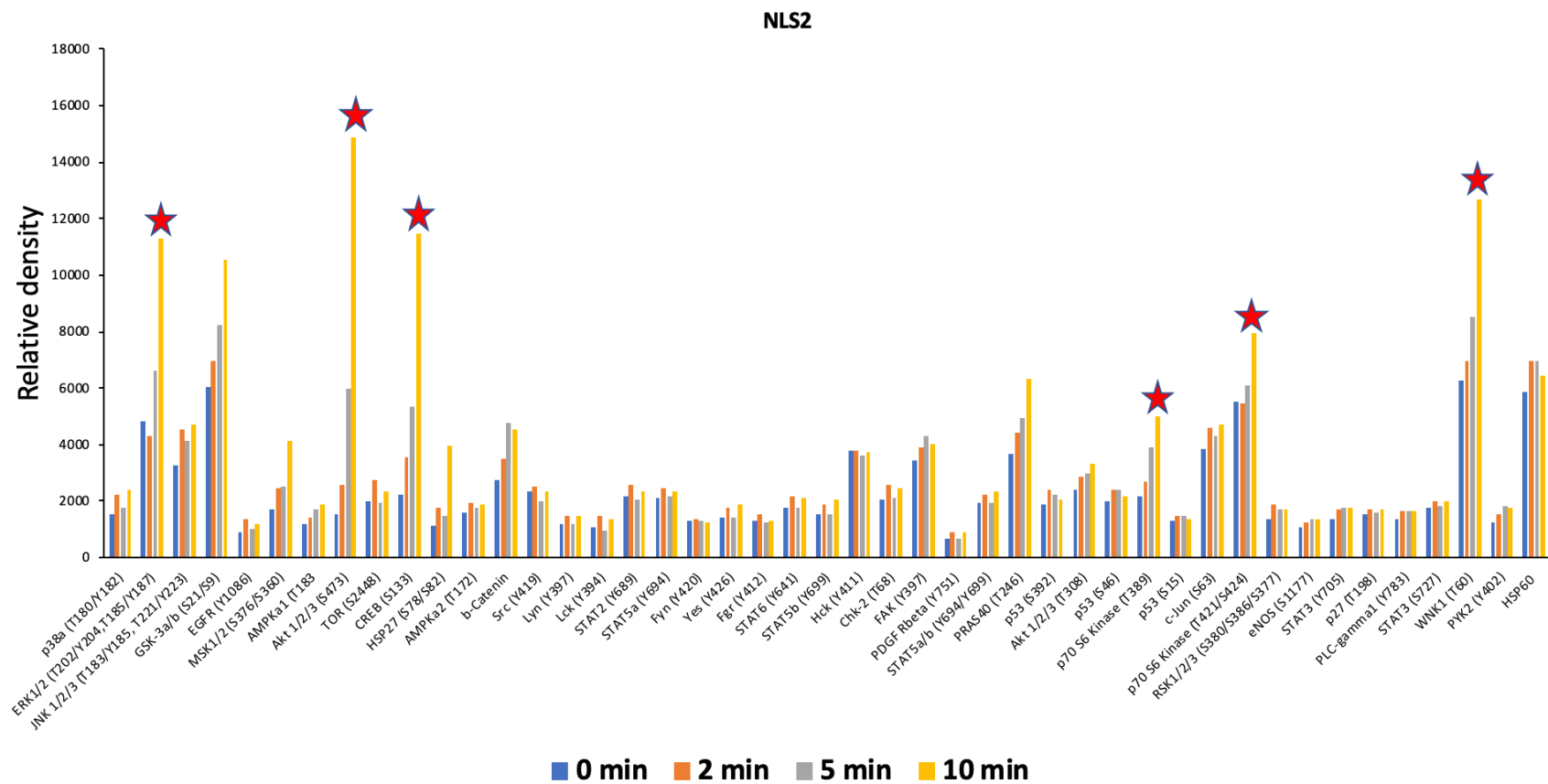


Figure 6.11 Densitometric analysis of phospho-kinase arrays in MCF-7 cells transfected with ZIP7 NLS2 with zinc stimulation.

MCF-7 cells were transfected with NLS2 for 18 hours. Zinc treatment was performed for 2, 5, and 10 minutes. Phosphorylation of selected kinases at the residues indicated in bracket was determined using the human phospho-kinase antibody arrays (R&D Systems). Densitometric data are presented as mean of the duplicate dots for each kinase \pm standard error (n=2). The kinases that show a marked increase (>5000 density units) after 10 minutes zinc treatment, compared with the control samples (no zinc treatment) are indicated with a red star.

NLS3

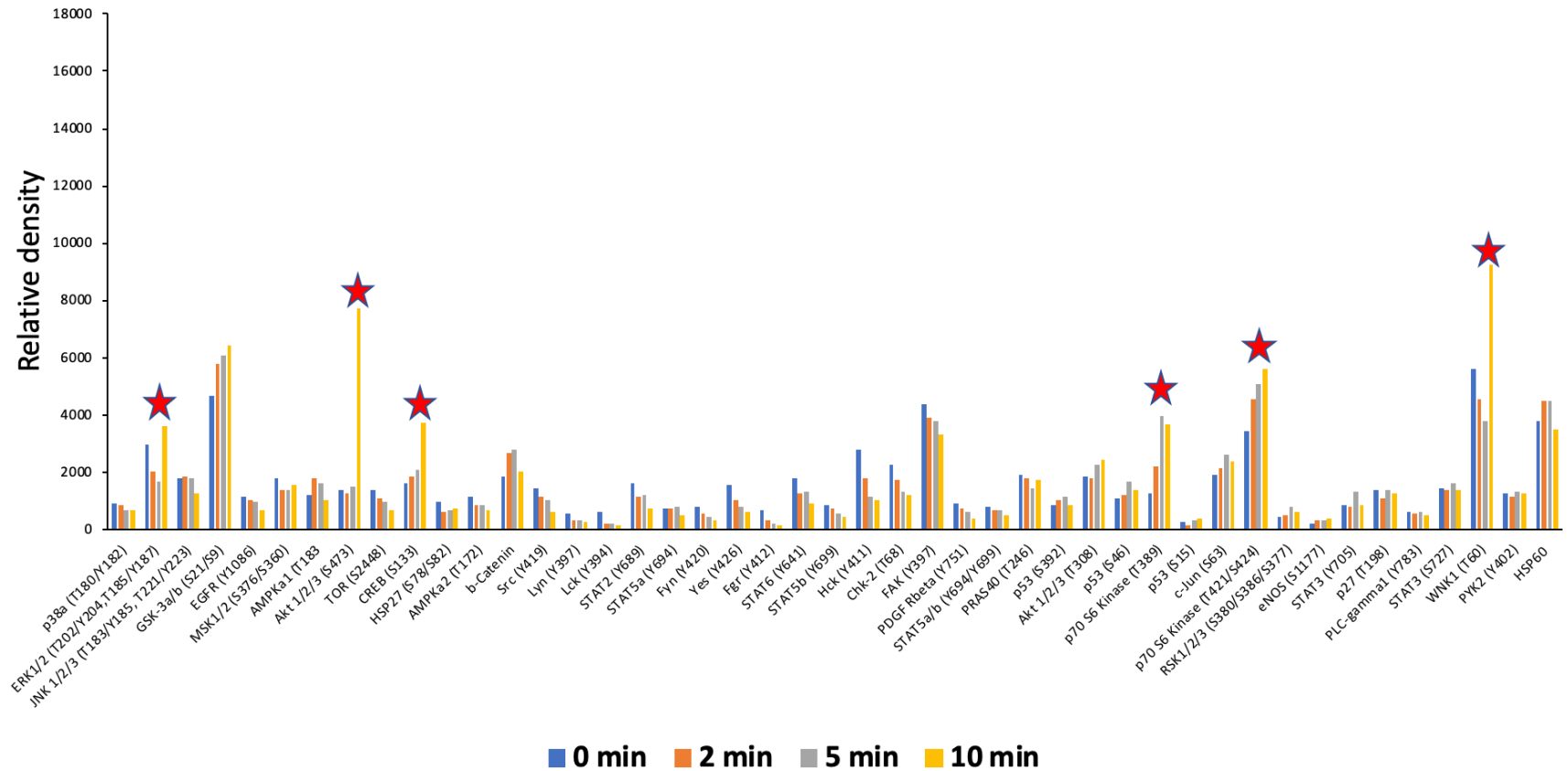


Figure 6.12 Densitometric analysis of phospho-kinase arrays in MCF-7 cells transfected with ZIP7 NLS3 plus zinc stimulation.

MCF-7 cells were transfected with NLS3 for 18 hours. Zinc treatment was performed for 2, 5, and 10 minutes. Phosphorylation of selected kinases at the residues indicated in bracket was determined using the human phospho-kinase antibody arrays (R&D Systems). Densitometric data are presented as mean of the duplicate dots for each kinase \pm standard error ($n=2$). The kinases that show a marked increase (>5000 density units) after 10 minutes zinc treatment, compared with the control samples (no zinc treatment) are indicated with a red star.

Figure 6.9 represents the kinases activated in cells expressing the WT ZIP7. The cells transfected with WT ZIP7 showed a mild increase (2000-5000 density units) in the phosphorylation of GSK-3 α/β (S21/S9) and a marked increase (> 5000 density units) in ERK1/2 (T202/Y204, T185/Y187), AKT 1/2/3 (S473), CREB (S133), p70S6 Kinase (T389), p70S6 Kinase (T421/S424), and WNK1 (T60) is seen after 10 minutes of zinc treatment, compared with the untreated samples. The markedly increased kinases compared with the untreated cells have been highlighted with a star on the graph in **Figure 6.9**. Interestingly, all these kinases have been shown to be immediately downstream of ZIP7-mediated zinc release from stores⁷⁴. It has been shown previously that the phosphorylation of AKT (S473) and ERK1/2 (T202/Y204, T185/Y187) is the result of ZIP7-mediated zinc release after phosphorylation by CK2 on residues S275 and S276¹⁶⁹. The phosphorylation level of p70S6 Kinase, CREB (S133) and WNK1 (T60) has been shown to be higher in the cells transfected with WT ZIP7 than in un-transfected cells, suggesting that p70S6 Kinase, CREB (S133), and WNK1(T60) are downstream effectors of ZIP7-mediated zinc release from cellular stores⁷⁴. Therefore, it is essential to assess the effect of these kinases in response to MCF-7 transfection with the NLS mutants.

Figure 6.10 represents the kinases activated in the cells expressing the ZIP7 NLS1 mutant. Treatment of the cells transfected with NLS1 mutant with 10 minutes of zinc showed a marked increase (>5000 density units) in phosphorylation of ERK1/2 (T202/Y204, T185/Y187), AKT 1/2/3 (S473), and CREB (S133) and a mild increase (2000-5000 density units) in WNK1 (T60) when compared to untreated cells, suggesting that NLS2 affects ZIP7 maximal activation. Cells transfected with the NLS2 mutant and treated with zinc for 10 minutes showed a marked increase (>5000 density units) in phosphorylation of ERK1/2 (T202/Y204, T185/Y187), AKT 1/2/3 (S473), CREB (S133), and WNK1 (T60) and a mild increase (2000-5000 density units) HSP27 (S78/S82), GSK-3 α/β (S21/S9), PRAS40 (T246), p70S6 Kinase (T389), p70S6 Kinase (T421/S424) when compared to untreated cells (**Figure 6.11**). Heat shock protein (HSP27) plays a significant role in inhibiting apoptosis²⁶⁷. HSP27 is present in both the cytoplasm and nucleus²⁶⁷. High expression of HSP27 is associated with metastasis, drug resistance, and poor prognosis in breast cancer, suggesting that HSP27 could be a proper target in breast cancer therapy²⁶⁸. The proline-rich Akt substrate of 40 kDa (PRAS40) is associated with the tumour progression of multiple cancers including melanoma and gastric cancer²⁶⁹. Interestingly, after 10 minutes of zinc treatment in cells transfected with the NLS3 mutant (**Figure 6.12**), only AKT 1/2/3 (S473) markedly increased while p70S6 Kinase (T389), and p70S6 Kinase

(T421/S424) mildly increased when compared to untreated cells. It is clear that in NLS3 transfected cells, there is a decrease in the level of several kinases, which equates to this mutant having a big effect on ZIP7 and its function. This mutant could prevent some ZIP7 from going to the nucleus, and that the differences were seen related to ZIP7 function in the nucleus compared to its function in the ER.

Zinc promotes activation of receptor tyrosine kinases and its downstream signaling pathways, which promote cell proliferation⁶⁹. Treating cells with exogenous zinc leads to ZIP7-mediated zinc release, which causes tyrosine phosphatase inhibition, leading to tyrosine kinase activation¹⁶⁹. Zinc treatment was done for between 2 and 10 minutes to see the difference in kinase activation over time. A large difference in the activity of the kinases was observed at 10 minutes of zinc treatment compared to untreated cells; therefore, 10 minutes of zinc treatment was chosen to confirm the array results with western blot in the next section. Five key kinases showed a marked increase after 10 minutes of zinc treatment in cells transfected with WT ZIP7, highlighted with a red star in **Figure 6.9**, and those kinases have been shown previously to be involved in the main downstream signalling pathways after ZIP7 activation⁷⁴.

ERK1/2 (T202/Y204, T185/Y187), extracellular signal-regulated kinases 1 and 2 (also known as MAPK) are part of the RAS-Raf-ERK signal transduction cascade²⁷⁰. Dysregulation in the MAPK cascade contributes to cancer²⁷¹. In WT ZIP7-transfected cells, ERK starts to increase at 5 minutes of zinc treatment and significantly increases at 10 minutes of zinc treatment (**Figure 6.13**). Protein kinase CK2 phosphorylates ZIP7 at S275 and S276, followed by an increase in cytosolic free zinc, which activates ERK1/2 and AKT¹⁶⁹. For NLS1 and NLS2-transfected cells, ERK is significantly increased at 5 minutes of zinc treatment, which is earlier than observed for WT ZIP7. In contrast, NLS3-transfected cells show a very low level of ERK activation compared to WT ZIP7, NLS1, and NLS2 at all time points. These results confirm the results of the array (**Figure 6.8**) and suggest that removal of the nuclear localization signal in the NLS3 mutant has a considerable effect on ZIP7 maximal activation.

AKT (S473) plays a key role in the downstream signalling pathway of ZIP7. Removal of ZIP7 by siRNA in tamoxifen-resistance breast cancer cell line significantly reduces AKT phosphorylation even after zinc stimulation⁶⁹. Cells transfected with WT ZIP7 showed a significant increase of AKT starting at 5 minutes of zinc treatment (**Figure 6.13**) which

confirmed a previous observation that zinc treatment in ZIP7-transfected cells increases ZIP7-mediated zinc release within two minutes¹⁶⁹. Like the cells transfected with WT ZIP7, those transfected with NLS1 showed a significant increase at 5 minutes; however, the amplitude is less than cells transfected with WT ZIP7. AKT in cells transfected with NLS2 mutant showed an earlier activation which started at 2 minutes of zinc treatment and significantly increased with longer zinc treatment. As expected, cells transfected with NLS3 mutant showed a very low level of AKT activation compared to WT ZIP7, NLS1, and NLS2 and only significantly increased at 10 minutes of zinc treatment (**Figure 6.13**).

CREB (cAMP response element-binding protein) is a 43 kDa nuclear transcription factor activated by phosphorylation at various serine residues²⁷². The best-understood phosphorylation is that of serine 133 (S133) by many different serine/threonine (Ser/Thr) protein kinases such as the mitogen-activated protein kinases (MAPK), Akt/protein kinase B (PKB), and protein kinase A (PKA)^{273,274}. In cells transfected with WT ZIP7, CREB phosphorylation was significantly increased at 5 minutes of zinc treatment, and more phosphorylation was observed at 10 minutes of zinc treatment (**Figure 6.13**). Cells transfected with NLS1 and NLS2 showed an earlier significant activation than cells transfected with WT ZIP7, which started at 2 minutes of zinc treatment. CREB activation in cells transfected with NLS3 is very low level compared to cells transfected with WT ZIP7, NLS1, and NLS3, which suggests that NLS3 affects zinc release into the nucleus, which is essential to activate zinc finger transcription factors such as CREB.

p70S6 Kinase is a mitogen-activated Ser/Thr protein kinase required for cell growth and G1 cell cycle progression²⁷⁵. p70S6 Kinase is phosphorylated at different Ser/Thre residues by different upstream kinases including AKT and ERK1/2²⁷⁶. p70S6 Kinase is a signaling protein in two mitogen-activated signaling pathways, including phosphoinositide-3 kinase (PI-3K) and the mammalian target of rapamycin (mTOR)²⁷⁵. In cells transfected with WT ZIP7 showed a gradual increase in p70S6 Kinase (T389) phosphorylation after zinc treatment, with a significant increase beginning at 5 minutes (**Figure 6.13**). Cells transfected with NLS1, NLS2, and NLS3 showed a significant increase of p70S6 Kinase (T389) starting at 5 minutes of zinc treatment, which is similar to cells transfected with WT ZIP7; however, the level of the activation is lower than with WT ZIP7. In cells transfected with WT ZIP7, p70S6 Kinase (T421/S424) showed a gradual increase with zinc treatment which is significant from 2 minutes

(Figure 6.13). Cells transfected with NLS1 and NLS2 showed a delay in p70S6 Kinase (T421/S424) activation compared with WT ZIP7, which is significantly increased at 10 minutes of zinc treatment. As expected, cells transfected with NLS3, p70S6 Kinase (T421/S424) showed a lower level of activation compared to WT ZIP7, NLS1, and NLS2.

WNKs (with no lysine [K]) are a protein kinase family that have been shown to play an essential role in the regulation of electrolyte homeostasis²⁷⁷. WNKs are also involved in cancer progression through three major cancers-associated signaling networks: PI3K-AKT, TGF- β , and NF- κ B²⁷⁷. Cells transfected with WT ZIP7 showed a significant increase of WNK1 (T60) level at 5 and 10 minutes of zinc treatment (**Figure 6.13**). Previous data from our group showed that WNK1 (T60) is markedly increased in cells transfected with WT ZIP7 and treated with zinc compared to the non-transfected zinc-treated MCF-7 cells which confirmed that the phosphorylation of WNK1 (T60) is ZIP7-dependent⁷⁴. Cells transfected with NLS1 showed a significant increase in WNK1 (T60) level at 10 minutes of zinc treatment. Cells transfected with NLS2 showed a significant increase at 5 and 10 minutes of zinc treatment, although a lower WNK1 (T60) phosphorylation level than WT ZIP7. As expected, cells transfected with NLS3 showed a low WNK1 (T60) level than WT ZIP7, NLS1, and NLS2, with a significant increase only at 10 minutes of zinc treatment.

The main advantage of using phospho-kinase arrays is the identification of a high number of signaling molecules within a sample of cells. ZIP7 is activated by phosphorylation on S275 and S276, resulting in zinc release from intracellular stores that inhibits protein tyrosine phosphatases¹⁶⁹. The array results in this study showed a significant increase in ERK1/2 (T202/Y204, T185/Y187), AKT 1/2/3 (S473), CREB (S133), p70S6 Kinase (T389), and p70S6 Kinase (T421/S424) in cells transfected with WT ZIP7 and treated with zinc which has also been confirmed previously⁷⁴. Interestingly, cells transfected with NLS3 showed a low level of these kinases, suggesting that the NLS3 mutant has a big effect on ZIP7 function in the nucleus. The highly phosphorylated proteins detected from these arrays were further verified by western blot in the next section.

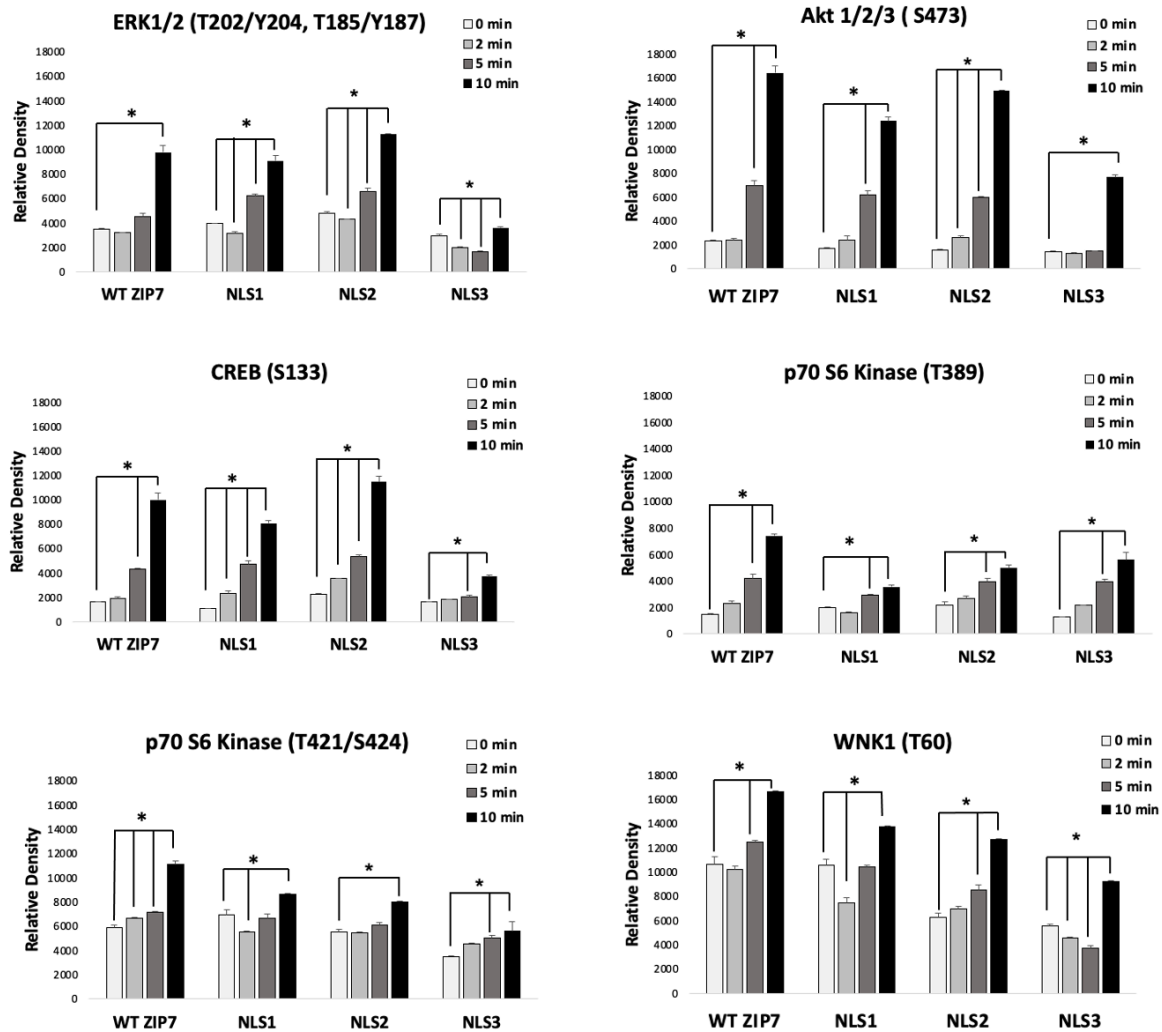


Figure 6.13 Cells transfected with NLS3 mutant shows less kinase activation than WT ZIP7, NLS1, and NLS2.

MCF-7 cells were transfected with WT ZIP7, and ZIP7 NLS mutants and treated with zinc for up to 10 minutes. Phosphorylation of selected kinases at the residues indicated in brackets after the names of the kinases was determined using the human phospho-kinase antibody arrays (R&D Systems). Average densities of the duplicate spots for the kinases that show marked increases in phosphorylation (>5000 density units) after 10 minutes zinc treatment when compared to the un-treated cells are demonstrated. Densitometric data are presented as mean of the duplicate dots for each kinase \pm standard error (n=2). Statistical significance of each mutant being compared at each time point to un-treated cells. * p < 0.05

6.3.6 Western blotting to confirm the kinases activated by ZIP7 and downregulated in cells transfected with NLS3 mutant:

Phospho-kinase arrays in the previous section were used as a screening method to investigate how NLS mutants affect many of the ZIP7 downstream pathways. All cells transfected with NLS mutants showed a lower phosphorylation level in most kinases than WT ZIP7. However, the double alanine mutation in NLS3 showed a big impact on ZIP7 downstream signalling pathways as all the kinases have a very low level compared to WT ZIP7, NLS1, and NLS2. To confirm the phosphorylation of the marked increase kinases due to ZIP7 overexpression and the negative effect of NLS3 on ZIP7 activation, western blot was performed in cells transfected with WT and NLS3 and treated with zinc for 10 minutes. Ten minutes of zinc treatment was chosen to confirm the array results because it shows the highest activation level of the kinases in cells transfected with WT ZIP7. We would like to see how cells transfected with NLS3 decrease this activation. The kinases selected to be confirmed by western blot were ERK1/2 (T202/Y204, T185/Y187), AKT 1/2/3 (S473), CREB (S133), p70S6 Kinase (T389), and p70S6 Kinase (T421/S424).

6.3.6.1 ZIP7 NLS3 transfection shows less ERK1/2 (T202/Y204, T185/Y187) activation than WT ZIP7:

Cells transfected with WT ZIP7 showed an increase of ERK1/2 (extracellular signal-regulated kinases 1 and 2) after 10 minutes of zinc treatment which was not statistically significant (**Figure 6.14**). Cells transfected with NLS3 showed a lower level of activated ERK1/2 in the untreated sample than WT ZIP7, suggesting ZIP7 mutant not able to function as well as the WT ZIP7 which confirm the data from the phospho-kinase arrays. This, in turn, suggests that the nuclear localisation of ZIP7 may be essential for activating ERK1/2 by ZIP7-mediated zinc release. Cells transfected with NLS3 showed a significant increase in ERK1/2 activation after 10 minutes of zinc treatment (**Figure 6.14**), suggesting this mutant is active and able to transport zinc but less extend than WT ZIP7.

The mitogen-activated protein kinase (MAPK) signaling pathways control many fundamental cellular processes such as growth, proliferation, migration, differential, and apoptosis²⁷⁸. Abnormalities in MAPK signalling play a critical role in the development and progression of

cancer, and many cancer treatments target MAPK²⁷⁰. The ERK pathway is dysregulated in approximately one-third of all human cancers²⁷⁸. ERK1/2 is activated by phosphorylation on residues T202/Y204 and T185/Y187²⁷⁹. A recent study in our group demonstrated that ZIP7-mediated zinc release activates downstream signalling pathways such as MAPK, mTOR, and PI3K-AKT⁷⁴. The array data and the western blot presented here confirm that ZIP7-mediated zinc release activates MAPK and also shows that inhibiting the nuclear localization of ZIP7 is a novel therapeutic target to decrease the phosphorylation level of MAPK.

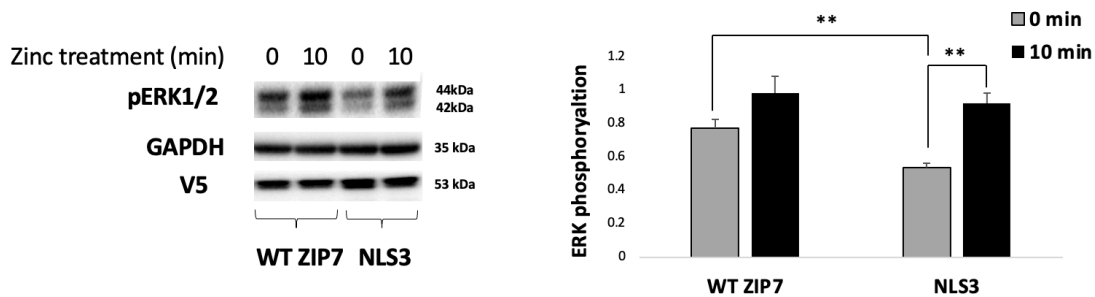


Figure 6.14 ERK1/2 activation downstream of ZIP7-mediated zinc release.

MCF-7 cells transfected with wild-type ZIP7 or NLS3 and then treated with zinc for 10 minutes and the cell lysates were analysed by western blot. Phospho-ERK (pERK), V5 and GAPDH antibodies were used to probe the membrane. Protein bands of pERK (44-42 kDa), V5 (53kDa) and GAPDH (35 kDa) are demonstrated. Densitometric data was normalised to V5 and demonstrated in relative density unit as mean values of $n = 4 \pm$ standard error. ** = $p < 0.01$

6.3.6.2 Cells transfected with NLS3 mutant shows less AKT 1/2/3 (S473) activation than WT ZIP7:

pAKT (S473) is known to be involved in cell proliferation and survival⁷⁴. As expected, there was undetectable pAKT (S473) in the untreated cells, and pAKT (S473) was significantly increased after 10 minutes of zinc treatment in cells transfected with WT ZIP7 (**Figure 6.15**), which is supported by the array data. In addition, the cells transfected with NLS3 showed a similarly low level of pAKT (S473) activation when un-treated to WT ZIP7 and then significantly increased after 10 minutes of zinc treatment. The pAKT (S473) phosphorylation level in NLS3 at 10 minutes of zinc treatment was less than the cells transfected with WT ZIP7 (**Figure 6.15**). These data suggest that nuclear localization of ZIP7 is essential for maximal ZIP7 activation as the level of pAKT (S473) was less in cells transfected with NLS3.

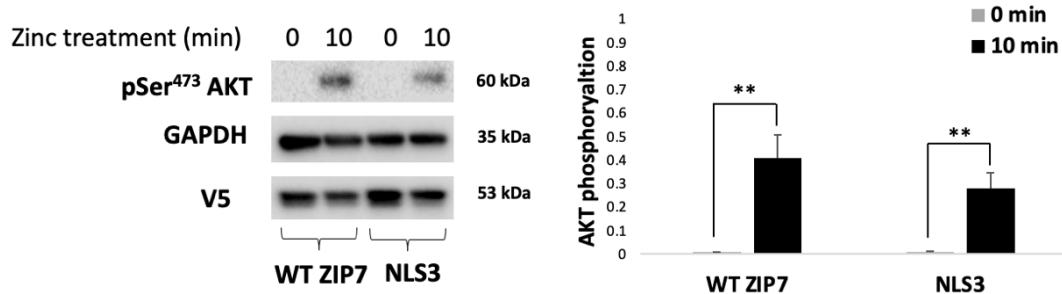


Figure 6.15 AKT activation upon ZIP7 mediated zinc release.

MCF-7 cells transfected with wild type ZIP7 or NLS3 and then treated with zinc for 10 minutes and the cell lysates were analysed by western blot. Phospho-AKT (pAKT), V5 and GAPDH antibodies were used to probe the membrane. Protein bands of pAKT (60 kDa), V5 (53kDa) and GAPDH (35 kDa) are demonstrated. Densitometric data was normalised to V5 and demonstrated in relative density unit as mean values of $n = 4 \pm$ standard error. ** = $p < 0.01$

6.3.6.3 Effect the removal of NLS3 on CREB (S133) activation

Previous studies have shown that zinc regulates the activity of many transcription factors such as metal-responsive transcription factors-1 (MTF-1), CREB, and CREB binding protein (CBP)¹⁶¹. CREB is a transcription factor localized in the nucleus²⁸⁰. It is activated by phosphorylation at S133 by different receptor-activated protein kinases, including protein kinase A (PKA) and mitogen-activated protein kinases (MAPK)²⁸⁰. Many transcription factors that regulate the expression of cytokines, growth factors and other essential molecules that have a role in cell death and proliferation are zinc finger proteins. Therefore, they depend on zinc for their activities²⁷⁴. So, targeting these transcription factors with upstream activation factors may be an attractive approach for antitumour strategies. To determine whether ZIP7 overexpression increases the phosphorylation of CREB, and whether removal of nuclear-located ZIP7 decreases CREB phosphorylation, western blot was performed in cells transfected with WT ZIP7 and the ZIP7 NLS3 mutant and treated with zinc for 10 minutes. In cells transfected with WT ZIP7, there was a low CREB (S133) level in untreated conditions, which was significantly increased after 10 minutes of zinc treatment (**Figure 6.16a**). Cells transfected with NLS3 mutant showed a low CREB (S133) activation when untreated and then increased slightly after 10 minutes of zinc treatment with no statistically significance (**Figure 6.16b**).

The results are represented as a percentage of the untreated state to understand how the NLS3 mutant response performed differently to zinc stimulation. This showed that CREB (S133) in only the WT ZIP7 transfected cells was significantly increased after 10 minutes of zinc treatment while NLS3 mutants showed an increase in the level of CREB (S133) after zinc treatment, but this was not statistically significant (**Figure 6.16c**). These results suggest the inability of ZIP7 NLS3 to phosphorylate CREB as usual and also suggesting that the nuclear localization of ZIP7 has a role in activating CREB. These findings support the hypothesis that nuclear ZIP7 has a role in transporting zinc into the nucleus.

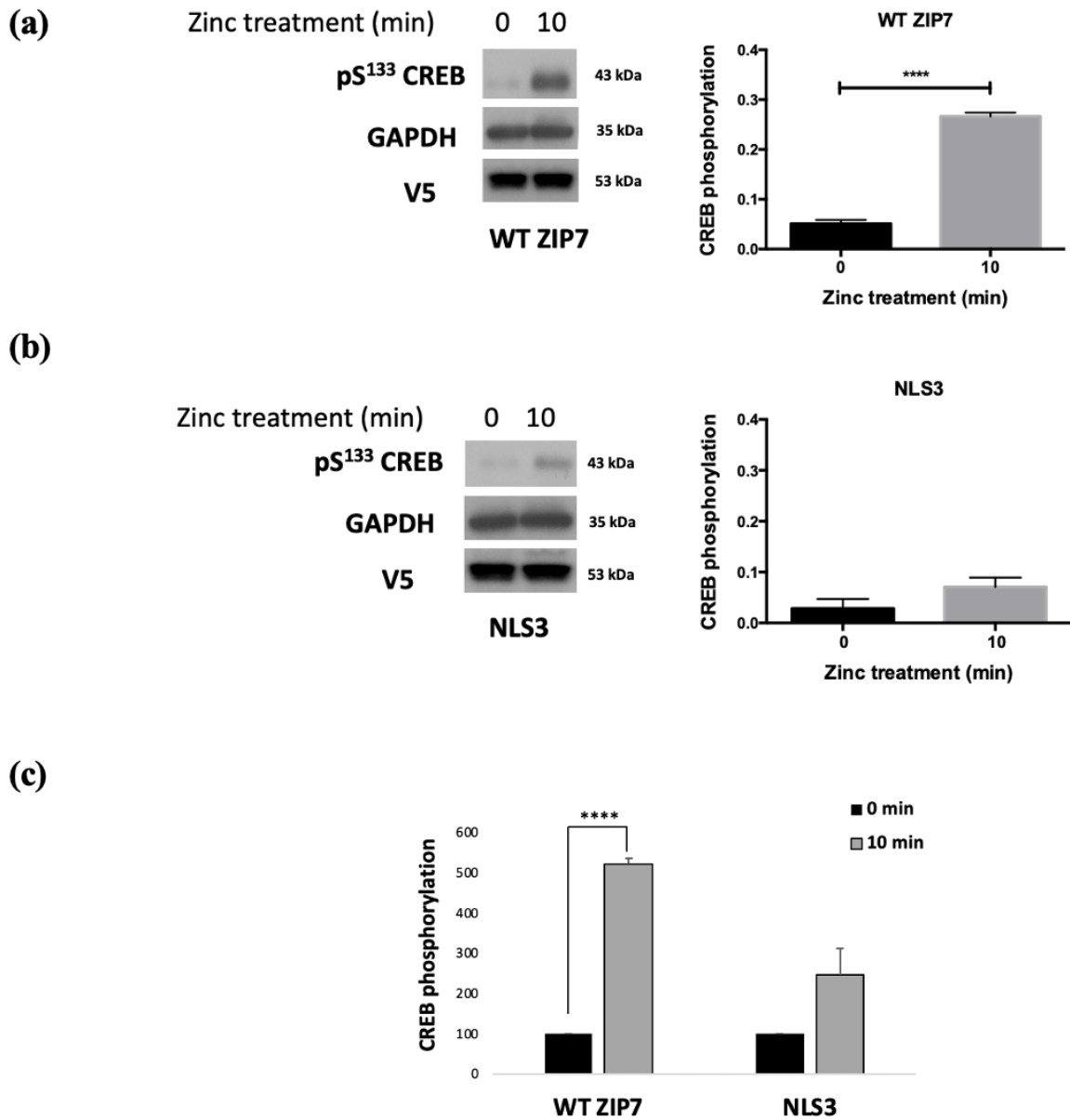


Figure 6.16 CREB activation upon ZIP7 mediated zinc release

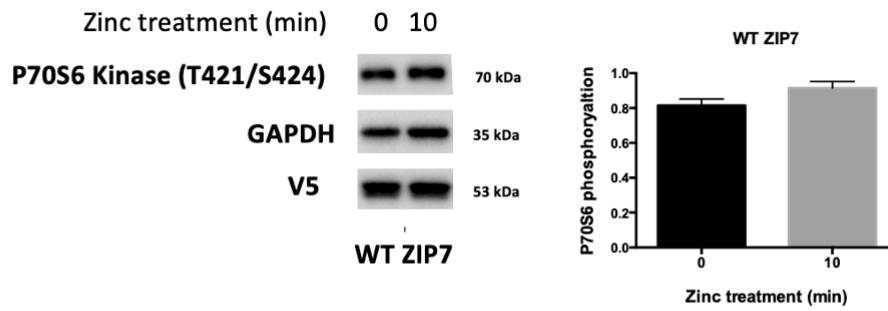
MCF-7 cells transfected with WT ZIP7 or NLS3 and then treated with zinc for 10 minutes and the cell lysates were analysed by western blot. Phospho-CREB (pCREB), V5 and GAPDH antibodies were used to probe the membrane. Protein bands of pCREB (43 kDa), V5 (53 kDa) and GAPDH (35 kDa) are demonstrated. Densitometric data was normalised to V5 and demonstrated in relative density units as mean values of $n = 4 \pm$ standard error. C, Graph represents the results expressed as percentage of the untreated constructs. *** = $p < 0.001$

6.3.6.4 Effect the removal of NLS3 on p70S6 Kinase (T389) and (T421/S424) activation

Next, the phosphorylation of p70S6 Kinase on T389 and T421/S424 was analysed. Phosphorylation of both sites is required for p70S6 Kinase activation²⁷⁶. p70S6 Kinase is regulated by two pathways: PI3K pathway and mTOR pathway, both of which have a critical role in breast cancer development^{281,282}. Cells transfected with WT ZIP7 showed a slightly increased p70S6 Kinase (T421/S424) after 10 minutes of zinc treatment (**Figure 6.17a**). A previous study in our group showed that p70S6 Kinase (T421/S424) increases significantly in cells transfected with WT ZIP7 compared to MCF-7 cells without transfection⁷⁴, which explains the high level of p70S6 Kinase (T421/S424) at the basal condition in cells transfected with WT ZIP7. Cells transfected with NLS3 mutant also showed a slightly increased p70S6 Kinase (T421/S424) after 10 minutes of zinc treatment (**Figure 6.17b**). The cells transfected with WT ZIP7 and NLS3 showed a significantly increased p70S6 Kinase (T389) after 10 minutes of zinc treatment (**Figure 6.18 a and b**). These results suggest that p70S6 Kinase (T389) is the critical residue for ZIP7 zinc mediated phosphorylation.

In summary, the array data and western blot presented in this chapter demonstrate that ZIP7 NLS mutants significantly affect ZIP7 signalling pathways, especially NLS3, which has a double alanine mutation. The cells transfected with NLS3 mutants have decreased ZIP7 in the nucleus, affecting the phosphorylation of nuclear kinases. However, there is still ZIP7 located in the ER responsible for transporting zinc from the ER to the cytoplasm. The nuclear localization signals of ZIP7 are essential for maximal activation of ZIP7, and removing those signals affects the downstream signaling pathways of ZIP7.

(a)



(b)

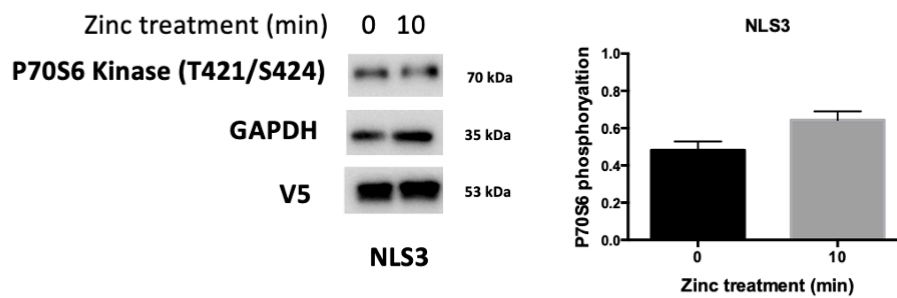


Figure 6.17 p70S6 Kinase (T421/S424) upon ZIP7 mediated-zinc release.

MCF-7 cells transfected with wild-type ZIP7 or NLS3 and then treated with zinc for 10 minutes and the cell lysates were analysed by western blot. p70S6K (T421/S424), V5 and GAPDH antibodies were used to probe the membrane. Protein bands of p70S6K (70 kDa), V5 (53kDa) and GAPDH (35 kDa) are demonstrated. Densitometric data was normalised to V5 and demonstrated in relative density units as mean values of $n = 3 \pm$ standard error.

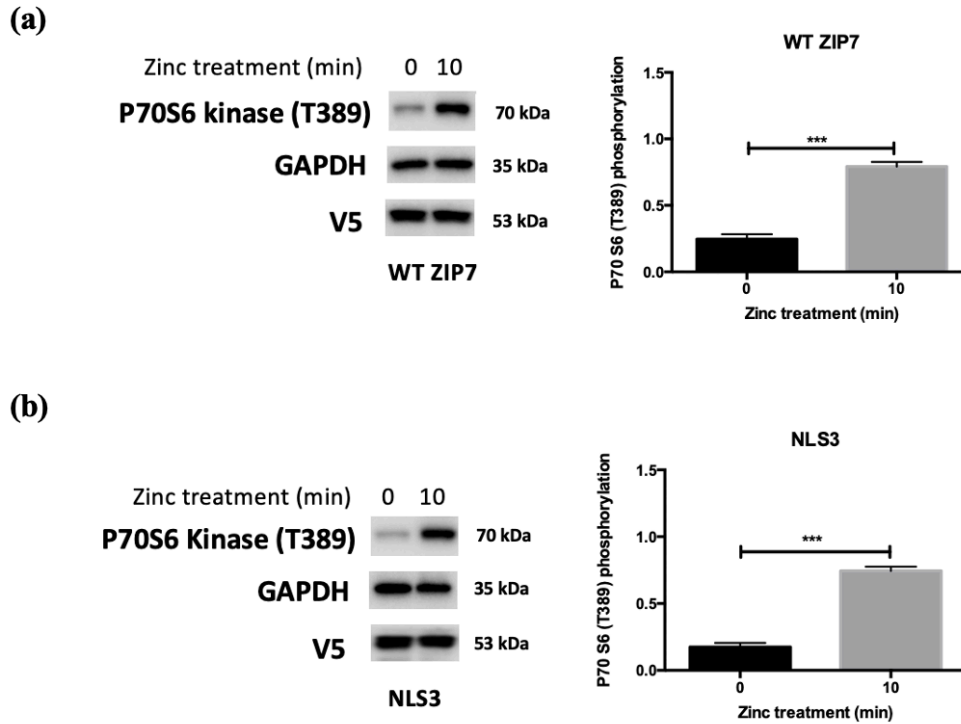


Figure 6.18 p70S6 Kinase (T389) upon ZIP7 mediated zinc release

MCF-7 cells transfected with wild-type ZIP7 or NLS3 and then treated with zinc for 10 minutes and the cell lysates were analysed by western blot. p70S6K (T389), V5 and GAPDH antibodies were used to probe the membrane. Protein bands of p70S6K (70 kDa), V5 (53kDa) and GAPDH (35 kDa) are demonstrated. Densitometric data was normalised to V5 and demonstrated in relative density unit as mean values of $n = 3 \pm$ standard error.

*** = $p < 0.001$

6.4 Chapter Summary

Having discovered three potential nuclear localisation motifs in Chapter 3, alanine mutation in the predicted NLS were performed by Mutagenex Inc (**Figure 6.1**) to assess the effect of NLS on ZIP7 localisation and downstream effect. Immunofluorescence was performed to investigate the cellular localisation of the ZIP7 NLS mutants. The Immunofluorescence results showed that NLS mutants have the same nuclear ring and ER staining, which suggests these mutations have little or no effect on the nuclear localisation of ZIP7 (**Figure 6.2**). Further investigation of the NLS mutant showed that the ZIP7 NLS mutant colocalises with Lamin B, which is located in INM (**Figure 6.3**). Western blot data showed that the predicted NLS is essential for the maximal effect of ZIP7 as none of the NLS mutants increased significantly in the level of pZIP7 after 10 minutes of zinc treatment (**Figure 6.5**). Furthermore, phosphokinase arrays were performed to examine the effect of NLS on the downstream effect of ZIP7 mediated zinc release. The arrays data showed a significant increase in ERK1/2 (T202/Y204, T185/Y187), AKT 1/2/3 (S473), CREB (S133), p70S6 Kinase (T389), and p70S6 Kinase (T421/S424) in cells transfected with WT ZIP7 and treated with zinc while in cells transfected with NLS3 showed a markedly low level of these kinases which all know to have a role in cancer progression. The data in this chapter showed that the nuclear localisation signals of ZIP7 are essential for ZIP7 maximal activation, and removal of these signals markedly decreased in the downstream signalling pathways of ZIP7-mediated zinc release.

7. Chapter 7: Discussion

Breast cancer is the most commonly occurring cancer in women and the second most common cancer overall²⁸³ with Belgium having the highest rate of breast cancer in women²⁸³. Screening and diagnosis of early breast cancer are crucial to reducing the overall morbidity and mortality^{171,172}. Cancer is a disease that is responsible for the uncontrolled growth and spread of abnormal cells. Cancer is a leading cause of death worldwide, with nearly 10 million deaths in 2020²²⁸. Identification of the molecular mechanism of breast cancer is crucial to its successful diagnosis, therapy, and prognosis. This is particularly true for aggressive types of breast cancer, which are still poorly understood. The main problem for the successful treatment of breast cancer patients is the ability of the cancer to develop resistance²⁸⁴. Unfortunately, the exact mechanism of resistance is still unclear. In recent years much has been done to develop a widespread chemotherapeutics strategy to treat all the different types of cancer; however, the overall death rate from this disease is still very high. As a result, there is an essential and urgent need to discover new targeted therapies that have a selective action against cancer cells and additionally develop more sensitive and specific biomarkers for patients with breast cancer. In order to understand the mechanism of cancer cells to enable proper treatment, it is essential to discover the signalling pathways involved in cell proliferation and apoptotic pathways associated with cell death.

Zinc is the second most abundant metal ion in the human body and as such plays an essential role in many biological processes. Zinc is required for normal cell growth and development²⁸⁵. Zinc has been associated with more than 3,000 enzymes and proteins, constituting approximately 10% of the proteome^{19,286}. According to the IUPAC system, zinc is the only metal detected in all classes of enzymes²⁸⁷. Therefore, zinc has an essential role in all cellular processes, including gene expression, signal transduction, and apoptosis⁶. Importantly, zinc acts as a second messenger as it is released from stores within minutes of an extracellular stimulus, leading to the activation of multiple intracellular cascades²⁵. The role of zinc as a second messenger was also further confirmed specifically in breast cancer cells as zinc release from stores after activation of zinc transporter ZIP7 leads to activation of multiple downstream signalling cascades within two minutes, resulting in cell growth and invasion^{69,74}. Therefore, the cellular zinc level has an important role in intracellular biological processes as its effect

can be observed on the time scale of minutes in contrast to zinc's transcription and DNA-binding properties, which take hours or days to accomplish²⁸⁸.

Dysregulation in zinc levels leads to dysfunction in many biological functions, which promotes a wide range of diseases such as cancer development, impaired growth, immunodeficiency, diabetes, and degenerative diseases^{289–291}. So, it is essential to maintain correct zinc homeostasis for human health. For this reason, in the last few years, much research has investigated zinc biology to understand exactly how zinc is controlled in cells in order to correct the imbalance. Still, little is known about the function of ZIP transporters, so this project has focused on ZIP7 to understand the functional mechanism and cellular localization. **Firstly**, the finding that ZIP7 is phosphorylated at S275 and S276 by CK2 protein kinase^{44,169} was expanded to investigate new potential phosphorylation sites. **Secondly**, the discovery that ZIP7 has a role in driving antihormone resistance in breast cancer^{69,167} was expanded to investigate the ZIP7 expression pattern and the survival outcome of ZIP7 in clinical samples representing different subtypes of breast cancer. **Thirdly**, the discovery that ZIP7 phosphorylation resulting in zinc release from the endoplasmic reticulum store into the cytosol, which activates MAPK, PI3K and mTOR⁷⁴ was expanded, and it has unveiled for the first time that ZIP7 is also located in the nuclear membrane resulting in the activation of nuclear pathways leading to cancer development.

The most remarkable breakthrough of this current project was the discovery of the nuclear localization of ZIP7 and by mutation of the nuclear localization signals resulting in a significant decrease in nuclear kinases that have a known role in cancer development. This novel new finding could lead to benefit for breast cancer patients, especially the aggressive type of breast cancer, as our bioinformatics analysis showed a much higher ZIP7 expression level in breast tumour samples than normal samples.

7.1 Overexpression of ZIP7 is a prognostic biomarker in human breast cancer

Zinc cannot passively traverse cell membranes, so cellular zinc homeostasis is achieved through the function of the ZnT family (SLC30A) acting as zinc efflux transporters and the ZIP family (SLC39A) acting as zinc influx transporters⁴⁹. ZnT transporter decrease the

cytosolic zinc while ZIP channels transport the zinc to the cytoplasm either from intracellular stores or from outside the cell. The ZIP family include four subfamilies: type I subfamily (SLC39A9), type II subfamily (SLC39A1-3), gnfA subfamily (SLC39A11), and LIV-1 subfamily (SLC39A4-8, 10, and 12-14)⁴⁴. Intracellular zinc is regulated by different zinc transporters, such as ZnT2 and ZnT4, decreasing cytoplasmic zinc by sequestering zinc inside the lysosome, while ZIP8 works in the opposite direction by increasing the cytoplasmic zinc level by releasing the zinc from the lysosome¹. Other essential zinc transporters responsible for increasing cytoplasmic zinc include ZIP9 and ZIP13, where they localize to the Golgi apparatus and are responsible for zinc release from this compartment to the cytosol¹. The primary regulator of intracellular zinc homeostasis is ZIP7 which is located in the endoplasmic reticulum and responsible for zinc release from the endoplasmic reticulum into cytoplasm^{58,292}. The endoplasmic reticulum is considered to be the major store of zinc with the cell^{1,58}. ZIP7 is phosphorylated by protein kinase CK2 on residues S275 and S276, resulting in zinc release from the intracellular store to the cytoplasm, which then activates signalling pathways such as MAPK, mTOR, and PI3K-AKT that are all known to be involved in cell survival and proliferation^{74,169}. In the present study, and for the first time, ZIP7 expression levels have been evaluated in different cancers using comprehensive bioinformatic analysis and resulting in a prognostic correlation of ZIP7 with breast cancer progression.

In this study, the expression level of ZIP7 was first determined in breast cancer based on bioinformatic analysis. The GEPIA online tool revealed a significant higher ZIP7 expression in many cancers compared to the corresponding normal tissue. Further investigation revealed that the expression of ZIP7 in the different subtypes of breast cancer was also significantly higher than that seen in normal tissue. Moreover, a positive association between ZIP7 expression and cancer stage, subclasses, nodal metastasis, menopause, patient age, ER, HER2, basal-like, and triple-negative breast cancer status was also seen. Subsequently, Kaplan-Meier plotters were used to study the prognostic role of ZIP7 in breast cancer, and the results showed that high ZIP7 expression was associated with poor relapse-free survival (RFS), overall survival (OS) and distant metastasis-free survival (DMFS). These findings suggest that increased ZIP7 expression may be a promising prognostic biomarker in breast cancer.

Many studies have shown that changes in the zinc level of tumour tissue are actually attributed to tissue-specific zinc dysregulation, resulting mainly from aberrant expressions of various ZIP

channels²⁹³. Among all the ZIP channels that have been implicated in cancers, ZIP7 has been most closely associated with breast carcinogenesis²⁹³. The results indicate that ZIP7 is highly expressed in different types of cancer tissues compared to normal relative samples, suggesting that controlling ZIP7 expression is essential for cancer patient treatment. The additional analysis demonstrates that high ZIP7 expression in breast cancer patients is positively associated with a worse prognosis value. According to the Oncomine cancer database, ZIP7 is present in over 25 common tumour types⁶³. Recently, the ZIP7 gene was shown to play an essential role in the survival and growth of lung adenocarcinoma²⁹⁴. In a gastric tumour model, it was reported that ZIP7 expression was remarkably up regulated^{295,296}. Furthermore, ZIP7 induced cell proliferation, migration, and inhibited apoptosis in gastric cancer via activation of the AKT/mTOR signalling pathway²⁹⁷. Further confirmation of this was provided by using knockdown of SLC39A7 to show inhibition of cell growth and induction of apoptosis in human colorectal cancer cells¹⁶⁶ and suppression of cell proliferation, migration, and invasion in cervical cancer²⁹⁸. In the present study, the ZIP7 gene was firstly found to be critical for the survival of breast cancer patients. ZIP7 mediated zinc release inhibits tyrosine phosphatases at physiological levels^{242,299} which activates downstream tyrosine kinases pathways such as EGFR³⁰⁰, IGF-1R³⁰¹, and Src³⁰² that promote the aggressive behaviour of tamoxifen resistance breast cancer cells³⁰³. Increasing the activation level of these kinases correlated with ZIP7 activation and an increased zinc level⁶⁹ whereas silencing of ZIP7 decreased the cytosolic zinc level and blocked growth factor responses and inhibited cell growth⁶⁹. These data linked the role of ZIP7 in tamoxifen resistance breast cancer²⁹³, which is reinforced by the association of ZIP7 expression in the Oncomine database with poor breast cancer outlook⁵⁷. Additionally, Zinc³⁰⁴ and AKT³⁰⁵ have both been shown to phosphorylate and inhibit glycogen synthase kinase-3 beta (GSK-3 β), a known suppressor of epithelial- mesenchymal transition (EMT)³⁰⁶. So, zinc release from the store after ZIP7 activation results in activation of AKT, which inhibits GSK-3 β and potently contributes to cell migration. These findings support the importance of ZIP7 as a gatekeeper of zinc release from stores and a hub of tyrosine kinases activation in the cell^{23,169}.

Tamoxifen is frequently used in treating estrogen receptor positive breast cancer patients. Most breast cancer patients are estrogen receptor positive and eligible for endocrine treatment; however, the development of resistance against endocrine therapy is an important issue that is a further driving force for future therapies. Interestingly, ZIP7 mRNA level increased

significantly in anti-estrogen resistant cell lines⁵⁷ providing further evidence of a role for ZIP7 in aggressive type of breast cancer. Estrogen receptor-positive breast cancer patients are mainly treated with antihormones such as tamoxifen or fulvestrant. However, resistance development to these drugs is a significant issue involving an altered and more aggressive breast cancer³⁰⁷. ZIP7 has been shown to be overexpressed in the tamoxifen-resistance model⁵⁷ and responsible for increasing the cell invasiveness and mobility³⁰⁸. The pZIP7 level, which is the active form of ZIP7 when phosphorylated on residues S275 and S276, was shown to increase significantly in TamR cells compared to MCF-7 cells¹⁶⁷. These data suggest that TamR cells use the zinc signalling pathways, controlled by ZIP7 mediated zinc release from stores, to bypass the inhibition provided by anti-hormone treatment. The aggressive phenotype of breast cancer is a term used to describe breast cancer with a poor prognosis and a higher chance of metastasis. Approximately 30% of treated breast cancer patients develop distance metastasis³⁰⁹, and these significantly account for 90% of breast cancer death³¹⁰. So, it is essential to develop a therapeutic strategy to target the metastasis^{311,312}. Understanding the effects and mechanism of ZIP7 in cancer may be beneficial for cancer treatment.

Genotype-Tissue Expression (GTEx) and the Cancer Genome Atlas (TCGA) projects contain RNA sequence data of normal and cancer samples, mainly used in cancer bioinformatics analysis to improve the diagnosis methods and treatment of cancer patients^{219,220}. In this project, different online bioinformatics prognostic tools³¹³ were used to appraise the expression pattern of ZIP7 in breast cancer patients. Using Kaplan-Meier plotter survival analysis tools¹⁸⁷ to generate a survival analysis plot showed that patients with higher ZIP7 expression are associated with worse relapse-free survival, overall survival, and distant metastasis-free survival compared to those with low ZIP7 expression. These findings will help us understand the consequences of higher ZIP7 expression and develop a novel strategy for targeting ZIP7 in cancer patients. ZIP7 is one of the 10% of genes whose overexpression is associated with poor prognostic states in terms of relapse rate, mortality rate and tendency to develop lymph node metastasis and invasion^{57,63}.

Furthermore, in a small clinical series, ZIP7 mRNA expression level is positively correlated with breast cancer progression indicators, including proliferation marker Ki-67, lymph node spread, the epidermal growth factor receptor ErbB3, and activator of transcription 3 (STAT3)⁵⁷. STAT3 has been well documented to be associated with breast cancer progression³¹⁴. This

study has demonstrated that higher ZIP7 expression is associated with a worse disease progression and spread of tumour to the lymph node of patients. In breast cancer patients, tumour metastasis to axillary lymph nodes is a significant risk factor for survival outcome or metastatic disease³¹⁵. These results together identify a potential role of ZIP7 in breast cancer progression and metastasis.

Moreover, ZIP7 level was investigated in breast cancer tissue samples where total ZIP7 protein level was highly elevated in breast tumour compared to normal breast samples. Furthermore, immunostaining of activated ZIP7 level (pZIP7) on clinical breast cancer samples showed that pZIP7 level is highly expressed in breast cancer samples, especially in cells associated with resistance and worse progression¹⁶⁷ which was further confirmed by elevated zinc level in TamR⁶⁹. In the present study, therefore, ZIP7 expression was shown to be increased in aggressive breast cancer samples, which suggests ZIP7 can be considered as a promising biomarker in breast cancer.

The data represented here showed that a higher level of ZIP7 is associated with a poor prognosis feature of high grade cancer, which further confirmed by other study that showed a significant increase in pZIP7 level in the higher grade tumour¹⁶⁷. A higher-grade tumour is associated with poor prognosis and endocrine resistance, which further suggests the role of ZIP7 in this process. pZIP7 level also had a positive correlation with MAPK activity¹⁶⁷ as pMAPK is a downstream target of pZIP7⁷⁴. Increased pMAPK level has been reported to be associated with endocrine resistant breast cancer³¹⁶. A recent study in our group identified activated ZIP7 is driving downstream pathways such as PI3K, MAPK, and mTOR, which are often hyperactivated in cancer and have implications with cancer survival and proliferation³¹⁷. These data further confirm the role of ZIP7 in breast cancer, especially related to endocrine resistance, a large unmet need in cancer. Furthermore, our study has also shown the correlation between ZIP7 expression in HER+ breast cancer patients and their survival. A previous study showed that tumours overexpressing HER2 receptor are more likely to be endocrine resistant due to the activation of growth factor pathways³¹⁸ and pZIP7 is shown to be associated with HER2, which reinforces the evidence that the activated form of ZIP7 has a role in promoting the poor prognosis of breast cancer.

In summary, the data represented here provided a comprehensive bioinformatic analysis of ZIP7 in breast cancer patients that showed that ZIP7 was more expressed in breast cancer than normal tissues and was correlated with worse survival. ZIP7 may serve as a potential novel biomarker and therapeutic target for patients with breast cancer. In the future, more laboratory experiments and clinical trials need to be performed to validate the finding in this study further.

7.2 Analysis of ER retention signals in the ZIP7 sequence

ZIP7 has been reported to reside on the membrane of endoplasmic reticulum and is responsible for zinc release from the endoplasmic reticulum store into the cytosol which inhibits protein tyrosine phosphatases leading to downstream activation of tyrosine kinases, such as mitogen-activated protein kinases (MAPK), and driving cell survival and proliferation^{58,74,169}. It is still unknown what sequence in ZIP7 is responsible for its location in the ER. Mutation of the four basic predicted ER retention signals present in the ZIP7 sequence had minimal effect on ZIP7 ER retention, leaving it predominantly localized in the ER, suggesting that ZIP7 could use other mechanisms for its ER localization. The endoplasmic reticulum (ER) is the largest intracellular compartment that extends throughout the cell, including the nuclear envelope. ER has a central role in the biosynthesis of lipid, steroid, membrane-bound and soluble proteins, and it is the main gateway of the secretory pathways²⁰⁹. Many proteins remain in the ER as a permanent resident, whereas others are exported to the Golgi stack for subsequent distribution to the cell surface, lysosomes, and secretory storage vesicles²⁰⁸. There is very little information available about the signals involved in the retention of an ER membrane protein other than that available on software prediction sites. ER-resident protein must possess specific signals to prevent their exit from the ER and/or to interact with receptors responsible for their retrieval from the Golgi apparatus²⁰⁸. Some ER retention sequences have been identified in both soluble³¹⁹ and transmembrane³²⁰ ER-resident proteins. The best characterized ER-retention motifs are Lys-Asp-Glu-Leu (KDEL) in the COOH terminal sequence found in many soluble ER proteins that accumulate in the ER lumen³²¹. Some proteins do not have KDEL signals, and yet they are still retained in the ER, possibly suggesting that they may be bound to other proteins that have a retention signal³²². Specific receptor proteins in post ER compartments recognize KDEL sequences to initiate the formation of COPI-coated vesicles, which are responsible for transporting the KDEL containing protein cargo from the Golgi to the ER³²³. Deleting the KDEL sequence in the C terminus of lysozyme

resulted in secretion of the mutated protein while adding the KDEL onto the C-terminus of lysozyme, the protein that is normally secreted, resulted in retention of lysozyme in the ER³¹⁹.

In the current study, four ER retention signals were identified in the sequence of ZIP7: either di-lysine (KK) or di-arginine (RxR) that could have a role in preventing ZIP7 to exist from the ER. All the predicted ER retention signals of ZIP7 occur in the cytoplasmic domains of ZIP7, which all could interact with a component in the cytoplasmic side of the ER membrane that confers ER residency. Many ER-resident mammalian and yeast membrane proteins contain signals in their cytosolic region, which facilitate their strict retention in the ER³²⁴⁻³²⁷ or their retrieval from the Golgi to the ER^{324,328,329}. Membrane proteins often contain a dibasic motif, either di-lysine (KK) or di-arginine (RxR), in their cytoplasmic domains, which is specifically responsible for the ER location^{208,330}. One motif that is present in the ZIP7 is ¹⁶³PRHR¹⁶⁶ which fit the criteria of di-arginine (RXR or RR) signals³³¹. These signals were first identified in a major histocompatibility complex (MHC) class 11 transport³³². An arginine containing motif (RXR) in the N terminus of type II membrane protein glycosidase I (GCSI) has an essential role in ER retention³³³. The RXR ER-retention/retrieval signal acts as a checkpoint for the surface expression of ATP-sensitive potassium channels³²⁹. The surface expression of several other transmembrane proteins such as GABA receptor³³⁴ and kainite receptor^{335,336}, which modulates the neurotransmitter release in the brain, is also regulated by the RXR motif. There is another type of motif present in ZIP7, ²⁷⁰KEK²⁷³ and ³⁷⁵SKK³⁷⁸ of ZIP7, which is similar to the first identified dilysine motifs (KKX and KXX) on the cytoplasmic C terminus of adenoviral E3 19 kDa (E19) protein in mammals which are known to interact with COPI^{320,337}. COPI is a heptameric protein complex that coats vesicles involved in retrograde protein transport from Golgi back to the ER^{338,339}. Normally, the protein is brought back to the ER through a direct interaction between the cytoplasmic domain of the membrane cargo protein and coat components³²³. The efficiency of a di-lysine motif for ER localization of the transmembrane protein in cells has been described in mammals, yeasts, and plants^{337,340-343}. This motif is found in a variety of cytosolic positions, including loops, at the C and N terminus of membrane proteins³⁴⁴. A cytosolic dilysine motif has been identified at the C-terminal end of many type I integral membrane proteins in the ER of yeast and animal cells^{328,345}. The C-terminal dilysine motif has been shown to mediate retrieval of type I membrane proteins from the Golgi to the ER in mammalian³⁴³ and yeast cells³⁴⁶. Delta opioid receptor, a type of G protein-coupled receptor, is shown to have a dilysine motif that interacts with COPI protein

complex to promote the retention of opioid receptors in the endoplasmic reticulum³⁴⁷. The COPI protein retrieval process is responsible for the ER-resident proteins by recognising an arginine and lysine-rich sequence or a KDEL sequence³⁴⁴. The discovery of these motifs in ZIP7, which have been verified in other transmembrane proteins located in the ER, suggesting that they may be responsible for the ER localization of ZIP7. So, alanine mutation was performed in the predicted ER retention signals of ZIP7 to investigate their effect on ZIP7 ER localization.

Mutation in the predicted retention signals of ZIP7 did not alter the ER localization of ZIP7, which suggests that ZIP7 could use other mechanisms to enable it to remain in the ER. Sec12p is a type II transmembrane glycoprotein that is mainly localized in the ER at a steady state³²⁵. ER localization of Sec12p involves two different mechanisms: static retention in the ER and a dynamic retrieval from the Golgi³²⁵. Transmembrane domain (TMD) regions of Sec12p have been shown to have a role in its ER localization in addition to its NH₂-terminal cytoplasmic domain³²⁵. In addition, removal of the double lysine motif from a mammalian endogenous ER enzyme (UDP-glycosyl transferases) does not result in the loss of ER retention³⁴³. This evidence suggests that the correct localization of ER membrane proteins may involve more than one mechanism, suggesting that ZIP7 could use another mechanism as well as the predicted ER retention signals to remain in the ER. ZIP7 contains eight transmembrane domains, and the TMD alone can localize the protein to the ER quite efficiently³²⁵. At the same time, the cytoplasmic domain can retain most of the molecules in the ER, which suggests that ZIP7 might use the TMD for retention in the ER membrane. The hydrophobic segment of the transmembrane domain with more than ten amino acid residues has been shown to be necessary to prevent the protein translocation almost completely³⁴⁸. It has been shown that increasing the length of transmembrane domains can disrupt ER retention of some proteins^{349–351}. Inserting transmembrane segments of an integral membrane protein into a secretory protein cause the modified protein to remain in the ER membrane and not translocate from the ER membrane³⁵². It has been suggested that proteins localized in the ER which do not have positive sorting signals, use their TMD sequence to interact with the lipid bilayer which enables retention in the ER³⁵¹. It is interesting to speculate that this may be the case for ZIP7 as alanine mutation in the predicted ER retention signals did not interfere with the ZIP7 ER localization. Generally, the transmembrane segment consists of non-polar, hydrophobic amino acid residues^{353,354}, and in many cases these are followed by positively charged amino acid residues^{355–357} as the

charged residues prevents transfer to other locations³⁴⁸. Transmembrane segments of an integral membrane protein has been demonstrated to stop the protein translocation from the ER membrane by anchoring the protein in the lipid bilayer³⁴⁸. The internal hydrophobic sequences in the transmembrane domain act as a signal sequence to keep an integral protein in the ER membrane³⁵⁴. These studies provide further examples confirming that ZIP7 could rely on its transmembrane segment to localize itself in the ER and not the predicted ER retention signals. Also, there is evidence that signals in the cytosol and the luminal part of the protein could coexist in the same membrane protein for their retention in the ER membrane³³³. Some ER-resident proteins do not have ER retention signals; however, they can indirectly be retained in the ER by interactions with some ER-resident proteins such as luminal chaperones, including BiP and calnexin and calreticulin³⁵⁸, which could be another mechanism of ZIP7 localization in the ER which needs further exploration.

7.3 The long cytoplasmic/nucleoplasm domain of ZIP7 contains multiple nuclear localization signals

ZIP7 is located in the endoplasmic reticulum and is responsible for zinc release from stores to the cytoplasm to activate many signaling pathways that have a role in cancer⁷⁴. However, this study for the first time has found that ZIP7 is also located on the nuclear membrane which suggests that ZIP7 not only transports zinc into the cytoplasm but also into the nucleus which could activate many nuclear kinases that also have a role in cancer development. Many researchers have shown the mechanism of transport of soluble molecules into the nucleus; however, much less is known about the mechanism of targeting integral membrane proteins into the inner nuclear membrane. It is important to know the exact mechanism of transfer, and the function of INM proteins as any alteration in their expression and structure may lead to cancer and nuclear envelopathies as evidenced by the following nuclear proteins. Lamina-associated polypeptide 2, Lap2b, is over-expressed in digestive tract cancers³⁵⁹. Mutation in Lamin B receptor, causes both Greenberg dysplasia, which leads to abnormal embryonic development³⁶⁰ or Pelger-Huet anomaly which is characterized by abnormal nuclear shape and chromatin organization in blood granulocytes³⁶¹ Mutation in emerin cause Emery-Dreifuss muscular dystrophy^{362,363}.

The nuclear envelope (NE) is a membrane system consisting of outer and inner nuclear membranes (ONM and INM) separated by a lumen³⁶⁴. The ONM, which is continuous with the ER, is facing the cytoplasm and covers all the nucleus except the areas where the nuclear pore complex are inserted³⁶⁴. The INM and ONM contain unique sets of membrane proteins called NETs (nuclear envelope transmembrane proteins, which include the lamin B receptor³⁶⁵ and the lamina-associated polypeptides 1 and 2 (LAP1 and LAP2)^{366,367}. Over 100 transmembrane proteins are found in the INM, of which only a relative few have been characterized³⁶⁸⁻³⁷¹. Integral membrane proteins of the inner nuclear membrane (INM) are positioned in the ER after their synthesis and then transported to their destination, which is the INM. In order for a protein to be located in the INM, the integral membrane protein needs to be transported through four continuous membrane domains. This membrane protein will move from the ER to the outer nuclear membrane, then to the highly curved membrane of the nuclear pore, and finally to the INM. The binding of an inner nuclear membrane protein to a nuclear ligand is required for their retention and unique inner nuclear localization³⁷². Many INM proteins contain nuclear localization signals, but it is still unclear if these are essential for INM targeting because mutation or deletion of these signals does not always affect the localization, which suggests another feature contributes to INM transport^{373,374}. SUN2 is an integral INM protein that relies on several sorting signals present in its sequence and also on its N terminal and C-terminal to mediate targeting to the INM³⁷⁴. Many INM proteins have essential functions in genome regulation³⁷⁵⁻³⁷⁷ and therefore it is crucial to understand the trafficking mechanisms of transmembrane proteins into the nuclear compartment. Imaging ZIP7 in MCF-7 cells has suggested that not only is ZIP7 present in the ER, but it is also located on the INM. ZIP7 is expected to be orientated on the INM so that it was able to transport zinc from the ER store into the nucleus. To date, no ZIP transporters have been located in the nucleus, however, there is much zinc in the nucleus which is required for DNA zinc fingers and transcription factor binding to the target gene, especially in cancer. Understanding how ZIP7 is targeted to the INM and its effect on nuclear kinases is crucial to treat cancer. Trafficking of soluble proteins between the cytoplasm and the nucleus has been well studied and accrues through the central channel of the NPC³⁷⁸⁻³⁸⁰, while trafficking of nuclear envelope transmembrane (NET) proteins into the nucleus remains in dispute^{368,381-385}.

The nuclear pore complex (NPC) is a large, multimeric structure that acts as a permeability barrier between the cytoplasm and nucleoplasm³⁸⁶. NPCs have been the primary mechanism

for nuclear translocation of NETs for over 20 years ago^{387,388}. There are two NPC-dependent mechanisms: free lateral diffusion retention and nuclear localization signal (NLS) dependent mechanism (**Figure 7.1**)^{84,389,390}. Both of these mechanisms require that NETs stay embedded in the membrane³⁹¹. So, while ZIP7 is located in the ER, its long loop between TM3 and TM4 is located in the cytoplasm, however, when ZIP7 is on the INM it would be expected that the long loop will be located in the nucleoplasm, and this could have a role in shuttling ZIP7 from the ER to the INM. ZIP7 could freely diffuse from the ER to the INM using the peripheral channel of the NPC (**Figure 7.1**). The peripheral channels are between the core NPC structure and the pore membrane shown by cryoelectronic microscopy ~10 nm in diameter^{392,393}. The nucleoplasm domain of an INM located protein should be <60 kDa to enable it to pass through the peripheral channel of the NPC^{372,382}. The translocation of the membrane protein through this pathway depends on the nucleocytoplasmic domain size, independently of whether it contains any NLSs or not. This process does not involve any energy dependant step in the targeting pathways. Several INM proteins use this model, including LAP1²⁵⁴, LAP2^{254,381}, MAN1³⁹⁴, emerin³⁹⁵, and LBR^{381,396,397}. Other NETs have also been shown to have nuclear localization signals in their nucleoplasm domain which is essential for their trafficking to the INM by allowing them to use transport receptors. However, the transport receptors are too big to fit through the peripheral NPC channel, so it has been shown to facilitate NET transport using the central channel of NPC³⁹⁸⁻⁴⁰⁰.

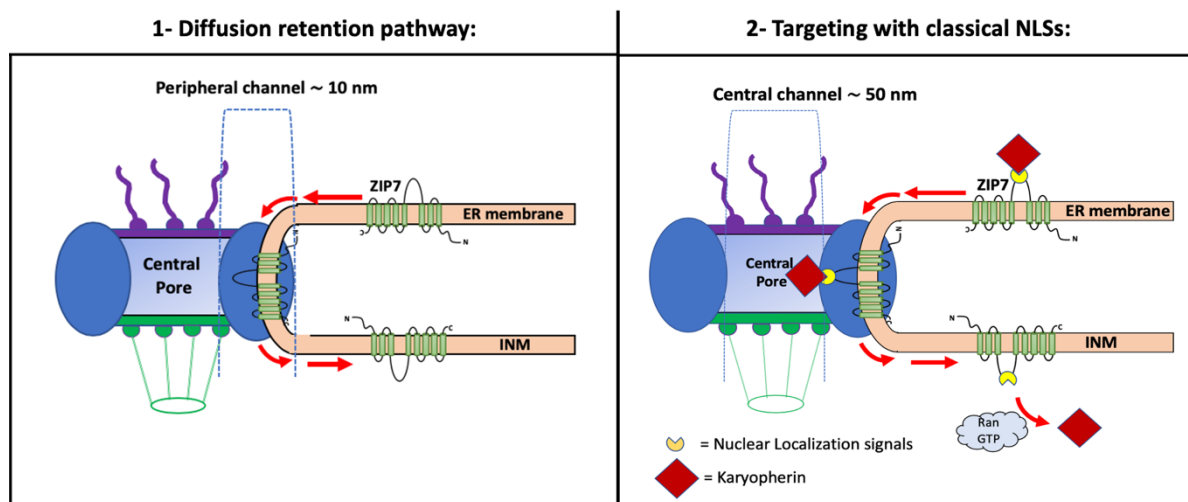


Figure 7.1 Proposed ZIP7 translocation mechanism into the nucleus.

The first proposed mechanism involves the free diffusion of ZIP7 from the ER to the INM using the peripheral channel of the NPC. The second proposed mechanism involves ZIP7 using an active transport mechanism which uses transport factors such as karyopherin which will bind to the NLS and facilitate the shuttle through NPC.

Subcellular localization of proteins can depend on their sorting or targeting signals, consisting of short stretch(es) of amino acids. Many of the protein localization mechanisms that rely on such signals have been identified using different predictors that recognize the wide variety of protein sorting signals⁴⁰¹. Nuclear proteins are transported into or out of the nuclei through the NPC by importin- β (Imp β), which can recognize specific targeting signals on cargo proteins⁴⁰². The NPC acts as a gate to allow transport molecules into the nucleus⁴⁰³. The NLSs are grouped into monopartite and bipartite signals⁴⁰⁴. A monopartite NLS is characterized by a single stretch of basic residues, while bipartite NLSs has two clusters of basic residues separated by a space region of 10-12 amino acids^{405,406}. Different online prediction methods have been used in this study, such as Nucpred²¹⁴, cNLSmapper²¹¹, NLStradamus²¹³, NucImport⁴⁰⁷, SeqNLS²¹⁵ to detect the NLSs of ZIP7, to understand by which mechanism ZIP7 is translocated to the INM. Computer analysis of the ZIP7 sequence revealed that ZIP7 has three nuclear localization signals: two monopartite NLSs and one bipartite NLS separated by 19 amino acids, all of which are in the nucleoplasm domain. The presence of these nuclear localization signals in ZIP7 may suggest that in order to move to the inner nuclear membrane ZIP7 uses an active transport mechanism and uses transport factors such as karyopherin, which will bind to the NLS and facilitate the shuttle of ZIP7 through the NPC (**Figure 7.1**). The central channel of the NPC

contains a nucleoporin containing phenylalanine-glycine (FG)-rich repeat, which promotes receptor-mediated transport of cargo containing nuclear import signals. Soluble cargo can go to the nucleus through the central channel of the NPC, while INM proteins must cross the pore close to the pore membrane. Ultrastructural analysis of NPCs has shown that the central channel of the NPC is approximately 50 nm while the lateral channel is a smaller size of approximately 10 nm in diameter⁴⁰⁸. If ZIP7 uses a receptor-mediated nuclear import pathway, then ZIP7 may use the central and lateral NPC channel to get transported into the INM. The three predicted NLS sites of ZIP7 are all in the cytoplasmic loop region between TM3 and 4. Moving ZIP7 through the side of the pore membrane will allow its NLS to be extended through the sideward opening of the lateral channel. The FG-Nups encode multiple phenylalanine and glycine (FG)-repeats that act as binding sites for soluble transport factors (Kaps)¹⁰⁰. There are studies that suggest that NLS containing proteins use receptor-mediated translocation through the central channel of NPC⁴⁰⁹. Examples of this are how depletion of importin α and importin β prevent the nuclear localisation of Heh1 and Heh2⁴¹⁰ and also how SUN, which is an INM protein is found to bind to importins³⁷⁴.

All this evidence suggests that the predicted NLS sites of ZIP7 could play a role in transporting ZIP7 from the endoplasmic reticulum into the inner nuclear membrane. The newly discovered NLS sites of ZIP7 fit the general criteria for nuclear targeting sequences which is to have a single or two clusters of a positively charged amino acid (arginine, R or lysine, K). In the monopartite NLS, short basic clusters such as (PKKKRKV) resemble the NLS of the simian virus 40 (SV40) protein which is responsible for directing the protein to the cell nucleus¹⁰⁶. INM proteins Src1/Heh1 and Heh2 (orthologs of mammalian MAN1 and LEM2) have NLS sites that bind to importin α/β to facilitate nuclear translocation and deletion of these NLS sites cause a mis-localization and accumulated in the ER³⁸⁵. The bipartite motif is characterized by two clusters of 1-3 positively charged amino acids separated by a linker⁴¹¹. The linker is usually ten amino acids, but it could be as high as 37 residues in the case of an adenovirus DNA binding protein⁴¹². The lamin B receptor is a protein that contains eight transmembrane domains and is located on the endoplasmic reticulum and INM. The nucleocytoplasmic domain of this inner nuclear membrane protein plays a major role in targeting the inner nuclear membrane and must fit through the lateral channels of the nuclear pore complex. The lamin B receptor contains a bipartite NLS, consisting of two basic segments (from Arg 63 to Arg79 and from Arg 93 to Lys 108) in its N-terminal nucleoplasm domain^{413,414}. Increasing the size of the

nucleocytoplasmic amino-terminal of lamin B receptor to 70 kDa actually prevented its nuclear localization³⁷², confirming the size restriction for this type of transport into the nucleus. The predicted nuclear localization signals of ZIP7 are located in the long cytoplasmic loop between TM3 and TM4. This long cytoplasmic loop is predicted to be located in the nucleus after targeting to the INM. According to Protein Molecular tools from Expasy, the size of the nucleocytoplasmic domain of ZIP7 is 8.82 kDa. To examine this mechanism, it would be possible to make a ZIP7 chimeric construct with nine copies of this ZIP7 nucleocytoplasmic domain, which would increase the size to be above the diffusion limit. If the theory was true, then this increased size in ZIP7 would prevent its nuclear location.

Knowing that ZIP7 has three predicted NLS sites, we further investigated these regions by mutating the key residues to alanine. The immunofluorescence results show that the NLS ZIP7 mutants have the same ER and nuclear ring localization as WT ZIP7, which means that these mutants still have access to the INM. Many INM proteins contain NLS sites, but in most cases, it is still unclear if these NLS regions are essential for INM transport as their mutation or deletion does not always seem to affect the nuclear localization, suggesting that there are additional features that contribute to INM targeting^{373,415}. However, a recent study showed that loss of NLS sites in the lamin B receptor reduced its transport rate to the INM and changed the transport mechanism from the central channel of the NPC to the peripheral channel which still allowed it to be localized on the INM³⁹¹. Immunofluorescence of the ZIP7 mutants with removed NLS sites suggested that ZIP7 still has access to the INM, however it might be at a reduced rate as it may have to use the peripheral channel of NPC instead of the central channel. The peripheral channels of the NPC are essential for INM transport as blocking this channel by using an antibody to the region of the transmembrane nucleoporin gp210 (anti-gp210)³⁸² completely inhibits the lamin B receptor transport through both the central and peripheral channel of NPC³⁹¹. Inhibition of the central channel of NPC has been achieved using microinjection of wheat germ agglutinin (WGA), a lectin that has been shown to bind O-glycosylated nucleoporins and dramatically reduce the transport through the central channel^{382,416,417}. Blocking the central channel by this mechanism prevented the lamin B receptor from using its normal route to the INM through the central channel, however it used the peripheral channel with a higher density diffusion rate³⁹¹. Single-molecule fluorescence recovery after photobleaching (smFRAP) is a new technique that provides quantitative information about the distribution and translocation rate of INM proteins in live cells²⁶³. It

would be important to use this technique to investigate the distribution of ZIP7 in INM and ONM.

Another proposed mechanism of how ZIP7 could translocate into the inner nuclear membrane could be during mitosis. During mitosis, the cells undergo structural changes, including chromosomal condensation, nuclear envelope breakdown and disassembly of the nuclear pore complex, lamins, and inner nuclear proteins⁸². In late Telophase, the last event of mitosis, the nuclear envelope membrane starts to reform from the existing endoplasmic reticulum where ZIP7 is located⁸². An *in vivo* study showed that the binding capacity of INM proteins to chromatin drive the spreading of the ER and collaborate to allow the rapid formation of the nuclear envelope at the end of mitosis and this was confirmed by knockdown of any part of the INM delaying the formation of NE⁴¹⁸. The location of ZIP7 in the ER would be ideal to allow it to be included in the new INM as it was reformed at the end of every mitosis cycle. This possibility is consistent with ZIP7 being localised to both the ER and the INM without the real need for any specific nuclear localisation signals and therefore may explain why little difference was observed when these NLS motifs in ZIP7 were removed. Furthermore, this would mean that ZIP7 was not only capable of transporting zinc from the ER into the cytoplasm, but also from the ER into the nucleus. This fact alone may explain why ZIP7 has such an important role to play in driving aggressive cancers such as tamoxifen resistant breast cancers as it is able to bring about signalling changes in the nucleus with ease.

7.4 Zinc and its role in the nucleus

ZIP7 is located in the ER and is phosphorylated by CK2, resulting in zinc release from stores, which activates many downstream signalling pathways known to have a role in breast cancer development^{58,69}. For the first time, this study has shown that ZIP7 is also located on the nuclear membrane as well as the ER and could be responsible for zinc release into the nucleus. This location of ZIP7 would be consistent with its ability to transport zinc from the ER lumen into the nucleus, where it could be used to regulate the structure and function of the genome⁴¹⁹. Transcription factors play a central role in regulating the gene expression⁴²⁰ and, according to DNA binding studies, most of the transcription factors are categorized into classical zinc finger containing proteins (ZNFs), which play an essential role in regulating their gene expression^{421–423}. Different types of zinc finger motifs have been shown to have a diverse role in gene

expression which control apoptosis, proliferation, differentiation, migration, and invasion⁴²⁰. Targeting the expression or activity of zinc finger proteins that have a role in cancer progression through decreased zinc levels could be a new therapeutic strategy against cancer development.

Different families of “zinc finger” proteins contain multiple cysteine and/or histidine residues that use zinc to stabilize their fold^{424–426}. Proteins containing the classical Cys2His2 zinc finger are among the most abundant in eukaryotic genomes, which were used for protein-DNA, protein-RNA, and protein-protein interaction^{21,427,428}. Thymidine kinase is often used as a marker of cell proliferation which is markedly increased during the G1 and early S phase of the cell cycle⁴²⁹. Although thymidine kinase is not a zinc metalloenzyme, zinc does regulate its transcription through zinc-dependent protein binding to the promoter region of the gene⁴³⁰. Several studies have reported that zinc depletion in tissues caused a reduction in the activity of DNA polymerase and thymidine kinase^{431–434}. Histochemical observation has shown that the cell nucleus, nucleolus, and chromosomes all contain zinc⁴³⁵. 30% to 40% of cellular zinc is localized in the nucleus whereas 50% is in the cytosol and cytosolic organelles⁴³⁶.

Zinc influences gene expression through transcription factors containing zinc finger domains⁴¹⁹. Metal response element binding transcription factor-1 (MTF-1) is one of the zinc-activated transcription factors that induce metallothionein in response to cellular zinc⁴³⁷. MTF-1 is a six-zinc finger protein that can bind to free cytoplasmic zinc and translocate to the nucleus to increase the expression of metallothionein (MT)⁴³⁷. MT is essential in regulating the cellular zinc level and the nucleolar translocation of zinc in the cell cycle and differentiation²⁴. The cellular free zinc level is very low because it is mainly bound to MT, which donates zinc to enzymes⁶¹ and zinc finger-domain transcription factors⁴³⁸. MT is a small cysteine-rich protein found primarily in the cytoplasm; however, it is translocated into the nucleus when a higher zinc level is required for DNA synthesis. MTF-1 is located in the cytoplasm in untreated mouse Hepa cells; however, increasing the level of zinc in the culture medium promotes its rapid translocation to the nucleus to enable it to activate the DNA binding activity of MTF-1⁴³⁷. Cytoplasmic zinc binding to MTF-1 allows its translocation to the nucleus to increase its DNA binding activity⁴³⁷. A zinc-MTF-1 complex binds to a metal response element (MRE) in the promoter region of the MT gene to induce MT gene expression⁴³⁷. Nuclear translocation of MT into the nucleus was observed during the early S-phase of growth factor-stimulated primary rat hepatocytes⁴³⁹ and in certain tumours such as thyroid tumours⁴⁴⁰ and bladder tumours⁴⁴¹. These

data provide evidence for a role of MT in trafficking zinc from the cytoplasm into the nucleus to activate gene expression.

Taking the above aspects together highlights the critical role of zinc in the nucleus, which has, until now, not been attributed to any zinc transporter. MT acts as a supplier for the transfer of zinc to nuclear proteins; however, MT requires upregulation by gene expression, so it cannot respond quickly to signalling events. This discovery that ZIP7 could transport zinc into the nucleus allows the nuclear zinc level to rise in seconds or minutes which is consistent with the ability to alter signalling pathways rapidly. This control of the zinc level in the nucleus will be important in normal cell conditions but also a problem if altered in diseases such as cancer.

7.5 ZIP7 signaling is involved in diverse kinase signaling pathways

ZIP transporters are mostly localized to the plasma membrane to transport zinc into cells from the extracellular space, however, ZIP7 is located in the ER and is responsible for the transport of zinc from the ER to the cytoplasm^{44,58,158}. The unique ER localization of ZIP7 enables it to play an essential role in regulating intracellular zinc levels, which has an important potential role in growth factor signalling. ZIP7 has already been implicated in cancer growth as it has been demonstrated to activate MAPK, PI3K-AKT and mTOR pathways⁷⁴. Using phospho-kinase arrays has confirmed the activation of AKT and ERK1/2 in response to ZIP7 activation which was amplified by zinc treatment. CK2 phosphorylates ZIP7 on residues S275 and S276 within 2 minutes of a stimulus resulting in ZIP7 activation and zinc release from stores into the cytosol¹⁶⁹. This released zinc can inhibit protein tyrosine phosphatase activity resulting in prolonged activation of tyrosine kinases²⁴¹. Cytosolic zinc released by ZIP7 has been shown to activate tyrosine kinase pathways in MCF-7 and tamoxifen-resistant cell lines, allowing stimulation of cell growth, cancer progression, and cell invasion^{63,69}. ZIP7-mediated zinc release activates EGFR³⁰⁰, IGF-1R³⁰¹, and Src³⁰², which all promote the aggressive behaviour of breast cancer cells that have tamoxifen resistance, which links ZIP7 to the mechanism of acquired tamoxifen resistance in breast cancer. Targeting ZIP7 in breast cancer could prevent inhibition of tyrosine phosphatases, decreasing the activation of tyrosine kinases and allowing normal cell signalling pathway activation.

7.6 ZIP7-mediated zinc release causes AKT and CREB phosphorylation

AKT⁴⁴² and ERK1/2²⁷⁸ pathways have been shown to be involved in the growth and proliferation of cancer. PI3K/AKT pathways are the most frequently mutated pathways in human cancer with are associated with tumorigenesis, drug resistance, and cancer progression⁴⁴³. AKT is one of the major downstream effectors of PI3K⁴⁴⁴. AKT is phosphorylated at Thr³⁰⁸ by PDK1 and at Ser⁴⁷³ by mTORC2 for the full activation of the enzyme⁴⁴³ (**Figure 7.2**). Increased AKT kinase activity has been reported in a broad range of human cancers, including breast⁴⁴⁵⁻⁴⁴⁷, prostate^{448,449}, gastric⁴⁵⁰, ovarian^{449,451,452}, pancreas⁴⁵³, and leukaemia⁴⁵⁴, and its activation has been shown to correlate with advanced disease and/or poor prognosis. AKT phosphorylates many cellular proteins that have a role in cell survival and cell cycle progression, such as GSK-3 α/β ⁴⁵⁵. AKT can phosphorylate and inactivate glycogen synthase kinase GSK-3 β (S9) and GSK-3 α (S21)¹¹⁶ which has a role in many signalling pathways. Inhibition of GSK-3 β promotes cell survival while hyperactive GSK-3 β contributes to cell death⁴⁵⁶⁻⁴⁵⁹. Dysregulation of GSK-3 activity is associated with many diseases, including cancers, and causes resistance to chemotherapy and radiotherapy⁴⁶⁰. GSK-3 α/β is overexpressed in many tumours such as liver, ovarian, pancreas, and colon⁴⁶¹⁻⁴⁶³. GSK-3 is known to drive cell proliferation by regulating the stability and synthesis of proteins involved in cell cycle entry⁴⁶⁴⁻⁴⁶⁷. GSK-3 is a potential therapeutic target in cancer that is resistant to treatment in ovarian carcinoma cells⁴⁶⁸, renal cell carcinoma⁴⁶⁹, and prostate cancer⁴⁷⁰. In addition, activated AKT phosphorylates mTORC1 which results in increased protein synthesis and cell survival by phosphorylation of p70S6 Kinase on residue threonine 389, which has a role in protein synthesis, cell growth, and survival through phosphorylation of ribosomal protein S6⁴⁷¹ (**Figure 7.2**). AKT has been shown to phosphorylate the transcription activator CREB, which is known to play an essential role in prostate carcinogenesis⁴⁷² (**Figure 7.2**). This evidence indicates that AKT activates several signalling pathways that are linked to tumorigenesis. The results presented in this thesis strongly suggest that ZIP7 activation can lead to AKT phosphorylation in a breast cancer cell line, which explains its role in driving cell proliferation and survival. Alteration in the PI3K/AKT/ mTOR pathway is strongly implicated in cancer pathogenesis and targeting the upstream effector that activates this pathway (ZIP7) is a promising therapeutic approach.

Using phospho-kinase arrays in this thesis showed that multiple kinases were phosphorylated due to ZIP7 mediated-zinc release from stores. Serine 473 phosphorylation of AKT is a major early event in the cellular response ZIP7 activation¹⁶⁹. Activation of the PI3K/AKT/mTOR pathway is seen in a wide variety of cancers, and it regulates essential cellular functions, including cell metabolism, migration, growth, survival, and angiogenesis⁴⁷³. Activation of PI3K/AKT/mTOR pathways is common in breast cancer and associated with resistance to endocrine and chemotherapy therapy⁴⁷⁴. Blocking this pathway could inhibit the proliferation of tumour cells, and several inhibitors are currently available such as everolimus, an oral mTOR inhibitor that has been approved for use in post-menopausal women with hormone receptor-positive breast cancer; it is also approved for use in other cancers, including renal cell carcinoma, and neuroendocrine tumours of the pancreas⁴⁷⁴. However, the use of these inhibitors is associated with a wide spectrum of adverse effects and resistance because the PI3K pathway involves a complex network of interactions with parallel cascades and its inhibition causes negative feedback resulting in activation of compensatory signalling pathways⁴⁷³. So, inhibiting ZIP7, upstream target of PI3K/AKT/mTOR in combination with endocrine therapy or with another single agent such as PI3K inhibitor in breast cancer may be possible to optimise the efficiency of cancer therapy by decreasing cell proliferation and enhancing cell death.

Transcription factors are key regulators of gene expression that have a critical role in cell proliferation, survival, and invasion. The function of transcription factors is mainly regulated through phosphorylation. cAMP-regulatory element-binding protein (CREB) is an oncogenic transcription factor, activated through phosphorylation of serine 133 by several kinases including AKT and ERK1/2^{273,472} (**Figure 7.2**). The results presented in this thesis showed that ZIP7-mediated zinc release from stores activates AKT and ERK1/2, which activates CREB, highlighting the role of ZIP7 in activating CREB that plays an essential role in malignant cellular behaviour. Of additional relevance is the fact that CREB often locates to the nucleus and due to the location of ZIP7 on the nuclear membrane, ZIP7 may be particularly well placed to activate CREB signalling.

Alteration in the function and expression of transcription factors such as CREB may occur as a central component of the molecular pathogenesis of a tumour, and inhibition of these transcription factors could reduce the malignant behaviour of many tumour types. CREB overexpression has been shown to be associated with tumour progression, metastasis,

chemotherapy resistance, and poor prognosis for cancer patients⁴⁷⁵. Immunohistochemical analysis of prostate and bone cancers showed that p-CREB staining was detectable in all the poorly differentiated prostate cancers and bone metastatic tissues specimens, suggesting that CREB is critically involved in tumour progression and metastasis⁴⁷⁶. In addition, increased CREB mRNA levels were detected in breast cancer tissues compared to normal mammary tissues and the level of the expression was correlated with disease progression and survival⁴⁷⁷. The results presented here indicate that ZIP7-mediated zinc release activates CREB. Given the role that CREB plays in carcinogenesis, inhibition of CREB through inhibition of the upstream pathways that activate it, provides ZIP7 as a potential therapeutic target in cancer.

Depletion of intracellular zinc is associated with the downregulation of CREB in hippocampal neurons⁴⁷⁸. CREB promotes cell growth and tumour angiogenesis in metastatic melanoma cells and silencing CREB shows suppression in tumour growth and metastasis^{479,480}. Also, CREB level have been shown to link to tumour stage, clinical outcome, and metastasis of gastric cancer⁴⁸¹. A high CREB expression level was observed in glioma, which highlighted the role of CREB as a transcription factor required for cancer cell proliferation, migration, and survival⁴⁸²⁻⁴⁸⁴. Several studies suggest that CREB promotes cell survival by upregulating the expression of anti-apoptotic proteins such as bcl-2⁴⁸⁵⁻⁴⁸⁸. ZIP4 overexpression in pancreatic cancer cells results in CREB phosphorylation, leading to increased cyclin D1 and, thereby, cell proliferation and tumour progression¹⁶¹. This evidence suggests that CREB plays a key role in mediating the malignant behaviour of tumour cells and that the successful targeting of CREB is a potential therapeutic consideration. CREB is involved in neoplastic transformation, so its inhibition becomes a potential therapeutic strategy for cancer⁴⁷⁵.

Knowing the molecular mechanisms involved in CREB expression and regulation will lead to therapeutic targets that inhibit the activity of CREB in cancer. Multiple Ser/Thr protein kinases could phosphorylate CREB, so the use of kinase inhibitors to inhibit CREB phosphorylation could potentially be used in cancer therapy. This study showed that ZIP7 overexpression caused increases in AKT and ERK1/2, which activated CREB resulting in increased cell proliferation and tumour progression of breast cancer. These results identified a new downstream target of ZIP7-mediated zinc release, which is CREB.

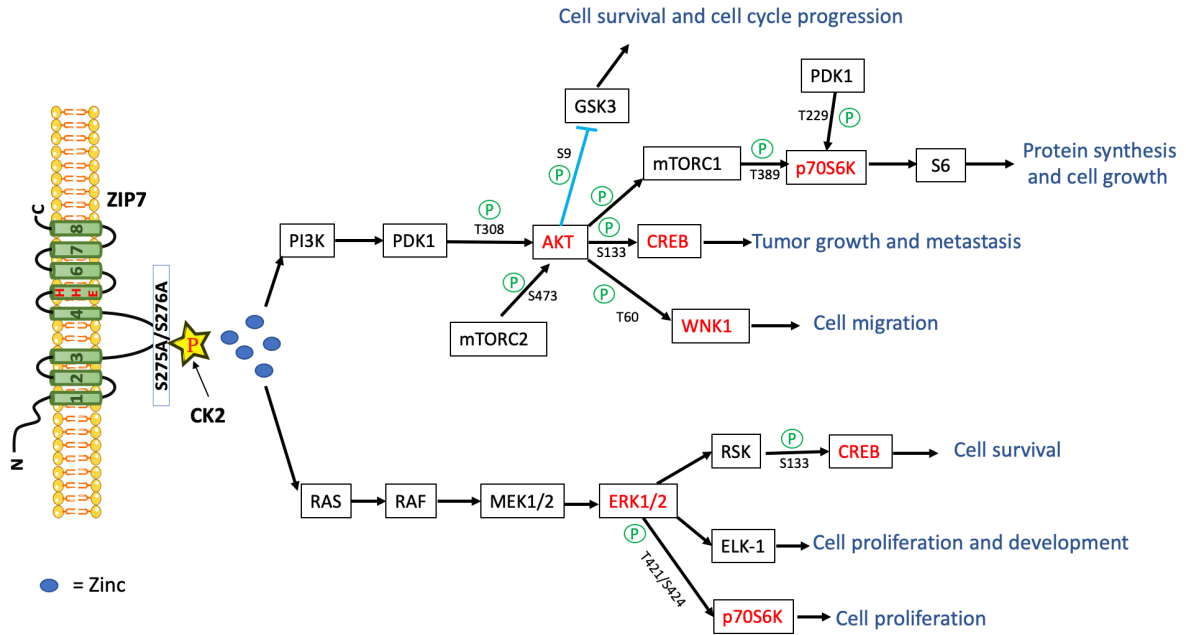


Figure 7.2 Downstream signalling pathways of ZIP7 mediated zinc release

ZIP7 is activated by CK2 phosphorylation on two serine residues on the long intracellular loop between TM3 and TM4. Phosphorylated ZIP7 results in zinc release from the ER into the cytosol and nucleus which activates several downstream signalling pathways that are known to be involved in cancer development. Red boxes are the key kinases that ZIP7-mediated zinc release activates.

7.7 Removal of the nuclear localization motifs from ZIP7 reduces the activation of AKT and CREB

This study has found that ZIP7 is located on the nuclear membrane and could transport zinc into the nucleus and activate many nuclear kinases that have a role in cancer development. Nuclear protein kinases have an essential role in regulating cellular proliferation⁴⁸⁹. In cancer, these nuclear kinases are often dysregulated and cause uncontrolled cell proliferation and growth⁴⁹⁰. It is necessary to develop a novel therapy that targets these nuclear kinases that have a role in cancer progression. In this study, three predicted NLS sites of ZIP7 have been identified, located in the long cytoplasmic/ nucleoplasmic loop that could have a role in trafficking ZIP7 to the INM. To investigate the role of these NLS signals on ZIP7 activation

and downstream effect, human phospho-kinase arrays were carried out using cells transfected with ZIP7 NLS mutants and treated with zinc for up to 10 minutes. The cells transfected with NLS3 mutant showed a lower level of AKT (S473) and CREB (S133) than cells transfected with WT ZIP7, suggesting the role of nuclear located ZIP7 in the activation of AKT and CREB.

The serine/threonine kinase AKT has a vital role in regulating many cellular functions involved in cell proliferation, survival, autophagy, metabolism, and angiogenesis⁴⁹¹. Dysregulation of AKT activity has been reported in many diseases, including cancer⁴⁹². AKT is known to function mainly in the cytoplasm, but also AKT has been reported to translocate to the nucleus in many cell types⁴⁹³. The presence of active and phosphorylated AKT in the nucleus was reported in the 1990s⁴⁹³. The FOXO family of transcription factors⁴⁹⁴ and transcription coactivator p300⁴⁹⁵ are both substrates of AKT and are all located in the nucleus. All the machinery that is necessary for AKT activation by phosphorylation at threonine 308, including PI3K⁴⁹⁶, PIP3⁴⁹⁷, and PDK1^{498,499} (**Figure 7.2**), is also located in the nucleus. Moreover, mTORC2 is localized in both the cytoplasm and nucleus⁵⁰⁰ and it has been hypothesized that it too could phosphorylate nuclear AKT at serine 473 in neoplastic thyroid cells⁵⁰¹. This data together suggests that AKT interaction with those signalling components in the nucleus may be as dynamic in the nucleus as it is already known to be in the cytoplasm.

Nuclear AKT is involved in cell cycle progression, cell survival, DNA repair, cell differentiation and tumorigenesis⁴⁹³. The presence of nuclear AKT has been reported in many cancers such as in breast⁵⁰², lung⁵⁰³, thyroid, and prostate cancer⁵⁰⁴, as well as in acute myeloid leukaemia^{505,506}. Moreover, nuclear AKT has been associated with invasion and metastasis of human thyroid cancer tissue⁵⁰⁷. In melanoma cells, both phosphorylated and unphosphorylated AKT were shown to be present in the nucleus⁵⁰⁸. The nuclear AKT could be used as an indicator of prostate cancer prognosis because it is increased during the progression from normal tissue to low grade prostatic intraepithelial neoplasia⁵⁰⁴, a neoplastic growth of epithelial cells within pre-existing benign prostatic ducts⁵⁰⁹. Furthermore, in prostate cancer the extent of AKT nuclear localization correlates with the Gleason score, which is the most potent predictor of tumour progression after prostatectomy⁵¹⁰. Moreover, nuclear AKT increases in invasive carcinoma, including glioblastomas⁵¹¹ and head and neck carcinoma cell lines⁵¹². The current study suggests that ZIP7 is located in the nuclear membrane and interestingly, when cells were transfected with the NLS3 mutant of ZIP7, there was a

significant reduction in the level of pAKT (S473). These data together demonstrate the importance of nuclear AKT, especially in driving cancer growth and development and additionally the nuclear localization of ZIP7 may play an important part in the activation of nuclear AKT.

AKT is capable of directly phosphorylating cyclic AMP-response element-binding protein (CREB) at Ser133⁴⁷² (**Figure 7.2**). The lower level of activated AKT observed in cells transfected with the ZIP7 NLS3 mutant was also followed by a low pS¹³³CREB level compared to cells transfected with WT ZIP7. Genome-wide screening for the CREB binding site showed that over 4000 genes involved in uncontrolled cell proliferation and tumorigenesis, might be controlled by CREB⁵¹³. This result suggests that pS¹³³CREB overexpression is promoting tumour initiation, progression, and metastasis⁵¹⁴. Therefore, pS¹³³CREB inhibition and downregulation is a potential therapeutic target for cancer. Currently, there are two strategies to inhibit CREB. The first, named “CREB inhibitors” directly affect CREB transcriptional activity through inhibition of CREB:CBP (CBP, CREB binding protein) or CREB:CRE-DNS interaction (CRE, cAMP response element)^{514,515}. The second, named “CREB-related pathways inhibitors” inhibit the signalling pathways that include CREB as a final effector^{514,515}. In this study, the results suggest that nuclear ZIP7 can activate different pathways that all have pS¹³³CREB as their final effector. Mutation of ZIP7 NLS sites causes a decrease in the activation of pS¹³³CREB which would be expected to decrease cell viability, growth properties and enhance apoptosis.

AKT activation is essential for glucose metabolism⁵¹⁶. The next generation AKT inhibitor, which is MK-2206 that inhibits AKT in adipocytes mainly develops complications such as insulin resistance, which may lead to an increased risk of diabetes⁵¹⁷. MK-2206 is an orally AKT inhibitor under development for treating solid tumours⁵¹⁷. These findings highlight the importance of regulating the cellular level of AKT to selectively block the increase of nuclear AKT. This study provides the first evidence that ZIP7 in the nucleus has an essential role to activate AKT and this was discovered by transfecting the cells with ZIP7 NLS3 and noticing the subsequent reduction in the level of nuclear pS⁴⁷³AKT and pS¹³³CREB. Therefore, ZIP7-mediated zinc signalling in the nucleus is an interesting target for cancer treatment which could potentially prevent activation of both AKT and CREB pathways in cancer.

7.8 ZIP7 overexpression activates ERK1/2

MAPK signalling pathways regulate many cellular processes involved in cell proliferation, differentiation, angiogenesis, tumour metastasis and apoptosis⁵¹⁸. ERK, a type of serine/threonine protein kinase, is a member of the MAPK family and is activated by phosphorylation on residues T202/Y204/T185/Y187⁵¹⁹. Stimulation of epidermal growth factor receptor (EGFR) or insulin-like growth factor receptor leads to RAS activation, which will activate RAF. Subsequently, RAF phosphorylates and activates MEK1/2 which in turn phosphorylates and activates ERK1/2. Once activated, ERK1/2 can regulate up to 250 potential substrates that have a role in apoptosis, DNA repair, and cell cycle⁵²⁰⁻⁵²². Activated ERK causes many pathological changes, including tumorigenesis^{523,524}. Activation of ERK has been observed in pancreas, melanoma, colorectal, basal-like breast, hepatic, and non-small cell lung cancer⁵²⁵. ERKs have been shown to promote cell survival by inhibiting apoptosis, inducing DNA damage repair and arresting the cell cycle⁵²¹. ERK is mainly located in the cytoplasm; however, it does get translocated to the nucleus after its initial activation where it can regulate transcription factor activity and gene expression⁵²⁰⁻⁵²². An *in vivo* study on mice has shown that increased activation of the ERK/MAPK pathways was related to colon carcinoma development as continuous activation of the ERK/MAPK signalling pathways promotes the transformation from normal cells into tumour cells⁵²⁶. Inhibition of this pathway can inhibit tumour growth, suggesting that ERK/MAPK is involved in tumour formation and providing a promising anticancer therapy⁵²⁶.

70-kDa ribosomal S6 kinase (p70S6K) has an important role in cell cycle progression and cell proliferation⁵¹⁸. p70S6K is a downstream target of ERK/MAPK (**Figure 7.2**) as well as AKT⁵¹⁸. The downregulation of p70S6K in ovarian tumours inhibits their growth and angiogenesis⁵²⁷. Angiogenesis is the formation of new blood vessels that play a critical role in the growth of cancer because solid tumours need to generate a new blood supply⁵²⁸. The primary cause of death for patients with cancer is metastatic growth of the tumour, which is the spreading of cancer cells from a primary tumour to a secondary site throughout the lymphatic circulatory system⁵²⁹. Invasion is the first step of metastasis, where the tumour cells penetrate their surrounding basement membrane and migrate through the extracellular matrix (ECM) into the surrounding tissue⁵³⁰. ERK/MAPK signalling pathway plays an important role

in tumour invasion and metastasis⁵³¹. So, MAPK is an important pathway that drives human cancer and blocking this pathway by targeting inhibitors is an essential anti-tumour strategy.

MAPK signalling pathways are often used as a target for cancer treatment because of their implication in cancer survival²⁷¹. A combination inhibitor of Raf (an upstream activator of MEK) and MEK inhibitors have been developed to target MAPK pathways; however, resistance to these antagonists accrues within one year, so discovering further new treatment options is necessary⁵³². ERK is the terminal kinase of MAPK pathways and inhibiting its effect is a promising strategy to treat a wide variety of cancer. However, available ERK inhibitors can cause resistance in clinics due to mutation in ERK1/2 which prevents the inhibitor binding to the mutant ERK molecule. Nevertheless, new ERK1/2-specific inhibitors are currently in early clinical trials to treat metastatic solid tumours⁵³³. The phosphokinase arrays presented in this thesis showed that activation of ERK1/2 is downstream of ZIP7 activation⁶⁹ by CK2¹⁶⁹. ZIP7 has been shown to increase growth and invasion of aggressive antihormonal resistance cells⁶⁹. ZIP7 is a highly promising therapeutic target of tumour growth, invasion and antihormonal resistance in breast cancer.

7.9 Decreased ERK1/2 activation in cells overexpressing ZIP7 NLS3

The phospho-array data revealed that ZIP7-mediated zinc release phosphorylates multiple kinases, and one of them involves the Mitogen-activated protein kinase (MAPK) cascade, confirming what was seen in a previous study⁷⁴. Treating tamoxifen-resistant breast cancer or MCF-7 cells with zinc showed CK2 phosphorylation of ZIP7 at Ser275 and Ser276 that peaks within 2 minutes, generating a downstream increase in cytosolic zinc and phosphorylation of ERK1/2 (T202/Y204/T185/Y187) and pS⁴⁷³AKT¹⁶⁹ (**Figure 7.2**). MAPK has an essential role in the regulation of cell proliferation, survival, and differentiation²⁷¹. Activated MAPK cascade has been reported in many diseases, including cancer²⁷¹. ERK1/2 is a downstream component of the Ras/Raf/MEK1/2 signaling cascade which has an important role in oncogenesis. Epidermal growth factor receptor (EGFR) is overexpressed in many cancers and Ras is the main downstream effector of EGFR^{534,535}. The previous study from our group showed that ZIP7-mediated zinc release from cellular stores resulted in activation of many receptor tyrosine kinases (RTKs) such as EGFR (ErbB1), ErbB2 and IGF-1R¹⁴ and this was further confirmed using phospho-RTK arrays⁷⁴. Taken together these data further support the involvement of

ZIP7-mediated zinc signalling in driving many signalling pathways that are known to be responsible for cellular carcinogenesis.

Activated ERK1/2 phosphorylates p90 ribosomal S6 kinases (RSK) downstream and both then translocate into the nucleus where they activate many transcription factors that lead to an increase in cell proliferation and survival⁵³⁶(**Figure 7.2**). Fluorescent staining in fibroblastic cells showed that MAPK, after mitogenic stimulation, is activated primarily in the cytoplasm and then moves to the nucleus⁵³⁷. In the nucleus, activated ERK1/2 can phosphorylate the cell cycle regulatory transcription factors such as Elk-1 while RSKs can phosphorylate CREB, which in turn also promotes cell survival⁵³⁸. Therefore, decreasing the nuclear effect of ERK1/2 has been investigated as a means of providing control in cancer development. The phospho-kinase arrays result in this study showed a significant reduction of ERK1/2 in cells transfected with the ZIP7 NLS3 mutant (**Figure 6.13**) which was also confirmed to be less than WT ZIP7 by western blot (**Figure 6.14**). These data confirmed the role of nuclear ZIP7 in ERK1/2 activation.

The discovery of the novel nuclear localization of ZIP7, suggests that it can transport zinc into both the cytosol and into the nucleus, which is a new discovery. Once ERK1/2 is activated, it will be able to phosphorylate proteins in the cytosol or nucleus that have a role in cell differentiation, proliferation, and apoptosis⁵³⁹. Zinc has a major role in ERK1/2 activation. A decrease in ERK1/2 phosphorylation and cell cycle arrest was observed in zinc-deficient IMR-32 cells (derived from neuroblastoma metastasis)⁵⁴⁰. These results suggest that targeting nuclear-located ZIP7 to reduce nuclear zinc and decrease activation of nuclear ERK1/2 would be a novel way to reduce cellular proliferation driven by the ERK1/2 pathway.

7.10 Decreased activation of p70S6 Kinases in cells overexpressing the ZIP7 NLS3 mutant

S6K is a ribosomal protein S6 kinase which is a member of the AGC family of serine/threonine kinases. This family also includes PKA, AKT (PKB), protein kinase C (PKCs), PKG, PDK-1, SGK and 90- kDa ribosomal S6 kinases (p90^{RSK})⁵⁴¹. p70S6K catalyses the phosphorylation of the S6 protein, which is a component of the 40S subunit of eukaryotic ribosomes^{275,542}. S6K is known to be involved in the regulation of protein synthesis, the G1/S transition of the cell

cycle, mRNA splicing, and ribosomal biogenesis^{543,544}, all factors required for increased cell growth and proliferation. Knockout studies of the S6 kinase gene in *Drosophila* and mice showed that the S6 kinases are essential for controlling cell size⁵⁴⁵, growth⁵⁴⁶, and glucose homeostasis⁵⁴⁷. Furthermore, microinjection studies with neutralizing p70S6 antibodies prevented cell entry into the S phase of the cell cycle and protein synthesis^{548,549}, showing that p70S6 is essential throughout G1 and p70S6 antibodies may exert their effect on protein synthesis through inhibition of S6 phosphorylation.

Two signaling pathways have been shown to activate p70S6 Kinase. The first pathway is regulated by PI3K and its downstream effectors PDK and AKT^{275,550,551} (**Figure 7.2**). The second pathway is mTOR^{552,553} an important target for breast cancer therapy as it is involved in cancer development and tumorigenesis^{554–556}. Both these pathways are activated as a result of ZIP7-mediated zinc release from stores⁷⁴. In fact, ZIP7-mediated zinc release from intracellular stores activates MAPK, mTOR, and PI3K-AKT pathways within 5 minutes of a stimulus. In this study, it was shown that ZIP7 overexpression leads to phosphorylation of p70S6 Kinase, which is also the downstream target of mTOR, and PI3K-AKT (**Figure 7.2**). Therefore, targeting p70S6 Kinase through inhibition of ZIP7 may represent a beneficial new avenue for cancer therapy.

p70S6 Kinase is activated by phosphorylation at different serine/threonine sites by different upstream kinases²⁷⁶. p70S6 Kinase activation is achieved by sequential phosphorylation on S⁴¹¹, S⁴¹⁸, T⁴²¹, S⁴²⁴, T³⁸⁹ and T²²⁹ residues^{557,558}. The first phosphorylation of p70S6 Kinase occurs at the C-terminal domain (S411, S418, T421, and S424)⁵⁵⁹. The kinases that can phosphorylate p70S6 kinase in the initial step are ERK (T⁴²¹/S⁴²⁴)⁵⁶⁰, JNK1 (S⁴¹¹/S⁴²⁴)⁵⁶¹ and mTOR (S⁴¹¹/T⁴²¹/S⁴²⁴)⁵⁶². The second phosphorylation step occurs on T389, which is catalysed by mTOR⁵⁶². Thr389 phosphorylation allows phosphatidylinositol dependent kinase 1 (PDK1) to phosphorylate T229²⁷⁶. The phosphorylation of T389 and T229 is essential for p70S6 kinases maximal activation⁵⁶³.

The phospho-kinase arrays showed a marked increase in p70S6 kinase phosphorylation on residues Thr389 and Thr421/Ser424 in cells transfected with WT ZIP7 and treated with zinc (**Figure 6.13**). A recent study in our group showed a significant increase in p70S6 Kinase (T421/S424) in untreated conditions in cells transfected with WT ZIP7 compared to non-

transfected cells confirming that ZIP7-mediated zinc release can activate p70S6 Kinase⁷⁴. ERK phosphorylates p70S6 Kinase on Thr421/Ser424⁵⁶⁰ and the western blot results of ERK activation in cells transfected with WT ZIP7 showed an increase after 10 minutes of zinc treatment that was not statistically significant (**Figure 6.14**). These results correlate with a nonsignificant increase in T421/S424 p70S6 Kinase phosphorylation level after 10 minutes of zinc treatment (**Figure 6.17**). Phosphorylation of p70S6 Kinase on Thr389 relies on mTOR activation⁵⁶². mTOR is a serine/threonine-protein kinase and a member of the PI3K-associated kinase protein family that regulates cell growth and proliferation⁵⁶⁴. mTORC1 is a downstream target of AKT and is activated by phosphorylated AKT²⁸¹. The western blot results of AKT in cells transfected with WT ZIP7 showed a significant increase of pS⁴⁷³AKT after 10 minutes of zinc treatment (**Figure 6.15**) and that correlated with a significant rise in p70S6 Kinase (T389) after 10 minutes of zinc treatment (**Figure 6.18**).

Zinc is essential for cell growth as it can stimulate the cell signalling activity of p70S6 Kinase through the PI3K signalling pathway⁵⁶⁵. In addition, zinc can stimulate mTOR, which is an important upstream kinase of p70S6 Kinase⁵⁶⁶. Using specific inhibitors of the p70S6 Kinase signalling pathways, such as wortmannin (a phosphatidylinositol 3-kinase [PI3-K] inhibitor) and rapamycin (an mTOR inhibitor), it has been demonstrated that zinc is an upstream activator of mTOR and PI3K as these inhibitors both inhibit the zinc-induced p70S6 Kinase activity⁵⁶⁵. ZIP7-mediated zinc release from stores activates the PI3K/mTOR pathway, leading to phosphorylation of p70S6 Kinase on residues T421/S424 and T389, and this pathway also has a well-known role in driving cell growth and proliferation⁵⁶⁷.

No direct inhibitor for p70S6 Kinase has been identified however the upstream signalling pathways involved in the regulation of p70S6 Kinase can be inhibited by wortmannin and immunosuppressant rapamycin and that inhibition subsequently can severely impair the progression of the cell cycle through the G1 phase⁵⁴³. Interestingly, combining mTOR inhibitors with endocrine therapy in a patient with estrogen receptor-positive breast cancer has also been shown to enhance antitumour activity and prolong the time to cancer progression^{568–570}. However, mTOR inhibitors can be involved in a negative feedback mechanism which produces a marked increase in AKT and ERK1/2 activation⁵⁷¹ which may be a potential unwanted side effect in the clinic. To prevent the cancer cells from finding another route for their proliferation, multiple inhibitory targets at different levels could alternatively be used.

Another novel target that has been highlighted in this study is the nuclear localized ZIP7. The ZIP7 NLS3 mutants showed a lower level of p70S6 Kinase, suggesting that nuclear ZIP7 has an indirect role in p70S6 Kinase activation.

7.11 Activation of WNK1 (T60) in cells overexpressing WT ZIP7

WNK is a protein kinase family that lacks lysine in the kinase subdomain II and its pathway is known to control blood pressure through regulation of the function of ion transport across the cell membrane^{572,573}. There are four WNK genes in human^{574,575}. Activated WNK kinases phosphorylate and stimulate oxidative stress response 1 (OSR1) and STE20/SPS1-related proline/alanine-rich kinase (SPAK) which directly phosphorylate cation-chloride-coupled cotransporters including Na-K-Cl cotransporter (NKCC1), (NKCC2), and Na-Cl cotransporter (NCC) that have a role in the pathogenesis of hypertension⁵⁷⁶⁻⁵⁷⁸. The PI3K-AKT cascade is a well-known carcinogenic pathway which activates numerous proteins involved in diverse cellular roles such as cell growth, proliferation, survival, and migration⁴⁴³. The with no lysine [K] protein kinase-1 (WNK1) is also shown to be involved in cell proliferation, invasion, migration, and autophagy⁵⁷⁹⁻⁵⁸³. Several studies have shown that WNK1 is one of the downstream signalling pathways of the PI3K-AKT cascade (**Figure 7.2**). Insulin-like growth factor stimulation of HEK-293 cells, induce WNK1 phosphorylation at threonine residue 60 by AKT, and WNK1 phosphorylation is inhibited by using a PI3K inhibitor^{584,585}. WNK1 is phosphorylated as a result of ZIP7-mediated zinc release from stores (**Figure 6.13**), confirming the results of a previous study in our group⁷⁴. Recently, many studies showed the link of WNK kinases to many cancer types however, the exact mechanism of how they act is not well understood. Large scale cancer genomic sequencing studies have identified point mutations of WNK1 in breast and colon cancer^{586,587}. There is evidence that WNK1 is important for cell migration in different cancer types, including prostate cancer⁵⁸⁸, non-small cell lung cancer⁵⁸⁹, glioblastoma⁵⁹⁰, and breast cancer^{591,592}. An in vitro study showed that depletion or inhibition of WNK1 in breast cancer decreased migration and invasion⁵⁹³.

The Secreted Protein Acidic and Rich in Cysteine (SPARC) has been shown to promote cell migration in a non-small cell lung cancer cell line through AKT activation and increased WNK1 phosphorylation at threonine residue 60⁵⁸⁹. Furthermore, WNK1 has been shown to regulate Wnt/ β -catenin positively in *Drosophila*⁵⁹⁴ where increased Wnt signalling and high β -catenin has been demonstrated to cause colon cancer⁵⁹⁵. Additionally, a few studies have

recently shown that β -Catenin is a transcription target of WNK1 and the proliferation of some cancer cells with high β -Catenin activity is dependent on WNK1^{583,596}. This data is consistent with the observed high expression of β -Catenin leading to many diseases including cancer⁵⁹⁷. The three kinases, WNK 1, WNK2 and WNK3, have all been shown to increase cell migration, invasion, and metastasis⁵⁹⁸⁻⁶⁰⁰ and are therefore considered important potential targets in cancer. Furthermore, WNK1 increases epithelial-mesenchymal transition (EMT) which enhances the accumulation of transcription factor Slug⁵⁸³, which would stimulate loss of cell attachment, an essential factor required for tumour invasion and development⁶⁰¹. Decreasing the expression of WNK1 in cultural endothelial cells caused reduced expression in a number of factors that promote angiogenesis including Slug, vascular endothelial growth factor A (VEGF-A), and matrix metalloproteinases⁵⁸³. These studies provide evidence that WNK1 has a role in tumour progression and metastasis. The results presented here are consistent with ZIP7 acting as an upstream effector of WNK1 and places ZIP7 as a new therapeutic target in breast cancer patients to attenuate tumour progression and metastasis.

Currently, there are no clinically approved drugs that target the WNK pathway being used to treat cancer; however, some compounds that inhibit OSR1 and SPAK activity have shown a promising effect in anticancer therapy. So, the link between ZIP7 and activation of these signalling pathways that are known to have a role in cancer progression does suggest that ZIP7-mediated zinc release signalling is an interesting target for cancer treatment.

7.12 How to target ZIP7

Many results in this thesis have concluded that ZIP7 is responsible for much aggressive cancer cell growth and that ZIP7 is therefore an appropriate target for preventing cancer progression. However, to date ZIP7 has only been inhibited by use of CK2 inhibitors such as CX-4945⁶⁰². There is no tertiary structure available for ZIP7 and without this it is difficult to design effective small molecule inhibitors. However, some data has recently provided some structural information of how the ZIP transporters are positioned in the membrane which may help this aim.

7.13 Summary

In summary, by using phospho-kinase arrays has enabled the multiple kinases phosphorylated as a direct result of ZIP7 mediated zinc release from stores to be confirmed. Interestingly, many of these kinases are linked together in an integrated network of carcinogenesis-related pathways, involving MAPK, PI3K-AKT, and mTOR pathways. ZIP7 is a gatekeeper for zinc release from cellular stores which can phosphorylate many kinases that have a role in carcinogenesis. These results have highlighted the role of ZIP7 in cancer development and suggest that ZIP7 is an interesting target for future cancer treatment. In this work, for the first time, it has been discovered that ZIP7 is additionally located in the nuclear membrane and capable of increasing the activation of multiple kinases in the nucleus, which has a direct effect on cell growth and proliferation. To date, no ZIP transporter has been located in the nucleus, and there is much zinc in the nucleus which is required for DNA zinc fingers and transcription factor binding to the target gene, especially in cancer.

Until now, it has been assumed that MT is involved in regulating nuclear zinc. However, MT requires transcription to get activated which can take hours and days, which is not very useful for signalling effects that occur in seconds or minutes. This discovery now explains the full reach of zinc transporters such as ZIP7 to not only activate signalling within the cytoplasm but also in the nucleus to guarantee cell growth and proliferation. The unique nuclear localization of ZIP7 has raised the question of its role in transporting zinc into the nucleus and activating the pathways leading to cancer development. Proving the role of ZIP7 in nuclear zinc transport could have significant implications for future cancer therapy. The phospho-arrays and western blot data demonstrated that ZIP7 NLS mutants significantly affect ZIP7 downstream signalling pathways, especially NLS3, which has a double alanine mutation. The cells transfected with NLS3 mutants decrease the amount of ZIP7 in the nucleus, affecting the phosphorylation of nuclear kinases. The nuclear localization signals of ZIP7 are essential for ZIP7 maximal activation, and removing those signals seriously reduces the downstream signalling pathways of ZIP7. This study provides the first evidence that ZIP7 is located on the INM, and its nuclear localization affects the downstream effect of ZIP7-mediated zinc release. This data should now position ZIP7 at the forefront of targets for new anti-cancer drugs. Inhibiting ZIP7 should prevent the activation of a multitude of signalling pathways, all with known oncogenic ability,

and may provide a useful alternative in the clinic that could potentially avoid the development of resistance by inhibiting multiple pathways together.

8 References

1. Kambe T, Tsuji T, Hashimoto A, Itsumura N. The Physiological, Biochemical, and Molecular Roles of Zinc Transporters in Zinc Homeostasis and Metabolism. *Physiol Rev.* 2015;95(3):749-784. doi:10.1152/physrev.00035.2014
2. Maret W. Zinc and Sulfur: A Critical Biological Partnership. *Biochemistry.* 2004;43(12):3301-3309. doi:10.1021/bi036340p
3. Maverakis E, Fung MA, Lynch PJ, et al. Acrodermatitis enteropathica and an overview of zinc metabolism. *J Am Acad Dermatol.* 2007;56(1):116-124. doi:10.1016/j.jaad.2006.08.015
4. Haase H. Zinc Signals and Immune Function. *Mol Genet Nutr Asp Major Trace Miner.* 2016;261-271. doi:10.1016/B978-0-12-802168-2.00021-X
5. Scott BJ, Bradwell AR. Identification of the serum binding proteins for iron, zinc, cadmium, nickel, and calcium. *Clin Chem.* 1983;29(4):629-633. <http://www.ncbi.nlm.nih.gov/pubmed/6831689>.
6. Hambidge KM, Krebs NF. Zinc Deficiency: A Special Challenge. *J Nutr.* 2007;137(4):1101-1105. doi:137/4/1101 [pii]
7. Wastney ME, Aamodt RL, Rumble WF, Henkin RI. Kinetic analysis of zinc metabolism and its regulation in normal humans. *Am J Physiol.* 1986;251(2 Pt 2):R398-408.
8. Prasad AS, Halsted JA, Nadimi M. Syndrome of iron deficiency anemia, hepatosplenomegaly, hypogonadism, dwarfism and geophagia. *Am J Med.* 1961;31:532-546.
9. Vallee BL, Falchuk KH. *The Biochemical Basis of Zinc Physiology.* Vol 73.; 1993.
10. Andreini C, Bertini I. A bioinformatics view of zinc enzymes. *J Inorg Biochem.* 2012;111:150-156. doi:10.1016/j.jinorgbio.2011.11.020
11. Chasapis CT, Spiliopoulou CA, Loutsidou AC, Stefanidou ME. Zinc and human health: An update. *Arch Toxicol.* 2012;86(4):521-534. doi:10.1007/s00204-011-0775-1
12. Ibs K-H, Rink L. Zinc-altered immune function. *J Nutr.* 2003;133(5 Suppl 1):1452S-6S. <http://www.ncbi.nlm.nih.gov/pubmed/12730441>.
13. Penny ME. Zinc supplementation in public health. *Ann Nutr Metab.* 2013;62(SUPPL.1):31-42. doi:10.1159/000348263
14. Rink L, Gabriel P. Zinc and the immune system. *Proc Nutr Soc.* 2000;59(4):541-552. doi:10.1017/S0029665100000781
15. Wise A. Phytate and zinc bioavailability. *Int J Food Sci Nutr.* 1995;46(1):53-63. <http://www.ncbi.nlm.nih.gov/pubmed/7712343>.
16. Sandström B. Bioavailability of zinc. *Eur J Clin Nutr.* 1997;51 Suppl 1:S17-9. <http://www.ncbi.nlm.nih.gov/pubmed/9023474>.
17. Kambe T, Hashimoto A, Fujimoto S. Current understanding of ZIP and ZnT zinc transporters in human health and diseases. *Cell Mol Life Sci.* 2014;71(17):3281-3295. doi:10.1007/s00018-014-1617-0
18. KEILIN D, MANN T. Carbonic Anhydrase. *Nature.* 1939;144(3644):442-443. doi:10.1038/144442b0
19. Andreini C, Banci L, Bertini I, Rosato A. Counting the zinc-proteins encoded in the human genome. *J Proteome Res.* 2006;5(1):196-201. doi:10.1021/pr050361j
20. King JC. Zinc: an essential but elusive nutrient. *Am J Clin Nutr.* 2011;94(2):679S-684S. doi:10.3945/ajcn.110.005744
21. Laity JH, Lee BM, Wright PE. Zinc finger proteins: new insights into structural and

- functional diversity. *Curr Opin Struct Biol.* 2001;11(1):39-46.
<http://www.ncbi.nlm.nih.gov/pubmed/11179890>.
22. Laity JH, Andrews GK. Understanding the mechanisms of zinc-sensing by metal-response element binding transcription factor-1 (MTF-1). *Arch Biochem Biophys.* 2007;463(2):201-210. doi:10.1016/j.abb.2007.03.019
 23. Hogstrand C, Zheng D, Feeney G, Cunningham P, Kille P. Zinc-controlled gene expression by metal-regulatory transcription factor 1 (MTF1) in a model vertebrate, the zebrafish. *Biochem Soc Trans.* 2008;36(6):1252-1257. doi:10.1042/BST0361252
 24. Beyersmann D, Haase H. Functions of zinc in signaling, proliferation and differentiation of mammalian cells. *Biometals.* 14(3-4):331-341.
<http://www.ncbi.nlm.nih.gov/pubmed/11831463>.
 25. Yamasaki S, Sakata-Sogawa K, Hasegawa A, et al. Zinc is a novel intracellular second messenger. *J Cell Biol.* 2007;177(4):637-645. doi:10.1083/jcb.200702081
 26. Yamashita S, Miyagi C, Fukada T, Kagara N, Che Y-S, Hirano T. Zinc transporter LIV1 controls epithelial-mesenchymal transition in zebrafish gastrula organizer. *Nature.* 2004;429(6989):298-302. doi:10.1038/nature02545
 27. Murakami M, Hirano T. Intracellular zinc homeostasis and zinc signaling. *Cancer Sci.* 2008;99(8):1515-1522. doi:10.1111/j.1349-7006.2008.00854.x
 28. Bell SG, Vallee BL. The Metallothionein/thionein system: An oxidoreductive metabolic zinc link. *ChemBioChem.* 2009;10(1):55-62. doi:10.1002/cbic.200800511
 29. Kim Y-H, Koh J-Y. The role of NADPH oxidase and neuronal nitric oxide synthase in zinc-induced poly(ADP-ribose) polymerase activation and cell death in cortical culture. *Exp Neurol.* 2002;177(2):407-418.
<http://www.ncbi.nlm.nih.gov/pubmed/12429187>.
 30. Colvin RA, Fontaine CP, Laskowski M, Thomas D. Zn²⁺ transporters and Zn²⁺ homeostasis in neurons. *Eur J Pharmacol.* 2003;479(1-3):171-185.
doi:10.1016/j.ejphar.2003.08.067
 31. Frederickson CJ, Koh J-Y, Bush AI. The neurobiology of zinc in health and disease. *Nat Rev Neurosci.* 2005;6(6):449-462. doi:10.1038/nrn1671
 32. Garai K, Sengupta P, Sahoo B, Maiti S. Selective destabilization of soluble amyloid beta oligomers by divalent metal ions. *Biochem Biophys Res Commun.* 2006;345(1):210-215. doi:10.1016/j.bbrc.2006.04.056
 33. Fukada T, Kambe T. Molecular and genetic features of zinc transporters in physiology and pathogenesis. *Metallomics.* 2011;3(7):662. doi:10.1039/c1mt00011j
 34. Chesters JK, Petrie L. A possible role for cyclins in the zinc requirements during G1 and G2 phases of the cell cycle. *J Nutr Biochem.* 1999;10(5):279-290.
<http://www.ncbi.nlm.nih.gov/pubmed/15539301>.
 35. Li Y, Maret W. Transient fluctuations of intracellular zinc ions in cell proliferation. *Exp Cell Res.* 2009;315(14):2463-2470. doi:10.1016/j.yexcr.2009.05.016
 36. Fraker PJ. Recent Advances in Nutritional Sciences Roles for Cell Death in Zinc. *Apoptosis.* 2004:359-362.
 37. Shankar AH, Prasad AS. Zinc and immune function: the biological basis of altered resistance to infection. *Am J Clin Nutr.* 1998;68(2 Suppl):447S-463S.
<http://www.ncbi.nlm.nih.gov/pubmed/9701160>.
 38. Hambidge M. Human zinc deficiency. *J Nutr.* 2000;130(5S Suppl):1344S-9S.
doi:10.1093/jn/130.5.1344S
 39. Song Y, Leonard SW, Traber MG, Ho E. Zinc Deficiency Affects DNA Damage , Oxidative Stress , Antioxidant Defenses , and DNA Repair. *J Nutr.* 2009;139:1626-1631. doi:10.3945/jn.109.106369.human
 40. Dufner-Beattie J, Weaver BP, Geiser J, et al. The mouse acrodermatitis enteropathica

- gene Slc39a4 (Zip4) is essential for early development and heterozygosity causes hypersensitivity to zinc deficiency. *Hum Mol Genet.* 2007;16(12):1391-1399. doi:10.1093/hmg/ddm088
41. Koh JY, Suh SW, Gwag BJ, He YY, Hsu CY, Choi DW. The role of zinc in selective neuronal death after transient global cerebral ischemia. *Science.* 1996;272(5264):1013-1016. <http://www.ncbi.nlm.nih.gov/pubmed/8638123>.
 42. Truong-Tran AQ, Carter J, Ruffin RE, Zalewski PD. The role of zinc in caspase activation and apoptotic cell death. *Biometals.* 14(3-4):315-330. <http://www.ncbi.nlm.nih.gov/pubmed/11831462>.
 43. Temple VJ, Masta A. Zinc in human health. *P N G Med J.* 2014;47(3-4):146-158. doi:10.1002/(SICI)1520-670X(1998)11:2/3<63::AID-JTRA2>3.0.CO;2-5
 44. Taylor KM, Nicholson RI. The LZT proteins; The LIV-1 subfamily of zinc transporters. *Biochim Biophys Acta - Biomembr.* 2003;1611(1-2):16-30. doi:10.1016/S0005-2736(03)00048-8
 45. Gaither LA, Eide DJ. Eukaryotic zinc transporters and their regulation. *Biometals.* 2016;14(3-4):251-270. doi:10.1023/A
 46. Eide D, Broderius M, Fett J, Guerinot ML. A novel iron-regulated metal transporter from plants identified by functional expression in yeast. *Proc Natl Acad Sci.* 1996;93(11):5624-5628. doi:10.1073/pnas.93.11.5624
 47. Rogers EE, Eide DJ, Guerinot M Lou. Altered selectivity in an Arabidopsis metal transporter. 2000.
 48. Lasswell J, Rogg LE, Nelson DC, Rongey C, Bartel B. Cloning and characterization of IAR1, a gene required for auxin conjugate sensitivity in *Arabidopsis*. *Plant Cell.* 2000;12(12):2395-2408. doi:10.1105/tpc.12.12.2395
 49. Lichten LA, Cousins RJ. Mammalian Zinc Transporters: Nutritional and Physiologic Regulation. *Annu Rev Nutr.* 2009;29(1):153-176. doi:10.1146/annurev-nutr-033009-083312
 50. Cousins RJ, Liuzzi JP, Lichten LA. Mammalian zinc transport, trafficking, and signals. *J Biol Chem.* 2006;281(34):24085-24089. doi:10.1074/jbc.R600011200
 51. Takagishi T, Hara T, Fukada T. Recent Advances in the Role of SLC39A/ZIP Zinc Transporters In Vivo. *Int J Mol Sci.* 2017;18(12):2708. doi:10.3390/ijms18122708
 52. Maret W. Oxidative metal release from metallothionein via zinc-thiol/disulfide interchange. *Proc Natl Acad Sci.* 1994;91(1):237-241. doi:10.1073/pnas.91.1.237
 53. Jiang L-J, Maret W, Vallee BL. The ATP–metallothionein complex. *Proc Natl Acad Sci.* 1998;95(16):9146-9149. doi:10.1073/pnas.95.16.9146
 54. Lu M, Fu D. Structure of the Zinc Transporter YiiP. *Science (80-).* 2007;317(5845):1746-1748. doi:10.1126/science.1143748
 55. Palmiter RD, Findley SD. Cloning and functional characterization of a mammalian zinc transporter that confers resistance to zinc. *EMBO J.* 1995;14(4):639-649. <http://www.ncbi.nlm.nih.gov/pubmed/7882967>.
 56. Ohana E, Hoch E, Keasar C, et al. Identification of the Zn²⁺ binding site and mode of operation of a mammalian Zn²⁺ transporter. *J Biol Chem.* 2009;284(26):17677-17686. doi:10.1074/jbc.M109.007203
 57. Taylor KM, Morgan HE, Smart K, et al. The Emerging Role of the LIV-1 Subfamily of Zinc Transporters in Breast Cancer. *Mol Med.* 2007;13(7-8):396-406. doi:10.2119/2007
 58. Taylor KM, Morgan HE, Johnson A, Nicholson RI. Structure-function analysis of HKE4, a member of the new LIV-1 subfamily of zinc transporters. *Biochem J.* 2004;377(Pt 1):131-139. doi:10.1042/BJ20031183
 59. Guerinot ML. The ZIP family of metal transporters. *Biochim Biophys Acta.*

- 2000;1465(1-2):190-198. doi:[https://doi.org/10.1016/S0005-2736\(00\)00138-3](https://doi.org/10.1016/S0005-2736(00)00138-3)
60. Gaither LA, Eide DJ. The Human ZIP1 Transporter Mediates Zinc Uptake in Human K562 Erythroleukemia Cells. *J Biol Chem.* 2001;276(25):22258-22264. doi:10.1074/jbc.M101772200
 61. Hooper NM. Families of zinc metalloproteases. *FEBS Lett.* 1994;354(1):1-6. doi:10.1016/0014-5793(94)01079-X
 62. Dardel F, Ragusa S, Lazennec C, Blanquet S, Meinnel T. Solution structure of nickel-peptide deformylase 1 Edited by A. R. Fersht. *J Mol Biol.* 1998;280(3):501-513. doi:10.1006/jmbi.1998.1882
 63. Hogstrand C, Kille P, Nicholson RI, Taylor KM. Zinc transporters and cancer: a potential role for ZIP7 as a hub for tyrosine kinase activation. *Trends Mol Med.* 2009;15(3):101-111. doi:10.1016/j.molmed.2009.01.004
 64. Wang K, Zhou B, Kuo Y-M, Zemansky J, Gitschier J. A novel member of a zinc transporter family is defective in acrodermatitis enteropathica. *Am J Hum Genet.* 2002;71(1):66-73. doi:10.1086/341125
 65. Ehsani S, Salehzadeh A, Huo H, et al. LIV-1 ZIP Ectodomain Shedding in Prion-Infected Mice Resembles Cellular Response to Transition Metal Starvation. *J Mol Biol.* 2012;422(4):556-574. doi:10.1016/j.jmb.2012.06.003
 66. Krężel A, Maret W. Zinc-buffering capacity of a eukaryotic cell at physiological pZn. *J Biol Inorg Chem.* 2006;11(8):1049-1062. doi:10.1007/s00775-006-0150-5
 67. Colvin RA, Holmes WR, Fontaine CP, Maret W. Cytosolic zinc buffering and muffling: Their role in intracellular zinc homeostasis. *Metallomics.* 2010;2(5):306. doi:10.1039/b926662c
 68. Colvin RA, Bush AI, Volitakis I, et al. Insights into Zn²⁺ homeostasis in neurons from experimental and modeling studies. *Am J Physiol Cell Physiol.* 2008;45701(294):726-742. doi:10.1152/ajpcell.00541.2007.
 69. Taylor KM, Vichova P, Jordan N, Hiscox S, Hendley R, Nicholson RI. ZIP7-mediated intracellular zinc transport contributes to aberrant growth factor signaling in antihormone-resistant breast cancer cells. *Endocrinology.* 2008;149(10):4912-4920. doi:10.1210/en.2008-0351
 70. Plum LM, Rink L, Hajo H. The essential toxin: Impact of zinc on human health. *Int J Environ Res Public Health.* 2010;7(4):1342-1365. doi:10.3390/ijerph7041342
 71. Chimienti F, Aouffen M, Favier A, Seve M. Zinc homeostasis-regulating proteins: new drug targets for triggering cell fate. *Curr Drug Targets.* 2003;4(4):323-338. doi:10.2174/1389450033491082
 72. Tapiero H, Tew KD. Trace elements in human physiology and pathology: Zinc and metallothioneins. *Biomed Pharmacother.* 2003;57(9):399-411. doi:10.1016/S0753-3322(03)00081-7
 73. Bin BH, Bhin J, Seo J, et al. Requirement of Zinc Transporter SLC39A7/ZIP7 for Dermal Development to Fine-Tune Endoplasmic Reticulum Function by Regulating Protein Disulfide Isomerase. *J Invest Dermatol.* 2017;137(8):1682-1691. doi:10.1016/j.jid.2017.03.031
 74. Nimmanon T, Ziliotto S, Morris S, Flanagan L, Taylor KM. Phosphorylation of zinc channel ZIP7 drives MAPK, PI3K and mTOR growth and proliferation signalling. *Metallomics.* 2017;9:471-481. doi:10.1039/C6MT00286B
 75. Taylor KM, Kille P, Hogstrand C. Protein kinase CK2 opens the gate for zinc signaling. In: ; 2012:1863-1864. doi:10.4161/cc.20414
 76. Motiwala T, Jacob ST. Role of protein tyrosine phosphatases in cancer. *Prog Nucleic Acid Res Mol Biol.* 2006;81:297-329. doi:10.1016/S0079-6603(06)81008-1
 77. Yde CW, Frogne T, Lykkesfeldt AE, Fichtner I, Issinger OG, Stenvang J. Induction of

- cell death in antiestrogen resistant human breast cancer cells by the protein kinase CK2 inhibitor DMAT. *Cancer Lett.* 2007;256(2):229-237. doi:10.1016/j.canlet.2007.06.010
78. Martins LR, Lúcio P, Melão A, et al. Activity of the clinical-stage CK2-specific inhibitor CX-4945 against chronic lymphocytic leukemia. *Leukemia.* 2014;28(1):179-182. doi:10.1038/leu.2013.232
 79. Zhang X, Yang X, Yang C, et al. Targeting protein kinase CK2 suppresses bladder cancer cell survival via the glucose metabolic pathway. *Oncotarget.* 2016;7(52):87361-87372. doi:10.18632/oncotarget.13571
 80. Ferrer-Font L, Villamañán L, Arias-Ramos N, et al. Targeting protein kinase CK2: Evaluating CX-4945 potential for GL261 glioblastoma therapy in immunocompetent mice. *Pharmaceuticals.* 2017;10(1):1-18. doi:10.3390/ph10010024
 81. Zheng Y, McFarland BC, Drygin D, et al. Targeting protein kinase CK2 suppresses prosurvival signaling pathways and growth of glioblastoma. *Clin Cancer Res.* 2013;19(23):6484-6494. doi:10.1158/1078-0432.CCR-13-0265
 82. Güttinger S, Laurell E, Kutay U. Orchestrating nuclear envelope disassembly and reassembly during mitosis. *Nat Rev Mol Cell Biol.* 2009;10(3):178-191. doi:10.1038/nrm2641
 83. Smoyer CJ, Katta SS, Gardner JM, et al. Analysis of membrane proteins localizing to the inner nuclear envelope in living cells. 2016:1-16.
 84. Katta SS, Smoyer CJ, Jaspersen SL. Destination: Inner nuclear membrane. *Trends Cell Biol.* 2014;24(4):221-229. doi:10.1016/j.tcb.2013.10.006
 85. Burke B, Ellenberg J. Remodelling the walls of the nucleus. *Nat Rev Mol Cell Biol.* 2002;3(7):487-497. doi:10.1038/nrm860
 86. Burke B, Stewart CL. The nuclear lamins: Flexibility in function. *Nat Rev Mol Cell Biol.* 2013;14(1):13-24. doi:10.1038/nrm3488
 87. Schirmer EC. Nuclear Membrane Proteins with Potential Disease Links Found by Subtractive Proteomics. *Science (80-).* 2007;318(5913):10-13. doi:10.1126/science.1088176
 88. Aebi U, Cohn J, Buhle L, Gerace L. The nuclear lamina is a meshwork of intermediate-type filaments. *Nature.* 1986;323(6088):560-564. doi:10.1038/323560a0
 89. Schwarz DS, Blower MD. The endoplasmic reticulum: Structure, function and response to cellular signaling. *Cell Mol Life Sci.* 2016;73(1):79-94.
 90. Gomez-Cavazos JS, Hetzer MW. Outfits for different occasions: tissue-specific roles of Nuclear Envelope proteins. *Curr Opin Cell Biol.* 2012;24(6):775-783. doi:10.1016/j.ceb.2012.08.008
 91. Suntharalingam M, Wentz SR, South A. Peering through the Pore : Nuclear Pore Complex Structure , Assembly , and Function. 2003;4:775-789.
 92. Kabachinski G, Schwartz TU. The nuclear pore complex - structure and function at a glance. *J Cell Sci.* 2015;128(3):423-429. doi:10.1242/jcs.083246
 93. Stewart C, Roux K, Burke B. Blurring the boundary: the nuclear envelope extends its reach. *Science (80-).* 2007;318(5848):1408-1412.
 94. Tran EJ, Wentz SR. Dynamic Nuclear Pore Complexes: Life on the Edge. *Cell.* 2006;125(6):1041-1053. doi:10.1016/j.cell.2006.05.027
 95. Beck M, Lüß V, Förster F, Baumeister W, Medalia O. Snapshots of nuclear pore complexes in action captured by cryo-electron tomography. *Nature.* 2007;449(7162):611-615. doi:10.1038/nature06170
 96. Bui KH, Von Appen A, Diguilio AL, et al. Integrated structural analysis of the human nuclear pore complex scaffold. *Cell.* 2013;155(6):1233-1243. doi:10.1016/j.cell.2013.10.055
 97. Terry LJ, Wentz SR. Flexible gates: Dynamic topologies and functions for FG

- nucleoporins in nucleocytoplasmic transport. *Eukaryot Cell*. 2009;8(12):1814-1827. doi:10.1128/EC.00225-09
98. Weis K. Regulating Access to the Genome : Nucleocytoplasmic Transport throughout the Cell Cycle Macromolecular transport between the cytoplasm and. *Cell*. 2003;112(4):441-451. doi:10.1016/S0092-8674(03)00082-5
 99. Moroianu J, Blobel G, Radu A. Previously identified protein of uncertain function is karyopherin alpha and together with karyopherin beta docks import substrate at nuclear pore complexes. *Proc Natl Acad Sci U S A*. 1995;92(6):2008-2011. doi:10.1073/pnas.92.5.1769
 100. Laba JK, Steen A, Veenhoff LM. Traffic to the inner membrane of the nuclear envelope. *Curr Opin Cell Biol*. 2014;28(1):36-45. doi:10.1016/j.ceb.2014.01.006
 101. Ye Q, Worman HJ. Primary structure analysis and lamin B and DNA binding of human LBR, an integral protein of the nuclear envelope inner membrane. *J Biol Chem*. 1994;269(15):11306-11311. <http://www.ncbi.nlm.nih.gov/pubmed/8157662>.
 102. Worman HJ, Yuan J, Blobel G, Georgatos SD. A lamin B receptor in the nuclear envelope. *Proc Natl Acad Sci U S A*. 1988;85(22):8531-8534. <http://www.ncbi.nlm.nih.gov/pubmed/2847165>.
 103. Simos G, Georgatos SD. The inner nuclear membrane protein p58 associates in vivo with a p58 kinase and the nuclear lamins. *EMBO J*. 1992;11(11):4027-4036. <http://www.ncbi.nlm.nih.gov/pubmed/1327755>.
 104. Jans DA, Xiao CY, Lam MHC. Nuclear targeting signal recognition: A key control point in nuclear transport? *BioEssays*. 2000;22(6):532-544. doi:10.1002/(SICI)1521-1878(200006)22:6<532::AID-BIES6>3.0.CO;2-O
 105. Fried H, Kutay U. Nucleocytoplasmic transport: Taking an inventory. *Cell Mol Life Sci*. 2003;60(8):1659-1688. doi:10.1007/s00018-003-3070-3
 106. Kalderon D, Richardson WD, Markham AF, Smith AE. Sequence requirements for nuclear location of simian virus 40 large-T antigen. *Nature*. 311(5981):33-38. <http://www.ncbi.nlm.nih.gov/pubmed/6088992>.
 107. Lanford RE, Butel JS. Construction and characterization of an SV40 mutant defective innuclear transport of T-antigen. *Cell*. 1984;37(July 1964):801-813.
 108. Kalderon D, Richardson WD, Markham AF, Smith AE. Sequence requirements for nuclear location of simian virus 40 large-T antigen. *Nature*. 1984;311(5981):33-38. <http://www.ncbi.nlm.nih.gov/pubmed/6088992>.
 109. Jans DA, Hubner S. Regulation of protein transport to the nucleus: central role of phosphorylation. *Physiol Rev*. 1996;76(3):651-685. http://www.ncbi.nlm.nih.gov/entrez/query.fcgi?cmd=Retrieve&db=PubMed&dopt=Citation&list_uids=8757785.
 110. Davey J, Dimmock NJ, Colman A. Identification of the sequence responsible for the nuclear accumulation of the influenza virus nucleoprotein in *Xenopus* oocytes. *Cell*. 1985;40(3):667-675. doi:10.1016/0092-8674(85)90215-6
 111. Dingwall C, Sharnick S V., Laskey RA. A polypeptide domain that specifies migration of nucleoplamin into the nucleus. *Cell*. 1982;30(2):449-458. doi:10.1016/0092-8674(82)90242-2
 112. Laskey RA, Honda BM, Mills AD, Finch JT. Nucleosomes are assembled by an acidic protein which binds histones and transfers them to DNA. *Nature*. 1978;275(5679):416-420. doi:10.1038/275416a0
 113. Hsu S-C, Hung M-C. Characterization of a novel tripartite nuclear localization sequence in the EGFR family. *J Biol Chem*. 2007;282(14):10432-10440. doi:10.1074/jbc.M610014200
 114. Haase H, Maret W. Intracellular zinc fluctuations modulate protein tyrosine

- phosphatase activity in insulin/insulin-like growth factor-1 signaling. *Exp Cell Res.* 2003;291(2):289-298. doi:10.1016/S0014-4827(03)00406-3
115. Wu W, Graves LM, Jaspers I, Devlin RB, Reed W, Samet JM. Activation of the EGF receptor signaling pathway in human airway epithelial cells exposed to metals. *Am J Physiol.* 1999;277(5):L924-31. doi:10.1152/ajplung.1999.277.5.L924
 116. Nagase H, Woessner JF. Matrix metalloproteinases. *J Biol Chem.* 1999;274(31):21491-21494. doi:10.1074/jbc.274.31.21491
 117. Bray F, Ferlay J, Soerjomataram I, Siegel RL, Torre LA, Jemal A. Global cancer statistics 2018: GLOBOCAN estimates of incidence and mortality worldwide for 36 cancers in 185 countries. *CA Cancer J Clin.* 2018;68(6):394-424. doi:10.3322/caac.21492
 118. Anastasiadi Z, Lianos GD, Ignatiadou E, Harissis H V., Mitsis M. Breast cancer in young women: an overview. *Updates Surg.* 2017;69(3):313-317. doi:10.1007/s13304-017-0424-1
 119. Perou CM, Sørlie T, Eisen MB, et al. Molecular portraits of human breast tumours. *Nature.* 2000;406(6797):747-752. doi:10.1038/35021093
 120. Colomer R, Aranda-López I, Albanell J, et al. Biomarkers in breast cancer: A consensus statement by the Spanish Society of Medical Oncology and the Spanish Society of Pathology. *Clin Transl Oncol.* 2018;20(7):815-826. doi:10.1007/s12094-017-1800-5
 121. Maughan KL, Lutterbie MA, Ham PS. Treatment of breast cancer. *Am Fam Physician.* 2010;81(11):1339-1346. <http://www.ncbi.nlm.nih.gov/pubmed/20521754>.
 122. Yeh W-L, Shioda K, Coser KR, Rivizzigno D, McSweeney KR, Shioda T. Fulvestrant-induced cell death and proteasomal degradation of estrogen receptor α protein in MCF-7 cells require the CSK c-Src tyrosine kinase. *PLoS One.* 2013;8(4):e60889. doi:10.1371/journal.pone.0060889
 123. Manni A, Arafah B, Pearson OH. Estrogen and progesterone receptors in the prediction of response of breast cancer to endocrine therapy. *Cancer.* 1980;46(12 Suppl):2838-2841. doi:10.1002/1097-0142(19801215)46:12+<2838::aid-cncr2820461421>3.0.co;2-a
 124. Travis RC, Key TJ. Oestrogen exposure and breast cancer risk. *Breast Cancer Res.* 2003;5(5):239. doi:10.1186/bcr628
 125. Frasor J, Danes JM, Komm B, Chang KCN, Lyttle CR, Katzenellenbogen BS. Profiling of estrogen up- and down-regulated gene expression in human breast cancer cells: insights into gene networks and pathways underlying estrogenic control of proliferation and cell phenotype. *Endocrinology.* 2003;144(10):4562-4574. doi:10.1210/en.2003-0567
 126. Butt AJ, Sutherland RL, Musgrove EA. Live or let die: oestrogen regulation of survival signalling in endocrine response. *Breast Cancer Res.* 2007;9(5):306. doi:10.1186/bcr1779
 127. Doisneau-Sixou SF, Sergio CM, Carroll JS, Hui R, Musgrove EA, Sutherland RL. Estrogen and antiestrogen regulation of cell cycle progression in breast cancer cells. *Endocr Relat Cancer.* 2003;10(2):179-186. doi:10.1677/erc.0.0100179
 128. Rozeboom B, Dey N, De P. ER+ metastatic breast cancer: past, present, and a prescription for an apoptosis-targeted future. *Am J Cancer Res.* 2019;9(12):2821-2831. <http://www.ncbi.nlm.nih.gov/pubmed/31911865>.
 129. Fabian CJ. The what, why and how of aromatase inhibitors: hormonal agents for treatment and prevention of breast cancer. *Int J Clin Pract.* 2007;61(12):2051-2063. doi:10.1111/j.1742-1241.2007.01587.x
 130. Osborne CK, Wakeling A, Nicholson RI. Fulvestrant: an oestrogen receptor antagonist

- with a novel mechanism of action. *Br J Cancer*. 2004;90(S1):S2-S6.
doi:10.1038/sj.bjc.6601629
131. Wakeling AE, Bowler J. Steroidal pure antioestrogens. *J Endocrinol*. 1987;112(3):R7-10. doi:10.1677/joe.0.112r007
 132. Slamon DJ, Clark GM, Wong SG, Levin WJ, Ullrich A, McGuire WL. Human breast cancer: correlation of relapse and survival with amplification of the HER-2/neu oncogene. *Science*. 1987;235(4785):177-182. doi:10.1126/science.3798106
 133. Clarke R, Liu MC, Bouker KB, et al. Antiestrogen resistance in breast cancer and the role of estrogen receptor signaling. *Oncogene*. 2003;22(47):7316-7339. doi:10.1038/sj.onc.1206937
 134. Knowlden JM, Hutcheson IR, Jones HE, et al. Elevated levels of epidermal growth factor receptor/c-erbB2 heterodimers mediate an autocrine growth regulatory pathway in tamoxifen-resistant MCF-7 cells. *Endocrinology*. 2003;144(3):1032-1044. doi:10.1210/en.2002-220620
 135. McClelland RA, Barrow D, Madden T-A, et al. Enhanced Epidermal Growth Factor Receptor Signaling in MCF7 Breast Cancer Cells after Long-Term Culture in the Presence of the Pure Antiestrogen ICI 182,780 (Faslodex)*. *Endocrinology*. 2001;142(7):2776-2788. doi:10.1210/endo.142.7.8259
 136. Knowlden JM, Hutcheson IR, Barrow D, Gee JMW, Nicholson RI. Insulin-like growth factor-I receptor signaling in tamoxifen-resistant breast cancer: A supporting role to the epidermal growth factor receptor. *Endocrinology*. 2005;146(11):4609-4618. doi:10.1210/en.2005-0247
 137. Farquharson MJ, Al-Ebraheem A, Geraki K, Leek R, Jubb A, Harris AL. Zinc presence in invasive ductal carcinoma of the breast and its correlation with oestrogen receptor status. *Phys Med Biol*. 2009;54(13):4213-4223. doi:10.1088/0031-9155/54/13/016
 138. Riesop D, Hirner A V., Rusch P, Bankfalvi A. Zinc distribution within breast cancer tissue: A possible marker for histological grading? *J Cancer Res Clin Oncol*. 2015;141(7):1321-1331. doi:10.1007/s00432-015-1932-3
 139. John E, Laskow TC, Buchser WJ, et al. Zinc in innate and adaptive tumor immunity. *J Transl Med*. 2010;8(1):118. doi:10.1186/1479-5876-8-118
 140. Cui Y, Vogt S, Olson N, Glass AG, Rohan TE. Levels of Zinc, Selenium, Calcium, and Iron in Benign Breast Tissue and Risk of Subsequent Breast Cancer. *Cancer Epidemiol Biomarkers & Prev*. 2007;16(8):1682-1685. doi:10.1158/1055-9965.EPI-07-0187
 141. Santoliquido PM, Southwick HW, Olwin JH. Trace metal levels in cancer of the breast. *Surg Gynecol Obstet*. 1976;142(1):65-70. <http://www.ncbi.nlm.nih.gov/pubmed/1244691>.
 142. Margalioth EJ, Schenker JG, Chevion M. Copper and Zinc levels in normal and malignant tissues. *Cancer*. 1983;52(5):868-872. doi:10.1002/1097-0142(19830901)52:5<868::AID-CNCR2820520521>3.0.CO;2-K
 143. R. LEE, W.WOO, B.WU, A.KUMMER, H.DUMINY AZX. Zinc Accumulation in N - Methyl- N -Nitrosourea-Induced Rat Mammary Tumors Is Accompanied by an Altered Expression of ZnT-1 and Metallothionein. :689-696. doi:228:689–696, 2003
 144. Jouybari L, Kiani F, Akbari A, et al. A meta-analysis of zinc levels in breast cancer. *J Trace Elem Med Biol*. 2019;56:90-99. doi:10.1016/j.jtemb.2019.06.017
 145. Gumulec J, Masarik M, Adam V, Eckschlager T, Provaznik I, Kizek R. Serum and tissue zinc in epithelial malignancies: a meta-analysis. *PLoS One*. 2014;9(6):e99790. doi:10.1371/journal.pone.0099790
 146. Gupta SK, Shukla VK, Vaidya MP, Roy SK, Gupta S. Serum trace elements and

- Cu/Zn ratio in breast cancer patients. *J Surg Oncol*. 1991;46(3):178-181. doi:10.1002/jso.2930460311
147. Memon A-R, Kazi TG, Afridi HI, et al. Evaluation of zinc status in whole blood and scalp hair of female cancer patients. *Clin Chim Acta*. 2007;379(1-2):66-70. doi:10.1016/j.cca.2006.12.009
 148. Cavallo F, Gerber M, Marubini E, et al. Zinc and copper in breast cancer. A joint study in northern Italy and southern France. *Cancer*. 1991;67(3):738-745. doi:10.1002/1097-0142(19910201)67:3<738::aid-cnrcr2820670335>3.0.co;2-#
 149. Piccinini L, Borella P, Bargellini A, Medici CI, Zoboli A. A case-control study on selenium, zinc, and copper in plasma and hair of subjects affected by breast and lung cancer. *Biol Trace Elem Res*. 1996;51(1):23-30. doi:10.1007/BF02790144
 150. Wu X, Tang J, Xie M. Serum and hair zinc levels in breast cancer: a meta-analysis. *Sci Rep*. 2015;5(1):12249. doi:10.1038/srep12249
 151. Woo W, Xu Z. Body zinc distribution profile during N-methyl-N-nitrosourea-induced mammary tumorigenesis in rats at various levels of dietary zinc intake. *Biol Trace Elem Res*. 2002;87(1-3):157-169. doi:10.1385/BTER:87:1-3:157
 152. Lee R, Woo W, Wu B, Kummer A, Duminy H, Xu Z. Zinc accumulation in N-methyl-N-nitrosourea-induced rat mammary tumors is accompanied by an altered expression of ZnT-1 and metallothionein. *Exp Biol Med (Maywood)*. 2003;228(6):689-696. <http://www.ncbi.nlm.nih.gov/pubmed/12773700>.
 153. Lu J, Stewart AJ, Sadler PJ, Pinheiro TJJ, Blindauer CA. Albumin as a zinc carrier: properties of its high-affinity zinc-binding site. *Biochem Soc Trans*. 2008;36(6):1317-1321. doi:10.1042/BST0361317
 154. Albrecht AL, Somji S, Sens MA, Sens DA, Garrett SH. Zinc transporter mRNA expression in the RWPE-1 human prostate epithelial cell line. *Biometals*. 2008;21(4):405-416. doi:10.1007/s10534-007-9129-0
 155. Desouki MM, Geradts J, Milon B, Franklin RB, Costello LC. hZip2 and hZip3 zinc transporters are down regulated in human prostate adenocarcinomatous glands. *Mol Cancer*. 2007;6:1-7. doi:10.1186/1476-4598-6-37
 156. Costello LC, Franklin RB. Novel role of zinc in the regulation of prostate citrate metabolism and its implications in prostate cancer. *Prostate*. 1998;35(4):285-296. <http://www.ncbi.nlm.nih.gov/pubmed/9609552>.
 157. Manning DL, McClelland RA, Knowlden JM, et al. Differential Expression of Oestrogen Regulated Genes in Breast Cancer. *Acta Oncol (Madr)*. 1995;34(5):641-646. doi:10.3109/02841869509094041
 158. Taylor KM, Morgan HE, Johnson A, Hadley LJ, Nicholson RI. Structure–function analysis of LIV-1, the breast cancer-associated protein that belongs to a new subfamily of zinc transporters. *Biochem J*. 2003;375(1):51-59. doi:10.1042/bj20030478
 159. Kagara N, Tanaka N, Noguchi S, Hirano T. Zinc and its transporter ZIP10 are involved in invasive behavior of breast cancer cells. *Cancer Sci*. 2007;98(5):692-697. doi:10.1111/j.1349-7006.2007.00446.x
 160. Li M, Zhang Y, Liu Z, et al. Aberrant expression of zinc transporter ZIP4 (SLC39A4) significantly contributes to human pancreatic cancer pathogenesis and progression. *Proc Natl Acad Sci U S A*. 2007;104(47):18636-18641. doi:10.1073/pnas.0709307104
 161. Zhang Y, Bharadwaj U, Logsdon CD, Chen C, Yao Q, Li M. ZIP4 regulates pancreatic cancer cell growth by activating IL-6/STAT3 pathway through zinc finger transcription factor CREB. *Clin Cancer Res*. 2010;16(5):1423-1430. doi:10.1158/1078-0432.CCR-09-2405
 162. Weaver BP, Zhang Y, Hiscox S, et al. Zip4 (Slc39a4) Expression is Activated in Hepatocellular Carcinomas and Functions to Repress Apoptosis, Enhance Cell Cycle

- and Increase Migration. Guan X, ed. *PLoS One*. 2010;5(10):e13158. doi:10.1371/journal.pone.0013158
163. Franklin RB, Levy BA, Zou J, et al. ZIP14 zinc transporter downregulation and zinc depletion in the development and progression of hepatocellular cancer. *J Gastrointest Cancer*. 2012;43(2):249-257. doi:10.1007/s12029-011-9269-x
 164. Sveen A, Bakken AC, Ågesen TH, et al. The exon-level biomarker SLC39A14 has organ-confined cancer-specificity in colorectal cancer. *Int J Cancer*. 2012;131(6):1479-1485. doi:10.1002/ijc.27399
 165. Miura K, Fujibuchi W, Unno M. Splice isoforms as therapeutic targets for colorectal cancer. *Carcinogenesis*. 2012;33(12):2311-2319. doi:10.1093/carcin/bgs347
 166. Sheng N, Yan L, You W, et al. Knockdown of SLC39A7 inhibits cell growth and induces apoptosis in human colorectal cancer cells. *Acta Biochim Biophys Sin (Shanghai)*. 2017;49(10):926-934. doi:10.1093/abbs/gmx094
 167. Ziliotto S, Gee JMW, Ellis IO, et al. Activated zinc transporter ZIP7 as an indicator of anti-hormone resistance in breast cancer. *Metallomics*. 2019;11(9):1579-1592. doi:10.1039/C9MT00136K
 168. Pan Z, Choi S, Ouadid-Ahidouch H, Yang J-M, Beattie JH, Korichneva I. Zinc transporters and dysregulated channels in cancers. *Front Biosci (Landmark Ed)*. 2017;22:623-643. <http://www.ncbi.nlm.nih.gov/pubmed/27814637> <http://www.pubmedcentral.nih.gov/articlerender.fcgi?artid=PMC5199720>.
 169. Taylor KM, Hiscox S, Nicholson RI, Hogstrand C, Kille P. Protein Kinase CK2 Triggers Cytosolic Zinc Signaling Pathways by Phosphorylation of Zinc Channel ZIP7. *Sci Signal*. 2012;5(210):ra11-ra11. doi:10.1126/scisignal.2002585
 170. Risbridger GP, Davis ID, Birrell SN, Tilley WD. Breast and prostate cancer: more similar than different. *Nat Rev Cancer*. 2010;10(3):205-212. doi:10.1038/nrc2795
 171. Mayor S. Screening for early breast cancer reduces invasive cancer, study finds. *BMJ*. December 2015:h6576. doi:10.1136/bmj.h6576
 172. Hamann M, Grill S, Struck J, et al. Detection of early breast cancer beyond mammographic screening: a promising biomarker panel. *Biomark Med*. 2019;13(13):1107-1117. doi:10.2217/bmm-2019-0085
 173. Arnedos M, Roulleaux Dugage M, Perez-Garcia J, Cortes J. Window of Opportunity trials for biomarker discovery in breast cancer. *Curr Opin Oncol*. 2019;31(6):486-492. doi:10.1097/CCO.0000000000000583
 174. Cserző M, Wallin E, Simon I, von Heijne G, Elofsson A. Prediction of transmembrane alpha-helices in prokaryotic membrane proteins: the dense alignment surface method. *Protein Eng*. 1997;10(6):673-676. <http://www.ncbi.nlm.nih.gov/pubmed/9278280>.
 175. Dobson L, Reményi I, Tusnády GE. CCTOP: a Consensus Constrained TOPology prediction web server. *Nucleic Acids Res*. 2015;43(W1):W408-W412. doi:10.1093/nar/gkv451
 176. Sprenger J, Lynn Fink J, Karunaratne S, Hanson K, Hamilton NA, Teasdale RD. LOCATE: a mammalian protein subcellular localization database. *Nucleic Acids Res*. 2007;36(Database):D230-D233. doi:10.1093/nar/gkm950
 177. Bernhofer M, Dallago C, Karl T, et al. PredictProtein - Predicting Protein Structure and Function for 29 Years. *Nucleic Acids Res*. 2021;49(W1):W535-W540. doi:10.1093/nar/gkab354
 178. Geourjon C, Deléage G. SOPMA: significant improvements in protein secondary structure prediction by consensus prediction from multiple alignments. *Comput Appl Biosci*. 1995;11(6):681-684. <http://www.ncbi.nlm.nih.gov/pubmed/8808585>.
 179. Nakai K, Horton P. PSORT: a program for detecting sorting signals in proteins and

- predicting their subcellular localization. *Trends Biochem Sci.* 1999;24(1):34-36. <http://www.ncbi.nlm.nih.gov/pubmed/10087920>.
180. Ikeda M, Arai M, Okuno T, Shimizu T. TMPDB: a database of experimentally-characterized transmembrane topologies. *Nucleic Acids Res.* 2003;31(1):406-409. doi:PMC165467
 181. Gnad F, Gunawardena J, Mann M. PHOSIDA 2011: The posttranslational modification database. *Nucleic Acids Res.* 2011;39(SUPPL. 1):253-260. doi:10.1093/nar/gkq1159
 182. Hornbeck P V., Zhang B, Murray B, Kornhauser JM, Latham V, Skrzypek E. PhosphoSitePlus, 2014: Mutations, PTMs and recalibrations. *Nucleic Acids Res.* 2015;43(D1):D512-D520. doi:10.1093/nar/gku1267
 183. Tang Z, Li C, Kang B, Gao G, Li C, Zhang Z. GEPIA: a web server for cancer and normal gene expression profiling and interactive analyses. *Nucleic Acids Res.* 2017;45(W1):W98-W102. doi:10.1093/nar/gkx247
 184. Chandrashekar DS, Bashel B, Balasubramanya SAH, et al. UALCAN: A Portal for Facilitating Tumor Subgroup Gene Expression and Survival Analyses. *Neoplasia.* 2017;19(8):649-658. doi:10.1016/j.neo.2017.05.002
 185. Jézéquel P, Gouraud W, Ben Azzouz F, et al. bc-GenExMiner 4.5: new mining module computes breast cancer differential gene expression analyses. *Database.* 2021;2021. doi:10.1093/database/baab007
 186. Thul PJ, Lindskog C. The human protein atlas: A spatial map of the human proteome. *Protein Sci.* 2018;27(1):233-244. doi:10.1002/pro.3307
 187. Györfy B, Lanczky A, Eklund AC, et al. An online survival analysis tool to rapidly assess the effect of 22,277 genes on breast cancer prognosis using microarray data of 1,809 patients. *Breast Cancer Res Treat.* 2010;123(3):725-731. doi:10.1007/s10549-009-0674-9
 188. Györfy B, Lanczky A, Szállási Z. Implementing an online tool for genome-wide validation of survival-associated biomarkers in ovarian-cancer using microarray data from 1287 patients. *Endocr Relat Cancer.* 2012;19(2):197-208. doi:10.1530/ERC-11-0329
 189. Györfy B, Surowiak P, Budczies J, Lanczky A. Online Survival Analysis Software to Assess the Prognostic Value of Biomarkers Using Transcriptomic Data in Non-Small-Cell Lung Cancer. Chellappan SP, ed. *PLoS One.* 2013;8(12):e82241. doi:10.1371/journal.pone.0082241
 190. Hogstrand C, Kille P, Ackland ML, Hiscox S, Taylor KM. A mechanism for epithelial-mesenchymal transition and anoikis resistance in breast cancer triggered by zinc channel ZIP6 and STAT3 (signal transducer and activator of transcription 3). *Biochem J.* 2013;455(2):229-237. doi:10.1042/BJ20130483
 191. Jenkitkasemwong S, Wang C-Y, Mackenzie B, Knutson MD. Physiologic implications of metal-ion transport by ZIP14 and ZIP8. *Biometals.* 2012;25(4):643-655. doi:10.1007/s10534-012-9526-x
 192. Girijashanker K, He L, Soleimani M, et al. Slc39a14 gene encodes ZIP14, a metal/bicarbonate symporter: similarities to the ZIP8 transporter. *Mol Pharmacol.* 2008;73(5):1413-1423. doi:10.1124/mol.107.043588
 193. Fujishiro H, Yano Y, Takada Y, Tanihara M, Himeno S. Roles of ZIP8, ZIP14, and DMT1 in transport of cadmium and manganese in mouse kidney proximal tubule cells. *Metallomics.* 2012;4(7):700-708. doi:10.1039/c2mt20024d
 194. Zhao N, Zhang A-S, Worthen C, Knutson MD, Enns CA. An iron-regulated and glycosylation-dependent proteasomal degradation pathway for the plasma membrane metal transporter ZIP14. *Proc Natl Acad Sci.* 2014;111(25):9175-9180.

- doi:10.1073/pnas.1405355111
195. Coleman J. Dual functions of the signal peptide in protein transfer across the membrane. *Cell*. 1985;43(1):351-360. doi:10.1016/0092-8674(85)90040-6
 196. Lai ZW, Petrera A, Schilling O. Protein amino-terminal modifications and proteomic approaches for N-terminal profiling. *Curr Opin Chem Biol*. 2015;24:71-79. doi:10.1016/j.cbpa.2014.10.026
 197. Blom N, Sicheritz-Pontén T, Gupta R, Gammeltoft S, Brunak S. Prediction of post-translational glycosylation and phosphorylation of proteins from the amino acid sequence. *Proteomics*. 2004;4(6):1633-1649. doi:10.1002/pmic.200300771
 198. Miller ML, Jensen LJ, Diella F, et al. Linear Motif Atlas for Phosphorylation-Dependent Signaling. *Sci Signal*. 2008;1(35):ra2-ra2. doi:10.1126/scisignal.1159433
 199. Olsen J V., Blagoev B, Gnäd F, et al. Global, In Vivo, and Site-Specific Phosphorylation Dynamics in Signaling Networks. *Cell*. 2006;127(3):635-648. doi:10.1016/j.cell.2006.09.026
 200. Cheng H-C, Qi RZ, Paudel H, Zhu H-J. Regulation and Function of Protein Kinases and Phosphatases. *Enzyme Res*. 2011;2011:1-3. doi:10.4061/2011/794089
 201. Filhol O, Cochet C. Protein kinase CK2 in health and disease: Cellular functions of protein kinase CK2: a dynamic affair. *Cell Mol Life Sci*. 2009;66(11-12):1830-1839. doi:10.1007/s00018-009-9151-1
 202. St-Denis NA, Litchfield DW. Protein kinase CK2 in health and disease: From birth to death: the role of protein kinase CK2 in the regulation of cell proliferation and survival. *Cell Mol Life Sci*. 2009;66(11-12):1817-1829. doi:10.1007/s00018-009-9150-2
 203. Meggio F, Pinna LA. One-thousand-and-one substrates of protein kinase CK2? *FASEB J*. 2003;17(3):349-368. doi:10.1096/fj.02-0473rev
 204. Griner EM, Kazanietz MG. Protein kinase C and other diacylglycerol effectors in cancer. *Nat Rev Cancer*. 2007;7(4):281-294. doi:10.1038/nrc2110
 205. Wang Z, Bhattacharya N, Weaver M, et al. Pim-1: a serine/threonine kinase with a role in cell survival, proliferation, differentiation and tumorigenesis. *J Vet Sci*. 2001;2(3):167-179. <http://www.ncbi.nlm.nih.gov/pubmed/12441685>.
 206. Zou Z, Tao T, Li H, Zhu X. mTOR signaling pathway and mTOR inhibitors in cancer: progress and challenges. *Cell Biosci*. 2020;10(1):31. doi:10.1186/s13578-020-00396-1
 207. Vijayaraghavan S, Moulder S, Keyomarsi K, Layman RM. Inhibiting CDK in Cancer Therapy: Current Evidence and Future Directions. *Target Oncol*. 2018;13(1):21-38. doi:10.1007/s11523-017-0541-2
 208. Teasdale RD, Jackson MR. Signal-mediated sorting of membrane proteins between the endoplasmic reticulum and the golgi apparatus. *Annu Rev Cell Dev Biol*. 1996;12:27-54. doi:10.1146/annurev.cellbio.12.1.27
 209. Lippincott-Schwartz J, Roberts TH, Hirschberg K. Secretory Protein Trafficking and Organelle Dynamics in Living Cells. *Annu Rev Cell Dev Biol*. 2000;16(1):557-589. doi:10.1146/annurev.cellbio.16.1.557
 210. Gardy JL. PSORT-B: improving protein subcellular localization prediction for Gram-negative bacteria. *Nucleic Acids Res*. 2003;31(13):3613-3617. doi:10.1093/nar/gkg602
 211. Kosugi S, Yanagawa H, Terauchi R, Tabata S. NESmapper: Accurate Prediction of Leucine-Rich Nuclear Export Signals Using Activity-Based Profiles. Prlic A, ed. *PLoS Comput Biol*. 2014;10(9):e1003841. doi:10.1371/journal.pcbi.1003841
 212. Cokol M, Nair R, Rost B. Finding nuclear localization signals. *EMBO Rep*. 2000;1(5):411-415. doi:10.1093/embo-reports/kvd092
 213. Nguyen Ba AN, Pogoutse A, Provart N, Moses AM. NLStradamus: a simple Hidden Markov Model for nuclear localization signal prediction. *BMC Bioinformatics*.

- 2009;10(1):202. doi:10.1186/1471-2105-10-202
214. Brameier M, Krings A, MacCallum RM. NucPred Predicting nuclear localization of proteins. *Bioinformatics*. 2007;23(9):1159-1160. doi:10.1093/bioinformatics/btm066
 215. Lin J, Hu J. SeqNLS: Nuclear Localization Signal Prediction Based on Frequent Pattern Mining and Linear Motif Scoring. Dalby AR, ed. *PLoS One*. 2013;8(10):e76864. doi:10.1371/journal.pone.0076864
 216. Diella F, Via A, Chica C, Luck K, Gould C, Gibson T. The Eukaryotic Linear Motif Resource (ELM): Regulatory Sites in Proteins. *Nat Preced*. April 2009. doi:10.1038/npre.2009.3152.1
 217. Negi S, Pandey S, Srinivasan SM, Mohammed A, Guda C. LocSigDB: a database of protein localization signals. *Database*. 2015;2015:bav003-bav003. doi:10.1093/database/bav003
 218. Tang Z, Li C, Kang B, Gao G, Li C, Zhang Z. GEPIA: a web server for cancer and normal gene expression profiling and interactive analyses. *Nucleic Acids Res*. 2017;45(W1):W98-W102. doi:10.1093/nar/gkx247
 219. Tomczak K, Czerwińska P, Wiznerowicz M. Review The Cancer Genome Atlas (TCGA): an immeasurable source of knowledge. *Współczesna Onkol*. 2015;1A:68-77. doi:10.5114/wo.2014.47136
 220. Barrett T, Wilhite SE, Ledoux P, et al. NCBI GEO: archive for functional genomics data sets—update. *Nucleic Acids Res*. 2012;41(D1):D991-D995. doi:10.1093/nar/gks1193
 221. Tang Z, Kang B, Li C, Chen T, Zhang Z. GEPIA2: an enhanced web server for large-scale expression profiling and interactive analysis. *Nucleic Acids Res*. 2019;47(W1):W556-W560. doi:10.1093/nar/gkz430
 222. Liu Y, Qiu P. Integrative analysis of methylation and gene expression data in TCGA. In: *Proceedings 2012 IEEE International Workshop on Genomic Signal Processing and Statistics (GENSIPS)*. IEEE; 2012:1-4. doi:10.1109/GENSIPS.2012.6507712
 223. Asplund A, Edqvist P-HD, Schwenk JM, Pontén F. Antibodies for profiling the human proteome-The Human Protein Atlas as a resource for cancer research. *Proteomics*. 2012;12(13):2067-2077. doi:10.1002/pmic.201100504
 224. Szász AM, Lánczky A, Nagy Á, et al. Cross-validation of survival associated biomarkers in gastric cancer using transcriptomic data of 1,065 patients. *Oncotarget*. 2016;7(31):49322-49333. doi:10.18632/oncotarget.10337
 225. Bland JM, Altman DG. The logrank test. *BMJ*. 2004;328(7447):1073. doi:10.1136/bmj.328.7447.1073
 226. Rich JT, Neely JG, Paniello RC, Voelker CCJ, Nussenbaum B, Wang EW. A practical guide to understanding Kaplan-Meier curves. *Otolaryngol Neck Surg*. 2010;143(3):331-336. doi:10.1016/j.otohns.2010.05.007
 227. Tonello F, Bergmann A, Abrahao K de S, Sales de Aguiar S, Adeodato Bello M, Santos Thuler LC. Impact of Number of Positive Lymph Nodes and Lymph Node Ratio on Survival of Women with Node-Positive Breast Cancer. *Eur J Breast Heal*. 2019;15(2):76-84. doi:10.5152/ejbh.2019.4414
 228. Sung H, Ferlay J, Siegel RL, et al. Global Cancer Statistics 2020: GLOBOCAN Estimates of Incidence and Mortality Worldwide for 36 Cancers in 185 Countries. *CA Cancer J Clin*. 2021;71(3):209-249. doi:10.3322/caac.21660
 229. Clarke R, Tyson JJ, Dixon JM. Endocrine resistance in breast cancer – An overview and update. *Mol Cell Endocrinol*. 2015;418:220-234. doi:10.1016/j.mce.2015.09.035
 230. Larionov AA, Miller WR. Challenges in defining predictive markers for response to endocrine therapy in breast cancer. *Futur Oncol*. 2009;5(9):1415-1428. doi:10.2217/fon.09.113

231. Gao Y-F, Mao X-Y, Zhu T, et al. COL3A1 and SNAP91: novel glioblastoma markers with diagnostic and prognostic value. *Oncotarget*. 2016;7(43):70494-70503. doi:10.18632/oncotarget.12038
232. Song M, Bode AM, Dong Z, Lee M-H. AKT as a Therapeutic Target for Cancer. *Cancer Res*. 2019;79(6):1019-1031. doi:10.1158/0008-5472.CAN-18-2738
233. Wilkinson B, Gilbert HF. Protein disulfide isomerase. *Biochim Biophys Acta - Proteins Proteomics*. 2004;1699(1-2):35-44. doi:10.1016/j.bbapap.2004.02.017
234. Gruber CW, Čemažar M, Heras B, Martin JL, Craik DJ. Protein disulfide isomerase: the structure of oxidative folding. *Trends Biochem Sci*. 2006;31(8):455-464. doi:10.1016/j.tibs.2006.06.001
235. Galligan JJ, Petersen DR. The human protein disulfide isomerase gene family. *Hum Genomics*. 2012;6(1):6. doi:10.1186/1479-7364-6-6
236. Sankavaram K, Freake HC. The effects of transformation and ZnT-1 silencing on zinc homeostasis in cultured cells. *J Nutr Biochem*. 2012;23(6):629-634. doi:10.1016/j.jnutbio.2011.03.006
237. Pratt EPS, Damon LJ, Anson KJ, Palmer AE. Tools and techniques for illuminating the cell biology of zinc. *Biochim Biophys Acta - Mol Cell Res*. 2021;1868(1):118865. doi:10.1016/j.bbamcr.2020.118865
238. Qin Y, Dittmer PJ, Park JG, Jansen KB, Palmer AE. Measuring steady-state and dynamic endoplasmic reticulum and Golgi Zn²⁺ with genetically encoded sensors. *Proc Natl Acad Sci U S A*. 2011;108(18):7351-7356. doi:10.1073/pnas.1015686108
239. Qin Y, Miranda JG, Stoddard CI, Dean KM, Galati DF, Palmer AE. Direct comparison of a genetically encoded sensor and small molecule indicator: implications for quantification of cytosolic Zn(2+). *ACS Chem Biol*. 2013;8(11):2366-2371. doi:10.1021/cb4003859
240. Vinkenborg JL, Nicolson TJ, Bellomo EA, Koay MS, Rutter GA, Merckx M. Genetically encoded FRET sensors to monitor intracellular Zn²⁺ homeostasis. *Nat Methods*. 2009;6(10):737-740. doi:10.1038/nmeth.1368
241. Haase H, Maret W. Protein Tyrosine Phosphatases as Targets of the Combined Insulinomimetic Effects of Zinc and Oxidants. *BioMetals*. 2005;18(4):333-338. doi:10.1007/s10534-005-3707-9
242. Bellomo E, Massarotti A, Hogstrand C, Maret W. Zinc ions modulate protein tyrosine phosphatase 1B activity. *Metallomics*. 2014;6(7):1229-1239. doi:10.1039/C4MT00086B
243. Dechat T, Adam SA, Taimen P, Shimi T, Goldman RD. Nuclear lamins. *Cold Spring Harb Perspect Biol*. 2010;2(11):a000547. doi:10.1101/cshperspect.a000547
244. Gerace L, Blobel G. The nuclear envelope lamina is reversibly depolymerized during mitosis. *Cell*. 1980;19(1):277-287. doi:10.1016/0092-8674(80)90409-2
245. Raices M, D'Angelo MA. Nuclear pore complex composition: a new regulator of tissue-specific and developmental functions. *Nat Rev Mol Cell Biol*. 2012;13(11):687-699. doi:10.1038/nrm3461
246. Muchir a, Worman HJ. The nuclear envelope and human disease. *Physiol*. 2004;19(Journal Article):309-314. doi:10.1152/physiol.00022.2004\r19/5/309 [pii]
247. Franke WW, Scheer U, Krohne G, Jarasch ED. The nuclear envelope and the architecture of the nuclear periphery. *J Cell Biol*. 1981;91(3 Pt 2):39s-50s. doi:10.1083/jcb.91.3.39s
248. Feldherr CM, Akin D. The permeability of the nuclear envelope in dividing and nondividing cell cultures. *J Cell Biol*. 1990;111(1):1-8. doi:10.1083/jcb.111.1.1
249. Huff J, Bergter A, Birkenbeil J, Kleppe I, Engelmann R, Krzic U. The new 2D Superresolution mode for ZEISS Airyscan. *Nat Methods*. 2017;14(12):1223-1223.

- doi:10.1038/nmeth.f.404
250. Korobchevskaya K, Lagerholm B, Colin-York H, Fritzsche M. Exploring the Potential of Airyscan Microscopy for Live Cell Imaging. *Photonics*. 2017;4(4):41. doi:10.3390/photonics4030041
 251. Wu X, Hammer JA. ZEISS Airyscan: Optimizing Usage for Fast, Gentle, Super-Resolution Imaging. In: ; 2021:111-130. doi:10.1007/978-1-0716-1402-0_5
 252. Tingey M, Mudumbi KC, Schirmer EC, Yang W. Casting a Wider Net: Differentiating between Inner Nuclear Envelope and Outer Nuclear Envelope Transmembrane Proteins. *Int J Mol Sci*. 2019;20(21):5248. doi:10.3390/ijms20215248
 253. Groves NR, McKenna JF, Evans DE, Graumann K, Meier I. A nuclear localization signal targets tail-anchored membrane proteins to the inner nuclear envelope in plants. *J Cell Sci*. January 2019. doi:10.1242/jcs.226134
 254. Yang L, Guan T, Gerace L. Integral membrane proteins of the nuclear envelope are dispersed throughout the endoplasmic reticulum during mitosis. *J Cell Biol*. 1997;137(6):1199-1210. <http://www.ncbi.nlm.nih.gov/pubmed/9182656>.
 255. Pleiner T, Bates M, Trakhanov S, et al. Nanobodies: site-specific labeling for super-resolution imaging, rapid epitope-mapping and native protein complex isolation. *Elife*. 2015;4. doi:10.7554/eLife.11349
 256. Kijanka M, van Donselaar EG, Müller WH, et al. A novel immuno-gold labeling protocol for nanobody-based detection of HER2 in breast cancer cells using immuno-electron microscopy. *J Struct Biol*. 2017;199(1):1-11. doi:10.1016/j.jsb.2017.05.008
 257. Yokoyama N, Hayashi N, Seki T, et al. A giant nucleopore protein that binds Ran/TC4. *Nature*. 1995;376(6536):184-188. doi:10.1038/376184a0
 258. Cordes VC, Reidenbach S, Rackwitz H-R, Franke WW. Identification of Protein p270/Tpr as a Constitutive Component of the Nuclear Pore Complex-attached Intranuclear Filaments. *J Cell Biol*. 1997;136(3):515-529. doi:10.1083/jcb.136.3.515
 259. Hell SW. Microscopy and its focal switch. *Nat Methods*. 2009;6(1):24-32. doi:10.1038/nmeth.1291
 260. Huang B, Bates M, Zhuang X. Super-Resolution Fluorescence Microscopy. *Annu Rev Biochem*. 2009;78(1):993-1016. doi:10.1146/annurev.biochem.77.061906.092014
 261. Godin AG, Lounis B, Cognet L. Super-resolution Microscopy Approaches for Live Cell Imaging. *Biophys J*. 2014;107(8):1777-1784. doi:10.1016/j.bpj.2014.08.028
 262. Chizhik AM, Ruhlandt D, Pfaff J, et al. Three-Dimensional Reconstruction of Nuclear Envelope Architecture Using Dual-Color Metal-Induced Energy Transfer Imaging. *ACS Nano*. 2017;11(12):11839-11846. doi:10.1021/acsnano.7b04671
 263. Mudumbi KC, Schirmer EC, Yang W. Single-point single-molecule FRAP distinguishes inner and outer nuclear membrane protein distribution. *Nat Commun*. 2016;7(1):12562. doi:10.1038/ncomms12562
 264. Chizhik AI, Rother J, Gregor I, Janshoff A, Enderlein J. Metal-induced energy transfer for live cell nanoscopy. *Nat Photonics*. 2014;8(2):124-127. doi:10.1038/nphoton.2013.345
 265. Prunuske AJ, Ullman KS. The nuclear envelope: form and reformation. *Curr Opin Cell Biol*. 2006;18(1):108-116. doi:10.1016/j.ceb.2005.12.004
 266. Macara IG. Transport into and out of the nucleus. *Microbiol Mol Biol Rev*. 2001;65(4):570-594, table of contents. doi:10.1128/MMBR.65.4.570-594.2001
 267. Choi, Kam, Kim, Park, Lee. Targeting Heat Shock Protein 27 in Cancer: A Druggable Target for Cancer Treatment? *Cancers (Basel)*. 2019;11(8):1195. doi:10.3390/cancers11081195
 268. Wei L, Liu T-T, Wang H-H, et al. Hsp27 participates in the maintenance of breast cancer stem cells through regulation of epithelial-mesenchymal transition and nuclear

- factor- κ B. *Breast Cancer Res.* 2011;13(5):R101. doi:10.1186/bcr3042
269. Lv D, Guo L, Zhang T, Huang L. PRAS40 signaling in tumor. *Oncotarget.* 2017;8(40):69076-69085. doi:10.18632/oncotarget.17299
 270. Roberts PJ, Der CJ. Targeting the Raf-MEK-ERK mitogen-activated protein kinase cascade for the treatment of cancer. *Oncogene.* 2007;26(22):3291-3310. doi:10.1038/sj.onc.1210422
 271. Roberts PJ, Der CJ. Targeting the Raf-MEK-ERK mitogen-activated protein kinase cascade for the treatment of cancer. *Oncogene.* 2007;26(22):3291-3310. doi:10.1038/sj.onc.1210422
 272. Johannessen M, Delghandi MP, Moens U. What turns CREB on? *Cell Signal.* 2004;16(11):1211-1227. doi:10.1016/j.cellsig.2004.05.001
 273. Sakamoto KM, Frank DA. CREB in the pathophysiology of cancer: implications for targeting transcription factors for cancer therapy. *Clin Cancer Res.* 2009;15(8):2583-2587. doi:10.1158/1078-0432.CCR-08-1137
 274. Lonze BE, Ginty DD. Function and regulation of CREB family transcription factors in the nervous system. *Neuron.* 2002;35(4):605-623. <http://www.ncbi.nlm.nih.gov/pubmed/12194863>.
 275. Pullen N, Thomas G. The modular phosphorylation and activation of p70 s6k. *FEBS Lett.* 1997;410(1):78-82. doi:10.1016/S0014-5793(97)00323-2
 276. Dennis PB, Pullen N, Pearson RB, Kozma SC, Thomas G. Phosphorylation Sites in the Autoinhibitory Domain Participate in p70 s6k Activation Loop Phosphorylation. *J Biol Chem.* 1998;273(24):14845-14852. doi:10.1074/jbc.273.24.14845
 277. Gallolu Kankanamalage S, Karra AS, Cobb MH. WNK pathways in cancer signaling networks. *Cell Commun Signal.* 2018;16(1):72. doi:10.1186/s12964-018-0287-1
 278. Dhillon AS, Hagan S, Rath O, Kolch W. MAP kinase signalling pathways in cancer. *Oncogene.* 2007;26(22):3279-3290. doi:10.1038/sj.onc.1210421
 279. Chen Z, Gibson TB, Robinson F, et al. MAP Kinases. *Chem Rev.* 2001;101(8):2449-2476. doi:10.1021/cr000241p
 280. Alberini CM. Transcription Factors in Long-Term Memory and Synaptic Plasticity. *Physiol Rev.* 2009;89(1):121-145. doi:10.1152/physrev.00017.2008
 281. Xu F, Na L, Li Y, Chen L. Roles of the PI3K/AKT/mTOR signalling pathways in neurodegenerative diseases and tumours. *Cell Biosci.* 2020;10(1):54. doi:10.1186/s13578-020-00416-0
 282. Sridharan S, Basu A. Distinct Roles of mTOR Targets S6K1 and S6K2 in Breast Cancer. *Int J Mol Sci.* 2020;21(4):1199. doi:10.3390/ijms21041199
 283. Society AC. American Cancer Society: Cancer Facts and Figures 2019. 2020.
 284. Dixon JM. Endocrine Resistance in Breast Cancer. *New J Sci.* 2014;2014:1-27. doi:10.1155/2014/390618
 285. Chen Y, Bai Y, Han Z, He W, Guo Z. Photoluminescence imaging of Zn²⁺ in living systems. *Chem Soc Rev.* 2015;44(14):4517-4546. doi:10.1039/C5CS00005J
 286. Passerini A, Andreini C, Menchetti S, Rosato A, Frasconi P. Predicting zinc binding at the proteome level. *BMC Bioinformatics.* 2007;8:1-13. doi:10.1186/1471-2105-8-39
 287. Micronutrients I of M (US) P on. *Dietary Reference Intakes for Vitamin A, Vitamin K, Arsenic, Boron, Chromium, Copper, Iodine, Iron, Manganese, Molybdenum, Nickel, Silicon, Vanadium, and Zinc.* Washington, D.C.: National Academies Press; 2001. doi:10.17226/10026
 288. Nimmanon Thirayost, M. Taylor K. Cellular Zinc Signalling Is Triggered by CK2. In: Switzerland: Springer International Publishing; 2015:141–157.
 289. Grattan BJ, Freake HC. Zinc and Cancer: Implications for LIV-1 in Breast Cancer. *Nutrients.* 2012;4(7):648-675. doi:10.3390/nu4070648

290. Lu Q, Haragopal H, Slepchenko KG, Stork C, Li Y V. Intracellular zinc distribution in mitochondria, ER and the Golgi apparatus. *Int J Physiol Pathophysiol Pharmacol*. 2016;8(1):35-43. <http://www.ncbi.nlm.nih.gov/pubmed/27186321>.
291. Fukada T, Kambe T. Molecular and genetic features of zinc transporters in physiology and pathogenesis. *Metallomics*. 2011;3(7):662. doi:10.1039/c1mt00011j
292. Woodruff G, Bouwkamp CG, de Vrij FM, et al. The Zinc Transporter SLC39A7 (ZIP7) Is Essential for Regulation of Cytosolic Zinc Levels. *Mol Pharmacol*. 2018;94(3):1092-1100. doi:10.1124/mol.118.112557
293. Nimmanon, T, Taylor KM. Zinc signalling and cancer. In: T. Fukada. Tokyo: Springer Japan; 2014:285–313.
294. Zhou H, Zhu Y, Qi H, et al. Evaluation of the prognostic values of solute carrier (SLC) family 39 genes for patients with lung adenocarcinoma. *Aging (Albany NY)*. 2021;13(4):5312-5331. doi:10.18632/aging.202452
295. Itadani H, Oshima H, Oshima M, Kotani H. Mouse gastric tumor models with prostaglandin E2 pathway activation show similar gene expression profiles to intestinal-type human gastric cancer. *BMC Genomics*. 2009;10(1):615. doi:10.1186/1471-2164-10-615
296. Ohashi W, Kimura S, Iwanaga T, et al. Zinc Transporter SLC39A7/ZIP7 Promotes Intestinal Epithelial Self-Renewal by Resolving ER Stress. Hershfinkel M, ed. *PLOS Genet*. 2016;12(10):e1006349. doi:10.1371/journal.pgen.1006349
297. Zhang Y, Bai J, Si W, Yuan S, Li Y, Chen X. SLC39A7, regulated by miR-139-5p, induces cell proliferation, migration and inhibits apoptosis in gastric cancer via Akt/mTOR signaling pathway. *Biosci Rep*. 2020;40(2). doi:10.1042/BSR20200041
298. Wei Y, Dong J, Li F, Wei Z, Tian Y. Knockdown of SLC39A7 suppresses cell proliferation, migration and invasion in cervical cancer. *EXCLI J*. 2017;16:1165-1176. doi:10.17179/excli2017-690
299. Wilson M, Hogstrand C, Maret W. Picomolar Concentrations of Free Zinc(II) Ions Regulate Receptor Protein-tyrosine Phosphatase β Activity. *J Biol Chem*. 2012;287(12):9322-9326. doi:10.1074/jbc.C111.320796
300. Knowlden JM, Hutcheson IR, Jones HE, et al. Elevated Levels of Epidermal Growth Factor Receptor/c-erbB2 Heterodimers Mediate an Autocrine Growth Regulatory Pathway in Tamoxifen-Resistant MCF-7 Cells. *Endocrinology*. 2003;144(3):1032-1044. doi:10.1210/en.2002-220620
301. Jones HE, Goddard L, Gee JMW, et al. Insulin-like growth factor-I receptor signalling and acquired resistance to gefitinib (ZD1839; Iressa) in human breast and prostate cancer cells. *Endocr Relat Cancer*. 2004;11(4):793-814. doi:10.1677/erc.1.00799
302. Hiscox S, Morgan L, Green TP, Barrow D, Gee J, Nicholson RI. Elevated Src activity promotes cellular invasion and motility in tamoxifen resistant breast cancer cells. *Breast Cancer Res Treat*. 2006;97(3):263-274. doi:10.1007/s10549-005-9120-9
303. Bourdeau A, Dubé N, Tremblay ML. Cytoplasmic protein tyrosine phosphatases, regulation and function: the roles of PTP1B and TC-PTP. *Curr Opin Cell Biol*. 2005;17(2):203-209. doi:10.1016/j.ceb.2005.02.001
304. Ilouz R, Kaidanovich O, Gurwitz D, Eldar-Finkelman H. Inhibition of glycogen synthase kinase-3 β by bivalent zinc ions: insight into the insulin-mimetic action of zinc. *Biochem Biophys Res Commun*. 2002;295(1):102-106. doi:10.1016/S0006-291X(02)00636-8
305. Lee S, Chanoit G, McIntosh R, Zvara DA, Xu Z. Molecular mechanism underlying Akt activation in zinc-induced cardioprotection. *Am J Physiol Circ Physiol*. 2009;297(2):H569-H575. doi:10.1152/ajpheart.00293.2009
306. Kao S-H, Wang W-L, Chen C-Y, et al. GSK3 β controls epithelial–mesenchymal

- transition and tumor metastasis by CHIP-mediated degradation of Slug. *Oncogene*. 2014;33(24):3172-3182. doi:10.1038/onc.2013.279
307. Nicholson RI, Johnston SR. Endocrine therapy – current benefits and limitations. *Breast Cancer Res Treat*. 2005;93(S1):3-10. doi:10.1007/s10549-005-9036-4
 308. Hiscox S, Morgan L, Barrow D, Dutkowski C, Wakeling A, Nicholson RI. Tamoxifen resistance in breast cancer cells is accompanied by an enhanced motile and invasive phenotype: Inhibition by gefitinib ('Iressa', ZD1839). *Clin Exp Metastasis*. 2004;21(3):201-212. doi:10.1023/B:CLIN.0000037697.76011.1d
 309. Johnston SRD. Enhancing the Efficacy of Hormonal Agents with Selected Targeted Agents. *Clin Breast Cancer*. 2009;9:S28-S36. doi:10.3816/CBC.2009.s.003
 310. Sporn MB. The war on cancer. *Lancet*. 1996;347(9012):1377-1381. doi:10.1016/S0140-6736(96)91015-6
 311. Lang K, Drell IV T, Zaenker K, Entschladen F. Inhibitors for Metastasis Development. *Recent Pat Anticancer Drug Discov*. 2006;1(1):69-80. doi:10.2174/157489206775246511
 312. Sleeman J, Steeg PS. Cancer metastasis as a therapeutic target. *Eur J Cancer*. 2010;46(7):1177-1180. doi:10.1016/j.ejca.2010.02.039
 313. Zheng H, Zhang G, Zhang L, et al. Comprehensive Review of Web Servers and Bioinformatics Tools for Cancer Prognosis Analysis. *Front Oncol*. 2020;10. doi:10.3389/fonc.2020.00068
 314. Gamero AM, Young HA, Wiltrout RH. Inactivation of Stat3 in tumor cells. *Cancer Cell*. 2004;5(2):111-112. doi:10.1016/S1535-6108(04)00028-5
 315. Carter CL, Allen C, Henson DE. Relation of tumor size, lymph node status, and survival in 24,740 breast cancer cases. *Cancer*. 1989;63(1):181-187. doi:10.1002/1097-0142(19890101)63:1<181::aid-cnrcr2820630129>3.0.co;2-h
 316. Razavi P, Chang MT, Xu G, et al. The Genomic Landscape of Endocrine-Resistant Advanced Breast Cancers. *Cancer Cell*. 2018;34(3):427-438.e6. doi:10.1016/j.ccell.2018.08.008
 317. Nishida H, Sohara E, Nomura N, et al. Phosphatidylinositol 3-Kinase/Akt Signaling Pathway Activates the WNK-OSR1/SPAK-NCC Phosphorylation Cascade in Hyperinsulinemic db/db Mice. *Hypertension*. 2012;60(4):981-990. doi:10.1161/HYPERTENSIONAHA.112.201509
 318. Lupien M, Meyer CA, Bailey ST, et al. Growth factor stimulation induces a distinct ER cistrome underlying breast cancer endocrine resistance. *Genes Dev*. 2010;24(19):2219-2227. doi:10.1101/gad.1944810
 319. Munro S, Pelham HRB. A C-terminal signal prevents secretion of luminal ER proteins. *Cell*. 1987;48(5):899-907. doi:10.1016/0092-8674(87)90086-9
 320. Nilsson T, Jackson M, Peterson PA. Short cytoplasmic sequences serve as retention signals for transmembrane proteins in the endoplasmic reticulum. *Cell*. 1989;58(4):707-718. doi:10.1016/0092-8674(89)90105-0
 321. Pfeffer SR, Rothman JE. Biosynthetic protein transport and sorting by the endoplasmic reticulum and Golgi. *Transport*. 1987.
 322. Nilsson T, Warren G. Retention and retrieval in the endoplasmic reticulum and the Golgi apparatus. *Curr Opin Cell Biol*. 1994;6(4):517-521. doi:10.1016/0955-0674(94)90070-1
 323. Wieland F, Harter C. Mechanisms of vesicle formation: insights from the COP system. *Curr Opin Cell Biol*. 1999;11(4):440-446. doi:10.1016/s0955-0674(99)80063-5
 324. Hardt B. (Arg)3 within the N-terminal domain of glucosidase I contains ER targeting information but is not required absolutely for ER localization. *Glycobiology*. 2003;13(3):159-168. doi:10.1093/glycob/cwg013

325. Sato M, Sato K, Nakano A. Endoplasmic reticulum localization of Sec12p is achieved by two mechanisms: Rer1p-dependent retrieval that requires the transmembrane domain and Rer1p-independent retention that involves the cytoplasmic domain. *J Cell Biol.* 1996;134(2):279-293. doi:10.1083/jcb.134.2.279
326. Nilsson T, Slusarewicz P, Hoe MH, Warren G. Kin recognition. A model for the retention of Golgi enzymes. *FEBS Lett.* 1993;330(1):1-4. doi:10.1016/0014-5793(93)80906-B
327. Cocquerel L, Meunier J-C, Pillez A, Wychowski C, Dubuisson J. A Retention Signal Necessary and Sufficient for Endoplasmic Reticulum Localization Maps to the Transmembrane Domain of Hepatitis C Virus Glycoprotein E2. *J Virol.* 1998;72(3):2183-2191. doi:10.1128/JVI.72.3.2183-2191.1998
328. Teasdale RD, Jackson MR. SIGNAL-MEDIATED SORTING OF MEMBRANE PROTEINS BETWEEN THE ENDOPLASMIC RETICULUM AND THE GOLGI APPARATUS. *Annu Rev Cell Dev Biol.* 1996;12(1):27-54. doi:10.1146/annurev.cellbio.12.1.27
329. Zerangue N, Schwappach B, Jan YN, Jan LY. A New ER Trafficking Signal Regulates the Subunit Stoichiometry of Plasma Membrane KATP Channels. *Neuron.* 1999;22(3):537-548. doi:10.1016/S0896-6273(00)80708-4
330. Jackson MR, Nilsson T, Peterson PA. Identification of a consensus motif for retention of transmembrane proteins in the endoplasmic reticulum. *EMBO J.* 1990;9(10):3153-3162. doi:2120038
331. Schutze MP, Peterson PA, Jackson MR. An N-terminal double-arginine motif maintains type II membrane proteins in the endoplasmic reticulum. *EMBO J.* 1994;13(7):1696-1705. <http://www.ncbi.nlm.nih.gov/pubmed/8157008>.
332. Bakke O, Dobberstein B. MHC class II-associated invariant chain contains a sorting signal for endosomal compartments. *Cell.* 1990;63(4):707-716. doi:10.1016/0092-8674(90)90137-4
333. Boulaflous A, Saint-Jore-Dupas C, Herranz-Gordo M-C, et al. Cytosolic N-terminal arginine-based signals together with a luminal signal target a type II membrane protein to the plant ER. *BMC Plant Biol.* 2009;9(1):144. doi:10.1186/1471-2229-9-144
334. Margeta-Mitrovic M, Jan YN, Jan LY. A Trafficking Checkpoint Controls GABAB Receptor Heterodimerization. *Neuron.* 2000;27(1):97-106. doi:10.1016/S0896-6273(00)00012-X
335. Nasu-Nishimura Y, Hurtado D, Braud S, Tang TT-T, Isaac JTR, Roche KW. Identification of an Endoplasmic Reticulum-Retention Motif in an Intracellular Loop of the Kainate Receptor Subunit KA2. *J Neurosci.* 2006;26(26):7014-7021. doi:10.1523/JNEUROSCI.0573-06.2006
336. Ren Z, Riley NJ, Garcia EP, Sanders JM, Swanson GT, Marshall J. Multiple Trafficking Signals Regulate Kainate Receptor KA2 Subunit Surface Expression. *J Neurosci.* 2003;23(16):6608-6616. doi:10.1523/JNEUROSCI.23-16-06608.2003
337. Jackson MR, Nilsson T, Peterson PA. Identification of a consensus motif for retention of transmembrane proteins in the endoplasmic reticulum. *EMBO J.* 1990;9(10):3153-3162. <http://www.ncbi.nlm.nih.gov/pubmed/2120038>.
338. Popoff V, Adolf F, Brugger B, Wieland F. COPI Budding within the Golgi Stack. *Cold Spring Harb Perspect Biol.* 2011;3(11):a005231-a005231. doi:10.1101/cshperspect.a005231
339. Jackson LP. Structure and mechanism of COPI vesicle biogenesis. *Curr Opin Cell Biol.* 2014;29:67-73. doi:10.1016/j.ceb.2014.04.009
340. Benghezal M, Wasteneys GO, Jones DA. The C-Terminal Dilysine Motif Confers Endoplasmic Reticulum Localization to Type I Membrane Proteins in Plants. *Plant*

- Cell*. 2000;12(7):1179-1201. doi:10.1105/tpc.12.7.1179
341. McCartney AW, Dyer JM, Dhanoa PK, et al. Membrane-bound fatty acid desaturases are inserted co-translationally into the ER and contain different ER retrieval motifs at their carboxy termini. *Plant J*. 2004;37(2):156-173. doi:10.1111/j.1365-313X.2004.01949.x
 342. Kabuß R, Ashikov A, Oelmann S, Gerardy-Schahn R, Bakker H. Endoplasmic reticulum retention of the large splice variant of the UDP-galactose transporter is caused by a dilysine motif. *Glycobiology*. 2005;15(10):905-911. doi:10.1093/glycob/cwi085
 343. Jackson MR, Nilsson T, Peterson PA. Retrieval of transmembrane proteins to the endoplasmic reticulum. *J Cell Biol*. 1993;121(2):317-333. doi:10.1083/jcb.121.2.317
 344. Michelsen K, Yuan H, Schwappach B. Hide and run. Arginine-based endoplasmic-reticulum-sorting motifs in the assembly of heteromultimeric membrane proteins. *EMBO Rep*. 2005;6(8):717-722. doi:10.1038/sj.embor.7400480
 345. Pagny S, Lerouge P, Faye L, Gomord V. Signals and mechanisms for protein retention in the endoplasmic reticulum. *J Exp Bot*. 1999;50(331):157-164. doi:10.1093/jxb/50.331.157
 346. Gaynor EC, te Heesen S, Graham TR, Aebi M, Emr SD. Signal-mediated retrieval of a membrane protein from the Golgi to the ER in yeast. *J Cell Biol*. 1994;127(3):653-665. doi:10.1083/jcb.127.3.653
 347. St-Louis É, Degrandmaison J, Grastilleur S, et al. Involvement of the coatamer protein complex I in the intracellular traffic of the delta opioid receptor. *Mol Cell Neurosci*. 2017;79:53-63. doi:10.1016/j.mcn.2016.12.005
 348. Kuroiwa T, Sakaguchi M, Mihara K, Omura T. Structural Requirements for Interruption of Protein Translocation across Rough Endoplasmic Reticulum Membrane1. *J Biochem*. 1990;108(5):829-834. doi:10.1093/oxfordjournals.jbchem.a123288
 349. Pedrazzini E, Villa A, Borgese N. A mutant cytochrome b5 with a lengthened membrane anchor escapes from the endoplasmic reticulum and reaches the plasma membrane. *Proc Natl Acad Sci*. 1996;93(9):4207-4212. doi:10.1073/pnas.93.9.4207
 350. Szczesna-Skorupa E, Kemper B. Endoplasmic Reticulum Retention Determinants in the Transmembrane and Linker Domains of Cytochrome P450 2C1. *J Biol Chem*. 2000;275(25):19409-19415. doi:10.1074/jbc.M002394200
 351. Yang M, Ellenberg J, Bonifacino JS, Weissman AM. The Transmembrane Domain of a Carboxyl-terminal Anchored Protein Determines Localization to the Endoplasmic Reticulum. *J Biol Chem*. 1997;272(3):1970-1975. doi:10.1074/jbc.272.3.1970
 352. Spencer Yost C, Hedgpeth J, Lingappa VR. A stop transfer sequence confers predictable transmembrane orientation to a previously secreted protein in cell-free systems. *Cell*. 1983;34(3):759-766. doi:10.1016/0092-8674(83)90532-9
 353. von Heijne G. Signal sequences. The limits of variation. *J Mol Biol*. 1985;184(1):99-105. doi:10.1016/0022-2836(85)90046-4
 354. Singer SJ, Maher PA, Yaffe MP. On the transfer of integral proteins into membranes. *Proc Natl Acad Sci*. 1987;84(7):1960-1964. doi:10.1073/pnas.84.7.1960
 355. Sabatini DD, Kreibich G, Morimoto T, Adesnik M. Mechanisms for the incorporation of proteins in membranes and organelles. *J Cell Biol*. 1982;92(1):1-22. doi:10.1083/jcb.92.1.1
 356. HEIJNE G, GAVEL Y. Topogenic signals in integral membrane proteins. *Eur J Biochem*. 1988;174(4):671-678. doi:10.1111/j.1432-1033.1988.tb14150.x
 357. Yamane K, Mizushima S. Introduction of basic amino acid residues after the signal peptide inhibits protein translocation across the cytoplasmic membrane of *Escherichia*

- coli. Relation to the orientation of membrane proteins. *J Biol Chem*. 1988;263(36):19690-19696. <http://www.ncbi.nlm.nih.gov/pubmed/3058705>.
358. Hammond C, Helenius A. Quality control in the secretory pathway. *Curr Opin Cell Biol*. 1995;7(4):523-529. <http://www.ncbi.nlm.nih.gov/pubmed/7495572>.
359. Kim H-J, Hwang S-H, Han M-E, et al. LAP2 Is Widely Overexpressed in Diverse Digestive Tract Cancers and Regulates Motility of Cancer Cells. Lee T, ed. *PLoS One*. 2012;7(6):e39482. doi:10.1371/journal.pone.0039482
360. Clayton P, Fischer B, Mann A, et al. Mutations causing Greenberg dysplasia but not Pelger anomaly uncouple enzymatic from structural functions of a nuclear membrane protein. *Nucleus*. 2010;1(4):354-366. doi:10.4161/nucl.1.4.12435
361. Hoffmann K, Dreger CK, Olins AL, et al. Mutations in the gene encoding the lamin B receptor produce an altered nuclear morphology in granulocytes (Pelger-Huët anomaly). *Nat Genet*. 2002;31(4):410-414. doi:10.1038/ng925
362. Ellis JA. Emery-Dreifuss muscular dystrophy at the nuclear envelope: 10 years on. *Cell Mol Life Sci*. 2006;63(23):2702-2709. doi:10.1007/s00018-006-6247-8
363. Manilal S. The Emery-Dreifuss muscular dystrophy protein, emerin, is a nuclear membrane protein. *Hum Mol Genet*. 1996;5(6):801-808. doi:10.1093/hmg/5.6.801
364. CALLAN HG, RANDALL JT, TOMLIN SG. An Electron Microscope Study of the Nuclear Membrane. *Nature*. 1949;163(4138):280-280. doi:10.1038/163280a0
365. Worman HJ, Evans CD, Blobel G. The lamin B receptor of the nuclear envelope inner membrane: a polytopic protein with eight potential transmembrane domains. *J Cell Biol*. 1990;111(4):1535-1542. doi:10.1083/jcb.111.4.1535
366. Foisner R, Gerace L. Integral membrane proteins of the nuclear envelope interact with lamins and chromosomes, and binding is modulated by mitotic phosphorylation. *Cell*. 1993;73(7):1267-1279. doi:10.1016/0092-8674(93)90355-T
367. Senior A, Gerace L. Integral membrane proteins specific to the inner nuclear membrane and associated with the nuclear lamina. *J Cell Biol*. 1988;107(6):2029-2036. doi:10.1083/jcb.107.6.2029
368. Schirmer EC, Florens L, Guan T, Yates JR, Gerace L. Nuclear membrane proteins with potential disease links found by subtractive proteomics. *Science*. 2003;301(5638):1380-1382. doi:10.1126/science.1088176
369. Olins AL, Rhodes G, Welch DBM, Zwerger M, Olins DE. Lamin B receptor. *Nucleus*. 2010;1(1):53-70. doi:10.4161/nucl.1.1.10515
370. Brachner A, Foisner R. Lamina-Associated Polypeptide (LAP)2 α and Other LEM Proteins in Cancer Biology. In: ; 2014:143-163. doi:10.1007/978-1-4899-8032-8_7
371. Barton LJ, Soshnev AA, Geyer PK. Networking in the nucleus: a spotlight on LEM-domain proteins. *Curr Opin Cell Biol*. 2015;34:1-8. doi:10.1016/j.ceb.2015.03.005
372. Soullam B, Worman HJ. Signals and structural features involved in integral membrane protein targeting to the inner nuclear membrane. *J Cell Biol*. 1995;130(1):15-27. doi:10.1083/jcb.130.1.15
373. Tapley EC, Ly N, Starr DA. Multiple mechanisms actively target the SUN protein UNC-84 to the inner nuclear membrane. Goldman RD, ed. *Mol Biol Cell*. 2011;22(10):1739-1752. doi:10.1091/mbc.e10-08-0733
374. Turgay Y, Ungricht R, Rothbaler A, et al. A classical NLS and the SUN domain contribute to the targeting of SUN2 to the inner nuclear membrane. *EMBO J*. 2010;29(14):2262-2275. doi:10.1038/emboj.2010.119
375. Gonzalez-Sandoval A, Towbin BD, Kalck V, et al. Perinuclear Anchoring of H3K9-Methylated Chromatin Stabilizes Induced Cell Fate in *C. elegans* Embryos. *Cell*. 2015;163(6):1333-1347. doi:10.1016/j.cell.2015.10.066
376. Solovei I, Wang AS, Thanisch K, et al. LBR and Lamin A/C Sequentially Tether

- Peripheral Heterochromatin and Inversely Regulate Differentiation. *Cell*. 2013;152(3):584-598. doi:10.1016/j.cell.2013.01.009
377. Wilson KL, Foisner R. Lamin-binding Proteins. *Cold Spring Harb Perspect Biol*. 2010;2(4):a000554-a000554. doi:10.1101/cshperspect.a000554
378. Fahrenkrog B, Aebi U. The nuclear pore complex: nucleocytoplasmic transport and beyond. *Nat Rev Mol Cell Biol*. 2003;4(10):757-766. doi:10.1038/nrm1230
379. Kubitscheck U, Grünwald D, Hoekstra A, et al. Nuclear transport of single molecules. *J Cell Biol*. 2005;168(2):233-243. doi:10.1083/jcb.200411005
380. Wagstaff KM, Jans DA. Importins and Beyond: Non-Conventional Nuclear Transport Mechanisms. *Traffic*. 2009;10(9):1188-1198. doi:10.1111/j.1600-0854.2009.00937.x
381. Ungricht R, Klann M, Horvath P, Kutay U. Diffusion and retention are major determinants of protein targeting to the inner nuclear membrane. *J Cell Biol*. 2015;209(5):687-704. doi:10.1083/jcb.201409127
382. Ohba T, Schirmer EC, Nishimoto T, Gerace L. Energy- and temperature-dependent transport of integral proteins to the inner nuclear membrane via the nuclear pore. *J Cell Biol*. 2004;167(6):1051-1062. doi:10.1083/jcb.200409149
383. Zuleger N, Kelly DA, Richardson AC, et al. System analysis shows distinct mechanisms and common principles of nuclear envelope protein dynamics. *J Cell Biol*. 2011;193(1):109-123. doi:10.1083/jcb.201009068
384. Boni A, Politi AZ, Strnad P, Xiang W, Hossain MJ, Ellenberg J. Live imaging and modeling of inner nuclear membrane targeting reveals its molecular requirements in mammalian cells. *J Cell Biol*. 2015;209(5):705-720. doi:10.1083/jcb.201409133
385. King MC, Lusk CP, Blobel G. Karyopherin-mediated import of integral inner nuclear membrane proteins. *Nature*. 2006;442(7106):1003-1007. doi:10.1038/nature05075
386. Strambio-De-Castillia C, Niepel M, Rout MP. The nuclear pore complex: bridging nuclear transport and gene regulation. *Nat Rev Mol Cell Biol*. 2010;11(7):490-501. doi:10.1038/nrm2928
387. Soullam B, Worman HJ. The amino-terminal domain of the lamin B receptor is a nuclear envelope targeting signal. *J Cell Biol*. 1993;120(5):1093-1100.
388. Soullam B, Worman HJ. Signals and structural features involved in integral membrane protein targeting to the inner nuclear membrane. *J Cell Biol*. 1995;130(1):15-27. doi:10.1083/jcb.130.1.15
389. Zuleger N, Kerr ARW, Schirmer EC. Many mechanisms, one entrance: membrane protein translocation into the nucleus. *Cell Mol Life Sci*. 2012;69(13):2205-2216. doi:10.1007/s00018-012-0929-1
390. Zuleger N, Korfali N, Schirmer EC. Inner nuclear membrane protein transport is mediated by multiple mechanisms. *Biochem Soc Trans*. 2008;36(6):1373-1377. doi:10.1042/BST0361373
391. Mudumbi KC, Czapiewski R, Ruba A, et al. Nucleoplasmic signals promote directed transmembrane protein import simultaneously via multiple channels of nuclear pores. *Nat Commun*. 2020;11(1):2184. doi:10.1038/s41467-020-16033-x
392. Hinshaw JE, Carragher BO, Milligan RA. Architecture and design of the nuclear pore complex. *Cell*. 1992;69(7):1133-1141. <http://www.ncbi.nlm.nih.gov/pubmed/1617726>.
393. Reichelt R, Holzenburg A, Buhle EL, Jarnik M, Engel A, Aebi U. Correlation between structure and mass distribution of the nuclear pore complex and of distinct pore complex components. *J Cell Biol*. 1990;110(4):883-894. doi:10.1083/jcb.110.4.883
394. Wu W, Lin F, Worman HJ. Intracellular trafficking of MAN1, an integral protein of the nuclear envelope inner membrane. *J Cell Sci*. 2002;115(Pt 7):1361-1371. <http://www.ncbi.nlm.nih.gov/pubmed/11896184>.
395. Ostlund C, Ellenberg J, Hallberg E, Lippincott-Schwartz J, Worman HJ. Intracellular

- trafficking of emerin, the Emery-Dreifuss muscular dystrophy protein. *J Cell Sci.* 1999;112 (Pt 1:1709-1719. <http://www.ncbi.nlm.nih.gov/pubmed/10318763>.
396. Smith S, Blobel G. The first membrane spanning region of the lamin B receptor is sufficient for sorting to the inner nuclear membrane. *J Cell Biol.* 1993;120(3):631-637. doi:10.1083/jcb.120.3.631
 397. Soullam B, Worman HJ. The amino-terminal domain of the lamin B receptor is a nuclear envelope targeting signal. *J Cell Biol.* 1993;120(5):1093-1100. doi:10.1083/jcb.120.5.1093
 398. Radu A, Blobel G, Moore MS. Identification of a protein complex that is required for nuclear protein import and mediates docking of import substrate to distinct nucleoporins. *Proc Natl Acad Sci.* 1995;92(5):1769-1773. doi:10.1073/pnas.92.5.1769
 399. Otsuka S, Iwasaka S, Yoneda Y, Takeyasu K, Yoshimura SH. Individual binding pockets of importin- for FG-nucleoporins have different binding properties and different sensitivities to RanGTP. *Proc Natl Acad Sci.* 2008;105(42):16101-16106. doi:10.1073/pnas.0802647105
 400. Bayliss R, Littlewood T, Strawn LA, Wentz SR, Stewart M. GLFG and FxFG Nucleoporins Bind to Overlapping Sites on Importin- β . *J Biol Chem.* 2002;277(52):50597-50606. doi:10.1074/jbc.M209037200
 401. Marfori M, Mynott A, Ellis JJ, et al. Molecular basis for specificity of nuclear import and prediction of nuclear localization. *Biochim Biophys Acta - Mol Cell Res.* 2011;1813(9):1562-1577. doi:10.1016/j.bbamer.2010.10.013
 402. Kimura M, Imamoto N. Biological Significance of the Importin- β Family-Dependent Nucleocytoplasmic Transport Pathways. *Traffic.* 2014;15(7):727-748. doi:10.1111/tra.12174
 403. Dingwall C, Laskey R. The nuclear membrane. *Science (80-).* 1992;258(5084):942-947. doi:10.1126/science.1439805
 404. Boulikas T. Nuclear localization signals (NLS). *Crit Rev Eukaryot Gene Expr.* 1993;3(3):193-227. doi:8241603
 405. Kosugi S, Hasebe M, Matsumura N, et al. Six Classes of Nuclear Localization Signals Specific to Different Binding Grooves of Importin α . *J Biol Chem.* 2009;284(1):478-485. doi:10.1074/jbc.M807017200
 406. Lisitsyna OM, Seplyarskiy VB, Sheval E V. Comparative analysis of nuclear localization signal (NLS) prediction methods. *Biopolym Cell.* 2017;33(2):147-154. doi:10.7124/bc.00094C
 407. Mehdi AM, Sehgal MSB, Kobe B, Bailey TL, Bodén M. A probabilistic model of nuclear import of proteins. *Bioinformatics.* 2011;27(9):1239-1246. doi:10.1093/bioinformatics/btr121
 408. Beck M. Nuclear Pore Complex Structure and Dynamics Revealed by Cryoelectron Tomography. *Science (80-).* 2004;306(5700):1387-1390. doi:10.1126/science.1104808
 409. Lusk CP, Blobel G, King MC. Highway to the inner nuclear membrane: rules for the road. *Nat Rev Mol Cell Biol.* 2007;8(5):414-420. doi:10.1038/nrm2165
 410. King MC, Lusk C, Blobel G. Karyopherin-mediated import of integral inner nuclear membrane proteins. *Nature.* 2006;442(7106):1003-1007. doi:10.1038/nature05075
 411. Lange A, McLane LM, Mills RE, Devine SE, Corbett AH. Expanding the Definition of the Classical Bipartite Nuclear Localization Signal. *Traffic.* 2010;11(3):311-323. doi:10.1111/j.1600-0854.2009.01028.x
 412. Dingwall C, Laskey RA. Nuclear targeting sequences — a consensus? *Trends Biochem Sci.* 1991;16:478-481. doi:10.1016/0968-0004(91)90184-W
 413. Robbins J, Dilworth SM, Laskey RA, Dingwall C. Two interdependent basic domains

- in nucleoplasm nuclear targeting sequence: Identification of a class of bipartite nuclear targeting sequence. *Cell*. 1991;64(3):615-623. doi:10.1016/0092-8674(91)90245-T
414. Nikolakaki E, Mylonis I, Giannakouros T. Lamin B Receptor: Interplay between Structure, Function and Localization. *Cells*. 2017;6(3):28. doi:10.3390/cells6030028
 415. Furukawa K, Panté N, Aebi U, Gerace L. Cloning of a cDNA for lamina-associated polypeptide 2 (LAP2) and identification of regions that specify targeting to the nuclear envelope. *EMBO J*. 1995;14(8):1626-1636. <http://www.ncbi.nlm.nih.gov/pubmed/7737115>.
 416. Nicolson SC, Samulski RJ. Recombinant Adeno-Associated Virus Utilizes Host Cell Nuclear Import Machinery To Enter the Nucleus. *J Virol*. 2014;88(8):4132-4144. doi:10.1128/JVI.02660-13
 417. Finlay DR, Newmeyer DD, Price TM, Forbes DJ. Inhibition of in vitro nuclear transport by a lectin that binds to nuclear pores. *J Cell Biol*. 1987;104(2):189-200. doi:10.1083/jcb.104.2.189
 418. Anderson DJ, Vargas JD, Hsiao JP, Hetzer MW. Recruitment of functionally distinct membrane proteins to chromatin mediates nuclear envelope formation in vivo. *J Cell Biol*. 2009;186(2):183-191. doi:10.1083/jcb.200901106
 419. Wu FYH, Wu CW. Zinc in DNA Replication and Transcription. *Annu Rev Nutr*. 1987;7(1):251-272. doi:10.1146/annurev.nu.07.070187.001343
 420. Jen J, Wang Y-C. Zinc finger proteins in cancer progression. *J Biomed Sci*. 2016;23(1):53. doi:10.1186/s12929-016-0269-9
 421. Krebs CJ, Zhang D, Yin L, Robins DM. The KRAB zinc finger protein RSL1 modulates sex-biased gene expression in liver and adipose tissue to maintain metabolic homeostasis. *Mol Cell Biol*. 2014;34(2):221-232. doi:10.1128/MCB.00875-13
 422. Ma X, Huang M, Wang Z, Liu B, Zhu Z, Li C. ZHX1 Inhibits Gastric Cancer Cell Growth through Inducing Cell-Cycle Arrest and Apoptosis. *J Cancer*. 2016;7(1):60-68. doi:10.7150/jca.12973
 423. Tupler R, Perini G, Green MR. Expressing the human genome. *Nature*. 2001;409(6822):832-833. doi:10.1038/35057011
 424. Berg JM, Godwin HA. LESSONS FROM ZINC-BINDING PEPTIDES. *Annu Rev Biophys Biomol Struct*. 1997;26(1):357-371. doi:10.1146/annurev.biophys.26.1.357
 425. Berg JM, Shi Y. The galvanization of biology: a growing appreciation for the roles of zinc. *Science*. 1996;271(5252):1081-1085. <http://www.ncbi.nlm.nih.gov/pubmed/8599083>.
 426. Coleman JE. ZINC PROTEINS: Enzymes, Storage Proteins, Transcription Factors, and Replication Proteins. *Annu Rev Biochem*. 1992;61(1):897-946. doi:10.1146/annurev.bi.61.070192.004341
 427. Shastry BS. Transcription factor IIIA (TFIIIA) in the second decade. *J Cell Sci*. 1996;109 (Pt 3:535-539. <http://www.ncbi.nlm.nih.gov/pubmed/8907699>.
 428. Mackay JP, Crossley M. Zinc fingers are sticking together. *Trends Biochem Sci*. 1998;23(1):1-4. doi:10.1016/S0968-0004(97)01168-7
 429. MacDonald RS. The Role of Zinc in Growth and Cell Proliferation. *J Nutr*. 2000;130(5):1500S-1508S. doi:10.1093/jn/130.5.1500S
 430. Chesters JK, Boyne R, Petrie L, Lipson KE. Role of the promoter in the sensitivity of human thymidine kinase to lack of Zn²⁺. *Biochem J*. 1995;308 (Pt 2:659-664. doi:10.1042/bj3080659
 431. MacDonald RS. The Role of Zinc in Growth and Cell Proliferation. *J Nutr*. 2000;130(5):1500S-1508S. doi:10.1093/jn/130.5.1500S
 432. Prasad AS. Zinc deficiency in human subjects. *Prog Clin Biol Res*. 1983;129:1-33.

- <http://www.ncbi.nlm.nih.gov/pubmed/6361778>.
433. Dreosti IE, Hurley LS. Depressed Thymidine Kinase Activity in Zinc-Deficient Rat Embryos. *Exp Biol Med*. 1975;150(1):161-165. doi:10.3181/00379727-150-38995
 434. Dreosti IE. Zinc and the gene. *Mutat Res Mol Mech Mutagen*. 2001;475(1-2):161-167. doi:10.1016/S0027-5107(01)00067-7
 435. FUJII T. Presence of zinc in nucleoli and its possible role in mitosis. *Nature*. 1954;174(4441):1108-1109. doi:10.1038/1741108a0
 436. Vallee BL, Falchuk KH. The biochemical basis of zinc physiology. *Physiol Rev*. 1993;73(1):79-118. doi:10.1152/physrev.1993.73.1.79
 437. Smirnova I V., Bittel DC, Ravindra R, Jiang H, Andrews GK. Zinc and Cadmium Can Promote Rapid Nuclear Translocation of Metal Response Element-binding Transcription Factor-1. *J Biol Chem*. 2000;275(13):9377-9384. doi:10.1074/jbc.275.13.9377
 438. Cano-Gauci DF, Sarkar B. Reversible zinc exchange between metallothionein and the estrogen receptor zinc finger. *FEBS Lett*. 1996;386(1):1-4. doi:10.1016/0014-5793(96)00356-0
 439. Tsujikawa K, Imai T, Kakutani M, et al. Localization of metallothionein in nuclei of growing primary cultured adult rat hepatocytes. *FEBS Lett*. 1991;283(2):239-242. doi:10.1016/0014-5793(91)80597-V
 440. Nartey N, Cherian MG, Banerjee D. Immunohistochemical localization of metallothionein in human thyroid tumors. *Am J Pathol*. 1987;129(1):177-182. <http://www.ncbi.nlm.nih.gov/pubmed/3661677>.
 441. Kuo SM, Kondo Y, Defilippo JM, Ernstoff MS, Bahnson RR, Lazo JS. Subcellular Localization of Metallothionein IIA in Human Bladder Tumor Cells Using a Novel Epitope-Specific Antiserum. *Toxicol Appl Pharmacol*. 1994;125(1):104-110. doi:10.1006/taap.1994.1054
 442. Liu P, Cheng H, Roberts TM, Zhao JJ. Targeting the phosphoinositide 3-kinase pathway in cancer. *Nat Rev Drug Discov*. 2009;8(8):627-644. doi:10.1038/nrd2926
 443. Mayer IA, Arteaga CL. The PI3K/AKT Pathway as a Target for Cancer Treatment. *Annu Rev Med*. 2016;67(1):11-28. doi:10.1146/annurev-med-062913-051343
 444. Burgering BMT, Coffey PJ. Protein kinase B (c-Akt) in phosphatidylinositol-3-OH kinase signal transduction. *Nature*. 1995;376(6541):599-602. doi:10.1038/376599a0
 445. Stål O, Pérez-Tenorio G, Åkerberg L, et al. Akt kinases in breast cancer and the results of adjuvant therapy. *Breast Cancer Res*. 2003;5(2):R37. doi:10.1186/bcr569
 446. Shi W, Zhang X, Pintilie M, et al. Dysregulated PTEN-PKB and negative receptor status in human breast cancer. *Int J Cancer*. 2003;104(2):195-203. doi:10.1002/ijc.10909
 447. Pérez-Tenorio G, Stål O. Activation of AKT/PKB in breast cancer predicts a worse outcome among endocrine treated patients. *Br J Cancer*. 2002;86(4):540-545. doi:10.1038/sj.bjc.6600126
 448. Malik SN, Brattain M, Ghosh PM, et al. Immunohistochemical demonstration of phospho-Akt in high Gleason grade prostate cancer. *Clin Cancer Res*. 2002;8(4):1168-1171. <http://www.ncbi.nlm.nih.gov/pubmed/11948129>.
 449. Sun M, Wang G, Paciga JE, et al. AKT1/PKB α Kinase Is Frequently Elevated in Human Cancers and Its Constitutive Activation Is Required for Oncogenic Transformation in NIH3T3 Cells. *Am J Pathol*. 2001;159(2):431-437. doi:10.1016/S0002-9440(10)61714-2
 450. NAM SY, LEE HS, JUNG G-A, et al. Akt/PKB activation in gastric carcinomas correlates with clinicopathologic variables and prognosis. *APMIS*. 2003;111(12):1105-1113. doi:10.1111/j.1600-0463.2003.apm1111205.x

451. Altomare DA, Wang HQ, Skele KL, et al. AKT and mTOR phosphorylation is frequently detected in ovarian cancer and can be targeted to disrupt ovarian tumor cell growth. *Oncogene*. 2004;23(34):5853-5857. doi:10.1038/sj.onc.1207721
452. Kurose K, Zhou X-P, Araki T, Cannistra SA, Maher ER, Eng C. Frequent Loss of PTEN Expression Is Linked to Elevated Phosphorylated Akt Levels, but Not Associated with p27 and Cyclin D1 Expression, in Primary Epithelial Ovarian Carcinomas. *Am J Pathol*. 2001;158(6):2097-2106. doi:10.1016/S0002-9440(10)64681-0
453. Schlieman MG, Fahy BN, Ramsamooj R, Beckett L, Bold RJ. Incidence, mechanism and prognostic value of activated AKT in pancreas cancer. *Br J Cancer*. 2003;89(11):2110-2115. doi:10.1038/sj.bjc.6601396
454. Min YH, Eom JI, Cheong JW, et al. Constitutive phosphorylation of Akt/PKB protein in acute myeloid leukemia: its significance as a prognostic variable. *Leukemia*. 2003;17(5):995-997. doi:10.1038/sj.leu.2402874
455. Manning BD, Cantley LC. AKT/PKB Signaling: Navigating Downstream. *Cell*. 2007;129(7):1261-1274. doi:10.1016/j.cell.2007.06.009
456. Pap M, Cooper GM. Role of Glycogen Synthase Kinase-3 in the Phosphatidylinositol 3-Kinase/Akt Cell Survival Pathway. *J Biol Chem*. 1998;273(32):19929-19932. doi:10.1074/jbc.273.32.19929
457. Bijur GN, Jope RS. Opposing Actions of Phosphatidylinositol 3-Kinase and Glycogen Synthase Kinase-3 β in the Regulation of HSF-1 Activity. *J Neurochem*. 2008;75(6):2401-2408. doi:10.1046/j.1471-4159.2000.0752401.x
458. Hetman M, Cavanaugh JE, Kimelman D, Xia Z. Role of Glycogen Synthase Kinase-3 β in Neuronal Apoptosis Induced by Trophic Withdrawal. *J Neurosci*. 2000;20(7):2567-2574. doi:10.1523/JNEUROSCI.20-07-02567.2000
459. Li X, Bijur GN, Jope RS. Glycogen synthase kinase-3 β , mood stabilizers, and neuroprotection. *Bipolar Disord*. 2002;4(2):137-144. doi:10.1034/j.1399-5618.2002.40201.x
460. SHIMURA T. Acquired Radioresistance of Cancer and the AKT/GSK3 β /cyclin D1 Overexpression Cycle. *J Radiat Res*. 2011;52(5):539-544. doi:10.1269/jrr.11098
461. Luo J. Glycogen synthase kinase 3 β (GSK3 β) in tumorigenesis and cancer chemotherapy. *Cancer Lett*. 2009;273(2):194-200. doi:10.1016/j.canlet.2008.05.045
462. Shakoory A, Ougolkov A, Yu ZW, et al. Deregulated GSK3 β activity in colorectal cancer: Its association with tumor cell survival and proliferation. *Biochem Biophys Res Commun*. 2005;334(4):1365-1373. doi:10.1016/j.bbrc.2005.07.041
463. Ougolkov A V., Fernandez-Zapico ME, Savoy DN, Urrutia RA, Billadeau DD. Glycogen Synthase Kinase-3 β Participates in Nuclear Factor κ B-Mediated Gene Transcription and Cell Survival in Pancreatic Cancer Cells. *Cancer Res*. 2005;65(6):2076-2081. doi:10.1158/0008-5472.CAN-04-3642
464. Diehl JA, Cheng M, Roussel MF, Sherr CJ. Glycogen synthase kinase-3 β regulates cyclin D1 proteolysis and subcellular localization. *Genes Dev*. 1998;12(22):3499-3511. doi:10.1101/gad.12.22.3499
465. Wei W, Jin J, Schlisio S, Harper JW, Kaelin WG. The v-Jun point mutation allows c-Jun to escape GSK3-dependent recognition and destruction by the Fbw7 ubiquitin ligase. *Cancer Cell*. 2005;8(1):25-33. doi:10.1016/j.ccr.2005.06.005
466. Welcker M, Singer J, Loeb KR, et al. Multisite Phosphorylation by Cdk2 and GSK3 Controls Cyclin E Degradation. *Mol Cell*. 2003;12(2):381-392. doi:10.1016/S1097-2765(03)00287-9
467. Yeh E, Cunningham M, Arnold H, et al. A signalling pathway controlling c-Myc degradation that impacts oncogenic transformation of human cells. *Nat Cell Biol*.

- 2004;6(4):308-318. doi:10.1038/ncb1110
468. Fu Y, Hu D, Qiu J, Xie X, Ye F, Lu W-G. Overexpression of Glycogen Synthase Kinase-3 in Ovarian Carcinoma Cells With Acquired Paclitaxel Resistance. *Int J Gynecol Cancer*. 2011;21(3):439-444. doi:10.1097/IGC.0b013e31820d7366
469. Kawazoe H, Bilim VN, Ugolokov A V., et al. GSK-3 inhibition in vitro and in vivo enhances antitumor effect of sorafenib in renal cell carcinoma (RCC). *Biochem Biophys Res Commun*. 2012;423(3):490-495. doi:10.1016/j.bbrc.2012.05.147
470. Thamilselvan V, Menon M, Thamilselvan S. Anticancer efficacy of deguelin in human prostate cancer cells targeting glycogen synthase kinase-3 β/β -catenin pathway. *Int J Cancer*. 2011;129(12):2916-2927. doi:10.1002/ijc.25949
471. Aoki M, Blazek E, Vogt PK. A role of the kinase mTOR in cellular transformation induced by the oncoproteins P3k and Akt. *Proc Natl Acad Sci*. 2001;98(1):136-141. doi:10.1073/pnas.98.1.136
472. Du K, Montminy M. CREB Is a Regulatory Target for the Protein Kinase Akt/PKB. *J Biol Chem*. 1998;273(49):32377-32379. doi:10.1074/jbc.273.49.32377
473. Rodon J, Dienstmann R, Serra V, Tabernero J. Development of PI3K inhibitors: lessons learned from early clinical trials. *Nat Rev Clin Oncol*. 2013;10(3):143-153. doi:10.1038/nrclinonc.2013.10
474. Lee JJ, Loh K, Yap Y-S. PI3K/Akt/mTOR inhibitors in breast cancer. *Cancer Biol Med*. 2015;12(4):342-354. doi:10.7497/j.issn.2095-3941.2015.0089
475. Steven A, Seliger B. Control of CREB expression in tumors: from molecular mechanisms and signal transduction pathways to therapeutic target. *Oncotarget*. 2016;7(23). doi:10.18632/oncotarget.7721
476. Wu D, Zhau HE, Huang W-C, et al. cAMP-responsive element-binding protein regulates vascular endothelial growth factor expression: implication in human prostate cancer bone metastasis. *Oncogene*. 2007;26(35):5070-5077. doi:10.1038/sj.onc.1210316
477. Chhabra A, Fernando H, Watkins G, Mansel RE, Jiang WG. Expression of transcription factor CREB1 in human breast cancer and its correlation with prognosis. *Oncol Rep*. 2007;18(4):953-958. <http://www.ncbi.nlm.nih.gov/pubmed/17786359>.
478. Liu J, Jiang Y-G, Huang C-Y, Fang H-Y, Fang H-T, Pang W. Depletion of intracellular zinc down-regulates expression of Uch-L1 mRNA and protein, and CREB mRNA in cultured hippocampal neurons. *Nutr Neurosci*. 2008;11(3):96-102. doi:10.1179/147683013X13789826942468
479. Dobroff AS, Wang H, Melnikova VO, et al. Silencing cAMP-response Element-binding Protein (CREB) Identifies CYR61 as a Tumor Suppressor Gene in Melanoma. *J Biol Chem*. 2009;284(38):26194-26206. doi:10.1074/jbc.M109.019836
480. Melnikova VO, Dobroff AS, Zigler M, et al. CREB Inhibits AP-2 α Expression to Regulate the Malignant Phenotype of Melanoma. Chammas R, ed. *PLoS One*. 2010;5(8):e12452. doi:10.1371/journal.pone.0012452
481. Wang Y-W, Chen X, Gao J-W, et al. High expression of cAMP responsive element binding protein 1 (CREB1) is associated with metastasis, tumor stage and poor outcome in gastric cancer. *Oncotarget*. 2015;6(12):10646-10657. doi:10.18632/oncotarget.3392
482. Tan X, Wang S, Zhu L, et al. cAMP response element-binding protein promotes gliomagenesis by modulating the expression of oncogenic microRNA-23a. *Proc Natl Acad Sci*. 2012;109(39):15805-15810. doi:10.1073/pnas.1207787109
483. Mantamadiotis T. Towards Targeting PI3K-Dependent Regulation of Gene Expression in Brain Cancer. *Cancers (Basel)*. 2017;9(12):60. doi:10.3390/cancers9060060
484. Rajesh Y, Pal I, Banik P, et al. Insights into molecular therapy of glioma: current

- challenges and next generation blueprint. *Acta Pharmacol Sin.* 2017;38(5):591-613. doi:10.1038/aps.2016.167
485. Ji L, Mochon E, Arcinas M, Boxer LM. CREB Proteins Function as Positive Regulators of the Translocated -2 Allele in t(14;18) Lymphomas. *J Biol Chem.* 1996;271(37):22687-22691. doi:10.1074/jbc.271.37.22687
486. Wilson BE, Mochon E, Boxer LM. Induction of bcl-2 expression by phosphorylated CREB proteins during B-cell activation and rescue from apoptosis. *Mol Cell Biol.* 1996;16(10):5546-5556. doi:10.1128/MCB.16.10.5546
487. Pugazhenth S, Miller E, Sable C, et al. Insulin-like Growth Factor-I Induces bcl-2 Promoter through the Transcription Factor cAMP-Response Element-binding Protein. *J Biol Chem.* 1999;274(39):27529-27535. doi:10.1074/jbc.274.39.27529
488. Riccio A, Ahn S, Davenport CM, Blendy JA, Ginty DD. Mediation by a CREB Family Transcription Factor of NGF-Dependent Survival of Sympathetic Neurons. *Science (80-).* 1999;286(5448):2358-2361. doi:10.1126/science.286.5448.2358
489. Pitts TM, Davis SL, Eckhardt SG, Bradshaw-Pierce EL. Targeting nuclear kinases in cancer: Development of cell cycle kinase inhibitors. *Pharmacol Ther.* 2014;142(2):258-269. doi:10.1016/j.pharmthera.2013.12.010
490. Harsha HC, Pandey A. Phosphoproteomics in cancer. *Mol Oncol.* 2010;4(6):482-495. doi:10.1016/j.molonc.2010.09.004
491. Risso G, Blaustein M, Pozzi B, Mammi P, Srebrow A. Akt/PKB: one kinase, many modifications. *Biochem J.* 2015;468(2):203-214. doi:10.1042/BJ20150041
492. Bellacosa A, Kumar CC, Cristofano A Di, Testa JR. Activation of AKT Kinases in Cancer: Implications for Therapeutic Targeting. In: ; 2005:29-86. doi:10.1016/S0065-230X(05)94002-5
493. Martelli AM, Tabellini G, Bressanin D, et al. The emerging multiple roles of nuclear Akt. *Biochim Biophys Acta - Mol Cell Res.* 2012;1823(12):2168-2178. doi:10.1016/j.bbamcr.2012.08.017
494. Arden KC, Biggs III WH. Regulation of the FoxO family of transcription factors by phosphatidylinositol-3 kinase-activated signaling. *Arch Biochem Biophys.* 2002;403(2):292-298. doi:10.1016/S0003-9861(02)00207-2
495. Huang W-C, Chen C-C. Akt Phosphorylation of p300 at Ser-1834 Is Essential for Its Histone Acetyltransferase and Transcriptional Activity. *Mol Cell Biol.* 2005;25(15):6592-6602. doi:10.1128/MCB.25.15.6592-6602.2005
496. NERI LM, MARTELLI AM, BORGATTI P, COLAMUSSI ML, MARCHISIO M, CAPITANI S. Increase in nuclear phosphatidylinositol 3-kinase activity and phosphatidylinositol (3,4,5) trisphosphate synthesis precede PKC- ζ translocation to the nucleus of NGF-treated PC12 cells. *FASEB J.* 1999;13(15):2299-2310. doi:10.1096/fasebj.13.15.2299
497. Neri LM, Bortul R, Tabellini G, et al. Erythropoietin (EPO)-induced erythroid differentiation of K562 cells is accompanied by the nuclear translocation of phosphatidylinositol 3-kinase and intranuclear generation of phosphatidylinositol (3,4,5) trisphosphate. *Cell Signal.* 2002;14(1):21-29. doi:10.1016/S0898-6568(01)00224-8
498. Scheid MP, Parsons M, Woodgett JR. Phosphoinositide-Dependent Phosphorylation of PDK1 Regulates Nuclear Translocation. *Mol Cell Biol.* 2005;25(6):2347-2363. doi:10.1128/MCB.25.6.2347-2363.2005
499. Kikani CK, Dong LQ, Liu F. "New"-clear functions of PDK1: Beyond a master kinase? *J Cell Biochem.* 2005;96(6):1157-1162. doi:10.1002/jcb.20651
500. Rosner M, Hengstschlager M. Detection of Cytoplasmic and Nuclear Functions of mTOR by Fractionation. In: ; 2012:105-124. doi:10.1007/978-1-61779-430-8_8

501. Liu J, Brown RE. Morphoproteomics demonstrates activation of mammalian target of rapamycin pathway in papillary thyroid carcinomas with nuclear translocation of MTOR in aggressive histological variants. *Mod Pathol*. 2011;24(12):1553-1559. doi:10.1038/modpathol.2011.121
502. Nicholson KM, Streuli CH, Anderson NG. Autocrine Signalling Through erbB Receptors Promotes Constitutive Activation of Protein Kinase B/Akt in Breast Cancer Cell Lines. *Breast Cancer Res Treat*. 2003;81(2):117-128. doi:10.1023/A:1025765215765
503. Lee SH, Kim HS, Park WS, et al. Non-small cell lung cancers frequently express phosphorylated Akt; an immunohistochemical study. *APMIS*. 2002;110(7-8):587-592. doi:10.1034/j.1600-0463.2002.11007811.x
504. Van de Sande T, Roskams T, Lerut E, et al. High-level expression of fatty acid synthase in human prostate cancer tissues is linked to activation and nuclear localization of Akt/PKB. *J Pathol*. 2005;206(2):214-219. doi:10.1002/path.1760
505. Cappellini A, Tabellini G, Zweyer M, et al. The phosphoinositide 3-kinase/Akt pathway regulates cell cycle progression of HL60 human leukemia cells through cytoplasmic relocalization of the cyclin-dependent kinase inhibitor p27Kip1 and control of cyclin D1 expression. *Leukemia*. 2003;17(11):2157-2167. doi:10.1038/sj.leu.2403111
506. Brandts CH, Sargin B, Rode M, et al. Constitutive Activation of Akt by Flt3 Internal Tandem Duplications Is Necessary for Increased Survival, Proliferation, and Myeloid Transformation. *Cancer Res*. 2005;65(21):9643-9650. doi:10.1158/0008-5472.CAN-05-0422
507. Vasko V. Akt activation and localisation correlate with tumour invasion and oncogene expression in thyroid cancer. *J Med Genet*. 2004;41(3):161-170. doi:10.1136/jmg.2003.015339
508. Coa LL, Abreu TF, Tashima AK, et al. AKT/protein kinase B associates with β -actin in the nucleus of melanoma cells. *Biosci Rep*. 2019;39(1). doi:10.1042/BSR20181312
509. Kim HL, Yang XJ. Prevalence of high-grade prostatic intraepithelial neoplasia and its relationship to serum prostate specific antigen. *Int Braz J Urol*. 28(5):413-416; discussion 417. doi:15748366
510. Montironi R, Mazzuccheli R, Scarpelli M, Lopez-Beltran A, Fellegara G, Algaba F. Gleason grading of prostate cancer in needle biopsies or radical prostatectomy specimens: contemporary approach, current clinical significance and sources of pathology discrepancies. *BJU Int*. 2005;95(8):1146-1152. doi:10.1111/j.1464-410X.2005.05540.x
511. SUZUKI Y, SHIRAI K, OKA K, et al. Higher pAkt Expression Predicts a Significant Worse Prognosis in Glioblastomas. *J Radiat Res*. 2010;51(3):343-348. doi:10.1269/jrr.09109
512. Giudice FS, Vechio AM da CD, Abrahão AC, Sperandio FF, Pinto-Junior D dos S. Different expression patterns of pAkt, NF- κ B and cyclin D1 proteins during the invasion process of head and neck squamous cell carcinoma: an in vitro approach. *J Oral Pathol Med*. 2011;40(5):405-411. doi:10.1111/j.1600-0714.2010.00960.x
513. Zhang X, Odom DT, Koo S-H, et al. Genome-wide analysis of cAMP-response element binding protein occupancy, phosphorylation, and target gene activation in human tissues. *Proc Natl Acad Sci*. 2005;102(12):4459-4464. doi:10.1073/pnas.0501076102
514. Sapio L, Salzillo A, Ragone A, Illiano M, Spina A, Naviglio S. Targeting CREB in Cancer Therapy: A Key Candidate or One of Many? An Update. *Cancers (Basel)*. 2020;12(11):3166. doi:10.3390/cancers12113166

515. Steven A, Friedrich M, Jank P, et al. What turns CREB on? And off? And why does it matter? *Cell Mol Life Sci.* 2020;77(20):4049-4067. doi:10.1007/s00018-020-03525-8
516. Whiteman EL, Cho H, Birnbaum MJ. Role of Akt/protein kinase B in metabolism. *Trends Endocrinol Metab.* 2002;13(10):444-451. doi:10.1016/S1043-2760(02)00662-8
517. Tan S, Ng Y, James DE. Next-generation Akt inhibitors provide greater specificity: effects on glucose metabolism in adipocytes. *Biochem J.* 2011;435(2):539-544. doi:10.1042/BJ20110040
518. Guo Y, Pan W, Liu S, Shen Z, Xu Y, Hu L. ERK/MAPK signalling pathway and tumorigenesis (Review). *Exp Ther Med.* January 2020. doi:10.3892/etm.2020.8454
519. Chang L, Karin M. Mammalian MAP kinase signalling cascades. *Nature.* 2001;410(6824):37-40. doi:10.1038/35065000
520. Boulton TG, Nye SH, Robbins DJ, et al. ERKs: A family of protein-serine/threonine kinases that are activated and tyrosine phosphorylated in response to insulin and NGF. *Cell.* 1991;65(4):663-675. doi:10.1016/0092-8674(91)90098-J
521. Lu Y, Liu B, Liu Y, Yu X, Cheng G. Dual effects of active ERK in cancer: A potential target for enhancing radiosensitivity (Review). *Oncol Lett.* 2020;20(2):993-1000. doi:10.3892/ol.2020.11684
522. Sun Y, Liu W-Z, Liu T, Feng X, Yang N, Zhou H-F. Signaling pathway of MAPK/ERK in cell proliferation, differentiation, migration, senescence and apoptosis. *J Recept Signal Transduct.* 2015;35(6):600-604. doi:10.3109/10799893.2015.1030412
523. Kim EK, Choi E-J. Compromised MAPK signaling in human diseases: an update. *Arch Toxicol.* 2015;89(6):867-882. doi:10.1007/s00204-015-1472-2
524. Balmanno K, Cook SJ. Tumour cell survival signalling by the ERK1/2 pathway. *Cell Death Differ.* 2009;16(3):368-377. doi:10.1038/cdd.2008.148
525. Neuzillet C, Tijeras-Raballand A, de Mestier L, Cros J, Faivre S, Raymond E. MEK in cancer and cancer therapy. *Pharmacol Ther.* 2014;141(2):160-171. doi:10.1016/j.pharmthera.2013.10.001
526. Sebolt-Leopold JS, Dudley DT, Herrera R, et al. Blockade of the MAP kinase pathway suppresses growth of colon tumors in vivo. *Nat Med.* 1999;5(7):810-816. doi:10.1038/10533
527. Huang P, Guo L, Xi J, Wang D. Angiotensin II type 2 receptor–interacting protein 3a inhibits ovarian carcinoma metastasis via the extracellular HMGA2-mediated ERK/EMT pathway. *Tumor Biol.* 2017;39(6):101042831771338. doi:10.1177/1010428317713389
528. Nishida N, Yano H, Nishida T, Kamura T, Kojiro M. Angiogenesis in cancer. *Vasc Health Risk Manag.* 2006;2(3):213-219. doi:10.2147/vhrm.2006.2.3.213
529. Lambert AW, Pattabiraman DR, Weinberg RA. Emerging Biological Principles of Metastasis. *Cell.* 2017;168(4):670-691. doi:10.1016/j.cell.2016.11.037
530. Krakhmal N V, Zavyalova M V, Denisov E V, Vtorushin S V, Perelmuter VM. Cancer Invasion: Patterns and Mechanisms. *Acta Naturae.* 7(2):17-28. <http://www.ncbi.nlm.nih.gov/pubmed/26085941>.
531. Sulzmaier FJ, Ramos JW. RSK Isoforms in Cancer Cell Invasion and Metastasis. *Cancer Res.* 2013;73(20):6099-6105. doi:10.1158/0008-5472.CAN-13-1087
532. Roskoski R. Targeting ERK1/2 protein-serine/threonine kinases in human cancers. *Pharmacol Res.* 2019;142:151-168. doi:10.1016/j.phrs.2019.01.039
533. Jaiswal BS, Durinck S, Stawiski EW, et al. ERK Mutations and Amplification Confer Resistance to ERK-Inhibitor Therapy. *Clin Cancer Res.* 2018;24(16):4044-4055. doi:10.1158/1078-0432.CCR-17-3674
534. Moodie S, Willumsen B, Weber M, Wolfman A. Complexes of Ras.GTP with Raf-1 and mitogen-activated protein kinase kinase. *Science (80-).* 1993;260(5114):1658-

1661. doi:10.1126/science.8503013
535. Vojtek AB, Hollenberg SM, Cooper JA. Mammalian Ras interacts directly with the serine/threonine kinase raf. *Cell*. 1993;74(1):205-214. doi:10.1016/0092-8674(93)90307-C
536. Roux PP, Blenis J. ERK and p38 MAPK-Activated Protein Kinases: a Family of Protein Kinases with Diverse Biological Functions. *Microbiol Mol Biol Rev*. 2004;68(2):320-344. doi:10.1128/MMBR.68.2.320-344.2004
537. Fukuda M. Interaction of MAP kinase with MAP kinase kinase: its possible role in the control of nucleocytoplasmic transport of MAP kinase. *EMBO J*. 1997;16(8):1901-1908. doi:10.1093/emboj/16.8.1901
538. Marais R, Wynne J, Treisman R. The SRF accessory protein Elk-1 contains a growth factor-regulated transcriptional activation domain. *Cell*. 1993;73(2):381-393. doi:10.1016/0092-8674(93)90237-K
539. Minichiello L. TrkB signalling pathways in LTP and learning. *Nat Rev Neurosci*. 2009;10(12):850-860. doi:10.1038/nrn2738
540. Adamo AM, Zago MP, Mackenzie GG, et al. The Role of Zinc in the Modulation of Neuronal Proliferation and Apoptosis. *Neurotox Res*. 2010;17(1):1-14. doi:10.1007/s12640-009-9067-4
541. Fenton TR, Gout IT. Functions and regulation of the 70kDa ribosomal S6 kinases. *Int J Biochem Cell Biol*. 2011;43(1):47-59. doi:10.1016/j.biocel.2010.09.018
542. Proud CG. p70 S6 kinase: an enigma with variations. *Trends Biochem Sci*. 1996;21(5):181-185. doi:10.1016/S0968-0004(96)10016-5
543. Valovka T, Verdier F, Cramer R, et al. Protein Kinase C Phosphorylates Ribosomal Protein S6 Kinase β II and Regulates Its Subcellular Localization. *Mol Cell Biol*. 2003;23(3):852-863. doi:10.1128/MCB.23.3.852-863.2003
544. Kosach V, Shkarina K, Kravchenko A, et al. Nucleocytoplasmic distribution of S6K1 depends on the density and motility of MCF-7 cells in vitro. *F1000Research*. 2018;7:1332. doi:10.12688/f1000research.15447.2
545. Montagne J. Drosophila S6 Kinase: A Regulator of Cell Size. *Science (80-)*. 1999;285(5436):2126-2129. doi:10.1126/science.285.5436.2126
546. Shima H. Disruption of the p70s6k/p85s6k gene reveals a small mouse phenotype and a new functional S6 kinase. *EMBO J*. 1998;17(22):6649-6659. doi:10.1093/emboj/17.22.6649
547. Pende M, Kozma SC, Jaquet M, et al. Hypoinsulinaemia, glucose intolerance and diminished β -cell size in S6K1-deficient mice. *Nature*. 2000;408(6815):994-997. doi:10.1038/35050135
548. Lane HA, Fernandez A, Lamb NJC, Thomas G. p70s6k function is essential for G1 progression. *Nature*. 1993;363(6425):170-172. doi:10.1038/363170a0
549. Reinhard C, Fernandez A, Lamb NJ, Thomas G. Nuclear localization of p85s6k: functional requirement for entry into S phase. *EMBO J*. 1994;13(7):1557-1565. doi:10.1002/j.1460-2075.1994.tb06418.x
550. Alessi DR, Cohen P. Mechanism of activation and function of protein kinase B. *Curr Opin Genet Dev*. 1998;8(1):55-62. doi:10.1016/S0959-437X(98)80062-2
551. Weng QP, Andrabi K, Klippel A, Kozlowski MT, Williams LT, Avruch J. Phosphatidylinositol 3-kinase signals activation of p70 S6 kinase in situ through site-specific p70 phosphorylation. *Proc Natl Acad Sci*. 1995;92(12):5744-5748. doi:10.1073/pnas.92.12.5744
552. Chung J, Kuo CJ, Crabtree GR, Blenis J. Rapamycin-FKBP specifically blocks growth-dependent activation of and signaling by the 70 kd S6 protein kinases. *Cell*. 1992;69(7):1227-1236. doi:10.1016/0092-8674(92)90643-Q

553. Brown EJ, Beal PA, Keith CT, Chen J, Bum Shin T, Schreiber SL. Control of p70 S6 kinase by kinase activity of FRAP in vivo. *Nature*. 1995;377(6548):441-446. doi:10.1038/377441a0
554. Tavares MR, Pavan ICB, Amaral CL, Meneguello L, Luchessi AD, Simabuco FM. The S6K protein family in health and disease. *Life Sci*. 2015;131:1-10. doi:10.1016/j.lfs.2015.03.001
555. Dey N, De P, Leyland-Jones B. PI3K-AKT-mTOR inhibitors in breast cancers: From tumor cell signaling to clinical trials. *Pharmacol Ther*. 2017;175:91-106. doi:10.1016/j.pharmthera.2017.02.037
556. Guerrero-Zotano A, Mayer IA, Arteaga CL. PI3K/AKT/mTOR: role in breast cancer progression, drug resistance, and treatment. *Cancer Metastasis Rev*. 2016;35(4):515-524. doi:10.1007/s10555-016-9637-x
557. Pearson RB, Dennis PB, Han JW, et al. The principal target of rapamycin-induced p70s6k inactivation is a novel phosphorylation site within a conserved hydrophobic domain. *EMBO J*. 1995;14(21):5279-5287. doi:10.1002/j.1460-2075.1995.tb00212.x
558. Ferrari S, Pearson RB, Siegmann M, Kozma SC, Thomas G. The immunosuppressant rapamycin induces inactivation of p70s6k through dephosphorylation of a novel set of sites. *J Biol Chem*. 1993;268(22):16091-16094. <http://www.ncbi.nlm.nih.gov/pubmed/8344891>.
559. Price DJ, Mukhopadhyay NK AJ. Insulin-activated protein kinases phosphorylate a pseudosubstrate synthetic peptide inhibitor of the p70 S6 kinase. *J Biol Chem*. 1991;5;266(25)(16281-4).
560. Lehman JA, Calvo V, Gomez-Cambronero J. Mechanism of Ribosomal p70S6 Kinase Activation by Granulocyte Macrophage Colony-stimulating Factor in Neutrophils. *J Biol Chem*. 2003;278(30):28130-28138. doi:10.1074/jbc.M300376200
561. Zhang J, Gao Z, Ye J. Phosphorylation and degradation of S6K1 (p70S6K1) in response to persistent JNK1 Activation. *Biochim Biophys Acta - Mol Basis Dis*. 2013;1832(12):1980-1988. doi:10.1016/j.bbadis.2013.06.013
562. Isotani S, Hara K, Tokunaga C, Inoue H, Avruch J, Yonezawa K. Immunopurified Mammalian Target of Rapamycin Phosphorylates and Activates p70 S6 Kinase α in Vitro. *J Biol Chem*. 1999;274(48):34493-34498. doi:10.1074/jbc.274.48.34493
563. Alessi DR, Kozlowski MT, Weng Q-P, Morrice N, Avruch J. 3-Phosphoinositide-dependent protein kinase 1 (PDK1) phosphorylates and activates the p70 S6 kinase in vivo and in vitro. *Curr Biol*. 1998;8(2):69-81. doi:10.1016/S0960-9822(98)70037-5
564. Wei, Luo, Chen. Roles of mTOR Signaling in Tissue Regeneration. *Cells*. 2019;8(9):1075. doi:10.3390/cells8091075
565. Kim S, Jung Y, Kim D, Koh H, Chung J. Extracellular Zinc Activates p70 S6 Kinase through the Phosphatidylinositol 3-Kinase Signaling Pathway. *J Biol Chem*. 2000;275(34):25979-25984. doi:10.1074/jbc.M001975200
566. Lynch CJ, Patson BJ, Goodman SA, Trapolsi D, Kimball SR. Zinc stimulates the activity of the insulin- and nutrient-regulated protein kinase mTOR. *Am J Physiol Metab*. 2001;281(1):E25-E34. doi:10.1152/ajpendo.2001.281.1.E25
567. Shaw RJ, Cantley LC. Ras, PI(3)K and mTOR signalling controls tumour cell growth. *Nature*. 2006;441(7092):424-430. doi:10.1038/nature04869
568. Bachelot T, Bourcier C, Cropet C, et al. Randomized Phase II Trial of Everolimus in Combination With Tamoxifen in Patients With Hormone Receptor-Positive, Human Epidermal Growth Factor Receptor 2-Negative Metastatic Breast Cancer With Prior Exposure to Aromatase Inhibitors: A GINECO Study. *J Clin Oncol*. 2012;30(22):2718-2724. doi:10.1200/JCO.2011.39.0708
569. Baselga J, Semiglazov V, van Dam P, et al. Phase II Randomized Study of

- Neoadjuvant Everolimus Plus Letrozole Compared With Placebo Plus Letrozole in Patients With Estrogen Receptor–Positive Breast Cancer. *J Clin Oncol*. 2009;27(16):2630-2637. doi:10.1200/JCO.2008.18.8391
570. Baselga J, Campone M, Piccart M, et al. Everolimus in Postmenopausal Hormone-Receptor–Positive Advanced Breast Cancer. *N Engl J Med*. 2012;366(6):520-529. doi:10.1056/NEJMoa1109653
571. Soares HP, Ni Y, Kisfalvi K, Sinnett-Smith J, Rozengurt E. Different Patterns of Akt and ERK Feedback Activation in Response to Rapamycin, Active-Site mTOR Inhibitors and Metformin in Pancreatic Cancer Cells. Pizzo S V., ed. *PLoS One*. 2013;8(2):e57289. doi:10.1371/journal.pone.0057289
572. Gagnon KBE, England R, Delpire E. Volume sensitivity of cation-Cl⁻ cotransporters is modulated by the interaction of two kinases: Ste20-related proline-alanine-rich kinase and WNK4. *Am J Physiol Physiol*. 2006;290(1):C134-C142. doi:10.1152/ajpcell.00037.2005
573. Huang C-L, Cha S-K, Wang H-R, Xie J, Cobb MH. WNKs: protein kinases with a unique kinase domain. *Exp Mol Med*. 2007;39(5):565-573. doi:10.1038/emm.2007.62
574. Xu B, English JM, Wilsbacher JL, Stippe S, Goldsmith EJ, Cobb MH. WNK1, a Novel Mammalian Serine/Threonine Protein Kinase Lacking the Catalytic Lysine in Subdomain II. *J Biol Chem*. 2000;275(22):16795-16801. doi:10.1074/jbc.275.22.16795
575. Verissimo F, Jordan P. WNK kinases, a novel protein kinase subfamily in multicellular organisms. *Oncogene*. 2001;20(39):5562-5569. doi:10.1038/sj.onc.1204726
576. Moriguchi T, Urushiyama S, Hisamoto N, et al. WNK1 Regulates Phosphorylation of Cation-Chloride-coupled Cotransporters via the STE20-related Kinases, SPAK and OSR1. *J Biol Chem*. 2005;280(52):42685-42693. doi:10.1074/jbc.M510042200
577. Vitari AC, Deak M, Morrice NA, Alessi DR. The WNK1 and WNK4 protein kinases that are mutated in Gordon's hypertension syndrome phosphorylate and activate SPAK and OSR1 protein kinases. *Biochem J*. 2005;391(1):17-24. doi:10.1042/BJ20051180
578. Anselmo AN, Earnest S, Chen W, et al. WNK1 and OSR1 regulate the Na⁺, K⁺, 2Cl⁻ cotransporter in HeLa cells. *Proc Natl Acad Sci U S A*. 2006;103(29):10883-10888. doi:10.1073/pnas.0604607103
579. Moniz S, Jordan P. Emerging roles for WNK kinases in cancer. *Cell Mol Life Sci*. 2010;67(8):1265-1276. doi:10.1007/s00018-010-0261-6
580. McCormick JA, Ellison DH. The WNKs: Atypical Protein Kinases With Pleiotropic Actions. *Physiol Rev*. 2011;91(1):177-219. doi:10.1152/physrev.00017.2010
581. Gallolu Kankanamalage S, Lee A-Y, Wichaidit C, et al. Multistep regulation of autophagy by WNK1. *Proc Natl Acad Sci*. 2016;113(50):14342-14347. doi:10.1073/pnas.1617649113
582. Sie Z-L, Li R-Y, Sampurna BP, et al. WNK1 Kinase Stimulates Angiogenesis to Promote Tumor Growth and Metastasis. *Cancers (Basel)*. 2020;12(3):575. doi:10.3390/cancers12030575
583. Dbouk HA, Weil LM, Perera GKS, et al. Actions of the protein kinase WNK1 on endothelial cells are differentially mediated by its substrate kinases OSR1 and SPAK. *Proc Natl Acad Sci*. 2014;111(45):15999-16004. doi:10.1073/pnas.1419057111
584. VITARI AC, DEAK M, COLLINS BJ, et al. WNK1, the kinase mutated in an inherited high-blood-pressure syndrome, is a novel PKB (protein kinase B)/Akt substrate. *Biochem J*. 2004;378(1):257-268. doi:10.1042/bj20031692
585. Jiang ZY, Zhou QL, Holik J, et al. Identification of WNK1 as a Substrate of Akt/Protein Kinase B and a Negative Regulator of Insulin-stimulated Mitogenesis in 3T3-L1 Cells. *J Biol Chem*. 2005;280(22):21622-21628. doi:10.1074/jbc.M414464200

586. Sjoblom T, Jones S, Wood LD, et al. The Consensus Coding Sequences of Human Breast and Colorectal Cancers. *Science* (80-). 2006;314(5797):268-274. doi:10.1126/science.1133427
587. Stephens P, Edkins S, Davies H, et al. A screen of the complete protein kinase gene family identifies diverse patterns of somatic mutations in human breast cancer. *Nat Genet.* 2005;37(6):590-592. doi:10.1038/ng1571
588. Fulford L, Milewski D, Ustiyani V, et al. The transcription factor FOXF1 promotes prostate cancer by stimulating the mitogen-activated protein kinase ERK5. *Sci Signal.* 2016;9(427):ra48-ra48. doi:10.1126/scisignal.aad5582
589. Hung J-Y, Yen M-C, Jian S-F, et al. Secreted protein acidic and rich in cysteine (SPARC) induces cell migration and epithelial mesenchymal transition through WNK1/snail in non-small cell lung cancer. *Oncotarget.* 2017;8(38):63691-63702. doi:10.18632/oncotarget.19475
590. Garzon-Muvdi T, Schiapparelli P, ap Rhys C, et al. Regulation of Brain Tumor Dispersal by NKCC1 Through a Novel Role in Focal Adhesion Regulation. Rich JN, ed. *PLoS Biol.* 2012;10(5):e1001320. doi:10.1371/journal.pbio.1001320
591. Shyamasundar S, Lim JP, Bay BH. miR-93 inhibits the invasive potential of triple-negative breast cancer cells in vitro via protein kinase WNK1. *Int J Oncol.* 2016;49(6):2629-2636. doi:10.3892/ijo.2016.3761
592. Pio GM, Xia Y, Piaseczny MM, Chu JE, Allan AL. Soluble bone-derived osteopontin promotes migration and stem-like behavior of breast cancer cells. Samant R, ed. *PLoS One.* 2017;12(5):e0177640. doi:10.1371/journal.pone.0177640
593. Jaykumar A, Jung J, Parida P, et al. WNK1 Enhances Migration and Invasion in Breast Cancer Models. 2021. doi:10.1101/2021.03.09.434610
594. Serysheva E, Berhane H, Grumolato L, et al. Wnk kinases are positive regulators of canonical Wnt/ β -catenin signalling. *EMBO Rep.* 2013;14(8):718-725. doi:10.1038/embor.2013.88
595. Clevers H, Nusse R. Wnt/ β -Catenin Signaling and Disease. *Cell.* 2012;149(6):1192-1205. doi:10.1016/j.cell.2012.05.012
596. Rosenbluh J, Nijhawan D, Cox AG, et al. β -Catenin-Driven Cancers Require a YAP1 Transcriptional Complex for Survival and Tumorigenesis. *Cell.* 2012;151(7):1457-1473. doi:10.1016/j.cell.2012.11.026
597. Shang S, Hua F, Hu Z-W. The regulation of β -catenin activity and function in cancer: therapeutic opportunities. *Oncotarget.* 2017;8(20):33972-33989. doi:10.18632/oncotarget.15687
598. Haas BR, Cuddapah VA, Watkins S, Rohn KJ, Dy TE, Sontheimer H. With-No-Lysine Kinase 3 (WNK3) stimulates glioma invasion by regulating cell volume. *Am J Physiol Physiol.* 2011;301(5):C1150-C1160. doi:10.1152/ajpcell.00203.2011
599. Mäusbacher N, Schreiber TB, Daub H. Glycoprotein Capture and Quantitative Phosphoproteomics Indicate Coordinated Regulation of Cell Migration upon Lysophosphatidic Acid Stimulation. *Mol Cell Proteomics.* 2010;9(11):2337-2353. doi:10.1074/mcp.M110.000737
600. Moniz S, Martinho O, Pinto F, et al. Loss of WNK2 expression by promoter gene methylation occurs in adult gliomas and triggers Rac1-mediated tumour cell invasiveness. *Hum Mol Genet.* 2013;22(1):84-95. doi:10.1093/hmg/dd5405
601. Alves CC. Role of the epithelial-mesenchymal transition regulator Slug in primary human cancers. *Front Biosci.* 2009;Volume(14):3035. doi:10.2741/3433
602. Siddiqui-Jain A, Drygin D, Streiner N, et al. CX-4945, an Orally Bioavailable Selective Inhibitor of Protein Kinase CK2, Inhibits Prosurvival and Angiogenic Signaling and Exhibits Antitumor Efficacy. *Cancer Res.* 2010;70(24):10288-10298.

doi:10.1158/0008-5472.CAN-10-1893

9. Appendices:

a- Materials, buffers and reagents for SDS-PAGE and western blot

- **Lysis buffer:**

- 50 mM Tris base pH 7.5, (Fisher;BP152-1)
- 150mM NaCl (sodium chloride) (Fisher;S/3160/65)
- 5mM EGTA (ethylene glycol tetra-acetic acid) (Sigma;3889)
- 1% Triton X-100 (Sigma;T8532)

We used 5M HCL to made up the pH to 7.6

- 100 mM NaVO₄ (sodium orthovanadate) → we used (2 µl/ dish)
- 1M Sodium fluoride (NaF) → we used (1 µl/ dish)
- Protease inhibitors cocktail 1:100 (Sigma;P8340)

The Protease inhibitors cocktail must be added just before use

- **Running buffer for SDS-PAGE pH 8.3 (10X concentrated stock)- 1 Litter**

- 30g TRIS base
- 144g Glycin (Fisher;G/P460/53)
- 10g SDS
- Distilled H₂O
- HCL (Hydrogen Chloride) 5M to adjust pH

The above reagents were dissolved in 800ml of distilled H₂O.pH of the solution was adjusted to 8.3 with 5M HCL (~ 6-7 ml) and make it up to 1 Litter with distal H₂O. For use in SDS-PAGE dilute the 10X concentrated stock 1 in 10 in distilled H₂O.

- **TRIS- Buffered Saline with Tween 20 (TBS-Tween), pH7.6 (10X concentrated stock)- 1 Litter**

- 12.1 g TRIS base
- 58 g NaCl
- 5 ml Tween 20

The above reagents were dissolved in 900ml of distilled H₂O. pH of the solution was adjusted to 7.6 with approximately 15 ml of 5M HCL and then the solution was make it up to 1 Litter with distilled H₂O. For western blot use, dilute the concentrated stock 1 in 10 with distilled H₂O (1X TBST).

- **Transfer Buffer- 1 Litter**

- 3.03 g TRIS base
- 14.4 g Glycine.
- 800 ml distilled H₂O
- 200 ml Methanol.(Fisher;10284580)

- **Laemmli Sample Buffer (Loading Buffer) 4X concentrated**

- 800 mg SDS (Sigma;L4390)
- 4 ml Glycerol (Sigma;G5516)
- 4.8 ml of 0.5M stacking gel buffer (pH 6.8) (Bio-Rad;161-0799)
- 1.2 ml distilled H₂O
- Bromophenol blue
- 308mg of Dithiothreitol (DDT)

DTT was added just before use because it is unstable in aqueous solution.
1x buffer made up from the 4x concentration stock in distilled H₂O

- **Ponceau S**

- Ponceau S 0.1 % (w/v)
- 5% acetic acid